Tissue engineering a ligamentous construct

by

Nazia Mehrban

A thesis submitted to

The University of Birmingham

for the degree of

DOCTOR OF PHILOSOPHY

Bioengineering

School of Chemical Engineering

University of Birmingham

ABSTRACT

Tendon and ligament damage causes extreme pain and decreased joint functionality. Current repair methods cannot restore original joint biomechanics nor promote regeneration of native tissue. Recent advances in tendon and ligament repair have involved engineering tissue using cell-seeded scaffolds. Self-aligned cellular structures, similar to those in ligaments and tendons, have been successfully formed, albeit with weak attachment between construct and bone. Calcium phosphates form an intimate bond with both soft and hard tissues and have successfully been used in tissue engineering bone, whilst hydrogels have often been used as cellular scaffolds.

This thesis explores agarose, gelatin, carrageenan and fibrin hydrogels as potential soft tissue scaffolds. Fibrin gel exhibited high cellular compatibility with highest metabolic activity on day 14. Although the cellular gel contracted significantly, it was found that the dry weight remained stable in both the acellular and cellular forms.

3D powder printed calcium phosphate scaffolds remained structurally stable after immersion in cell culture media with immersion in protein-rich sera promoting tenocyte attachment. Bracket designs were developed to enhance grip of the cell-seeded fibrin. Ligament constructs were self-supporting and exhibited structural characteristics similar to native connective tissue. Tenocyte density peaked on day 14, with added L-proline and ascorbic acid inducing a constant level of glycosaminoglycans and 7.4 ± 1.5 % w/w collagen. This research may significantly enhance the clinical application of tissue engineered ligaments and tendons.

ACKNOWLEDGEMENTS

My sincerest thanks go to my supervisor Dr. Liam Grover for his helpful comments and guidance throughout my PhD. I extend special thanks to Dr. James Bowen for the scientific discussions, equipment training, motivational speeches and helping me to figure out solutions to seemingly impossible problems.

I would also like to express my gratitude to the help provided by staff at the Department For Functional Materials in Medicine and Dentistry in Würzburg, Germany, in particular Dr. Uwe Gbureck, Dr. Andrea Ewald, Elke Vorndran and Isabell Biermann.

I extend a huge thank you to the Grover group for their support over the years and offering a helping hand when needed, especially Dr. Paxton. I would also like to thank all the staff at the Biochemical Engineering building, including Hazel Jennings and Elaine Mitchell and members of other departments for helpful discussions and encouragement.

I would also like to acknowledge the Biotechnology and Biological Sciences Research Council for their financial support and Advanced Materials (AM2), funded by Advantage West Midlands (AWM) and part funded by the European Regional Development Fund (ERDF), for use of their equipment.

Finally, I am eternally grateful for the love, patience and motivation provided by my parents, Nasreen and Mohammed Mehrban, brothers, Kamran, Adnan and Imran and friends, especially Doreen Ray, throughout my PhD. Your encouragement has played a big role in my achievements.

TABLE OF CONTENTS

LIST OF FIGURES

LIST OF TABLES

LIST OF EQUATIONS

LIST OF ABBREVIATIONS AND ACRONYMS

ABAM	Antibiotic-antimycotic
AFM	Atomic force microscopy
ANOVA	Analysis of variance
BSA	Bovine albumin
$CaCl_2$	Calcium chloride
CAD	Computer-aided design
Calcein-AM	Calcein- acetoxymethyl ester
CaP	Calcium phosphate
DMEM	Dulbecco's Modified Eagle's Medium
DMSO	Dimethyl sulphoxide
DNA	Deoxyribonucleic acid
ECM	Extracellular matrix
EDTA	Ethylenediaminetetraacetic acid
FBS	Foetal bovine serum
GJ	GraftJacket
H&E	Hematoxylin and eosin
HA	Hydroxyapatite

HAM	Nutrient mixture Ham's F-12K
HEPES	4-(2-hydroxyethyl)-1 piperazineethane-sulfonic acid
***κ*-carrageenan**	Kappa-carrageenan
KCl	Potassium chloride
MSC	Mesenchymal stem cells
MTT	3-(4,5-Dimethylthiazol-2-yl)-2,5-diphenyltetrazolium bromide
Pen-strep	Penicillin-streptomycin
PGA	Poly(glycolic acid)
PI	Propidium iodide
PLA	Poly(lactic acid)
PLGA	Poly(lactic-co-glycolic acid)
rhBMP-2	Recombinant human bone morphogenetic protein-2
S-DMEM	Supplemented Dulbecco's Modified Eagle's Medium
SEM	Scanning electron microscopy
S-HAM	Supplemented nutrient mixture Ham's F-12K
SIS	Small intestinal submucosa
SPSS	Statistical package for the social sciences
Std. Dev.	Standard deviation
TCP	Tricalcium phosphate
TEM	Transmission electron microscopy

USB	Universal serial bus
XRD	X-ray diffraction
α-TCP	alpha-tricalcium phosphate
β-TCP	beta-tricalcium phosphate
***ι*-carrageenan**	Iota-carrageenan

CHAPTER 1: INTRODUCTION

Tendon and ligament injuries are very common with 800,000 connective tissue injuries occurring every year in the USA (Butler *et al*. 2003). Some connective tissue problems are caused by disease, such as rheumatoid arthritis (Holmbeck *et al*. 1999), although most are caused by sport related injuries through overuse, leading to rupture or tear (Paoloni *et al*. 2011). Such injuries cause considerable pain and decreased movement at and around the site of the rupture (Louie *et al*. 1998). Native tendons and ligaments heal slowly due to their low mitotic activity and severe injuries can cause irreparable damage in which the orientation of the aligned fibril bundles making up tendons and ligaments is destroyed.

With so many injuries occurring each year and the low healing capacity of native connective tissue, surgical intervention is necessary. Some of the methods currently used to repair the damaged tissue include silastic sheets (Chen *et al*. 2008), fibrin glue (Patel *et al*. 2010), sutures and pins (Brown and Ahmad 2007) and grafts (Nutton *et al*. 1999). Methods to stitch, glue or pin the soft tissue back to either the muscle or bone regularly fail as the stress concentrations dissipated in four distinct zones in native tissue are not replicated in the repair (Sano *et al*. 2007). Such repair often requires further surgery and leads to an altered gait as the repair method leads to a considerably shorter tendon or ligament than is naturally present at the site (Bohnsack *et al*. 2000). Introduction of grafts to the injury site can also lead to problems related to donor site morbidity (Mastrokalos *et al*. 2005), inflammation (Dagher *et al*. 2009) and disease transmission

(Nutton *et al*. 1999) with lengthy operating times and sometimes the need for further surgery at the injury site. Often the problems with such repair methods eventually outweigh the benefits of temporary relief from the injury.

As a result of the problems associated with current repairs there is a great need for an alternative method of connective tissue repair. Tissue engineering may enable the production of a tissue replacement tailored to the wound site with no cytotoxic side effects and inflammation caused by disease transmission or graft rejection. As the tissue may be specifically tailored to the individual, the dimensions of the engineered tissue can be varied, reducing the risks of permanent gait disturbance. One approach to ligament regeneration uses knitted biodegradable polyester scaffolds to investigate the attachment of porcine bone marrow stromal cells (BMSCs) which showed that the knitting technique aided cellular growth and proliferation and may be used for the engineering of tendons and ligaments (Sahoo *et al*. 2007). Other research on tendon and ligament repair include using hybrid scaffolds such as chitosan-based hyaluronan as demonstrated by Majima *et al*. (2007) who found that their hybrid scaffold showed good cellular compatibility. By aiding cellular migration, attachment and proliferation, both researchers have shown a reduced risk of an inflammatory response *in vivo*, using sterile synthetic materials to further avoid the transmission of diseases.

Recent advances in the repair of damaged tendons and ligaments have involved the use of biological scaffolds, such as small-intestinal submucosa, impregnated with native cells (Badylak *et al*. 1995 and Dejardin *et al*. 2001). The matrix of a tendon can also be directly reconstructed using natural materials including collagen (Marenzana *et al*. 2006), silk fibres (Lu *et al*. 2005) and fibrin (Ahmed *et al*. 2000) as well as synthetic materials such as poly-L-lactic acid (Cooper

et al. 2006) and poly(lactic-co-glycolic acid) (Qin *et al*. 2005). However, the problem with most of the scaffolds is that they cannot withstand the mechanical stresses native tissues can (Sahoo *et al*. 2006).

Problems also lie in fully testing the *in vitro* models as the structural weakness of the gels means that they are prone to premature tearing when attempting to conduct mechanical tests (Ikema *et al*. 2007). Mechanical testing is particularly important as *in vivo* these tissues are responsible for dissipation of stresses in joints and therefore contain high levels of collagen to maintain flexibility. Some researchers have attempted to overcome this issue by providing cyclic mechanical stimulation as the tissue matures to induce higher metabolic activity in cell (Juncosa-Melvin *et al*. 2007 and Chokalingam *et al*. 2009), thereby increasing the amount of ECM produced and creating a more robust network. Specific reasons for the early tear in developed constructs include gripping problems. The metallic mechanical grips often introduce stress concentrations at the interface with soft tissues creating weaknesses in the structure. This causes the tissue to tear at the end region and not the middle as is desired for a true interpretation of material strength.

This thesis aims to address some of these drawbacks by engineering ligament-like tissue between calcium phosphate based anchor points. After a description of tendon and ligament background and a comparison of existing research in the field, several scaffolds are described for use as tissue engineering scaffolds. An initial exploration of the suitability of selected polymeric gels for tissue engineering has been made followed by a comparison of three hydrogels and their use in creating a ligamentous construct. A discussion of the suitability of fibrin as a soft tissue scaffold has been provided alongside an assessment of CaP as a bone scaffold for the enthesis region of the

construct. Finally the use of powder printing technology has been explored and utilised to rapidly and accurately produce large batches of bespoke calcium phosphate based brackets to maximise the gripping of the soft gel without causing tear at the ends of the scaffold. Combination of the two tissue types has been explored to develop bespoke ligaments. The capabilities of the constructs have been explored in comparison to native tendons and ligaments with particular focus on cell compatibility and matrix production.

CHAPTER 2: TENDON AND LIGAMENT ENGINEERING: INJURIES, REPAIR AND LIMITATIONS

Tendons and ligaments are vital in guiding joint movement and their damage results in the impairment of mobility and a significant reduction in the quality of life. This chapter provides a background of the structure and function of tendinous and ligamentous connective tissue as well as a comparison of tendon and ligament injuries. Current methods of injury repair are discussed and their limitations highlighted leading to an introduction to tissue engineering, focussing particularly on the recreation of the enthesis region.

2.1 Structure and function of tendinous and ligamentous connective tissue

2.1.1 Tendons and ligaments

Tendons and ligaments are fibrous connective tissue. Tendons connect muscle to bone and ligaments connect bone to bone. Both tissues are similar in that they function primarily in tension and induce or guide joint movement (Doroski *et al*. 2007). Tendons are made up of approximately 70% H_2O (Ker 2007). Of all the tendons in the human body, the Achilles tendon

is the largest. The Achilles tendon connects the calcaneus to the calf muscle as shown in Figure 2.1 (Rufai *et al*. 1995).

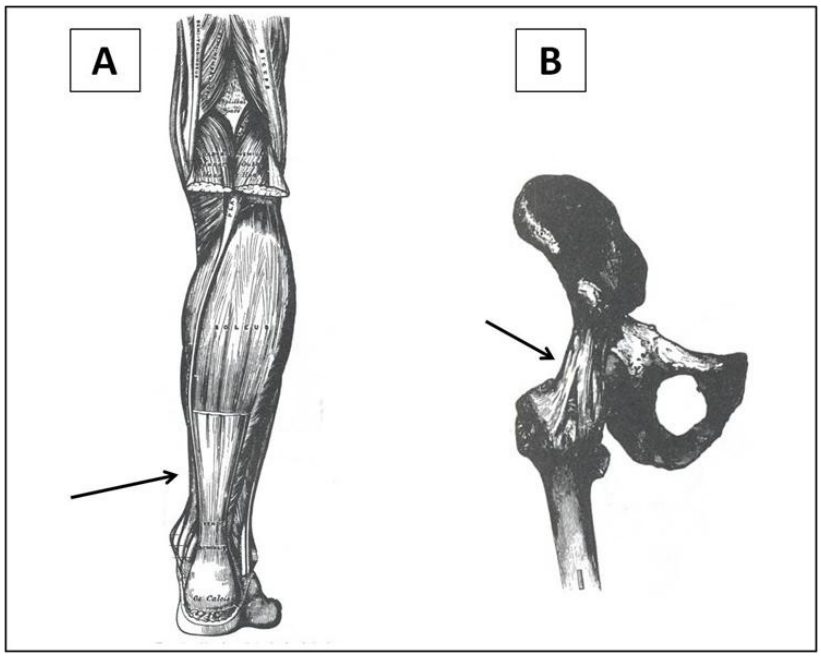

Figure 2.1 An illustration of the Achilles tendon, A and the iliofemoral ligament, B (images reproduced from Pick and Howden 1974).

Similarly, the iliofemoral ligament, also known as the Y-ligament or the ligament of Bigelow, is one of the strongest in the body (able to withstand a tensile force of 350N) (Schuenke *et al*. 2006) and is part of a group of ligaments responsible for movements of the hip joint.

2.1.2 Structure of tendons and ligaments

Tendons and ligaments have been proposed to be the most simple form of connective tissue. However, recent work has shown that the structure is more complex than previously thought and the tissue is composed of highly specialised mesenchyme-derived cells embedded in a three-dimensional network of extracellular matrix (ECM) (Fini *et al*. 2007). Structurally, tendons and ligaments are very similar. The Kastelic *et al*. (1978) model of the hierarchical structure of tendons may be used to describe the make-up of tendons (Figure 2.2). No set nomenclature exists for tendons and this figure is only a guide as natural variation occurs in all native tendons (Kannus 2000). The fibroblasts in native tendon connective tissue attach end to end and side to side to form the fibrils which are assembled parallel to one another forming fibrils which have a woven appearance. Parallel fibrils form collagen fibres, which are the smallest structural components that are visible using light microscopy (Kannus 2000). The stability and strength of collagen is maintained by covalent crosslinks between the fibres. Formation of macroaggregrate bundles occurs through the development of these crosslinks between the collagen fibres. Research conducted by Doroski *et al*. (2007) suggests that these crosslinks are more abundant in younger collagen suggesting that older collagen is therefore less stable.

The endotendon sheath is responsible for enveloping the collection of fibres to form the individual bundles whilst the peri-tendons and epi-tendons bind the bundles together to form the macroscopic tendon structure.

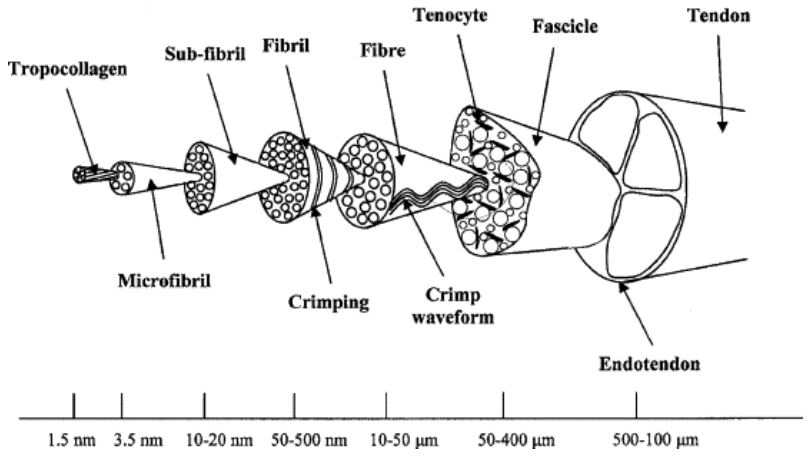

Figure 2.2 The hierarchical structure of a typical tendon (Image reproduced from Screen *et al.* 2004).

The densely packed collagen fibrils are naturally 'crimped', a term used to describe the sinusoidal wave-like structure of the collagen fascicles (Doroski *et al*. 2007). The crimp disappears when the tendon is strained (Calve *et al*. 2004) and appears as alternate light and dark bands at low magnifications under polarised light (Cribb and Scott 1995). Screen *et al*. (2004) and Ker *et al*. (2007) have suggested that the crimp is partly responsible for the tendon's flexibility and has shock-absorbing capabilities. Kannus (2000) stated that the crimp varies in angle and regularity suggesting that certain parts of the tendon structure may be weaker than others.

The collagen molecules within the fibrils are distributed in a 'quarter-stagger' arrangement (Figure 2.3) with fibres being bound together by the previously described crosslinks, giving the overall tendon stability and strength (Dee *et al*. 2002).

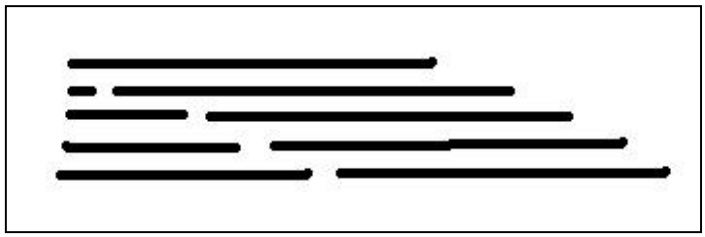

Figure 2.3 Quarter-stagger arrangement of collagen molecules within fibrils.

Ker *et al*. (2007) used the term 'multi-stranded wire' to describe the overall structure and flexibility of the tendon. This flexibility, supported by the loose binding nature between the fibrous units, is necessary for the tendon to be able to withstand great stresses in tension whilst retaining full movement.

To ensure that their movement over bone is smooth, tendons are able to move through canals and sheaths. Synovial fluid contained within these sheaths improves lubrication (Lin *et al*. 2004). Furthermore, ligaments have a high concentration of elastin between each layer to facilitate flexibility, change of movement or direction (Houglum 2010). Blood supply to tendons and ligaments is limited by poor vascularisation. In tendons blood is supplied from the muscles to which they are attached whereas ligaments are supplied by a network of vessels in the synovial membrane of joints they pass over (Petersen and Tillmann 1999).

2.1.3 Fibril length

Whilst fibril orientation and their role in tendon and ligament connective tissue integrity is clear, the length of individual fibrils is a much debated issue. The diameter of fibrils is well known (50-500 nm, Hiltner *et al*. 1985), as is the fact that ligament fibril diameter is considerably smaller than that of tendons (50-300 µm), but there appears to be no definite length recorded. Provenzano and Vanderby (2006) were unable to determine the length of a tendon whilst investigating rat bovine and feline tendon fibril ends. In an earlier study by Trotter and Wofsy (1989) transmission electron microscopy (TEM) was used to examine 5639 fibrils. Although 2 fibril ends were found in that instance, the low number meant that statistically the results were insignificant.

The lack of data available in this area could mean that it is possible that the fibril length exceeds the overall tendon length. Although some researchers have supported this theory (Graham *et al*. 2000 and Holmes *et al*. 1998) others such as Caprise *et al*. (2001) and Robinson *et al*. (2004) have suggested that fibril length may actually be short and discontinuous. Birk *et al*. (1997) reports that the length of fibrils varies depending on how mature they are, regardless of whether they are continuous or discontinuous. They predicted that the mean fibril length was 60 µm and that variation in length usually occurred after 18 days when fibrils started to mature and therefore fuse together. Length of fibrils may also be affected by fibril bifurcations and fusions, where regions of fibrils are not well aligned (Provenzano and Vanderby 2006). Caprise *et al*. (2001) also proposed the 'sliding fibril' theory. It was stated that fibrils were connected by reversible interfibrillar bonds or a stress transfer matrix whereby fibrils are able to slide past one another and bond again at a different site without structurally damaging the tendon itself. This theory does account for changes in fibril length at different stages of maturation as proposed by Birk *et*

al. (1998) although Screen *et al*. (2005) disagreed noting that a change in fibril length through sliding inevitably affects the overall tendon length and therefore the structure.

2.1.4 Fibroblasts and tenocytes

Whilst fibril length is debatable, cellular composition of tendons and ligaments is not. Throughout literature on ligamentous and tendinous connective tissue, fibroblasts and tenocytes have both been used interchangeably to mean the same cell type. Fibroblasts are the most abundant type of cells found in fibrous connective tissue, usually organised in columns between fibrils (Provenzano and Vanderby 2006). There appears to be little histological difference between fibroblasts and tenocytes (Lie *et al*. 2006). Although Kannus (2000) noted that tenocytes are elongated fibroblasts which lie between the collagen fibres it is generally accepted that fibroblasts cut in different planes can vary in shapes and may appear triangular, rectangular and trapezoidal (Amiel *et al*. 1984). Similarly Okuda *et al*. (1987) researched the structure of tenocytes and showed that they are narrow and tapered in shape, although it was ascertained that in terms of function, biomechanical, biochemical and nutritional factors strongly influence the tenocyte's capability to adapt to the environment. Fu *et al*. (2007) also showed that the function of these cells changes at different stages of tendon healing, haemorrhage, inflammation, proliferation and maturation and it has been reported that isolation of tenocytes from tendons can cause defects in the tendon (Liu *et al*. 2006). Furthermore, it has been shown that certain cells, such as mesenchymal stem cells (MSCs), can be stimulated through mechanical stress to differentiate into other cell types, including fibroblasts (Doroski *et al*. 2007).

2.1.5 Extracellular matrix (ECM)

The primary function of fibroblasts, or tenocytes, found along the collagen fibres is excretion of the extracellular matrix (ECM), which makes up 20% of tendons and ligaments (Doroski *et al*. 2007). The ECM has many functions, some of which have been listed by Pecheva *et al*. (2007) including acting as a scaffold, directing cellular movement and regulating cell differentiation and growth. The ECM is made up of H_2O, cells, collagen, ground substance, such as proteoglycans, glycoproteins and plasma proteins, and elastin (Dahlgren *et al*. 2007).

In the creation of the KK-Periome transcriptome database, Nushida *et al*. (2007) found that 13 of the 617 expressed sequence clusters assembled were related to the ECM protein genes. The study expresses the complexity of ECM which provides a highly tuned environment for the complex functions to occur (Pedersen and Swartz 2005).

Okuda *et al*. (1987) found that compressive loading and continuous stress can affect the matrix composition and therefore its overall function whilst Provenzano and Vanderby (2006) noted that the stresses in ECM can increase by up to three times as an animal matures. Furthermore, increased mechanical stress at the myotendinous junction, the junction where the tendon attaches to muscle, leads to an increased production of proteins, minimising structural damage (Larkin *et al*. 2006). Therefore, assessment and maintenance of the ECM in engineered tendons is vital.

2.1.6 Collagen and proteoglycans

Yoon and Halper (2005) assign the main components of ECM into three main categories, collagen, proteoglycans and glycoproteins.

Although there are over 20 different types of collagens (Carpenter and Hankenson 2004) Collagen I and III are the most abundant proteins in ECM, over 90% of the ECM in tendons and ligaments being Collagen type I with ligaments also having a higher concentration of Collagen type III, approximately 10% in ligaments in comparison to 1-5% in tendons. Collagen is responsible for supporting cellular attachment, migration, proliferation, differentiation and survival which accounts for the strength of fibrous connective tissue (Zhai and Cui 2006 and Yoon and Harper 2005). A decrease in the amount of collagen in tendon and ligaments can have a substantial effect on tissue function. A defect in the collagen production in ligaments can cause joint hypermobility syndrome, where an individual is referred to as being 'double-jointed' with the joint movement not being restrained (Everman and Robin 1998).

Proteoglycans make up less than 1% of the dry weight of most tendons (Vogel 2004). Proteoglycans as a whole have varied functions and are responsible for viscoelastic and other mechanical properties of ligamentous connective tissue. Fini *et al*. (2007) further explain that proteoglycans are responsible for overall structural integrity, helping to guide individual fibril maturation, maintaining hydration and facilitating slippage between adjacent and intertwined fibrils during loading. This is further supported by research conducted by Yoon and Halper (2005) who showed that in fact two separate groups of proteoglycans exist, small leucine-rich and large modular lecticans, and exercise or tension based changes in those groups are responsible for

the structural integrity and mechanical function of tendons. Therefore, the changes are caused by a variation in mechanical loads. Furthermore, the importance of proteoglycan regulation was highlighted by Vogel (2004) who showed that in the absence of decorin alone, collagen fibrils become thick. In supporting research conducted by Mendias *et al*. (2007) it was found that inhibition of myostatin receptors caused the tendons of mice to also become brittle and stiff. The structure and binding of proteoglycans can vary along the length of the same tendon (Screen *et al*. 2005) and are strongly influenced by changes in age (Cribb and Scott 1995).

Proteoglycans are also responsible for type I collagen production and it is shown that increased exercise leads to high amounts of collagen I forming with decreased maturation of the tendon due to a stimulation of cytokines and growth factors, such as insulin-like growth factor (IGF-1) and interleukin-6 (Olesen *et al*. 2007). However, new members of the proteoglycan family are constantly being discovered and the most often quoted decorin, biglycan, fibromodulin and lumican, are not the only proteoglycans found in tendons.

2.1.7 Enthesis

The junction where bone and tendons or ligaments interface with bone is known as the enthesis or the osteotendinous junction (Sharma and Maffulli 2005). Ligaments partially cover the bone to which they are attached creating a capsular sac or joint capsule (Stine and Vangsness Jr. 2009) via the periosteum, a fibrous membrane covering bone. Although the enthesis varies in shape and size from location to location, not all tendons have an enthesis and attachment can occur via Sharpey's fibres (Doschak and Zernicke 2005; Benjamin *et al*. 2006). The entheses balance

varying elastic moduli of tendon and skeletal tissue and involves the gradual calcification of fibrocartilage (Hashimoto *et al*. 2007) existing in two forms, fibrous, direct attachment usually located near joints, and fibrocartilaginous, indirect attachment usually located near the diaphysis (Benjamin *et al*. 2002 and Paulson *et al*. 2000).

Hashimoto *et al*. (2007) outlined four histologically distinct zones of the fibrocartilaginous form; tendon (the aforementioned aligned collagen and elastic fibres mainly composed of fibroblasts), unmineralised fibrocartilage (150-400µm in width, consisting of rounded chondrocytes visible in pairs or rows within lacunae), calcified fibrocartilage (an abrupt change seen between the second and third zones approximately 100-300 µm in width with the separation often seen as a blue basophilic line) and bone (Cooper and Misol 1970). Collagen fibre orientation varies depending on direct or indirect insertion. Research conducted by Moffat *et al*. (2008) shows that variation in collagen fibre orientation, and mineral content through the four regions of indirect insertion accounts for the change in mechanical strength along the enthesis. Thus failure caused by trauma rarely occurs at the enthesis and usually occurs at the bone end or soft tissue end. In their research Moffat *et al*. (2008) attempted to regenerate the enthesis by injecting the recombinant human bone morphogenetic protein-2 (rhBMP-2) into rabbit tendon. Although enthesis-like tissue formed after four weeks, the junction remained relatively weak. Cellular interaction with bone, as outlined by Pecheva *et al*. (2007), strongly depends on wettability, surface chemistry, surface charge and roughness, although research by Claudepierre and Voisin (2005) also shows that the presence of Sharpey's fibres add additional anchorage by directly inserting into the bone.

The development of the enthesis begins with the endochondral ossification of hyaline cartilage forming bony trabeculae whilst at the same time tendon and ligament cells undergo metaplasia

and form a fibrocartilage layer of cartilage cells (Caludepierre and Voisin 2005). This would suggest that inducing the metaplasia stage and erosion of the hyaline cartilage can lead to control of fibrocartilage development. It has also previously been shown that the presence of type I and type II collagen fibres indicate the presence of fibrocartilage within a tendon structure (Hashimoto *et al*. 2007).

Earlier research by Rufai *et al*. (1995) showed that the four zones were rarely separated and defects in the four zones may occur in the form of bone spurs, longitudinal fissures and transverse tears. Bone spurs, exostoses, involve extension of the bone into the tendon. Fissures and tears occur where the fibrous ECM is poorly organised and the gaps left are sometimes filled with adipose cells or vascular connective tissue.

These defects and changes to native enthesis, known as enthesopathies, make it difficult to recreate the junction successfully with researchers often labelling enthesis grafts as incompatible (Claudepierre and Voisin 2005). Previous attempts by Gottsauner-Wolf *et al*. (1994) and Pendegrass *et al*. (2004) to attach tendons to prostheses by anchoring sutures, plates with/ without spikes, porous metallic surfaces and porous coatings have been unsuccessful. Weak attachment often leads to other complications such as tendon shortening, detachment and a permanently altered gait.

It has also been noted (Lin *et al*. 2004) that tendons themselves can usually withstand considerably more strain than the muscle to which they are attached.

2.1.8 Hard tissue at the interfacial region

In discussing the enthesis and its role in native tissue, it is important to discuss the hard tissue, i.e. bone. In adult humans, bone may be described as trabecular (also known as spongy or cancelous), such as vertebral bone and cortical (also known as compact), such as the tibia or both, such as the femur (Wehrli 2007 and Wear 1999). The latter dense bone accounts for ~80% of the total adult skeleton dry weight (Weinstein and Buckwalter 2005) and usually covers the highly porous cancellous bone (Spiekermann *et al*. 1995). In terms of cells, native bone consists of a mixture of osteoblasts responsible for ECM production and mineralisation, osteoclasts responsible for the degeneration of the bone osteoid matrix and osteocytes are thought to be responsible for response to loading (Bilezikian *et al*. 2002).

The main function of bone is to structurally support the body by protecting the internal organs, guiding movement, withstanding heavy loads and storing minerals (Salgado *et al*. 2004) as well as blood production and pH regulation (Porter *et al*. 2009). Unlike tendons and ligaments, bone is a highly vascularised tissue with the ability to heal readily after most injuries (Sommerfeldt and Rubin 2001). Any large injuries or defects caused by trauma or disease, such as osteoarthritis (Ameye and Chee 2006) and osteoporosis (Parfitt *et al*. 1983), can dramatically affect an individual's quality of life by greatly reducing mobility.

2.2 Tendon and ligament related injuries

2.2.1 Fatigue/ Stress

Everyday activities mean that tendons and ligaments encounter load continuously as forces are transmitted from bone or muscle to the rest of the skeleton. Tendons or ligament can be loaded in compression, tension or shear, each type of loading causing a characteristic strain within the soft tissue. A typical stress-strain curve for tendons and ligaments can be seen in Figure 2.4.

Cribb and Scott (1995) identified three regions of the stress-strain curve for tendons and ligaments;

1. Toe-region where the dark and light bands of the crimp, visible on the fibrils start to disappear as tension increases.

2. Linear region where the tissue is still reversibly extendable.

3. Yield and failure region where too much tension causes permanent damage to the soft tissue.

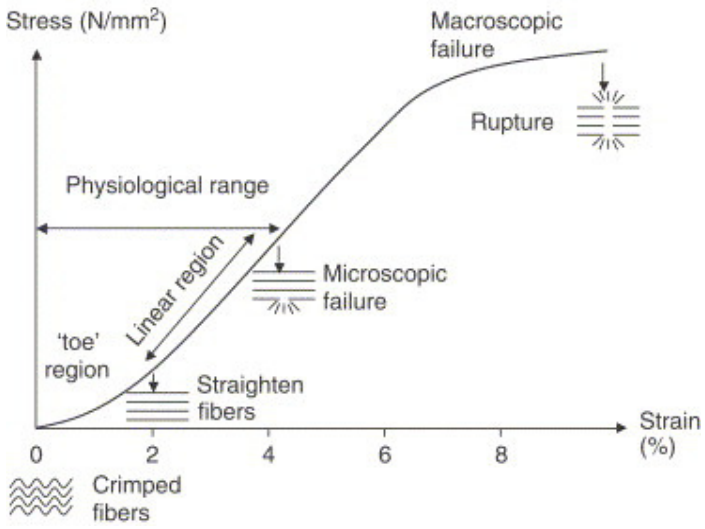

Figure 2.4 Stress-strain curve for tendons and ligaments (from Wang *et al*. 2006).

For the enthesis, at each zone a different material composition surrounds the collagen fibres and therefore the stiffness and modulus varies across the length of the transitional zone (Doschak and Zernicke 2005). A diagrammatic representation of these zones can be seen in Figure 2.5.

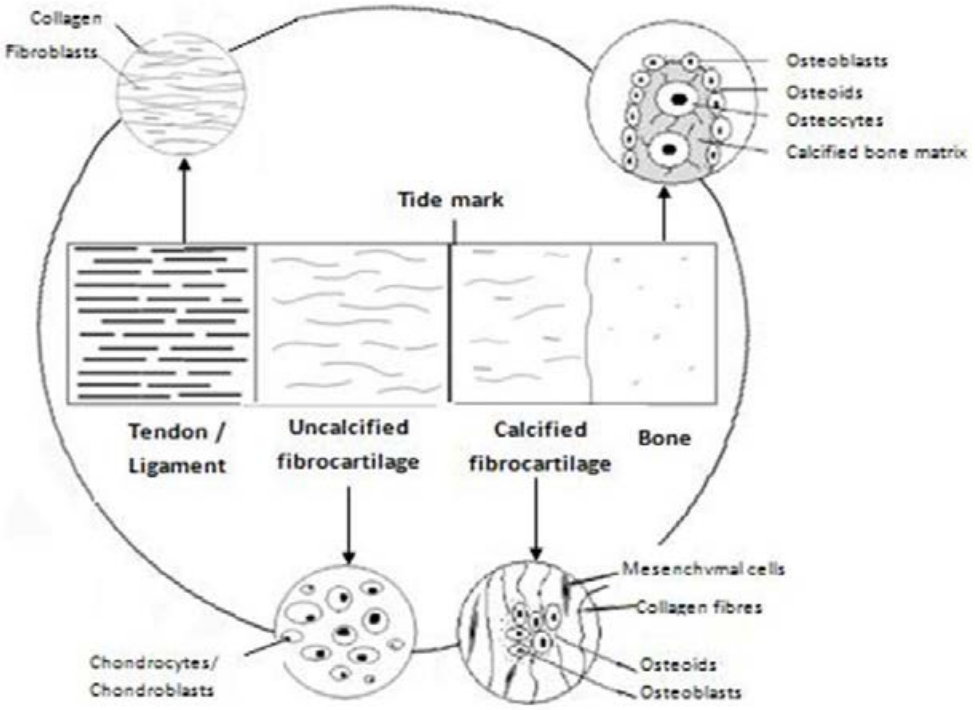

Figure 2.5 The four zones of tendinous and ligamentous entheses, soft tissue, uncalcified fibrocartilage, calcified fibrocartilage and bone.

Continuous stress with repeated loading is therefore shown to create permanent damage to a tendon or ligament, although the exact effect depends on the origin of the tissue and its maturity. Generally three modes of failure have been defined in tendons and ligaments. Noyes *et al*. (1974) showed that in ligament-bone attachment these failures occur in the ligament (frayed appearance), the bone (fracture) or the enthesis.

It is thought that by introducing cyclic strain, without causing permanent deformation, at an early stage in tendon and ligament engineering, thinning and fatigue damage is avoided (Ker *et al*. 2007), especially if the scaffold used to support the cells creates tissue of poor tensile strength. Researchers such as Liu *et al*. (2006) and Larkin *et al*. (2006) have shown that improving the tensile strength in a construct is beneficial. In a PGA scaffold seeded with fibroblasts, Liu *et al*. (2006) were able to show that the engineered tendons had 75% the tensile strength of native tendons after 26 weeks (31.0 ± 2.2 MPa).

2.2.2 Tendon and ligament related injuries

Tendons and ligaments are prone to injury due to the constant strain they are under. Tendinous connective tissue may be damaged by overuse (repetitive motion and stress) or lack of use (e.g. being bedridden), with most tendon and ligament related injuries occurring amongst athlete, particularly in the knee region for ligaments. According to Whitlock *et al*. (2007) over half of the 30 million musculoskeletal injuries reported in USA are related to soft tissue injuries. In the UK, Rufai *et al*. (1995) reported that problems related to the Achilles tendon alone included Haglund's deformity (a bony enlargement at the back of the heel often called 'pump bumps'), ectopic calcification of the tendon, calcaneal spurs and retrocalcaneal bursitis, inflammation at the back of the heel (Stephens 1994). These problems and conditions such as tendinitis, where the repetitive movement causes the tendon to stiffen and then tear, can cause extreme pain, swelling and decrease the functionality of the joint (Hoffmann and Gross 2006).

2.3 Native repair and engineering tissue

2.3.1 Native healing of tendinous and ligamentous connective tissue

Native tendons and ligaments have poor regenerative capabilities due to low mitotic activity and a low density of the cells, approximately 20% of the tissue volume (Calve *et al*. 2004). Healing occurs in stages (inflammation, proliferation and remodelling). Inflammation occurs immediately after injury. Proliferation accounts for an increase in cell number and more matrix which leads to the remodelling stage where the scar diminishes, collagen fibrils are aligned and crosslinks between the fibres form (Lin *et al*. 2004). All three phases can be seen in Figure 2.6.

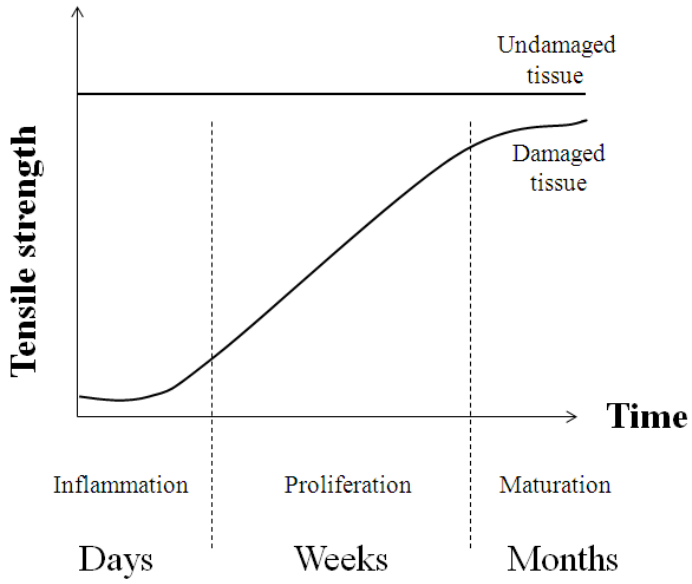

Figure 2.6 Tensile strength during the three phases of tendon healing (inflammation, proliferation and tissue maturation) in comparison to undamaged tissue.

Although the phases of tendon healing are discussed at length by many researchers, two opposing theories exist explaining the healing process, extrinsic and intrinsic. The extrinsic model states that tendons themselves have no healing ability of their own and it is the migration of external cells (such as fibroblasts) which accumulate at the wound site and begin the healing process. The intrinsic model states that healing occurs by the proliferation of epitenon and endotenon cells from within the tendon matrix (Lin *et al*. 2004). Both models have supporters and strong research exists for both sides of the argument. It may be that the complex healing process of tendons is perhaps a combination of both models. Whatever the actual process is, it is agreed that the structural, organisational and mechanical properties of naturally healed tendons are the cause of their weakness (Lin *et al*. 2004).

2.3.2 Current methods of repair and tissue engineering

With the previously mentioned 'attachment' methods for ligament and tendon tissue repair leading to further problems, there is a great need for an alternative method. Tissue engineering involves introducing a cell-seeded temporary scaffold to the injury site, specifically tailored to the wound, creating new functional tissue by stimulating the proliferation of cells and degrading at a predictable rate without causing inflammation. To minimise rejection, tissue engineering attempts to mimic the natural processes of the body. Methods currently used to enhance repair and regeneration of tendons and ligaments include cell therapy, growth factors, gene delivery systems and biological scaffolds (Calve *et al*. 2004; Hildebrand *et al*. 2004; Kuroda *et al*. 2010 and Chen *et al*. 2009). Orthopaedic devices have also been used as outlined earlier, as well as

grafts (autografts, allografts and xenografts), sutures and fibrin glue. A less invasive method of repair is prolotherapy, or proliferative injection therapy, which involves the injection of dextrose or natural glycerine to the site of injury stimulating the immune system and enhancing repair function at the site (Reeves and Hassenein 2003). Furthermore, prolotherapy stimulates cell proliferation where fibroblast growth would ordinarily be low. Although extensive research exists on tissue engineering, most methods have problems with restoring original joint biomechanics, due to poor integration into host tissue, and maintaining good healing at the site of injury (Doroski *et al*. 2007) as well as the added risk of disease transmission. Transplants are limited in terms of availability, lack of full movement recovery and tendency to degrade (Hairfield-Stein *et al*. 2007) ultimately leading to implant failure and requiring further surgery. Some treatments such as corticosteroid may even impair the healing process (Fini *et al*. 2007). Tendons and ligaments are ideal for tissue engineering as they are relatively avascular in nature, reducing the complexity of new tissue required. Ideally tissue engineering aims to not only restore functionality but also accelerate the natural healing process of tendons (Carpenter and Hankenson 2004).

2.3.3 Tissue engineering of scaffolds

Biodegradable matrices, scaffolds, are temporary supports used in tissue engineering. Cells similar to the injured tissue are seeded onto these constructs in order to enhance repair or to generate new tissue. In order to minimise cytotoxic side effects, it is necessary to ensure that scaffold composition and makeup are similar to the conditions found *in vivo*. Therefore, the

scaffold must be able to degrade at a rate which is predictable and commensurate with new tissue regeneration whilst ensuring the by-products do not encourage an inflammatory response. Other ideal qualities desired in scaffolds include;

- naturally derived to avoid an inflammatory response
- cytocompatible
- micro-architecture to encourage biological entities to develop native tissue
- sufficient biomechanical integrity
- allow cell proliferation

There are many different types of suitable scaffold materials available, both natural and synthetic, some of which will be discussed later in the thesis.

As an example of some commercially available scaffolds, Fini *et al*. (2007) tested two, the GraftJacket (GJ) and the SIS- small intestinal submucosa. The SIS scaffold is mainly based on collagen and growth factor β1 whilst the GJ is said to retain the major biological components of the dermis, including collagen (types I, III, IV and VII), elastin and proteoglycans. Both matrices mimic natural ECM histologically although in that particular study GJ was said to be more superior. Other commercially available scaffolds include Restore, TissueMend, CuffPatch and Permacol (Chen *et al*. 2009).

Huang *et al*. (2005) tested a naturally derived fibrin scaffold successfully promoting cellular migration and proliferation through the binding to growth factors whilst inducing proteolytic digestion of the scaffold. The variety of natural and commercially available scaffolds will be discussed in depth in Chapter 4.

As a general comparison of natural and synthetic scaffolds, it was noted that whilst some of the natural scaffolds lacked the tensile strength required for successful tissue engineering, synthetic scaffolds (including PGA) created antimitotic and cytotoxic by-products. In the research of Liao *et al*. (2007) polymer membranes were shown to directly degrade to acid which if accumulated could present inflammatory problems.

Earlier research by Tateishi *et al*. (2006) and Doroski *et al*. (2007) further stressed the need to recreate original tissue strength in restoring original functionality. Therefore, ideal scaffold qualities outlined by Tateishi *et al*. (2006) were primarily based upon cell adhesion, mechanical strength and high porosity to encourage cellular adhesion. Tateishi *et al*. (2006) also explored the use of PGA, PLA (polylactic acid) and PLGA (polylactic-co-glycolic-acid) as scaffolds. It was found that all three allowed easy control of the pore structure, easy control of degradation and exhibited good mechanical strength. However, the hydrophobic property of the scaffolds hindered successful cell seeding and it was suggested that a combination of natural and synthetic scaffolds may provide a better alternative by combining the wettability and consequently easier seeding of collagen matrices with the strength exhibited by PLA/PGA matrices.

Furthermore, Lin *et al*. (2004) noted that motion and tension following tissue repair improves tendon tensile properties. Therefore, scaffolds alone may not be able to account for good

mechanical strength and although attempts have been made to create ideal scaffolds, Liu and Cao (2007) noted that all scaffolds behave differently *in vivo* to *in vitro*, between different mammals and different locations on the same animal. They also disagreed with previous researchers, suggesting that an inflammatory response was necessary to ensure fibrotic adhesion did not take place. Some researchers have suggested that the role of the highly complex ECM in developing mechanical strengths is highly significant. However, as noted by Pedersen and Swartz (2005), the complexity of the ECM means that *in vitro* studies could not possibly hope to mimic all the functions controlled and regulated by the ECM.

2.3.4 Bone repair and tissue engineering

As previously mentioned, tendon and ligament failure can sometimes occur at the bone end. Current methods of bone repair, after injury when natural healing is insufficient, include autografts, allografts, xenografts, prostheses, and whilst they may provide some support, almost all the repair methods have some problems, such as disease transmission (Sogal and Tofe 1999), tissue availability limitations (Fröhlich *et al*. 2008), lengthy operating procedures (Gabl *et al*. 1999), infections (Matsuno *et al*. 2006), poor integration with native tissue (Becktor *et al*. 2008) and rejection of tissue (Seitz *et al*. 2005), associated with them.

For all its diverse functions, it is necessary to ensure any form of repair on bone attempts to mimic native hard tissue as closely as possible and therefore restore functionality as soon as possible. When this cannot be satisfactorily achieved alternative means of repair are sought. Tissue engineering offers injury specific repair with focus on integration to native tissue,

restoring the injured bone by using pluripotent cells such as MSCs (Mauney *et al*. 2005). As temporary supports several materials have been investigated for bone tissue engineering including collagen (Sachlos *et al*. 2003), chitosan (Zhang *et al*. 2003 and Baran *et al*. 2004), hyaluronic acid (Solchaga *et al*. 1999), poly(ε-caprolactone) (Washburn *et al*. 2002) and poly(carbonate) (Choueka *et al*. 1996).

Since 70% of the inorganic component of bone consists of CaPs, with the rest composed of glycoproteins, proteoglycans and bone sialoproteins, CaP compatibility with endogenous bone is high and this is an obvious choice of material for bone tissue engineering. Therefore CaP based cements, such as brushite, monetite and hydroxyapatite (HA) (Becker *et al*. 2004 and Prado Da Silva *et al*. 2001) have been widely used for tissue engineering bone by coating prostheses (Hayakawa *et al*. 2000 and Goyenvalle *et al*. 2003), cell delivery vehicles (Ginebra *et al*. 2006) and scaffolds (von Doernberg *et al*. 2006). HA is the most stable form of CaP but the lack of degradation presents a problem in trying to regenerate new tissue. Many researchers, such as So *et al*. (2006), have combined HA with a different material, such as glass, to increase its degradability. Brushite has a higher solubility rate than HA and is easily resorbable (Gbureck *et al*. 2005). This makes the mineral ideal for use as the junction between soft and hard tissue. It has often been used in orthopaedic, dental and maxillofacial applications (Tamimi *et al*. 2009) due to its nonantigenicity, mechanical stability and ability to directly bond with bone. Furthermore, the use of synthetic materials decreases operating times, donor site morbidity and allows each scaffold to be constructed specific to the patient's needs.

2.3.5 Tendon and ligament clamping

Whilst repair of fibrous connective tissue may involve focussing on tissue engineering, examination of connective tissue mechanical strength still presents a challenging task as the individual units comprising the tendon or ligament are difficult to clamp. Unbalanced stress caused by clamping result in serious distortions of the structure and premature failure. Ker *et al*. (2007) found freezing the ends to be clamped was effective, although if the tendon is thick, the technique is still not adequate. Freezing also introduces further stress at the point where the frozen section meets the unfrozen and general 'drying' of the ends means that the tendon becomes stiffer and thinner although a single tendon possesses unbalanced mechanical abilities and therefore stiffness in a native tendon varies along its entire length, with the tissue becoming stiffer nearer to the bone (Paxton and Baar 2007). This is further supported by Arruda *et al*. (2006) who showed that stress experienced near the muscle is 5 times greater than that experienced near the bone in tendons. This would suggest that the mechanical analysis of whole tendons would be different to small sections of tendon and by manipulating the ends for ease of testing, an accurate representation of the entire tendon or ligament is not acquired.

2.3.6 In vitro and in vivo testing

Furthermore, it has been noted that whilst research may be carried out *in vitro*, it usually serves as a precursor to more complex *in vivo* methods. *In vitro* experiments are usually cheaper with fewer ethical issues whilst *in vivo* experiments allow for a more clinically realistic model to be used with the conditions experienced in an animal model being more comparable to humans.

Some of the commonly used animals from which tissue is extracted for *in vitro* experiments include rats, mice, rabbits, dogs, monkeys and pigs.

Some of the research on tendon tissue regeneration includes the extraction of fibroblasts from the rat Achilles tendon and their successful growth in a self-assembled, aligned form between two anchor points (Calve *et al*. 2004). Although the diameter of the fibrils was very small and the overall structure only had the tensile strength of an embryonic chick tendon, no artificial scaffold was used.

In 2007 Fini *et al*. used tenocytes extracted from rat cuff tendons and cultured them on SIS and GJ matrices for a cellular compatibility comparison of native tissue on the synthetic scaffolds.

The tenocytes used for experiments in this thesis have been isolated from adult rat tail tendons and although only adult models were available, Ker (2007) found that only 2% of tenocytes extracted from adult rat tails were viable whilst 40% were found in 5 day old tail tendons. This research confirmed an earlier study of Calve *et al*. (2004) who found that as a tendon matures the number of fibroblasts decreases. This would suggest that the use of a younger rat tail tendon is more beneficial when compared to an older one in tissue engineering. Furthermore, some researchers believe the use of preserved or deep-frozen cells does not accurately reflect *in vivo* conditions as the preservation process alters the properties of the tenocytes (Maganaris and Paul 1999). For this purpose cells were isolated immediately after tissue dissection and cultured directly onto tissue culture plastic.

2.4 Aim

The aim of this study is to create a ligamentous construct using CaP, in the form of 3D printed brushite, as the bonding material to a hydrogel soft tissue scaffold. The most suitable soft tissue scaffold will display similar characteristics to the native tissue whilst hard tissue formation is required to be fast and reproducible.

CHAPTER 3: MATERIALS AND METHODS

3.1 Introduction

Chapter 3 outlines the methods used for the studies presented in this thesis. For each of the main equipment used for the research, a background is provided with technique limitations outlined where they relate or may specifically affect the acquisition of data for the thesis. The brief equipment introduction is followed by the specific technique used.

3.2 Gel preparation

3.2.1 Agarose

Agarose gel was prepared using 500 mg agarose powder (UltraPure, Invitrogen, Paisley, UK) in 50 mL distilled H_2O, heated on a hotplate (Heidolph magnetic hotplate stirrer, Heidolph Mr Hei-Standard, Scientific Laboratory Supplies, Nottingham, UK) to a temperature of 37°C. The powder was mixed thoroughly and the solution was left at room temperature until gelation occurred.

3.2.2 Gelatin

Gelatin was prepared using 1 g gelatin (Type B: From bovine skin powder, Sigma Aldrich, Poole, UK) in 50 mL H_2O, heated on a hotplate (Heidolph magnetic hotplate stirrer, Heidolph Mr Hei-Standard, Scientific Laboratory Supplies, Nottingham, UK) to a temperature of 70°C. The powder was mixed thoroughly and the solution was left at room temperature until gelation occurred.

3.2.3 κ-carrageenan and ι-carrageenan

Carrageenan was prepared using 500 mg *κ*-carrageenan (Commercial grade, Type I, Sigma Aldrich, Poole, UK) and *ι*-carrageenan powder (Commercial grade, Type II) and 125 mg KCl and NaCl powder in 50 mL H_2O, heated on a hotplate (Heidolph magnetic hotplate stirrer, Heidolph Mr Hei-Standard, Scientific Laboratory Supplies, Nottingham, UK) to a temperature of 60°C. *κ*-carrageenan gels were separately prepared substituting NaCl with KCl, S-DMEM and various concentrations of sucrose 0-5% w/v sucrose). The solutions were then left at room temperature until gelation occurred. For cellular samples hydrocolloids were autoclaved at 121°C for 15 min and maintained at 37°C before use.

3.2.4 Fibrin

Thrombin was prepared by adding 1 mg/mL BSA to F12K Ham media and adding 5 mL of the BSA-HAM mix to 1KU thrombin. After filtration 50 µL thrombin solution was added to 1 mL S-

HAM. 500 μL of the S-HAM-thrombin mix was added drop wise to 200 μL sterile fibrinogen (20 mg/mL to non-supplemented F-12K HAM media). The solution mix was incubated at 37°C for a minimum of 4 h for formation of clotted fibrin.

3.3 Assessing clotting and gelation times

A stopwatch was used to determine gelation times by visual inspection of the gels. The stopwatch was started after the solutions were fully homogenous with gelation determined by visual inspection. Times were recorded for gelation at 24°C (ambient temperature) and 37°C. For gelation experiments at 37°C the gels were lowered into a preheated water bath (JB1, Grant Instruments Ltd, Cambridge, UK). The stopwatch was started after the sample was fully homogenous and lowered into the water bath. Gels were given a maximum period of 3 h for gelation to occur after which 'no gelation' was recorded if the solutions remained liquid.

3.4 Mechanical testing

3.4.1 Gel compression

A series of 35 mm diameter cylindrical agarose, gelatin, κ-carrageenan and ι-carrageenan gels were formed in Iwaki 6-welled flat bottomed microplates (Scientific Laboratory Supplies, Nottingham, UK) at ambient conditions for each gel.

A TA.XT-Plus texture analyser (Stable Micro Systems, Surrey, UK) was used set at a strain of up to 20% and a test speed of 0.25 mm/sec to obtain deformation data for the gels. Stress-strain graphs for these values were created to show the relationship between the two.

3.4.2 Compression testing of CaP

The compressive strength of CaPs was determined by loading cylindrical samples of the cements in parallel to their long axes at a constant cross head speed of 1 mm/min using a Universal Testing Machine (Z030, Zwick, Leominster, UK) equipped with a 30 kN load cell. For the immersed samples, the cements were first incubated in the cell culture media at 37°C prior to testing. After failure the fragments were collected and dried in ambient conditions prior to further characterisation.

3.4.3 Assessing adhesive strength of gels using atomic force microscopy

Atomic force microscopy (AFM) is a type of scanning probe microscopy (SPM) involving a Si or Si_3N_4 cantilever, the tip of which, on the order of nm, probes the sample surface in a controlled manner through piezoelectric elements. As the cantilever approaches the sample surface, forces between the tip and the sample cause some degree of deflection in the cantilever, based on Hooke's law, whereby;

$$F = -kx \qquad (3.1)$$

Here x is the displacement of the spring end after application of force measured by a laser spot reflected back from the top of the cantilever, F is the force exerted by the material and k is the spring constant, also known as the stiffness of the cantilever.

The AFM is able to measure a number of forces including mechanical contact forces, capillary forces, electrostatic forces and van der Waals forces and may be operated in the contact (static) mode or the non-contact (vibrational) mode.

Acquisition of adhesion data for agarose, gelatin, κ-carrageenan, ι-carrageenan and fibrin was performed using a NanoWizard II AFM (JPK, Germany) employing a CellHesion module (JPK, Germany), operating in contact mode at 18˚C and 40 % relative humidity. A minimum of 5 measurements were performed, employing rectangular 130 µm length Si cantilevers with 6 µm nominal radius SiO_2 colloid probes at their apex (NovaScan, USA). Cantilever spring constants were on the order 25-30 N/m, as calibrated according to the method reported by Bowen *et al.* (2010). SiO_2 probes were chosen as a model for mammalian cells (which have an overall negative charge) to measure their interaction with the gel surfaces investigated.

3.5 General cell culture procedures

All cell culture procedures were conducted under sterile conditions in a laminar flow hood (BSB 3-S, Gelaire ICN Biomedicals, UK). The hood was cleaned with virkon disinfectant (Fisher Scientific, UK) and 70% v/v ethanol in water was used to sterile hands and all equipment needed. Cells were maintained in an incubator (MCO-15AC, Sanyo Electric Co. Ltd., UK) at 37°C, 5% CO_2 and 100% relative humidity with the media being changed every 3 days. Unless stated

otherwise, all cell culture chemicals were purchased from Sigma Aldrich, Poole, UK. Sterilisation of solutions was done by autoclaving at 121˚C for 20 min. All other sterilisation was performed by using 70% ethanol.

3.5.1 Fibroblasts

The NIH 3T3 murine fibroblast cell line was purchased from LGC (Middlesex, UK). Upon receipt, the cells were suspended in S-DMEM and incubated in cell culture flasks.

3.5.2 Tenocyte isolation

200g Wistar male rats were killed by a schedule 1 method (supplied dead by the Biomedical Science Unit, University of Birmingham, UK) and the tendons were teased out of their sheaths from the rat tails. After cutting the extracted tendons into small pieces, they were digested in 25 mL Collagenase type I (1 mg/ mL in PBS) and 15 mL trypsin (25 mg/mL) for 6 h at 37°C with continuous stirring. The enzymes were inactivated by the addition of 3 mL FBS. Tissue debris was filtered out using nylon gauze and the suspension was centrifuged at 1000 rpm for 3 min. The cell pellet formed was re-suspended in S-HAM and incubated.

3.5.3 Media preparation

3.5.3.1 3T3

3T3 cell growth media were prepared by supplementing high glucose Dulbecco's Modified Eagle's Medium (DMEM) with 10% v/v FBS (PAA, Somerset, UK), 1% v/v pen-strep, 2.5% v/v L-glutamine and 2.5% v/v 1M 4-(2-hydroxyethyl)-1 piperazineethane-sulfonic acid (HEPES buffer).

3.5.3.2 Tenocyte

Tenocyte growth media were prepared by supplementing HAM's nutrient mixture (HAM, F12) with 20% v/v FBS (PAA, Somerset, UK), 1 mM L-glutamine and 1% v/v ABAM.

3.5.4 Preparation of FBS for degradation studies

For acellular FBS studies, FBS was prepared by diluting FBS (PAA, Somerset, UK) with double distilled H_2O to the required concentration and adding 0.1% w/v sodium azide.

3.5.5 Freezing cells

Unused viable cells were suspended in supplemented media containing 10% v/v DMSO and stored at -80°C for a minimum of 48 h before storage in liquid N_2.

3.5.6 Thawing cells

Cells were thawed in a water bath at 37°C and immediately added to fresh supplemented media under sterile conditions. Care was taken to ensure thawed cells were added to fresh media quickly as the DMSO used in the freezing process to prevent crystal formation is toxic to cells in its liquid state. Thawed cells were incubated and re-fed the next day to remove cell debris.

3.5.7 Re-feeding cells

All incubated cells were re-fed every 3 days by removing old media from the flask, washing with copious amounts of PBS and replenishing with enough supplemented media to at least cover the cell surface.

3.5.8 Passaging

After cells reached ~70% confluency, they were detached from the wall of the cell culture flask using enough trypsin to cover the base of the flask. After 3 min of incubation, an equal amount of supplemented media to the trypsin was added and the cell slurry was transferred to a sterile centrifuge tube before spinning at 1000rpm for a further 3 min (MSE Mistral 2000, Global Medical Instrumentation Inc., UK). The supernatant was carefully removed and the cells re-suspended in 3 mL of supplemented media, split 1:3 and incubated.

3.6 Cell counting using Trypan blue exclusion method

Trypan blue is a diazo dye which cannot penetrate through intact semi-permeable cellular membranes. Ruptured cell membranes allow intrusion of dye which stains the dead cells deep blue whilst living cells are not stained.

Growth of cells was determined by counting the number of cells in 1 mL of 0.4 % w/v trypan blue in PBS stained cell suspension using an inverted microscope (Olympus BH-2, Global Medical Instrumentation Inc., UK) and a Neubauer haemocytometer of 0.1 mm depth (Hawksley, London, UK). The approximate number of viable cells present in the suspension were calculated in accordance with equations 3.2 and 3.3;

$$Cells\ per\ mL\ =\ \frac{number\ of\ viable\ cells\ counted}{number\ of\ grids\ counted\ \times\ 10^{4}\times\ dilution\ factor} \tag{3.2}$$

$$Total\ number\ of\ cells\ =\ cells\ per\ mL\ \times\ volume\ of\ original\ cell\ suspension \tag{3.3}$$

3.7 Cell seeding

3.7.1 Encapsulation in carrageenan

0.75 x 10^6 NIH 3T3 fibroblasts were encapsulated in 2% sterile carrageenan (w/v) solutions to form 3 mL gel discs (created in 12-well culture plates). To ensure cells were evenly distributed within the gel, the cell suspension was repeatedly pipetted in liquid gel. Gelled discs were incubated at 37°C for 3 h to ensure gelation. All discs were topped with 3 mL supplemented media and incubated. The media were changed every 3 days to ensure a fresh supply of nutrients reached the cells.

3.7.2 Cell-seeded fibrin

Fibrin gel was formed as previously stated in 12-well plates with 1 mL thrombin and 400 μL fibrinogen. Isolated tenocytes were counted using the trypan blue exclusion method and added to the surface of the clotted gel at a seeding density of 0.75 x 10^6.

3.7.3 Surface seeding on gels

2% sterile carrageenan (w/v) solutions were prepared to form 3 mL gelled discs in 12-well cell culture plates and incubated at 37°C for 3 h. The gelled discs were seeded with 0.75 x 10^6 NIH 3T3 fibroblasts and 3 mL supplemented media. Discs were incubated at 37°C and the media changed every 3 days.

3.7.4 Surface seeding on CaP discs

Printed and post-treated CaP discs were immersed overnight in autoclaved sterile PBS at room temperature to reduce acidity. The discs were then washed in 70% ethanol, dried in a laminar flow and sterilised under ultraviolet light overnight. Before use in cellular experiments, the sterile discs were immersed overnight in neat FBS. The discs were placed in 12-well plates and seeded with 0.75 x 10^6 isolated tenocytes topped with 3 mL S-HAM. Discs were incubated at 37°C and the media changed every 3 days.

3.8 Live/ dead staining

Calcein-AM and propidium iodide are popularly used to assess live and dead cells using fluorescent microscopy. Hydrophobic calcein-AM (with acetoxymethyl ester) does not fluoresce. However, once taken up by living cells it is hydrolysed into the green fluorescent hydrophilic anion calcein by intracellular cytoplasmic esterases. Calcein-AM is used because it has low toxicity and is not influenced by intracellular pH (Braut-Boucher *et al*. 1995).

Propidium iodide (PI) is also non-fluorescent until it interacts with DNA. However, as PI cannot penetrate through the plasma membrane of cells, it may only enter the cell and fluoresce through the disrupted cell membranes of dead cells. Upon interacting with DNA, the dye fluoresces red, indicating dead cells (Kaneshiro *et al*. 1993). Although staining cellular samples with calcein-AM and PI is quick and easy, problems include low initial fluorescence intensity and bleaching upon continuous exposure to light.

7 µL calcein-AM (50 µg/mL DMSO) was added to 1 mL of cell-seeded gel samples and supplemented media. The calcein and media were repeatedly pipetted to ensure homogenisation. The mixture was allowed to stand in the dark for 5 min before 25 µL PI (100 µg/mL water) was added and left for further 2 min in the dark. The stained samples were cut to approximately 1 mm thickness using a sterile scalpel and observed using a fluorescence microscope fitted with a mercury lamp (Carl Zeiss Ltd, Hertfordshire, UK) at magnifications of X10 and X20. Since PI and Calcein can both be excited at 490 nm, both dead and live cells can be viewed simultaneously. Live and dead cells were photographed using a Canon digital camera (Powershot G5, Canon UK Ltd., Surrey, UK) attached to the microscope (Carl Zeiss Ltd, Hertfordshire, UK).

3.9 MTT assay

The MTT (3-(4,5-Dimethylthiazol-2-yl)-2,5-diphenyltetrazolium bromide) assay is a colourimetric assay used to assess the metabolic activity of cells by the reduction of yellow MTT, a tetrazolium salt, to purple formazan. The tetrazolium ring is cleaved by dehydrogenase enzymes present in the active mitochondria of cells; therefore only viable cells are indicated. Endocytosis, cell receptor mediated uptake, is responsible for the uptake of MTT and exocytosis is responsible for the transport of formazan into the extracellular space (Molinari *et al*. 2005). The amount of formazan crystals formed is directly proportional to the number of living cells (WoldeMeskel 2005).

3.9.1 MTT assay in a cell culture flask

The metabolic rate of cells grown on cell culture plastic was assessed by adding 10% v/v MTT solution to the well. The MTT solution consisted of 10% w/v tetrazolium MTT in PBS. Calibration plots were initially created to determine the incubation time needed to obtain the maximum dissolution of MTT using HCl-isopropanol (1 mL HCl in 24 mL isopropanol). After 4 h of MTT incubation, 3 mL HCl-isopropanol was added to the well and incubated at 37°C for a further 45 min. Absorbance was measured on a daily basis, in triplicate, at 620 nm (Glomax multi detection system, Promega, UK). Absorbance measurements obtained from the MTT assay were used to calculate the number of metabolising cells present in each daily sample.

3.9.2 MTT of cells encapsulated and surface-seeded on gels

The proliferation of encapsulated and surface-seeded cells was evaluated by adding 200µL MTT (10% tetrazolium MTT in phosphate buffer solution) to a 2 mL gelled disc. Calibration plots were again created to determine the amount of MTT needed per gelled disc and the incubation time needed to obtain the maximum dissolution of MTT using HCl-isopropanol. After 18 h incubation at 37°C, 3 mL HCl-isopropanol was added to the well and incubated further at 37°C for 45 min. Absorbance readings were taken in triplicate, at 620 nm (Glomax multi detection system, Promega, UK) and used to calculate the number of metabolising cells present in each sample.

3.9.3 MTT of cells grown on the surface of CaP

The proliferation of cells seeded on the surface of CaP discs was evaluated by adding 300µL MTT (10% tetrazolium MTT in phosphate buffer solution) to a printed disc. Calibration plots were created to determine the amount of MTT needed per disc and the incubation time needed to obtain the maximum dissolution of MTT using HCl-isopropanol. After 18 hs incubation at 37°C, 3 mL HCl-isopropanol was added to the well and incubated further at 37°C for 45 min. After repeated pipetting to ensure complete dissolution of formazan crystals, absorbance readings were taken in triplicate, at 620 nm (Glomax multi detection system, Promega, UK) and used to calculate the number of metabolising cells present in each sample.

3.10 Scanning electron microscopy

Electron microscopy is a visualisation method based on concentrating a beam of electrons onto the sample surface in a vacuum state. Electron microscopy is used in many forms, including transmission electron microscopy, scanning electron microscopy, reflection electron microscopy, scanning transmission electron microscopy and low voltage electron microscopy. Scanning electron microscopy was used for all materials imaged via electron microscopy in this thesis. As a sample surface is bombarded with electrons through a focussed electron beam, the energy of the beam is altered and converted to either heat, generation of secondary electrons with a lower energy, light or X-rays. SEM maps from which the SEM images are produced, consist of the depiction of the varying energies.

3.10.1 Biological samples

The cell-seeded samples were fixed using 2.5% v/v glutaraldehyde (in 0.1M PBS) for 1 h and dehydrated with graded ethanol 50%, 70%, 90% and 100% v/v ethanol for 30 min each. The samples were then placed in liquid CO_2 at 1070 psi and 31°C for 60 min. Finally, the specimens were Au coated by a sputtering method using 25 mA and 1.5 kV (Polaron SC7640 sputter coater, UK); the thickness of sputtered Au was between 10 and 12 nm. A JEOL JSM 6060 LV SEM (Oxford Instrument Inca, UK) was used at an operating voltage of 20 kV, a working distance of 10 mm and spot size 3 to obtain images.

3.10.2 Cements

To evaluate cement microstructure, the samples were first vacuum dried and sputter coated (Polaron SC7640 sputter coater, UK). The Au sputtered cement fracture (Polaron SC7640 sputter coater, UK) surfaces were examined using SEM (JEOL JSM 6060 LV, Oxford Instrument Inca, UK) at an accelerating voltage of 20kV, a working distance of 10 mm and a spot size of 3.

3.11 Assessment of degradation

3.11.1 Gels

Degradation of gels with and without encapsulated cells was conducted by measuring daily wet and dry weights. For the wet weights, samples were carefully blotted on paper towels before weighing. Dry weights were obtained by vacuum drying (Edwards model EF03 freeze dryer, High Vacuum Ltd., Crawley, UK). All measurements were taken in triplicate.

3.11.2 Cements

Acellular and cellular CaP discs were submerged and incubated for 28 days in 3 mL PBS, DMEM, S-DMEM, HAM and S-HAM and the media were changed three times weekly. The wet mass was taken in triplicate after blotting the discs on paper towel to remove surface moisture. Dry mass of the samples was taken in triplicate on days 0, 3, 7, 14, 21 and 28 after slow vacuum drying in a vacuum freeze-drier (Edwards model EF03 freeze dryer, High Vacuum Ltd., Crawley, UK) overnight.

3.12 Raman spectroscopy

Based on Rayleigh scattering, the analytical technique detects scattered photons from irradiated samples. Shifts in the excitation of chemical bonds within the sample cause light to be scattered at different wavelengths, which are characteristic of the chemical properties of that sample. These shifts may be bond data or different phases of the same materials. As the process is quick,

requires little or no sample preparation and is compatible with aqueous samples, the technique is very useful in looking at specimens in a biologically relevant environment. Other than the laser being concentrated for too long on a given area, fluorescence from the sample can interfere with the Raman spectra, although photo-bleaching and baseline corrections can partially eliminate this effect. The burning effect may also be reduced by scanning a larger area and reducing the laser intensity. Intensity of peaks in the final spectra allows quantitative as well as qualitative data to be obtained. The aforementioned intensities are proportional to the concentration of the compounds (Penel *et al*. 1999). Raman imaging is also a useful tool, where a predefined area for spectral data may be used to map an image with areas of high and low Raman intensity. This may be correlated to the spectra produced. Red areas signify areas of high Raman intensity and blue signifies areas of low intensity.

Composition of CaP powders, printed CaP discs, fibrinogen, thrombin and fibrin was evaluated using a Raman microscope (WiTec Confocal Raman, LOT Oriel, UK). Raman spectral data for the cement samples were collected using a Peltier element cooled CCD detector in backscattering geometry and a grating set at 300 g/mm. High resolution scans with a spectral resolution of 3 cm^{-1} were obtained. For excitation, a 785 nm solid state single frequency diode laser was used.

3.13 Assessment of water uptake ratio

Assessing water uptake is important in the assessment of materials composed mostly of liquid, such as hydrogels. Not only does the amount of fluid absorbed change the structure and dimensions of the material, the water uptake ratio is also a good indication of nutrient uptake

when such materials are used as scaffolds for tissue engineering purposes. The water uptake ratio is defined as the ratio of weight increase (Equation 3.4 as described by Zhao *et al*. 2008). Fibrin gels were made using 60% v/v thrombin. The gels were incubated at 37°C in distilled water and the weights were recorded in triplicate over 18 h (Scout Pro, Ohaus Corporation, UK). The water uptake ratio was calculated using the equation outlined earlier.

$$Weight\ increase = W_t - W_0 \tag{3.4}$$

Where;

W_t is the end weight

W_0 is the initial weight

3.14 Rheometry

Rheometry of gels involving oscillatory shear is the application of a small sinusoidal wave of strain at a given frequency (ω) on the surface of the polymeric system between two parallel metallic discs. However, the stress transmitted through the sample is dependent on the gel type. Viscoelastic gels can exhibit steady-state flow and will fracture/ tear under steady shear deformation when applied beyond the elastic limit of the gel (Ferry 1980).

The measurement of the different phase components occurs through the extraction of phase and amplitude difference between stress and strain waves. The storage modulus, i.e. the elastic component of the gel, is given the term *G'* (the ratio of in-phase stress divided by strain) with the loss modulus (90° out-of-phase stress to strain) given the term *G"*. For a Hookean material *G'* is independent of the frequency of oscillation and therefore a constant. For a Newtonian liquid the stress and strain rate is linearly proportional, i.e. the viscosity is independent of the shear rate.

3.14.1 Gelation kinetics

The effect of thrombin concentration (5-40 U/mL) on the gelation kinetics of fibrin gel was measured using an AR-G2 rheometer (TA Instruments, UK) operating a 40 mm diameter sand-blasted stainless steel parallel plate geometry at 37°C. 600 μL of fibrinogen was first added to the bottom plate with the concentration of thrombin to be assessed, made up separately in 1.5 mL aliquots and added drop wise to the fibrinogen. After mixing the two solutions with a pipette tip, the rheometer was immediately started, at a plate separation distance of 1 mm. The upper plate was oscillated at a frequency of 1 Hz and a strain of 0.05 for 3 h with the storage and loss moduli being recorded throughout.

3.14.2 Assessment of a frequency dependent response

Upon formation of fibrin gel directly between the rheometer plates, as described in 3.2.4, at the thrombin concentration used for cellular experiments (20 U/mL) the storage and loss moduli were assessed over a range of oscillation frequencies up to 100 rad/s employing a strain of 0.05.

3.15 Fibrin contraction

Contraction of cell-seeded fibrin was assessed using optical microscopy methods. Fibrin gels for this assessment were produced in 5 cm diameter petri dishes. The petri dishes were first lined with 5 mL Sylgard (Type 184 silicone elastomer, Dow Corning Corporation, Midland, MI, USA) and left to cure for 1 week. After the Sylgard had set, 1 cm x 1 cm squares were cut and the petri dishes sterilised using 70% v/v ethanol and overnight ultraviolet sterilisation in a laminar flow hood. The square was then filled with 600 mL fibrinogen (20 mg/mL HAM) and 1.5 mL thrombin (200 U/mL S-HAM). After agitation, the gel was incubated and allowed to clot at 37°C for 4h. 0.75 x 10^6 tenocytes were seeded onto the surface of each gel square and re-incubated for a further 3h. The cell-seeded samples were topped with 6 mL S-HAM. Images of fibrin contraction were captured using a universal serial bus (USB) digital microscope (GX Optical, UK).

3.16 Cement preparation

3.16.1 3D powder printing

Tricalcium phosphate (TCP) was synthesised by heating an equimolar mixture of diCalcium phosphate anhydrous (DCPA, $CaHPO_4$, monetite) (Merck, Darmstadt, Germany) and calcium carbonate ($CaCO_3$, calcite) (Merck, Darmstadt, Germany) to a temperature of 1400°C for 14h followed by quenching at room temperature. The sintered cake was crushed with a pestle and mortar and passed through a 160 µm sieve. Milling was performed in a planetary ball mill (PM400, Retsch, Germany) at 200 rpm with 500 mL agate jars, four agate balls with a diameter of 30 mm and a load of 125 g TCP per jar for 30 min. Cement samples were printed with a multi-colour 3D-powder printing system (Spectrum ZS10, Z-Corporation, USA) using the TCP powder and a binder solution of 20% phosphoric acid (Merck, Darmstadt, Germany) with a layer thickness of 125 µm, a binder/ volume ratio of 0.371 and an isotropic scaling x=y=z= 1.0. Structural geometries were designed using the Thinkdesign 2007 software (Think3, Munich, Germany) to produce cylinders of height 12 mm and diameter 6 mm, discs of height 3 mm and diameter 16 mm. The large brackets were printed at a height of 6 mm, 24 mm length, 16 mm diameter, a channel diameter of 3 mm and depth of 1 mm. Small brackets were produced with a height of 3 mm, length of 6 mm, diameter of 4 mm and channel diameter and depth of 1 mm. After printing, the loose powder on the samples was removed using compressed air and the exterior hardened by triplicate immersion in 20% phosphoric acid for 30 s.

3.16.2 Hand-moulded cements

Hand-moulded brushite cements were made by combining β-TCP (β-tricalcium phosphate) with phosphoric acid (3.5 M + 200 mM citric acid + 200 mM sodium pyrophosphate) at a powder to liquid ratio of 3.5 g/mL. The cement paste was cast into cylindrical PTFE moulds to give samples of height 12 mm and diameter 6 mm. Cement cylinders were left to set at 37°C overnight before being removed from the mould.

3.17 Interferometry

Interferometry is the measurement of surface topography for a given material. It is a non-contact optical profiling method which works by constructive and destructive interference of a split beam creating interferometric fringes which appear as the plane of the sample surface is brought into focus. There are many types of interferometers, such as the Michelson interferometer, the Fabry-Perot interferometer and the Fizeau interferometer based on visible light (to measure length of objects based on the wavelengths of light), radio waves (usually used in astronomy to map celestial sources of radio waves) or acoustic waves (to measure sound waves through gases and liquids).

The interferometer used for this study was based on the original Michelson interferometer and involves the recombination of a split beam from a single light source by using two mirrors, one fixed and the other moveable, creating the Interferometric fringes. A 3D map is created by moving through the focal planes of a sample surface, forming a series of images for the scanned area (Hariharan 2007).

Interferometric measurements of cement samples were performed using a MicroXAM2 interferometer (Omniscan, UK), operating using a white light source. Samples were imaged at 10X magnification, acquiring images in a 4x4 grid array, with 45% overlap, which were subsequently stitched together. The final image had dimensions of 2.28 mm x 1.69 mm. Scanning Probe Image Processor software (Image Metrology, Denmark) was employed for the analysis of acquired images, yielding S_a and S_q values for surface roughness.

3.18 X-ray diffraction

X-ray diffraction (XRD) is a non-destructive technique involving the scattering of X-rays through a crystal. The X-rays are picked up by a detector to determine the precise geometry of that crystal as it is rotated 180° around the X-ray source. The diffractometer works by bombarding a rotating sample with a focussed monochromatic X-ray beam. The pattern produced depends on the structural organisation of the sample. Therefore, for a crystalline material this pattern is regular but for a solid comprising of random arrangement, there is no distinctive pattern. The intensity of X-rays detected are plotted against the 2θ angle yielding a unique signature for a given material. The X-ray intensity peaks produced through constructive interference may be explained by Bragg's Law;

$$n\lambda = 2d\sin(\theta) \tag{3.5}$$

Where n is an integer, λ is the wavelength of X-rays, θ is the angle between incident beam and crystal surface and d is the distance between the atomic planes.

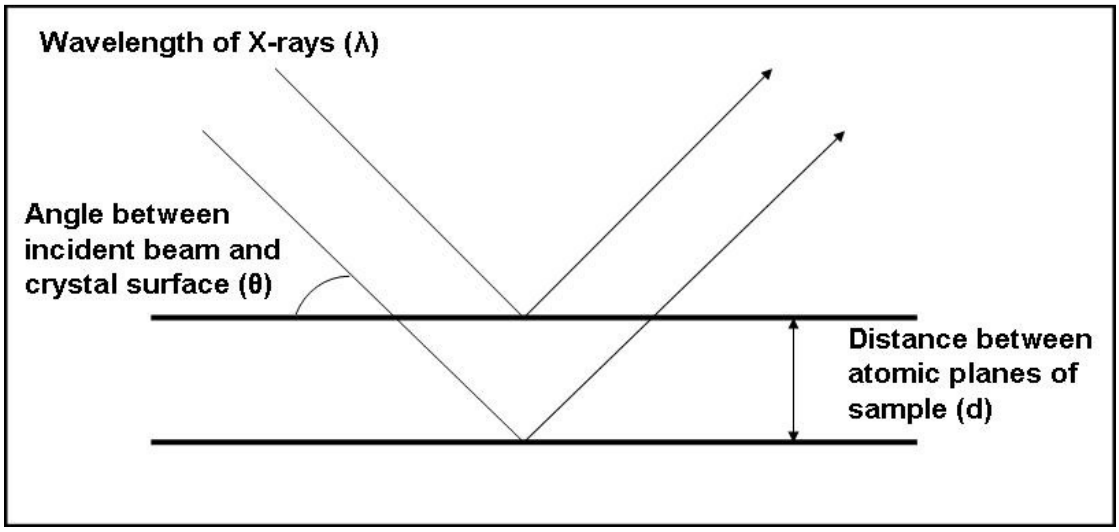

Figure 3.1 A diagrammatic representation of X-ray diffraction off two planes of a crystal lattice, based on Bragg's Law.

The crystalline compositions of the cement samples were determined using XRD. XRD patterns were recorded for printed and hand-moulded samples using an X-ray diffractometer equipped with an autosampler (D8, Bruker, Coventry, UK). Data were collected in the 2θ range 5° to 60° with a step size of 0.009° and a normalised count time of 1 s/step, using monochromatic $CuK_{\alpha 1}$ radiation from a Ge primary beam monochromator.

3.19 Helium pycnometry

Helium pycnometry is a non-destructive technique measuring the true density of a material. The technique is based on Archimedes' principle and measures true/ strut density through two chambers. There is an increase of pressure in the empty chamber as a central valve opens between the two sections. The resulting pressure changes in the sample chamber, previously calibrated to a known volume, are then measured from which the volume of the sample is calculated.

The true density of dried cement fragments was determined using a helium pycnometer (AccuPyc II 1340, Micromeritics, Dunstable, UK) with 10 purges prior to 10 measurements. Ten samples were measured for each condition, making the reported values an average of 100 measurements. The apparent density of the cement samples was calculated from geometrical measurements taken using a digital caliper (Mitutoyo, UK) and the mass of the specimens, dividing the mass of the sample by the volume. Relative porosity was then calculated using the values for apparent and true density, dividing the apparent density calculated by the true density measured and subtracting the calculated value from 1.

3.20 Mercury porosimetry

Porosimetry is the measurement of pore size distribution and relative porosity of a material. Pores within the sample structure are only intruded when the mercury is put under pressure (Abell *et al*. 1999). Mercury penetration into the small pores is governed by the Washburn equation:

$$D = -\left(\frac{1}{P}\right) 4\gamma\cos\theta \qquad (3.6)$$

Where D is pore diameter, P is the applied pressure, γ is the surface tension of mercury at 25˚C (generally accepted to be 0.485 N/m as it varies with mercury purity), and θ is the contact angle between the mercury and the porous solid. Whilst this equation is generally accepted as the relationship between pressure and pore size, the equation actually describes pores of a cylindrical nature and this is rarely the case in actual materials (Galarneau *et al*. 2008). This is a major limitation of the method.

A mercury porosimeter operates by filling a previously calibrated glass penetrometer chamber with mercury over an increasing pressure range. Data for pore volume is dependent on the stem size of the penetrometer as well as the chamber size since the intrusion of mercury at high pressures, i.e. mercury vacating the stem, allows the volume of mercury remaining to be determined. Therefore, the sample volume as a function of pressure is determined. As the pressure is increased, pores of smaller diameter are intruded with mercury.

To determine the pore size distribution of the printed cement structures, samples structures were dried in a freeze dryer, weighed and added to a solid sample 3 mL bulb volume glass penetrometer with a stem volume of 0.412cc. The penetrometer was sealed and analysed in the two chambers, one at low pressure (for the evacuation of gases from the penetrometer chamber and backfilling with mercury up to the lowest pressure point which in this case was 50 psia) and the other at high pressure (collection of data points in the high pressure region up to 33,000 psia)

on a mercury porosimeter (Micromeritics AutoPore IV 9500, UK). Data was recorded on the AutoPore software provided by the manufacturer.

3.21 Construct preparation

Ligament constructs were prepared by soaking the printed brackets overnight in sterile PBS. After immersion in 70% ethanol, the brackets were dried in a laminar flow hood and sterilised overnight under ultraviolet light. The printed half of the anchors were placed 3 cm apart in an 8.5 cm petri dish for the large constructs and 2 cm apart in 5 cm petri dishes for small constructs. 600 µL fibrinogen solution (20 mg/mL HAM) was added to the petri dishes so that the added brackets were completely submerged. To this 1.5 mL thrombin solution (200 U/mL S-HAM with 50 µM Ascorbic acid, 50 µM proline, 2 µL/ mL Aminohexanoic acid and 2 µL/ mL Aprotinin) was added drop wise with regular agitation of the petri dish to ensure homogenisation. The solutions were allowed to clot in an incubator at 37°C for 3 h after which 0.75 x 10^6 isolated tenocytes were added to each of the constructs and the top half of the bracket was placed into position using sterile tweezers.

The gelled constructs were topped with 6 mL S-HAM which was replenished every 3 days and incubated at 37°C.

3.22 Histological analysis of soft tissue constructs

Histology is a qualitative technique for the assessment of cell structure, general morphology and intercellular composition. Visualisation may be made of native and synthetic tissue sections, or cells which have been fixed to a slide, which have been dyed using stains which chemically bind to specific parts of a cell. Images of the stained samples are usually taken by a camera attached to a light microscope or electron microscope.

After chemical fixation to preserve the samples and retain their morphology, the samples are embedded in medium which replaces the water in the samples with a solidifying chemical, such as paraffin wax, allowing thin sections of the sample to be made. The dyes used to stain the samples specifically target certain components of the sample or cell. A typical example of such a dye is hematoxylin and eosin (H and E) where hematoxylin which binds to nucleic acids in the cell nucleus and stains them blue whilst eosin provides information on the cytoskeleton of the cell by staining the cytoplasm pink (Stevens and Lowe 1997). The dyes are usually a vibrant colour to provide a strong contrast with the rest of the sample and, as is the case for *H and E*, the sample may be stained with multiple dyes at the same time, each highlighting a different part of the cell.

Histological sections of fixed constructs (4% formaldehyde in PBS) were made by first setting the samples in Embedding medium (Sigma Aldrich, Poole, UK) and then sectioning with a sample thickness of 6 μm in a cryostat (Bright Starlet 2212, Cambridge, UK) at -25°C.

Sectioned slides were fixed overnight in Bouin's solution and washed in running tap water to remove the yellow colour. After 5 min staining in working Weigert's iron hematoxylin solution the slides were again washed under running tap water for 5 min. After rinsing in deionised water,

the slides were stained in Beibrich scarlet-acid fuschin for 5 min and rinsed again in deionised water. The slides were then placed in working Phosphotungstic/ Phosphomolybdic acid solution (1 volume of Phosphotungstic acid with 1 volume of Phosphomolybdic acid and 2 volumes of deionised water) for 5 min. After staining the slides in Analine blue solution for 5 min they were rinsed in 1% acetic acid for 2 min. Finally the stained slides were rinsed in running tap water, dehydrated through 5 min rinses in 70%, 80%, 90%, 95% and 100% ethanol cleared in Histo-clear solution and mounted using Histomount after the slides were dry. All histological solutions were purchased from Sigma Aldrich, UK.

3.23 Glycosaminoglycan assay for assessing extracellular matrix production in constructs

Proteoglycans, with glycosaminoglycan (GAG) side chains around a protein core, are a major component of the ECM (Karousou *et al*. 2008). By measuring the amount of GAG present within a cellular sample, the amount of proteoglycan, and therefore ECM production, can be approximated. GAGs are non-branching polysaccharide chains with a repeating disaccharide unit, such as chondroitin sulphate, hyaluronic acid and heparin (Yoon and Halper 2005). Since all GAGs except hyaluronic acid, contain sulphate, a dye such as 1,2-Dimethymethylene blue, the sulphate content may be used to calorimetrically assess the GAG content of a given sample when compared to the standard curve.

The GAG content of ligament constructs, indicating matrix production, was assessed by first oven drying the samples for 30 min at 110°C and then weighing them. To each sample 500 μL papain buffer (2 U/mL papain, 5 mM cysteine and 5 mM EDTA in sterile PBS) was added before

incubating at 60°C for 24h to induce sample digestion. After cooling, 100 µL of the samples was added in triplicate to 24-well plates (Scientific Laboratory Supplies, UK) before adding 2.5 mL dimethymethylene dye (16 mg 1,2-dimethymethylene blue, 3.04 g glycine, 2.37 g NaCl and 95 mL 0.1M HCl, dissolved in 1 L distilled water, pH 3) and reading the absorbance at 525 nm on a spectrophotometer (Glomax multi detection system, Promega, UK).

For the calibration curve, 1 mg/mL standard of Chondroitin sulphate was prepared in papain buffer, serial diluted, dyed with dimethylmethylene blue and the absorbance read. GAG content in the samples was determined using the linear equation derived from the calibration curve.

3.24 Hydroxyproline assay for the assessment of collagen in constructs

Hydroxyproline, (2S,4R)-4-Hydroxyproline or L-hydroxyproline ($C_5H_9O_3N$) is a non-essential amino acid, produced by the conversion of proline through ascorbic acid, also known as vitamin C (Hausmann and Neuman 1961). Therefore, vitamin C deficiency often leads to poor hydroxyproline generation and therefore breakdown of connective tissue, which in turn leads to the excretion of any stored hydroxyproline. The conversion is mediated through the enzyme prolyle hydroxylase and occurs in the lumen of the endoplasmic reticulum (Kaelin Jr. 2005).

Through the formation of hydrogen bonds, the amino acid maintains the structural integrity of collagen and its triple-helical structure. Hydroxyproline is not often found outside collagen, in mammals it is only found in collagen and elastin (Bentley and Hanson 1969). The hydroxyproline is a quantitative assay based on colorimetry, used to estimate the amount of collagen produced by cells by comparison to a calibration curve.

To assess the collagen content of ligament constructs, 200 µL 6 M HCl was added to 1 mg of dried cell-seeded sample as well as 0.5 mg dried native tendon and hydrolysed at 130°C for 3h in a dry bath (Accublock digital dry bath, Labnet International, UK). The HCl was then evaporated at 130°C for a further 1h in a fume hood and cooled overnight. 200 µL buffer pH 6.5 (16.6 g citric acid, 4 mL acetic acid, 40 mg sodium acetate, 11.4 g sodium hydroxide, 500 mL distilled water and 0.25 mL toluene) was added to each sample and repeatedly pipetted to facilitate sample dissolution. 200 µL L-4-hydroxyproline standards were prepared (0 µg/mL, 4 µg/mL, 6 µg/mL, 8 µg/mL, 10 µg/mL, 20 µg/mL, 30 µg/mL). The samples and standards were mechanically agitated (Rotamixer, Baird and Tatlock, UK) before the addition of 150 µL Chloramine-T reagent (14.1 mg/ 1 mL distilled water) to each sample and standard . Again these wereall agitated in a rotary mixer. After 20 min at room temperature, 150 µL aldehyde-perchloric acid solution (1.5 g P-dimethylaminobenzaldehyde, 6 mL propan-1-ol and 2.6 mL perchloric acid) was added to each sample and heated to 60°C in a dry bath for 15 min. After cooling, the absorbance of each solution was read at 550 nm on a spectrophotometer (Glomax multi detection system, Promega, UK). All absorbance readings were taken in triplicate.

Collagen content of samples was calculated using the methodology outlined by Neuman and Logan (1950) where the µg hydroxyproline, derived from the absorbance spectra for the samples against calibration curves, is used as follows;

$$Collagen\ content\ =\ \left(\frac{\mu g\ \ hydroxyproline\ in\ 1mL\ lysate}{\mu g\ \ tissue\ in\ 1mL\ lysate}\right)\ \times\ 100\ \times\ 13.34 \qquad (3.7)$$

Equation 3.7 is based on the assumption that native collagen contains 13.34% w/v hydroxyproline (Neuman and Logan 1950).

3.25 Statistical analysis

Statistical significance ($P<0.05$) between test groups was determined by one-way analysis of variance (ANOVA) and Tukey-Kramer Honestly Significant Difference post-hoc test (www.Brightstat.com).

CHAPTER 4: EVALUATING BIOPOLYMER GELS AS TISSUE ENGINEERING SCAFFOLDS

4.1 Introduction

In utilising the tissue engineering principles mentioned in Chapter 2, a suitable scaffold is needed to support, promote and maintain cellular growth. Hydrogels are ideal for tissue engineering as their morphological structure closely resembles the extracellular matrix (ECM) of native tissue and can produce minimal or no cytotoxic by-products (Drury and Mooney 2003; Sant *et al*. 2010 and Van Vlierberghe *et al*. 2011). These polymeric scaffolds may be naturally derived, such as agarose, alginate, carrageenan and gelatin, or, synthetic, such as poly(hydroxyethylmethacrylate), poly(vinyl alcohol) and polypeptides. Synthetic scaffolds have specifically been tailored to increase functionality of the gels as tissue engineering scaffolds. The gels used in this research are naturally derived. An overview of some of the natural gels and their advantages and disadvantages in tissue engineering may be seen in Table 4.1.

Table 4.1 The advantages and disadvantages of some natural hydrogels used in tissue engineering.

Polymer name	Advantages	Disadvantages	References
Collagen and gelatin	Easy to gel and manipulate No cell toxicity Thermally reversible gel structures Improved mechanical properties through chemical crosslinking	Poor mechanical properties Chemical modification is time and money consuming Crosslinking agents likely to be harmful to cells	Cen *et al.* 2008 Barnes *et al.* 2007 Pan *et al.* 2010 McGuigan and Sefton 2007
Hyaluronate	Already present in GAGs	Degrades through serum and hyaluronidase from cells Extra purification step needed Poor mechanical properties Possibility of disease transmission	Nesti *et al.* 2008 Zheng Shu *et al.* 2004 Calderon *et al.* 2010 Allison and Grande-Allen 2006
Fibrin	Naturally created in the body for wound healing Non-toxic Easily forms gel at room temperature Degradation may be controlled by proteinase inhibitors such as aprotinin	Contracts once cells are added Poor mechanical strength	Vinatier *et al.* 2006 Johnson *et al.* 2010 Jockenhoevel *et al.* 2001
Alginate	Low toxicity Cheap Easy to gel and manipulate	Degrades through ionic exchange with surrounding media Minimal cellular interaction Proteins not easily adsorbed	Li *et al.* 2005 Kim *et al.* 2011 Wang *et al.* 2003
Agarose	Thermally reversible Easy to control pore sizes	Larger pores ideal for cellular growth introduce structural instability	Mauck *et al.* 2000 Stokols *et al.* 2006
Chitosan	Structurally similar to GAGs compatible with cells	Difficult to dissolve	Heinemann *et al.* 2009 Ragetly *et al.* 2010
Carrageenan	Easy to manipulate Can get reversible and non-reversible	Difficult to maintain good cellular compatibility when the structure is strengthened Temperature, pH and cation concentration controlled	Daniel-da-Silva *et al.* 2007 Santo *et al.* 2009
Dextran	Crosslinking density may be varied	Slow degradation rate Minimal cellular interaction	Jukes *et al.* 2010 Lévesque *et al.* 2005

As well as mimicking the morphology of the ECM and causing little or no inflammation, these scaffolds must exhibit structural integrity while maintaining a porous network for nutrient diffusion. Certain hydrogels, such as poly(hydroxyethylmethacrylate) (PHEMA) are able to retain water at a concentration similar to living tissue but degrade slowly. Having a predictable degradation rate is an important factor since the gel acts as a temporary support to the cells, allowing the cells to grow and proliferate. Furthermore, they should provide mechanical support whilst the scaffold dissolves and is cleared from the body. The swelling of the gels allows nutrients to diffuse into the network whilst allowing cellular waste to diffuse out (Jeon *et al*. 2007). Mechanical properties of gels are also affected by the surfaces to which they adhere, i.e hybrid materials, as was noted by Jeon *et al*. (2007) who studied the mechanical stability and degradation rates of hyaluronic acid at various concentrations with the addition of molecular weight and density controlled poly(ethylene glycol) (PEG) crosslinking agent. Below is a description of some natural hydrogels used for tissue engineering.

4.1.1 Agarose

Agarose is a linear polymer extracted from agarophyte seaweed and composed of a repeating D-galactose and 3,6-anhydro-L-galactopyranose disaccharide unit, known as an agarobiose unit. Agarose forms thermoreversible hydrogels as the dispersion medium (i.e. water) is cooled from near boiling point to less than 30°C. With applications in gel electrophoresis, tissue culture, pharmacy and food technology, agarose is easily manipulated by varying the agarose powder concentration (Narayanan *et al*. 2006). Jain *et al*. (2006) used agarose to support 3D neurite

extension *in vivo* and deliver trophic factors, more specifically brain derived neurotrophic factor, to promote neuronal growth. Agarose has also been used in conjunction with other natural polymers, such as chitosan and gelatin, to form cartilage tissue scaffolds (Bhat *et al*. 2010) or manipulated to form osteoblast-loaded agarose stamps for the transfer of cells onto a secondary scaffold (Stevens *et al*. 2005).

4.1.2 Gelatin

Gelatin is derived from the breakdown of the insoluble collagen triple-helical structure and exists in two forms, gelatin A, extracted from collagen via acid pretreatment, and gelatin B, extracted from collagen via alkaline pretreatment (Pal *et al*. 2006). Gelatin is composed of α, β and γ peptide chains with a sequence of 18 amino acids (Gillmor *et al*. 1999). The breakdown of collagen occurs through thermal denaturation, physical treatment or hydrolysis. Gelation of gelatin occurs through hydrogen bonding as the temperature of dissolved gelatin is decreased to <30°C, independent of concentration, and an organised triple-helical structure forms. This is a reversible process whereby the solid structure collapses and forms a random orientation of peptide coils at temperatures above 40°C.

Gelatin is often used in the food industry, for surgery as absorbent pads or wound dressing (Choi *et al*. 1999) and more recently the tissue engineering field both as a cell delivery vehicle and as a potential scaffold due to its gelation close to core temperature and chemical similarity to native collagen (McGuigan and Sefton 2007; Yung *et al*. 2007 and Sakai *et al*. 2007). As discussed in the previous section, gelatin has been used with other gels to manipulate specific characteristics.

Sakai *et al*. (2007) formed an agarose-gelatin conjugate as a tissue engineering scaffold and successfully maintained a high cell viability therein.

4.1.3 Carrageenan

Carrageenan is a high molecular weight polysaccharide composed of repeated galactose and 3,6 anhydrogalactose (3,6-AG) units, both sulphated and non-sulphated. These units are joined by alternating α 1-3 and β 1-4 glycosidic linkages (Nickerson *et al*. 2010). Differences between the three main forms of carrageenan, kappa (κ), iota (ι) and lambda (λ) lie in the number and position of the ester sulphate groups on the galactose units (Santo *et al*. 2008). Low levels of ester sulphate promote gelation whereas high levels of ester sulphate lowers the solubility temperature, producing weaker gels. κ-carrageenan has one sulphate group on its polymer chain and therefore forms a strong, rigid gel through disulphide crosslinking. Gelation is further affected by variations in temperature and salt concentrations as demonstrated by Özbek and Pekcan (2004) who researched the thermal phase transitions of κ-carrageenan in pure water and KCl solution.

The gelation of κ-carrageenan occurs through the addition of cations, such as K^+, Rb^+, Cs^+ and Na^+ (MacArtain *et al*. 2003). Loose polymer coils begin to form as the temperature rises above the melting point of the gel. Coaxial double helices form upon cooling which may be grouped together to form 'domains' where helix-helix aggregation from different domains occurs through the presence of cations, forming a closely crosslinked structure by suppressing electrostatic repulsion between the polymer helices, in accordance to Robinson *et al*. (1991), or 'fibrils' (Morris *et al*. 1998) whereby the coils begin aligning end-to-end in the early stages of

aggregation and thicken as the polymer and/ or salt concentration is increased. Gels containing cations become so tightly aggregated that they often result in syneresis even without an external load. Syneresis is the accumulation of moisture on the gel surface. The process of gelation mostly associated with *κ*-carrageenan domain model is depicted in Figure 4.1.

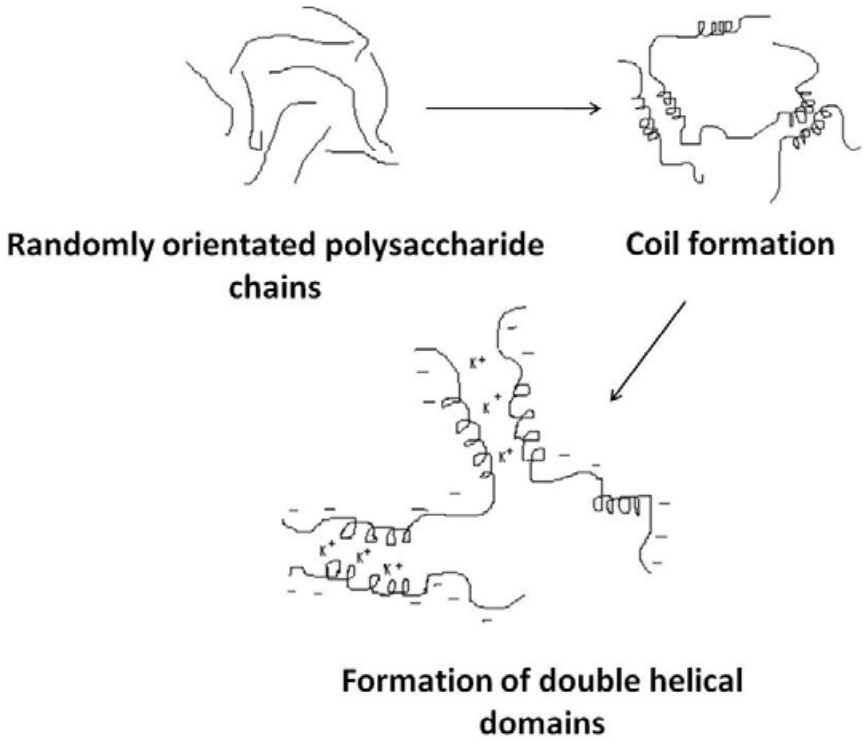

Figure 4.1 Gelation of *κ*-carrageenan from loose polymer chains to ordered helical structures and eventually to cation-bound aggregates.

Carrageenan is often used in the food and cosmetic industries as a stabiliser and thickening agent (Granero *et al*. 2010) and more recently combined with other gels, such as chitosan, for drug delivery (Picker 1999 and Grenha *et al*. 2010). In this chapter the use of three naturally derived hydrogels, agarose, gelatin and carrageenan have been evaluated as possible tissue engineering scaffolds for tendons and ligaments. Evaluation of the gels has included gelation temperatures, the compressive strength of the networks, cellular compatibility and the degradation of the gels with and without incorporated cells.

4.2 Results and discussion

Preliminary studies were conducted to ascertain gelation times for agarose, gelatin and κ-carrageenan. In addition to understanding the gelation behaviour of the gels, these initial studies served as a guide to selecting a gel which would be suitable for the encapsulation fibroblasts.

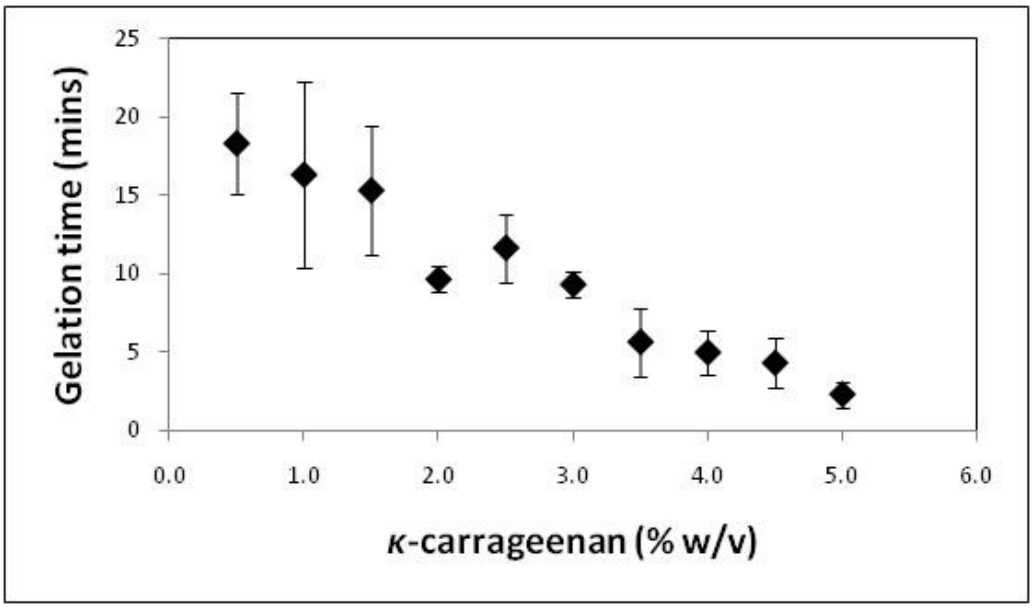

Figure 4.2 Gelation times for *κ*-carrageenan at 24°C. The error bars shown represent the standard error of the mean.

A 1h time frame was chosen to study the gelation of agarose, gelatin and *κ*-carrageenan at 24°C. The gelation time frame was chosen specifically to allow sufficient time for cell encapsulation. A period of longer than 1h would compromise cell viability. From the experiments it was found that gelatin does not gel at 24°C within the time period specified. Furthermore, agarose only gelled at higher concentrations (>4.5 % w/v) and took over 45 min to coagulate at 4.5 % w/v. Figure 4.2 shows the gelation times for *κ*-carrageenan at 24°C as the concentration of the polysaccharide is increased. Shorter gelation times were achieved when the *κ*-carrageenan concentration was increased. Furthermore, the lowest concentration investigated (0.5% w/v) required 18 min to gel, an ideal time to encapsulate cells and replenish with fresh supplements.

The decrease in gelation time may be explained by the number of polysaccharide chains present in the medium. By increasing the polysaccharide concentration in the dispersion medium, coil-coil interactions were increased, enabling rapid agglomerate formation in the presence of cations. The gel as a soft solid takes form when the secondary structures, seen in the second step of the gelation mechanism (Figure 4.1), are present in sufficient quantity to agglomerate and form an ordered structure. If these loose coils are present in high quantity, then a gelled network is likely to develop sooner, as seen in Figure 4.1.

As well as investigating the effect of increased polymer concentration, the effect of increasing the cation (K^+) concentration on the gelation time of κ-carrageenan at 24°C was studied. It was found, as shown in Figure 4.3 that changing either the cation or the polysaccharide concentration had a similar effect on the time taken for κ-carrageenan to crosslink. Increasing the cation concentration in the dispersion medium increased the availability of the crosslinking agent, allowing loose polymer coils to agglomerate into an organised structure faster as the rate of cation availability increased.

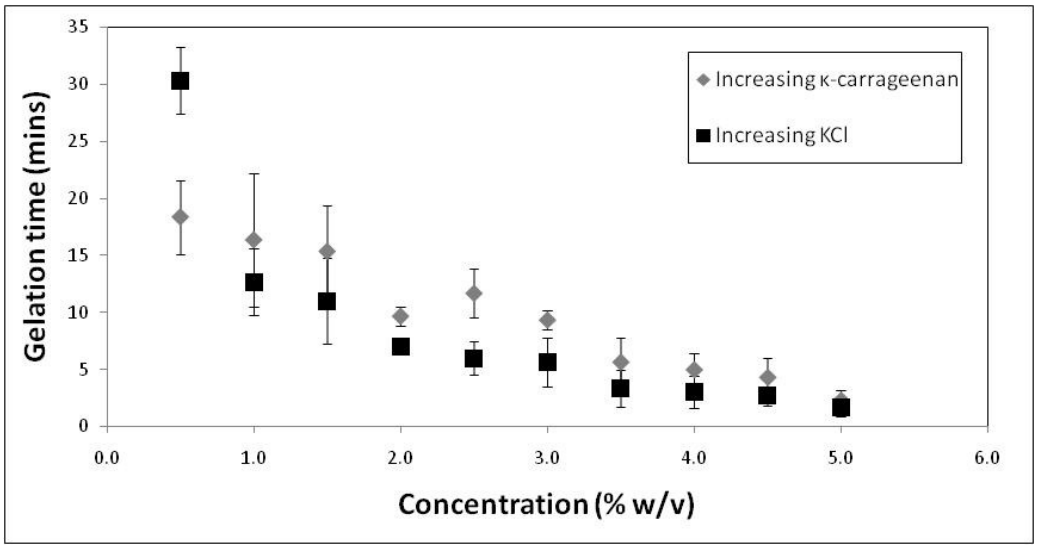

Figure 4.3 Gelation times for *κ*-carrageenan at 24°C with an increasing *κ*-carrageenan concentration (0.25% w/v KCl concentration) and with an increasing KCl concentration (1% w/v *κ*-carrageenan concentration). The error bars shown represent the standard error of the mean.

The influence of temperature on gelling of the carrageenan is also of great importance as the gel will be transferred from liquid to solid following manufacture. Figure 4.4 depicts changes in the gelation times of *κ*-carrageenan at 24°C and 37°C as the *κ*-carrageenan concentration was increased (A) and as the KCl concentration was increased (B). The gelation kinetics are similar in the variation of *κ*-carrageenan and KCl concentrations at 24°C and 37°C, suggesting that manipulation of the gel for cell seeding purposes will not be hindered by the increase in temperature.

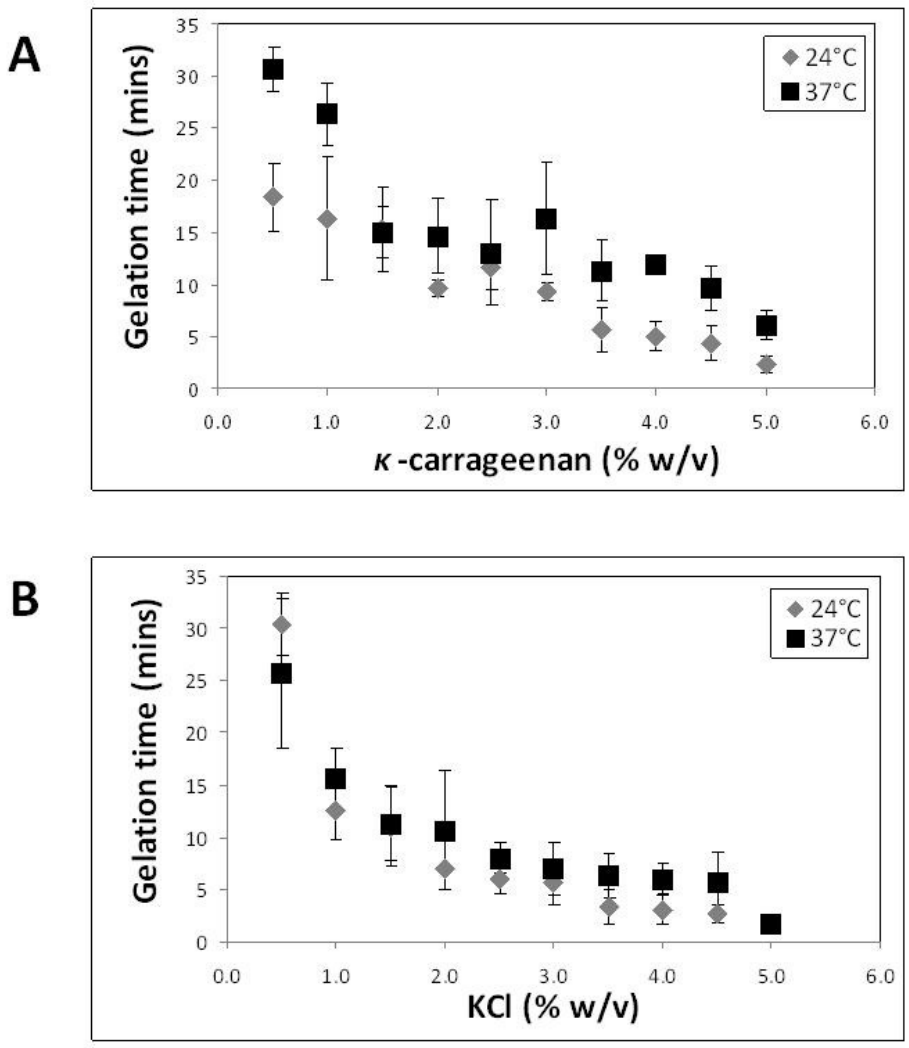

Figure 4.4 Gelation times for *κ*-carrageenan at 24°C and 37°C with varying *κ*-carrageenan concentration and 0.25% w/v KCl concentration (A) varying KCl concentration and 1% w/v *κ*-carrageenan concentration (B). The error bars shown represent the standard error of the mean.

Literature also shows (Rees 1981) that the K^+ cation is the strongest crosslinker for *κ*-carrageenan. Table 4.2 shows a comparison in *κ*-carrageenan gelation times when the K^+ cation

(Table 4.2B) is substituted for Ca^{2+} (Table 4.2 A). It can be seen that at 0.3% w/v the gelation time of κ-carrageenan with Ca^{2+} is 44 min at 37˚C, with a similar concentration of K^+ taking less than 0.1 min to gel. It is only when the concentration of Ca^{2+} ions in the medium is increased by almost 7-fold that the time taken to form a gelled structure is reduced to <0.1 min. These results indicate, as previously shown by Nijenhuis (1997), that the K^+ forms an ionic bond with the sulphated groups and the coils are brought together by electrostatic forces. However, Lai *et al*. (2000) have suggested that the popularly believed cationic binding theory may be challenged by the fact that impurities within the polysaccharide, such as different types of carrageenan, and other conditions may produce a stronger gel when a combination of cation types, such as K^+ and Ca^{2+}, is used. The data obtained for this study also shows that a strong variation in gelation times exists when using different cations in the same gel and keeping all other conditions the same.

Table 4.2 Gelation time of *κ*-carrageenan at 37°C for $CaCl_2$ at different concentrations and 1% w/v *κ*-carrageenan (A) and KCl at different concentrations and 1% w/v *κ*-carrageenan (B).

A

Concentration of $CaCl_2$ (% w/v)	Mean gelation time (mins)
0.30	44.33 ± 7.00
0.50	30.67 ± 2.50
0.70	<0.10
0.90	<0.10

B

Concentration of KCl (% w/v)	Mean gelation time (mins)
0.10	32.67 ± 1.60
0.15	<0.10
0.20	<0.10
0.25	<0.10

Furthermore, studies by Nishinari *et al*. (1990) showed that the addition of sucrose and glucose also had an effect on the gelation of *κ*-carrageenan. At 37°C, it was shown that a *κ*-carrageenan gel took longer to crosslink as the sucrose concentration was increased (Figure 4.5). At a sucrose concentration of 5% w/v the gel took twice as long to form a crosslinked network (12.6 min) in comparison to when no sucrose was added (6.3 min). Nishinari *et al*. (1990) suggested that this may be due to sucrose promoting the formation of hydrogen bonds which stabilises the gelled network. However, this would suggest an equilibrium was established and hydrogen bonds can no longer form. This is not evident in Figure 4.5, certainly not by a sucrose concentration of 5% w/v. It may be necessary to investigate higher concentrations in order to prove or refute the

findings of Nishinari *et al*. (1990). Such an investigation is beyond the purpose of this research finding a suitable scaffold for engineering tissues whereby the addition of sucrose to an already 2-part gelation process, before the addition of cells, would counteract the need for investigating suitable gelation times for cell seeding as well as the fact that the media in which the cells are suspended contain less than 5% w/v sucrose. However, the inclusion of cations, specifically K^+ ions, as established in Figure 4.3, is a necessity in the formation of carrageenan double helices.

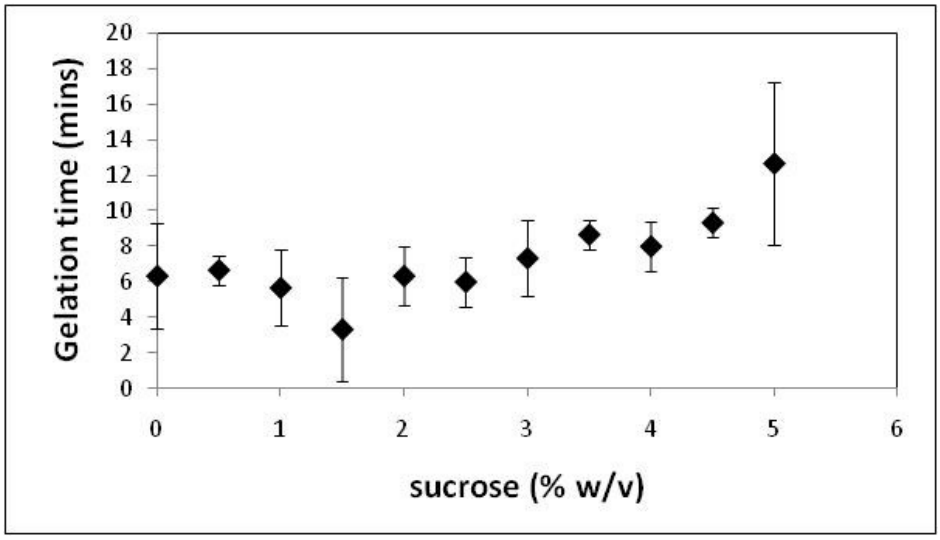

Figure 4.5 Gelation time for 1% w/v *κ*-carrageenan and 0.25% KCl at 37°C with added sucrose at various concentrations. The error bars shown represent the standard error of the mean.

Cell culture medium (Dulbecco's Modified Eagle's Medium (DMEM) in this work) contains many cations. The DMEM used for the experiments in this chapter contains 6.4 g/L NaCl (0.64%

w/v). Since cells suspended in DMEM, will be added to the κ-carrageenan, it is important to investigate the effects these extra cations would have on the polymer gelation. Table 4.3A shows the gelation time for κ-carrageenan at 37°C when supplemented DMEM (S-DMEM) was used as the crosslinking agent. Table 4.3B shows the effect of varying κ-carrageenan concentration in the same process. When the concentration of S-DMEM was increased to 40% v/v, gelation occurred at <0.1 min. Concentrations less than 40% v/v are considered to be insufficient to create a network with the necessary number of cations to form a rigid structure. Contrastingly when the concentration of κ-carrageenan required for network formation is increased with 50% v/v S-DMEM, it is not until the κ-carrageenan concentration is increased to 2% w/v that a network was formed with sufficient mechanical integrity to maintain its structure when removed from the mould. κ-carrageenan was added gradually to the heated water to avoid formation of insoluble agglomerates. The even dispersion of the polysaccharide within the medium may be insufficient to allow the formation of helix-helix agglomerates. The results of the gelation kinetics of κ-carrageenan with the addition of S-DMEM experiment show that it is possible to form rigid κ-carrageenan networks using S-DMEM alone as the crosslinking agent. However, the transition from a loose coil network to a fully formed rigid structure is so rapid that it is likely that the cell slurry will not be dispersed evenly before gelation starts to occur, i.e. premature local gelation leading to the formation of a heterogeneous gel network. Table 4.3B suggests that there may be a window of opportunity for the manipulation of κ-carrageenan and S-DMEM concentration for the successful seeding of cells, set between 1-1.5% w/v κ-carrageenan.

Table 4.3 Gelation times for *κ*-carrageenan at 37°C with varying concentrations of S-DMEM and 1% w/v *κ*-carrageenan (A) and *κ*-carrageenan and 40% v/v S-DMEM (B) with <0.1 min indicating immediate gelation.

A

Concentration of S-DMEM (% v/v)	Gelation times (mins)
5	No gelation
10	No gelation
20	No gelation
30	No gelation
40	<0.1
60	<0.1
80	<0.1
100	<0.1

B

Concentration of *κ*-carrageenan (% w/v)	Gelation times (mins)
0.5	No gelation
1	25
1.5	7
2	<0.1
2.5	<0.1
3	<0.1
3.5	<0.1
4	<0.1
4.5	<0.1
5	<0.1

The compressive strengths of the gels used in this chapter were determined to understand more about the structural integrity of the potential scaffolds. Figure 4.6 shows a comparison of the nominal stress exhibited by the two gelling forms of carrageenan, *κ*-carrageenan and *ι*-carrageenan at strains up to 20%. For comparative purposes, the stress exhibited by agarose and gelatin under the same conditions are also presented. Figure 4.6 shows that the potassium

chloride bound *κ*-carrageenan is the strongest of the four gels tested , withstanding a compressive stress of up to 2.1 kPa. Calcium chloride bound *ι*-carrageenan is a much weaker gel than the *κ*-carrageenan gel (withstanding 702 Pa compressive stress under the same test conditions). This structural weakness may be explained by the fewer sulphate groups on the galactose units of *ι*-carrageenan polysaccharide in comparison to the *κ*-carrageenan polysaccharide. Upon aggregation the fewer bonding sites in *ι*-carrageenan lead to a less ordered gel structure than the comparable *κ*-carrageenan gel and is therefore weaker. Finally Figure 4.6 shows that agarose and gelatin gels are the weaker of the four gels tested at up to 20 % strain exhibiting compressive stresses of 273 Pa (gelatin) and 143 Pa (agarose) respectively.

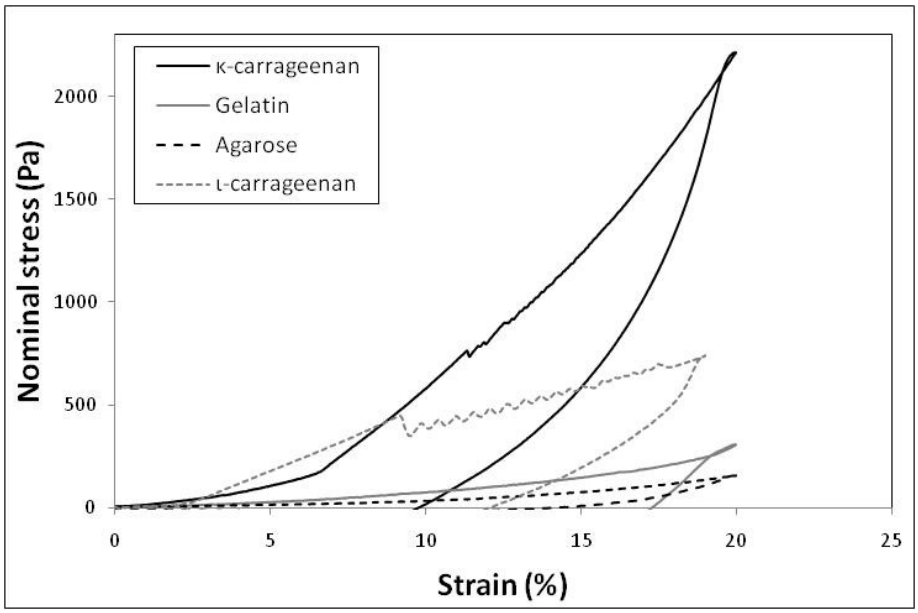

Figure 4.6 Comparison of stress exhibited by *κ*-carrageenan, *ι*-carrageenan, gelatin and agarose at up to approximately 20% strain.

The testing procedure for gel surface adhesion has been outlined in Figure 4.7, whereby the pull-out force of a 6 µm radius SiO_2 colloid probe from the surface of the gels is measured. The pull-off force for *κ*-carrageenan at 1% w/v polysaccharide was measured as 5.48 ± 0.02 µN whilst at 2% w/v polysaccharide it was measured as 6.32 ± 0.09 µN. The force measured for 1% w/v κ-carrageenan is in agreement with the capillary force (5.43 µN) expected for water under similar experimental conditions (Equation 4.1).

$$F = 4\pi\gamma R \qquad (4.1)$$

Where F is the force, γ is the surface tension (γ_{water} = 0.072 N/m at 20˚C) and R is the probe radius (Israelachvili 1991).

The pull-off force obtained for *κ*-carrageenan could be due to syneresis on the surface of the gel or that the compressive normal load applied by the probe has deformed the gel to a depth sufficient to cause extrusion of water from the bulk material. As the concentration of the polysaccharide is increased the adhesion force also increases (5.48 ± 0.02 µN at 1% w/v polysaccharide and 6.32 ± 0.09 µN at 2% w/v polysaccharide). The difference between the two *κ*-carrageenan gels is the number of disulphide bridges forming within the gel. The force is greater than the previously reported water capillary force suggesting that the effect is caused by the gel surface itself. This suggests that there is an interaction between the SiO_2 colloid probe and the

disulphide bridges. To understand this relationship a number of studies based on contact pressures and probe surface chemistries would need to be conducted. In comparison the pull-off force for *ι*-carrageenan is measured as 7.42 ± 0.40 μN. Whilst there are a decreased number of sulphate groups in the iota form, the formation of a crosslinked structure occurs through the presence of Na^+ as opposed to K^+ for *κ*-carrageenan. The surface charge density of Na^+ is higher than K^+ (Aylward 2007). The molar concentration of Na^+ for 2 % w/v *ι*-carrageenan is higher than the molar concentration of K^+ in *κ*-carrageenan. The SiO_2 probe presents a surface of silanol bonds (Si-OH) which contain hydroxyl moieties and will interact favourably with cations (Iler 1979). Therefore for a given contact area, there will be a greater number of interactions between the probe and the iota form than the probe and the kappa form of the gel and as such the adhesion force could be expected to be greater for *ι*-carrageenan than *κ*-carrageenan.

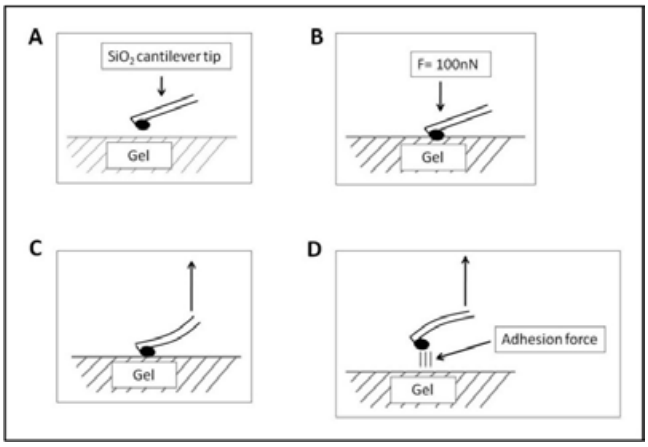

Figure 4.7 A diagrammatic representation of the AFM adhesion procedure where A is the procedural setup, B is the direction of the force applied, C is the pull-off motion and D is the adhesion force measured. The holding time between the AFM probe and the substrate surface is 5s.

In order to consider a material as a potential tissue engineering scaffold, it is necessary to investigate cellular compatibility. Figure 4.8 shows the growth curve for 3T3 fibroblast cells used for part of the research presented in this thesis. The curve consists of an initial adjustement phase (Figure 4.8A), rapid growth phase (Figure 4.8B), stationary/ plateau phase (Figure 4.8C) and a death phase (Figure 4.8D). Section A of the graph, representing the adjustment phase, accounts for the period after the cells have been harvested from the cell culture flask and re-seeded onto a cell culture plate, re-attaching and adapting to the new conditions after the ECM is digested during trypsinisation. The cells in this phase have a very rounded morphology. The rapid growth phase, section B on the graph, includes population doublings where there is a rapid growth and spread, i.e. proliferation, of cells due to space and a fresh supply of nutrients from the media

which is typically replenished every 3 days. The length of the rapid growth phase depends on the initial seeding density, the rate of growth of the cells and the overall density of the cells within the well/ plate where cells compete for space to grow and proliferate. It is at this stage that cells are usually harvested as the cell viability is high. For the research presented here the cells were harvested when they had covered approximately two thirds of the flask surface. Eventually the cells reach full confluency, signifying the end of the rapid growth phase and the beginning of the stationary phase, section C on Figure 4.8.

The stationary phase is the plateau reached by the cells when there is no room for growth, there is a build-up of toxins and nutrient availability is limited. At this point cell growth is reduced and due to the compact nature of the confluent exponential phase, less of the cell surface is available to the nutrients and their motility is considerably reduced (contact inhibition). The slowed growth rate, reduction in the amount of nutrients available, competition for nutrients and free space and a build-up of by-products and dead cells lead to the death phase, section D on the graph. Replenishing the medium and agitation of the culture plate/ well to break up the compact monolayer temporarily created more surface area for the cells to grow on. However, with only some areas being exposed for further cellular growth and proliferation, the new cells began to create multiple layers.

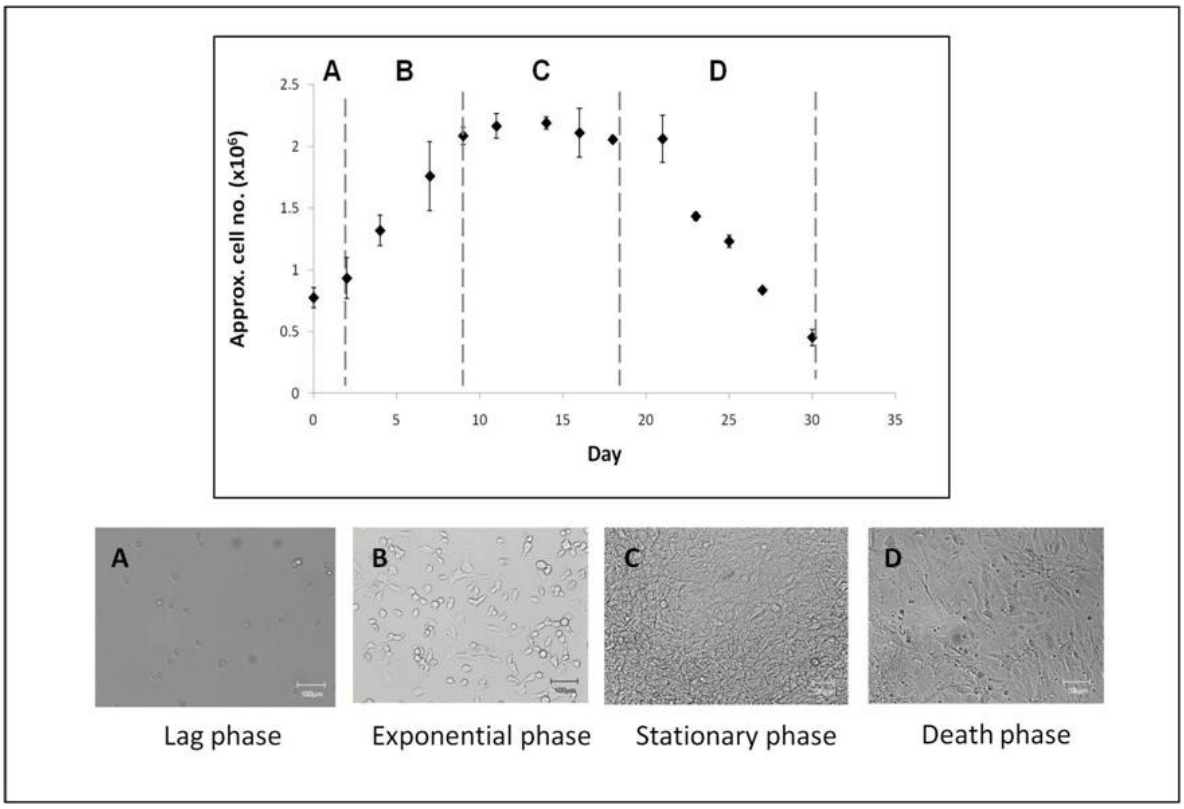

Figure 4.8 An MTT growth curve for murine NIH 3T3 fibroblasts showing the end of the adjustment phase whereby the cells are becoming accustomed to a changed environment (A), rapid growth phase (B), stationary phase (C) and the death phase (D). Scale bar on the SEM images represents 100µm. The error bars shown represent the standard error of the mean.

Murine NIH 3T3 fibroblasts were encapsulated in κ-carrageenan gelled using $CaCl_2$, KCl and S-DMEM. Figure 4.9 shows representative live/ dead images of the encapsulated cells on days 3, 6 and 10. Figure 4.9A, B and C (day 3 post-encapsulation) show a rounded cellular morphology with >95% of cells appearing green/ alive in all gels. This morphology is typically associated

with cells which are not attached to the material. From the number of viable cells visible on these images, it may be assumed that nutrients are readily diffusing through the gels. By day 6, small clusters of cells (Figure 4.9D) are beginning to form inside the $CaCl_2$ gel, whilst cells encapsulated in the KCl gel (Figure 4.9E) have a similar rounded morphology to day 3. Finally, for the cells encapsulated in the S-DMEM-gelled network, very few cells are now visible. This is because although S-DMEM did crosslink the *κ*-carrageenan, the resulting gel was very weak and subsequently repeated washing and nutrient replenishment led to a degradation of the gel with much of the gel being lost with the removal of waste media. By day 10, there was a general elongation of the cells in the $CaCl_2$ gelled network (Figure 4.9G). Furthermore, cytoplasmic projections can also be seen, strongly indicating cell attachment to the gel. The KCl gel (Figure 4.9H) still contained a high number of cells, suggesting that cells are not being lost through scaffold degradation. However, the number of dead cells, indicated by the red colour, also increased due to the fact that this particular cell type begins competing for nutrients and space as it enters the stationary phase, as indicated in section C in Figure 4.8. Furthermore, cellular morphology was still very similar to day 3, the start of the study. Finally, whilst a few cell aggregates may be seen in Figure 4.9I, the S-DMEM gel, the loss of mass greatly reduced the number of cells encapsulated. Overall, it is apparent that whilst *κ*-carrageenan takes longer to gel in the presence of $CaCl_2$, as shown previously in Table 4.2, cell viability is high when the cells are encapsulated within the gel. As previously explained, K^+ crosslinks the kappa form of the gel strongest in comparison to all other cations, which produces a highly organised network structure, reducing cellular migration and proliferation. In comparison Ca^{2+} produces a weaker network whereby the cells are not constricted promoting proliferation. Comparatively, the S-DMEM gel

although much less ordered, led to premature degradation which is not ideal for tissue engineering applications, a property which may be more suited to cell delivery.

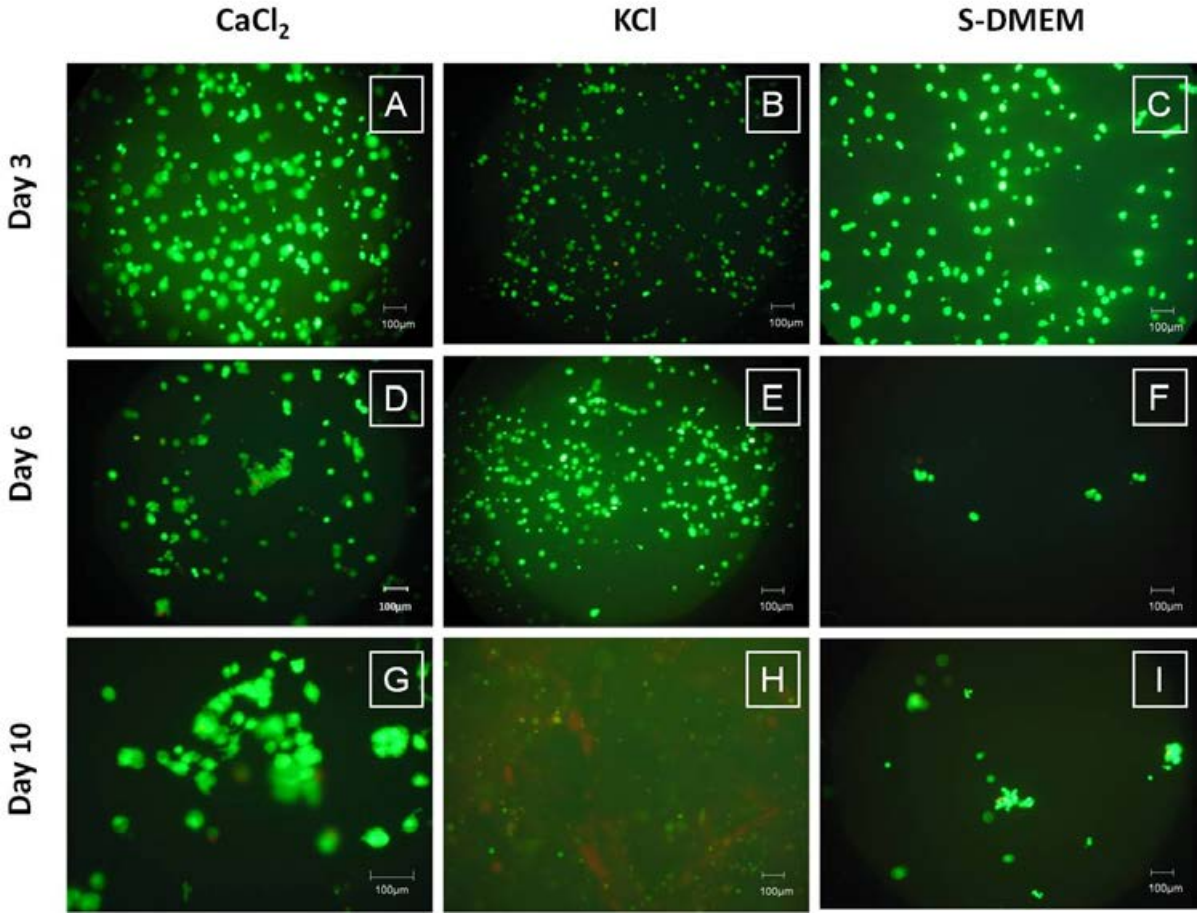

Figure 4.9 Live/ dead fluorescent images for murine NIH 3T3 fibroblasts encapsulated in κ-carrageenan gelled with $CaCl_2$ (A, D and G), KCl (B, E and H) and S-DMEM (C, F and I). Representative images have been shown for days 3, 6 and 10 post-encapsulation. Scale bars represent 100µm.

As mentioned previously, the use of KCl and S-DMEM to gel κ-carrageenan as a tissue engineering scaffold is more promising than $CaCl_2$ and whilst encapsulation of NIH 3T3 fibroblasts in both gel types has been investigated, the opportunity to surface seed the scaffolds is also available. Figure 4.10 shows live/ dead images for the fibroblasts seeded on the surface of κ-carrageenan gels formed using the afore mentioned crosslinking agents (Figure 4.10A, B, C, G, H and I) in comparison to cells encapsulated within the networks (Figure 4.10D, E, F, J, K and L). It is immediately apparent that cell attachment, indicated by elongation of cells and proliferation, indicated by an increase in the number of live cells visible, is marginally improved by seeding the cells onto the surface of the two gels. For the KCl crosslinked gel (Figure 4.10A-F) where previously cellular morphology remained unchanged over 10 days, there is now vast agglomeration from day 3 (Figure 4.10A), forming large colonies by day 6 (Figure 4.10B). Although by day 10 (Figure 4.10C) an increase is seen in the number of dead cells, which corresponds to the nutrient and contact inhibited stationary phase shown in Figure 4.8, the amassment of cells remain agglomerated and a large proportion remain viable. Similarly from Figure 4.10G-I it is seen that cell attachment and proliferation is greatly improved by seeding cells on the surface. Unlike the cells encapsulated within this gel (Figure 4.10J-L) they remain attached to the gel surface in large numbers, which would indicate less degradation than in their encapsulated form. It is evident from Figure 4.10I that a number of cell agglomerates have formed on the surface of S-DMEM gelled κ-carrageenan. It is likely that these colonies will merge together as the cells utilise the free space in between them. Although this may be beneficial in the early stages of a seeded tissue engineering scaffold, this rapid growth may need to be controlled by incorporating inhibitors into the gel matrix, such as the drug tranilast (Isaji *et*

al. 1997), or receptor specific inhibitors, such as NF449 (Hechler *et al*. 2005). This is to minimise uncontrolled growth of cells within the scaffold and allow the release of a degraded scaffold later as the tissue begins to form. Furthermore, as previously mentioned, it is possible that these cells will now begin to form multi-layers as the intercolony space diminishes. Control of this is also necessary to avoid formation of cell aggregates which would not allow nutrients to reach the centre of the agglomerate and so the tissue would begin to deteriorate from the inside out.

The number of dead cells on day 10 (Figure 4.10I) is much less than those on the surface of the KCl gel (Figure 4.10C). This is because the media used to gel these samples (Figure 4.10G-L) is supplemented with the nutrients required to maintain fibroblastic growth. Therefore, as well as the surface-seeded cells receiving nutrients from the regularly replenished source, as is normal cell laboratory practice, extra nutrients are also provided by the gel network itself. However, these 'inter-gel nutrients' are limited and will eventually become depleted and as such cellular viability is likely to approach a similarity to that on the surface of the KCl gel. It is evident by the marked difference in the number of dead cells in Figure 4.10C and Figure 4.10I that this nutrient-depleted stage has not yet been reached. It would be necessary to conduct a long-term study in order to understand this effect further. For this short-term study it has been revealed that κ-carrageenan should not be discounted as a tissue engineering scaffold based on the seemingly initial lack of cell proliferation.

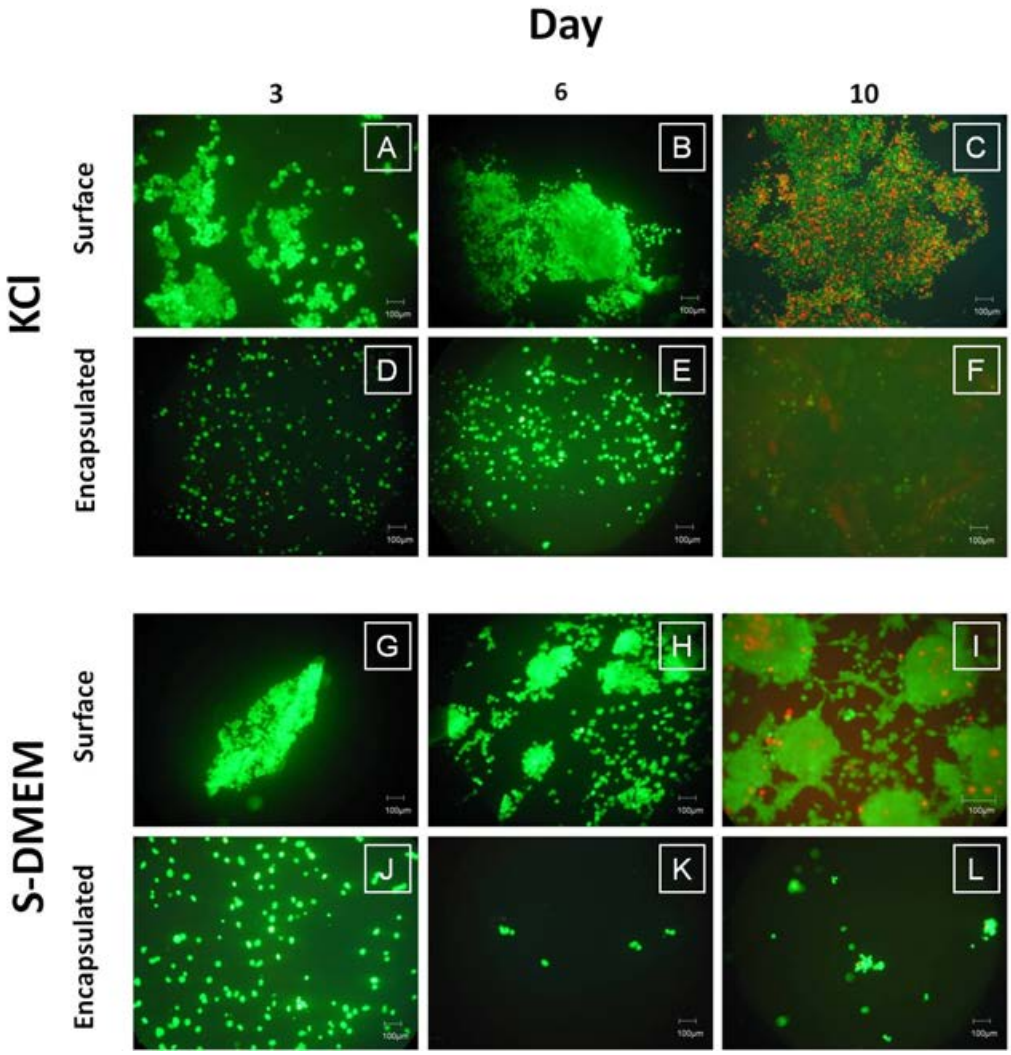

Figure 4.10 Live/ dead fluorescent images for murine NIH 3T3 fibroblasts surface-seeded and encapsulated in κ-carrageenan gelled with KCl and S-DMEM. Representative images are shown for days 3, 6 and 10 post-seeding. Scale bars represent 100µm.

As mentioned earlier in this chapter, carrageenan is available in three forms, κ-carrageenan, ι-carrageenan and λ-carrageenan. Although λ-carrageenan does not gel, ι-carrageenan does. In Figure 4.11A-L live/ dead images are shown representing cellular morphology after cells have been encapsulated in the two gels and seeded onto their surface. Furthermore, the cumulative metabolic rate for the cells has been presented (Figure 4.11M-P). Whilst the effect of the seeding method has previously been discussed, the opposite is true for the morphology of cells in and on an ι-carrageenan scaffold in comparison to κ-carrageenan. Notably, the number of cells has reduced considerably (Figure 4.11G-L) which may be attributed to scaffold degradation for ι-carrageenan due to ι-carrageenan forming a weaker gel than κ-carrageenan (as previously discussed in Figure 4.6). However in comparing images J-L to the MTT results depicting the approximate number of living cells on the surface of the gel (Figure 4.11O), it would appear there is an exponential increase in the metabolic rate of the cells as a whole which implies a proliferation of cells. This would suggest that the proliferation seen in Figure 4.11I is not a single occurrence and that these agglomerates, which show good attachment to the gel through cytoplasmic projections, are dispersed evenly in the gel. Comparatively, the MTT data for cells encapsulated in κ-carrageenan, confirm the results presented in Figure 4.11D-F. Figure 4.11D-F show that the number of proliferating cells reach a plateau by day 5 at approximately 5 x 10^6 cells and start to reduce after day 8, resulting finally in 0.3 x 10^6 cells by day 14. If cell proliferation has occurred, this has diminished by the end of this short-term study which would suggest that the cells cannot migrate and/ or there is an insufficient provision of fresh nutrients reaching the cells.

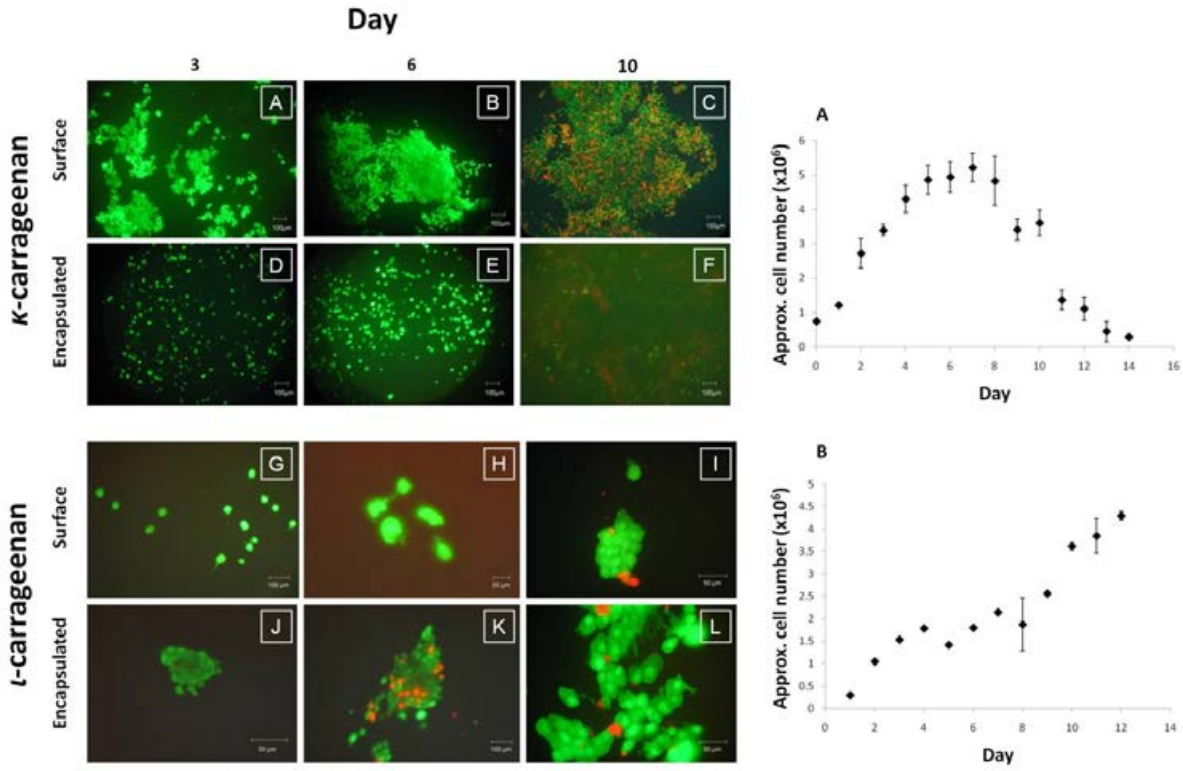

Figure 4.11 Live/ dead fluorescent images for murine NIH 3T3 fibroblasts surface-seeded and encapsulated in *ι*-carrageenan and *κ*-carrageenan. Representative images are shown for days 3, 6 and 10 post-seeding. The metabolic rate for encapsulated cells is shown in graph A for *κ*-carrageenan and B *ι*-carrageenan. The error bars shown represent the standard error of the mean.

Finally, it is also important to consider the degradation of the scaffold as a scaffold which is too stable will not allow enough room for cellular growth and a scaffold which degrades too quickly will provide insufficient support to the cells, not allowing them to proliferate and introducing the risk of cell migration beyond the specific site where the tissue is needed. Figure 4.12 shows the degradation of acellular and cellular *ι*-carrageenan and *κ*-carrageenan. Figure 4.12A shows a

comparison of percentage mass change in acellular and cellular κ-carrageenan where it is evident that whilst the acellular gel does not lose mass over 12 days, there is a 6% decrease in mass between days 0 and 28 when cells have been encapsulated in the gel. Similarly, the cellular ι-carrageenan samples appear to lose up to 4% mass over the 12 days (Figure 4.12B). However, this difference in mass for Figure 4.12B is not statistically significant. The loss in mass seen in Figure 4.12A is attributed to cell proliferation, as indicated by Figure 4.11 M and O, disrupting the network and therefore production of ECM, containing a vast array of enzymes, leads to premature scaffold degradation. Whilst the gel type used in Figure 4.12A and 4.12B is different, the cell type used is the same and therefore the enzymatic production should be measured. If the ECM produced is of similar quantities in both sets of data, it may be that the ι-carrageenan experiment should be repeated. As a comparison of cellular ι-carrageenan and κ-carrageenan (Figure 4.12D) it can be seen that for both gel types scaffold integrity is maintained throughout the study with no statistical difference in mass between days 0 and 28. The results collected for Figure 4.12 were based on 3 samples per time point. In order to obtain more conclusive results, the experiments need to be repeated with a greater sample number.

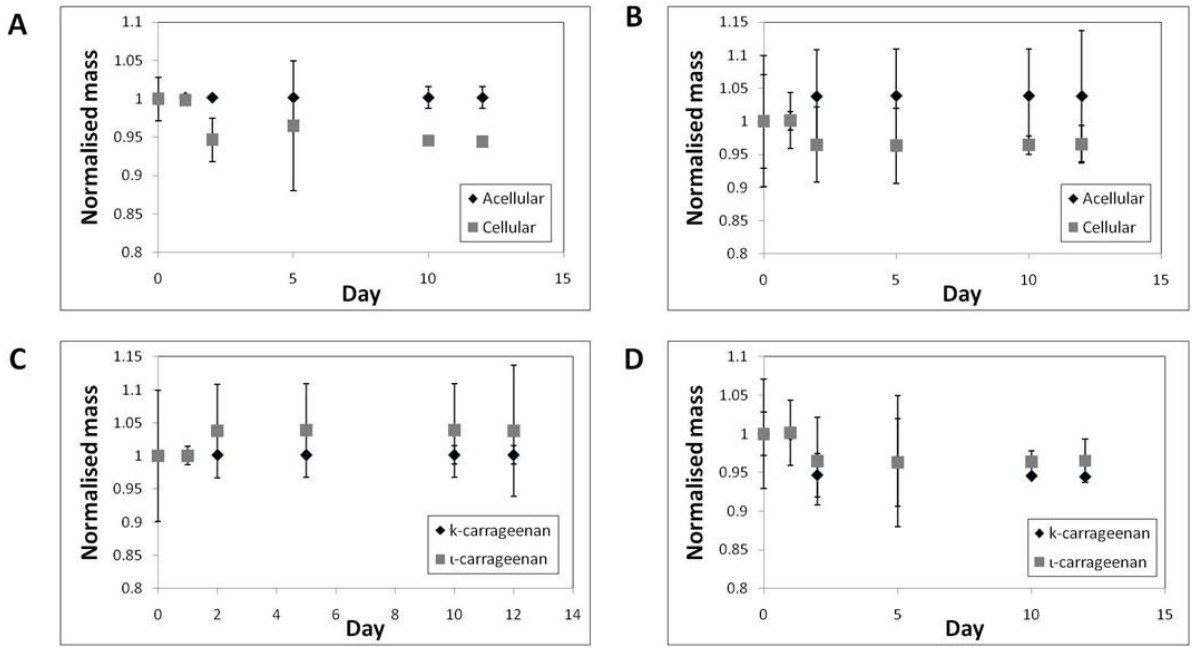

Figure 4.12 Scaffold degradation shown as normalised mass for acellular and cellular *κ*-carrageenan (A), acellular and cellular *ι*-carrageenan (B), acellular *κ*-carrageenan and *ι*-carrageenan (C) and cellular *κ*-carrageenan and *ι*-carrageenan (D). The error bars shown represent the standard error of the mean.

4.3 Conclusion

In this chapter three natural polymer scaffolds were tested for their suitability for tissue engineering applications. Initial experiments focused on the gelation times of the potential scaffolds. Agarose and gelatin were not suitable for this purpose as gelatin did not gel at 24˚C and agarose took 45 mins to gel at a concentration of 4.5 % w/v. *κ*-carrageenan was found to gel in 18 mins at low concentration (0.5 % w/v) in the presence of K^+ cations and was considered

ideal for cell encapsulation studies. Increasing the κ-carrageenan concentration lead to a decreased gelation time and therefore control of the gelation time was achievable. Further control was attained by changing the cation concentration. Increased cation concentrations lead to the rapid formation of polymer coils and an organised structure. However, when the K^+ cation was replaced by Ca^+, the gelation times were strongly affected, with 0.3 % w/v Ca^+ causing the κ-carrageenan to crosslink at 44 mins whilst the same concentration of K^+ ions taking less than 0.1 min to gel. It was shown therefore, that the K^+ cation was the strongest crosslinking agent between the two for crosslinking κ-carrageenan.

Further studies of gelation properties at 37˚C showed no difference to 24˚C, further adding to the suitability of the gel as a tissue engineering scaffold. Gelation was also found to be achieved by adding supplemented media to κ-carrageenan and no additional cations. It was found that whilst the salts in the media were sufficient in allowing polymer coils to be formed in κ-carrageenan, the concentrations of both the polymer and the media would need to be optimised to avoid forming a heterogeneous structure.

κ-carrageenan was also shown to withstand the highest compressive stress when tested against ι-carrageenan, gelatin and agarose at up to 20 % strain.

Cellular compatibility of the two gelling forms of carrageenan showed that encapsulation of murine fibroblasts within ι-carrageenan induced higher proliferative activity of the cells than seeding on the surface whereas the opposite was true for κ-carrageenan. This was attributed to the fact that ι-carrageenan forms a looser network than κ-carrageenan when crosslinked.

Finally the stability of *ι*-carrageenan and *κ*-carrageenan was compared, both in the acellular and the cellular forms. Although it was found that there was a difference in mass in the acellular and cellular forms of *κ*-carrageenan, the data presented for *ι*-carrageenan was not significant.

While it appears that there are many benefits to using carrageenan and perhaps both types, there is mounting evidence that carrageenan may be carcinogenic. Initial studies suggested that the degraded type of carrageenan, poligeenan, is the only type to cause cancer. However, more current research by Tobacman (2001) suggests that the ungraded type (native carrageenan with a higher molecular weight) of carrageenan may also be associated with malignancies through food preparation steps and spontaneous metabolism as part of the digestive process.

Based on these findings while the use of carrageenan merits future application, it is necessary to investigate an alternative scaffold material for engineering tendons and ligaments.

CHAPTER 5: INVESTIGATING THE SUITABILITY OF FIBRIN AS A TISSUE ENGINEERING SCAFFOLD

Hydrogels are used in many industries which include tissue engineering (Chapter 4) of which the use of agarose, gelatin and carrageenan as potential scaffolds for tendon and ligament engineering has been investigated. Whilst agarose and gelatin have gelation properties unsuitable for tendon and ligament engineering, carrageenan showed cellular compatibility. However, owing to increasing worries about the carcinogenic effects of carrageenan, an alternative scaffold material is sought. In this chapter a protein naturally found in the body, fibrin, has been investigated as an alternative gel scaffold.

5.1 Introduction

Fibrin is a naturally occurring, soluble blood glycoprotein which is 45nm in length (Williams 1981) and composed of fibrin fibres, formed by the polymerisation of fibrinogen (commercially available crystal morphology seen in Figure 5.1A), a protein abundantly present in blood, via the proteolytic enzyme thrombin (morphology of commercially available thrombin crystals shown in Figure 5.1B) and Ca^{2+} although preliminary experiments have shown that other serum proteases in supplemented media can cause gelation (McManus *et al*. 2006).

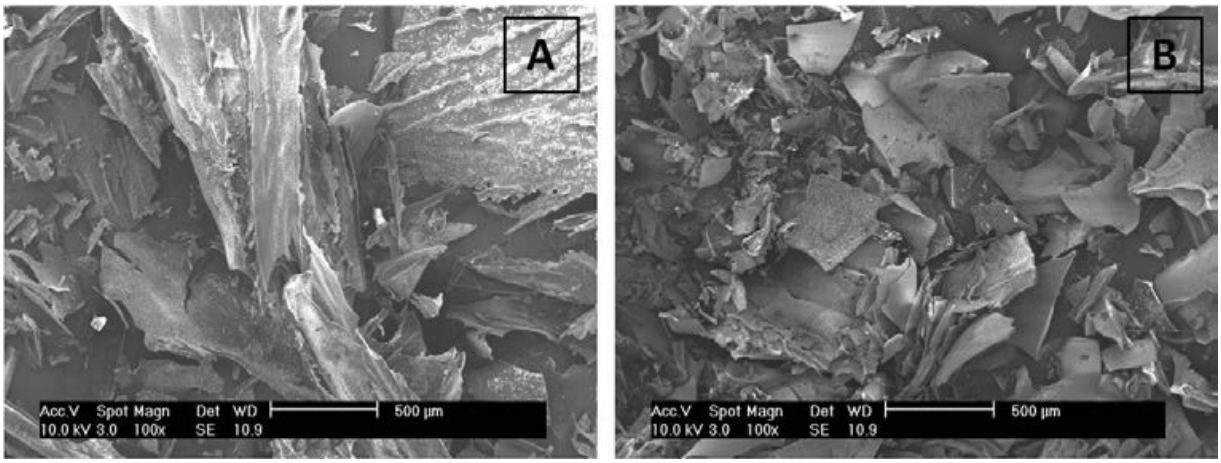

Figure 5.1 SEM images showing the crystal structure of flat sheet-like fibrinogen (A) and short, irregular shaped crystals of thrombin (B).

Fibrinogen is composed of three pairs of polypeptide chains, (AαBβγ)2 , held together by 29 disulphide bonds (Weisel 2005). The central region of the fibrinogen molecule connects the amino termini of the polypeptide chains and connects to the end domains by the α-helical coiled coils. The distal end regions are composed of the C-terminal γ-chains while the proximal ends are composed of the C-terminal Bβ-chains. Finally, the Aα-chains are folded back to form the fourth strand of the coiled coil, connecting to the αC-domains. The αC-domains are bound to the central region as shown in Figure 5.2. The central region contains the fibrinopeptides A and B which are cleaved by thrombin, derived from the glycoprotein prothrombin, at specific Arg-Gly residues.

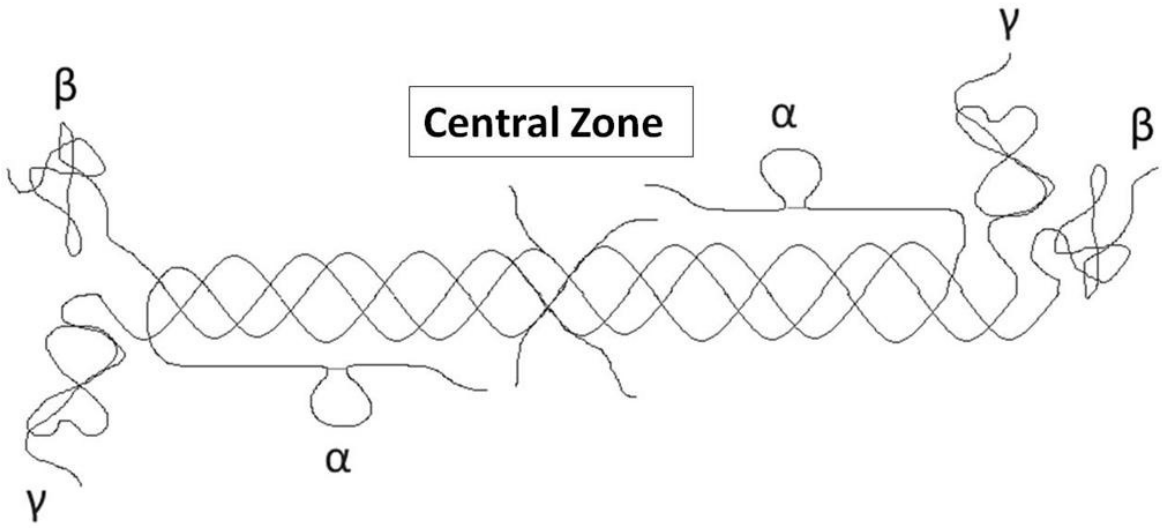

Figure 5.2 Diagrammatic representation of the coiled fibrinogen coil (adapted from Yee *et al*. 1997). Thrombin cleaves at the central zone, where the amino terminals of the coil meet and tether to each other, in effect attaching two 6-polypeptide chains.

The formation of a fibrin hydrogel, or clot, occurs through the linking of a glutamine residue of one fibrinogen molecule to a lysine residue on another fibrinogen, resulting in crosslinking of the fibrin fibres (Mitkevich *et al*. 1998). A diagrammatic representation of the gelation mechanism of fibrin and the interaction between thrombin and fibrinogen is shown in Figure 5.3 where knobs 'A' in fibrinopeptides A, cleaved more rapidly in comparison to fibrinopeptides B, complement holes 'a', exposed towards the end of the molecule in the γ-C module. Similarly, knobs 'B' exposed by the removal of B fibrinopeptides, compliment holes 'b' in the β-C module. Interactions between these knobs and holes yield different protofibrils. For the 'A' knob and 'a' hole interaction, the monomers within the protofibrils are found to be half-staggered with the

centre of one molecule binding to the end of the next molecule. For B fibrinopeptide cleavage, lateral aggregation is seen through the presence of fibrin oligomers, ultimately producing thick fibres composed of the cleavage of both fibrinopeptides. It has been suggested that the removal of B fibrinopeptides occurs via a combination of B-b interactions, αC-domain release and B peptide binding (Weisel 2007). Oligomers are lengthened through the addition of more monomers, forming multi-stranded protofibrils. Through specific protein-protein interactions between weak protein bonds and chloride ions (Di Stasio *et al*. 1998) the protofibrils then assemble and aggregate to form fibres.

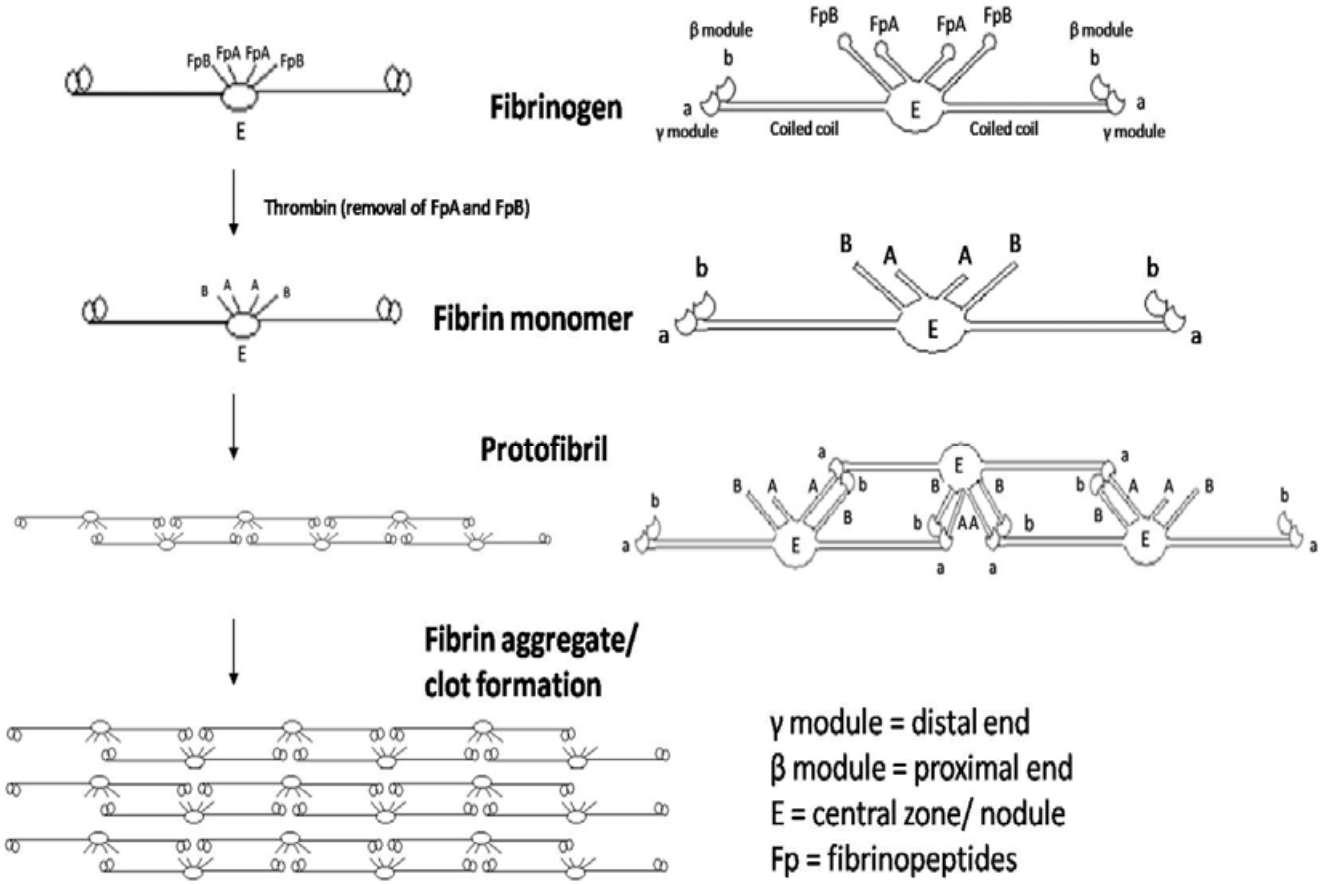

Figure 5.3 Schematic of the fibrin monomer structure and assembly into an aggregate (adapted from Janmey *et al*. 2009).

The three-dimensional network which constitutes the fibrous mesh is such that fibre ends are difficult to find in normal clots. Gelation of fibrinogen may occur through serum proteases other than thrombin. However, these factors are likely to affect the properties of the gelled network in terms of individual fibre thickness, the extent to which they branch and pore sizes. Low concentration of thrombin, for example, produces clots with large pore sizes and thick fibres with very few branch points. Similarly, the addition of stabilising factors, such as factor XIIIa which is derived from the enzyme factor XIII, creates a mechanically stable gel with a greater resistance to proteolytic digestion by covalently crosslinking the γ chains (Lewis *et al*. 1985).

Furthermore, fibroblasts seeded in fibrin gel have been shown to readily cause contraction (Tuan *et al*. 1996), a feature of fibrin matrix reorganisation and remodelling fibroplasia. Tuan *et al*. (1996) seeded fibroblasts on fibrin hemispheres with a gradual reduction in gel thickness rather than diameter, thus causing tension between the fibrin fibrils as they develop, similar to conditions in native wound repair and fibroplasia. Studies have also shown that fibroblasts seeded on fibrin gel cause a 10% reduction in original thickness (Tuan *et al*. 1996). This is primarily caused by the reorganization of fibrin fibrils due to fibroblast proliferation, ultimately leading to a dense arrangement of fibrils with water being excluded in the process. However, this contraction may be reduced by varying the protein content of the scaffold (Bell *et al*. 1979). The production of collagen by fibroblasts has also been shown to increase in attached gels, with tension, compared to floating gels without tension by Nakagawa *et al*. (1989).

Fibroblasts have often been seeded on autologously sourced fibrin gels, avoiding the risk of foreign body or viral infections following implantation (Rowe *et al*. 2007). Fibrin may be autologous, allogeneic, xenogeneic or recombinant. The two most popular forms used are either

as an adhesive/ sealant in the form of fibrin glue or a non-porous hydrogel (Linnes *et al*. 2007). As described previously, increasing the porosity of fibrinogen is seen as a necessity for certain tissue engineering purposes, such as bone formation, with pore size affecting cell attachment, growth and differentiation (Yang *et al*. 2007). Some researchers have electrospun fibrinogen, by charging the solution and forcing the solution out of a nozzle to an oppositely charged target to produce dry, fibrous mats mimicking fiber diameters in native fibrin clots (~80-500 nm). Furthermore, the interconnected pores have been reported to facilitate cellular organization and diffusion of nutrients and waste products (McManus *et al*. 2006). The diameter of these fibres may also be controlled, by varying the concentration of fibrinogen in the electrospinning solution.

The use of fibrin as a scaffold material can be further enhanced by preconditioning fibrin networks in specialised bioreactors before implantation. It has been shown that when a constant tensile strain of >25% is applied to a 3 mg/mL fibrin gel, the cells encapsulated within the gel begin to divide and align (Matsumoto *et al*. 2007). It is the ease of thrombin-controlled gelation and addition of contraction inhibitors to manipulate the network, which allows fibrin to be a suitable scaffold for tissue engineering applications.

Furthermore, addition of growth factors, such as TGF-β which controls growth, proliferation and apoptosis, have been shown to increase gel contraction and collagen synthesis although researchers have shown that there is no significant difference in fibroblast proliferation between the two gel types (Gillery *et al*. 1989).

Some researchers have also explored the rapid production of gel networks to form fibrin networks with varied 'patterns' on the surface. Campbell *et al*. (2005) used an ink-jet printing

method to add FGF-β (basic fibroblast growth factor) to specific areas of a fibrin film and showed preferential cell adherence to areas where the growth factor was incorporated. This particular method would be ideal for producing fibrin bandages where growth factors or clot components may be contained to a certain area to facilitate wound healing.

Other uses of fibrin gel include glue, as a suture replacement method to reduce bleeding (Srinivasan *et al*. 2009), mesh fixation for hernia repair, nerve reattachment, skin graft adhesion and microsurgical anastomoses stabilisation (Martins *et al*. 2005 and Andree *et al*. 2008). Furthermore, fibrin is an ideal drug delivery vehicle for the enhancement of tissue repair as it is relatively easy to manipulate, can easily be injected into the wound site, degrades naturally and can stimulate the body's own repair mechanism (Janmey *et al*. 2009). As well as drugs, fibrin may also be used for the delivery of cells. Fibrin is necessary in the migration, proliferation and differentiation of cells within a tissue. Not only does it allow cells to migrate freely within the fibrin gel matrix, fibrin also readily binds to growth factors and clot components such as the ECM glycoprotein fibronectin. Finally, some researchers have further gone on to form fibrin based hybrid scaffolds such as combinations with poly(lactic-co-glycolic acid) and sepharose (Eyrich *et al*. 2007; Chernousov and Carey 2003).

In this chapter the agglomeration of fibrin from fibrinogen and thrombin has been investigated and the effects that the clotting agent, thrombin, has on the structural morphology and integrity of the gel have been studied. Cellular compatibility using the 3T3 fibroblast cell line, was investigated as well as an introduction to tendon-specific tenocytes and their effect on the degradation of the scaffold.

5.2 Results and discussion

Fibrin formation consists of the agglomeration of two proteins, fibrinogen and thrombin. Whilst Figure 5.1 depicts the crystal structure of fibrinogen and thrombin, Figure 5.4 shows the Raman spectra for these components as well as the final clotted gel. These spectra provide a unique chemical signature for the individual components present in fibrin. The spectra shown in Figure 5.4 have been baseline corrected. From the spectra it can be seen that the Raman peaks for fibrinogen and thrombin are very similar. This is because both components of the gel are proteins and the peaks obtained reflect typical protein bond signatures. Few literature studies have focussed on the Raman spectra for fibrinogen, thrombin and fibrin. An 1979 analysis of the clotting behaviour of fibrin through Raman spectroscopy provides the best explanation not only for the chain of events in fibrin agglomeration but also the bonds to be expected (Marx *et al.* 1979). From this study bond presence and type has been deduced for Figure 5.4. Initial peaks (from 935-1117 cm^{-1}) represent the stretching modes of the αC-C interaction (Figure 5.2) in the formation of fibrin coils. Raman shifts at 1234 and 1238 cm^{-1} in fibrinogen and thrombin are indicative of Amide III, the peptide backbone whilst 1311-1442 cm^{-1} indicate deformation of C-H bonds and presence of tryptophan, an aromatic side chain, an amino acid, the authors show to be present in proteins. Peaks at 1539-1545 cm^{-1} in fibrinogen and thrombin indicate CH_2 and CH_3 deformation, whilst an additional peak at 1598 cm^{-1} in the fibrinogen indicates the presence of another aromatic side chain, tyrosine. Finally a strong peak for all three materials is seen between 1638 and 1657 cm^{-1} which indicates the presence of Amine I. This is also said to indicate the formation of the α-helix in fibrin. Whilst it can be seen in Figure 5.4 that strong peaks are visible for fibrinogen and thrombin, those for fibrin appear ‘noisy’ and with little definition at lower

intensities. This is due to accumulation of water on the surface of the gel, syneresis, which made it difficult to acquire a spectrum even when high concentrations of thrombin and fibrinogen were used. Drying the surface liquid allowed more to exude out of the gelled structure and it was noted that continued dehydration would eventually lead to a change/ collapse of the gel. The data accumulated for the proteins in Figure 5.4 allow a chemical fingerprint to be assigned to the separate constituents, fibrinogen and thrombin, as well as fibrin. These may be used to identify fibrin where other species are present.

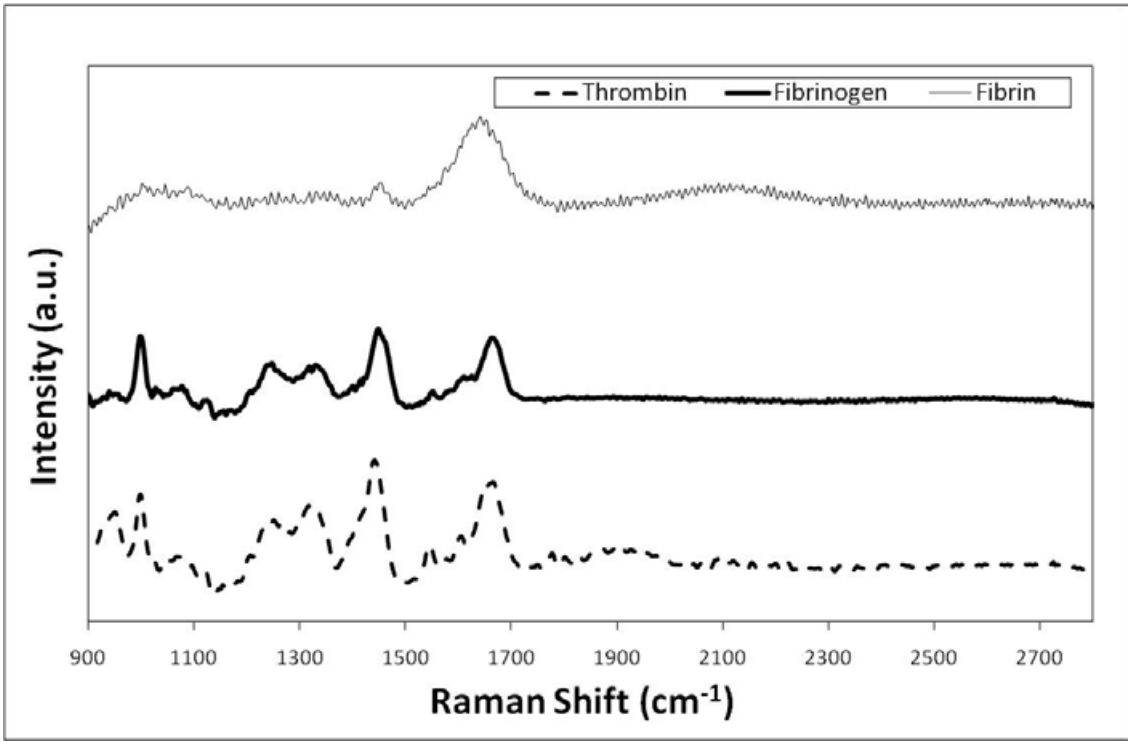

Figure 5.4 Raman spectra showing vibrational frequencies for thrombin (solid line), fibrinogen (bold solid line) and fibrin (dashed line).

Whilst definition of Raman peak intensity is difficult, an outline has been established of the chemical bond presence for the proteins and an initial insight into the gelation behaviour of fibrin through the formation of α-helix coils. It has previously been mentioned that thrombin is an important factor in governing gelation behaviour whereby changes in the concentration of the clotting agent affect the gelation time of the gel. It should be noted that the formation of fibrin is commonly referred to as clotting, owing to the nature of its formation in the body after an injury, therefore both agglomeration and clotting will be used to describe the same process. Figure 5.5 shows that as the concentration of thrombin is increased, the gelation time for fibrin decreases. Similarly to carrageenan gelation as the concentration of the cation is increased (Figure 4.3), the availability of thrombin per fibrinogen chain unit has increased, thus allowing fibrin monomers (depicted in Figure 5.3) to form sooner.

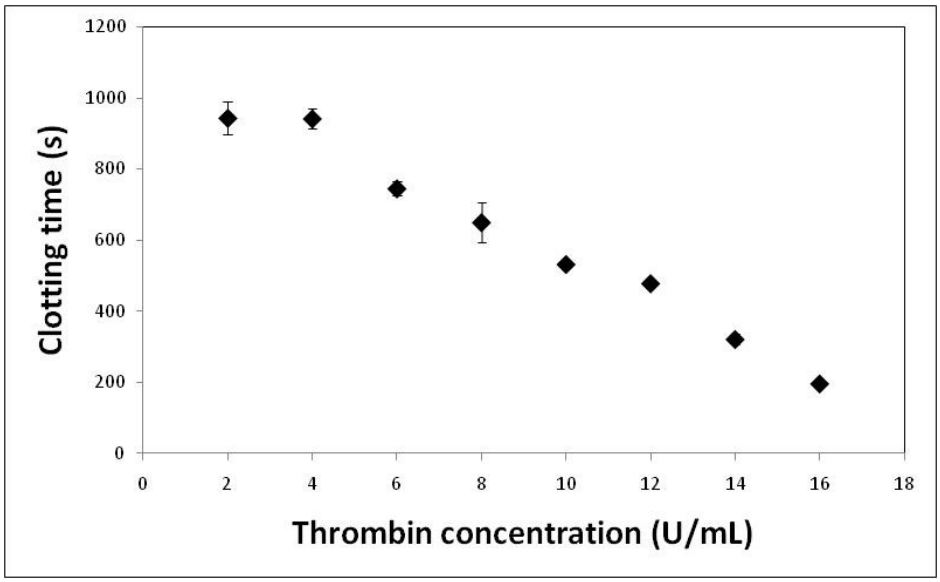

Figure 5.5 The effect of thrombin concentration on the clotting time of fibrin at 37°C. The error bars shown represent the standard error of the mean.

Whilst a change in the clotting behaviour of fibrin is evident from Figure 5.5, the structure of fibrin, as previously described, would also vary considerably. Figure 5.6 shows scanning electron microscopy (SEM) images of fibrin gels formed with an increasing concentration of thrombin. It can be seen that as the concentration of thrombin is increased the fibril morphology changes from being short, thick fibres to long thin fibres. This has previously been demonstrated by Zhao *et al.* (2008) who proposed that the change in fibril morphology was due to a faster fibrinopeptide cleavage rate which leads to a shorter clotting time. However, it was also stated that as the thrombin concentration is increased the network becomes tighter and therefore the porosity decreases. Contrastingly, although the actual porosity was not calculated for the gels, it can be seen from the images in Figure 5.6 that the thin fibril arrangement (Figure 5.6D) leads to a very

porous network. This can be explained by the fact that as the thrombin concentration is increased, the fibrinogen concentration decreases. This decrease in fibrinogen chains available leads to fewer monomers forming, fewer protofibrils and subsequently a primarily loose network. Ultimately, more test methods would be needed to show this as the dehydration steps of the SEM process affect the size of the fibres and although attempts have been made to estimate the actual fibre size in fibrin networks, no definitive measurement exists for either the fibre size or the spacing between individual fibres (Pedersen and Swartz 2005) as fibres interweave making it difficult to view an entire fibre end-to-end. The complex structural properties of fibrin and variation in forms, induced by changes in gelation kinetics allow fibrin to be manipulated in a way in which the gel is composed of thick fibers or thin fibers which in turn may be used for different purposes.

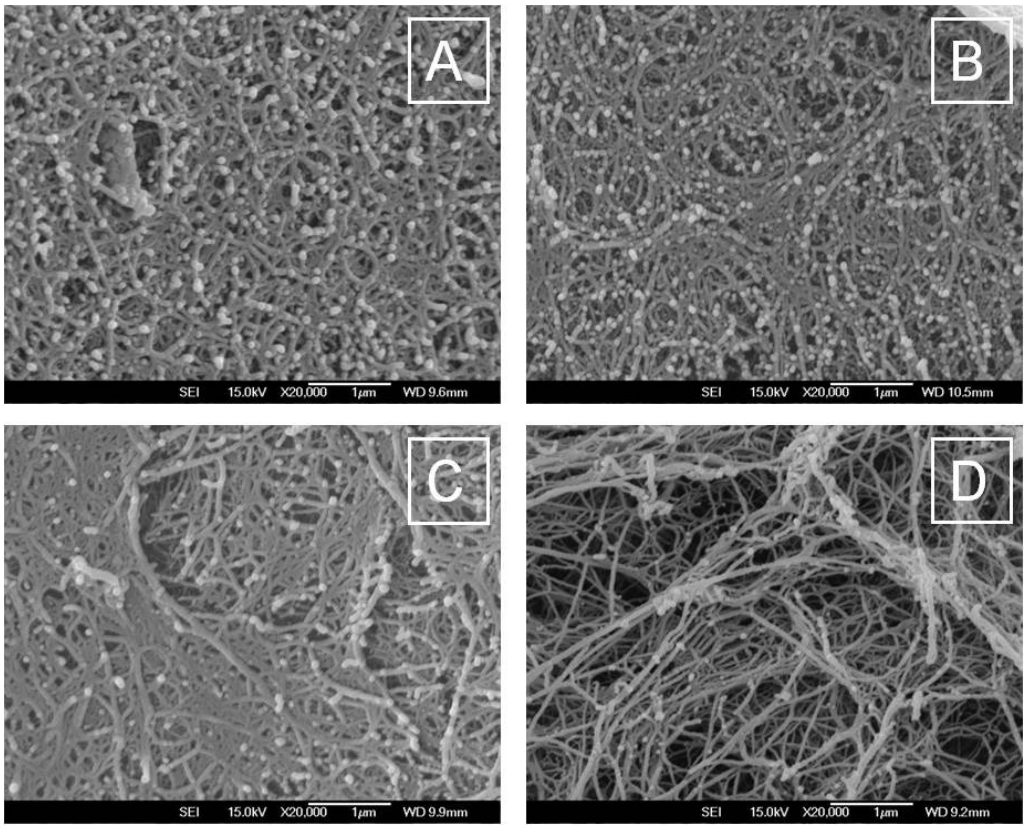

Figure 5.6 SEM microstructure of fibrin gels clotted with 20% v/v thrombin (A), 40% v/v thrombin (B), 60% v/v thrombin (C) and 80% v/v thrombin (D).

The effect thrombin concentration has on the structure of the final gel formed, especially the porosity, affects gels structure which also affects the degree of swelling, i.e. the ability of the fibrin network to expand and absorb nutrients when in solution. Figure 5.7 shows the water uptake ratio, calculated by the change in mass over time, at 37°C which is the temperature at which cellular experiments are conducted. These results have been collated on the assumption that the gelled network swells uniformly in all directions. It can be seen from the results shown in

Figure 5.7 shows that the water uptake ratio decreased with time up until 9 h by which point a constant level was reached. A proposed hypothetical mechanism is as follows. The initial decrease may be caused by relaxation of the porous scaffold structure as it becomes hydrated. As it does so it is possible that the larger molecules from the DMEM in which the thrombin and fibrinogen are initially dissolved leach out of the network. Once the network is fully expanded, trapped larger molecules leave the network and equilibrium is reached, the gel cannot take up any more water and a constant weight is achieved. This suggests that gel morphology and indeed the volume of the gel after introduction to solutions changes significantly and will impact on the final size of scaffold needed. Thus, the uptake of solution is equally as important as the ability of the gel to contract upon cellular introduction to the network although the phenomenon would need further investigation, especially below the 2 h time point where currently the immediate effect of gel submersion in water has not been studied.

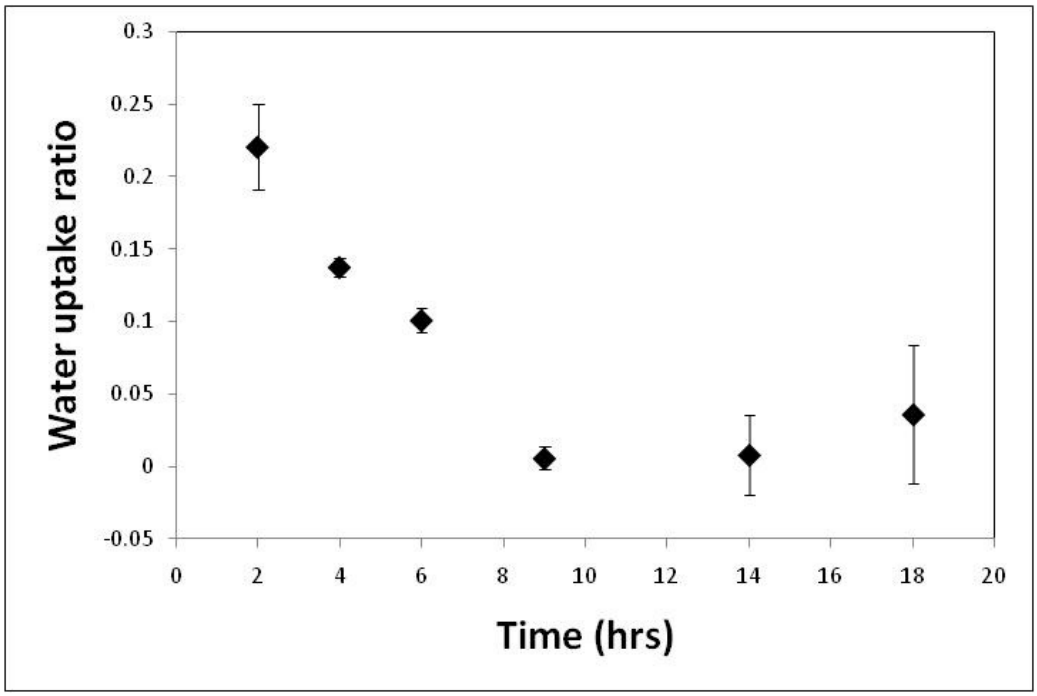

Figure 5.7 Water uptake ratio for fibrin gel at 37°C. All gels were produced in 12-well tissue culture plates. The error bars shown represent the standard error of the mean.

Furthermore, as shown in the previous chapter, the degradation of the potential scaffold is an important issue to consider as loss of scaffold mass must be proportional to cellular proliferation. *In vivo*, the natural degradation of fibrin occurs via fibrinolysis, by the enzyme plasmin, and its degradation products are cleared by the kidneys and liver (Gans and Lowman 1967). This degradation may take anywhere between a few days to a few weeks (Schenes and Hubbell 1999) and a lack of degradation can lead to illnesses such as acute renal failure (Wardle and Taylor 1968). It is evident from Figure 5.7 that during the first 9 h after immersion in liquid, the gelled network uptakes water and expands. In doing so, it is necessary to investigate the effect

submersion has on the structural integrity of clotted fibrin and more importantly whether the excess liquid causes the structure to become weaker. Figure 5.8A shows that there was no change in the mass of fibrin after submersion in water, presented as a continuation of the data accumulated in Figure 5.7, DMEM and PBS whilst Figure 5.8B, C and D show that by day 28 these acellular gels all maintained structural integrity and were strong enough to support their own weight after submersion in all three liquids. DMEM and PBS were included in the study as they are solutions typically used for the maintenance of cell cultures. The fibrin structure maintains its integrity for 28 days (Figure 5.8), the minimum time required for fibroblastic cells to go through a complete life cycle (Figure 4.8). Although the structure remains stable under the conditions specified, long-term stability needs to be considered. Should the structural integrity decrease prematurely, research suggests that the stability may be enhanced by increasing calcium concentrations which accelerates the formation of fibrin and protects the structure against proteolytic digestion and denaturation through heat (Yee *et al*. 1997).

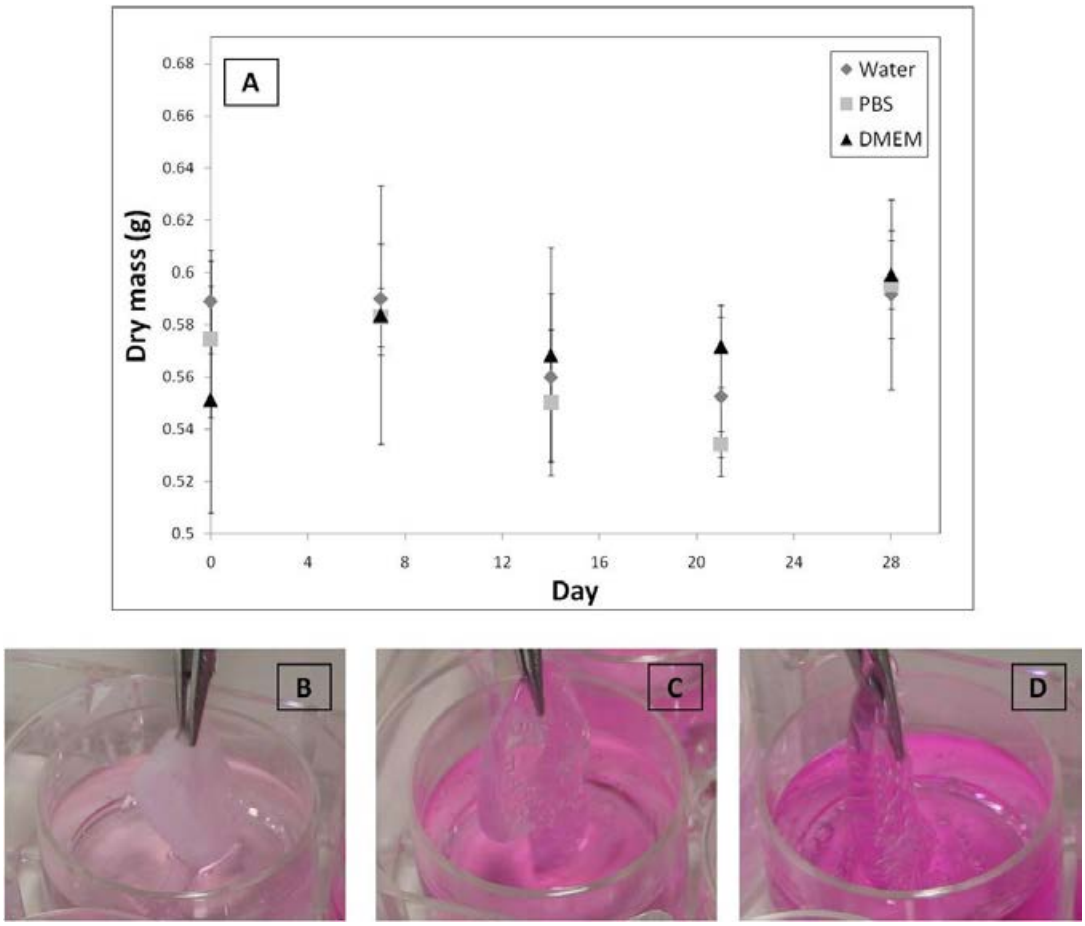

Figure 5.8 Degradation of acellular fibrin gel at 37°C in water, PBS and DMEM (A) and images of self-supporting fibrin structures after 28 days in water (B), PBS (C) and DMEM (D). All gels were formed in 12-well cell culture plates. The error bars shown represent the standard error of the mean.

Indeed, as previously mentioned, manipulation of fibrin has been shown to increase the degradation time to several months (Linnes *et al*. 2007). Furthermore, although upon observation (Figure 5.8B, C and D) the fibrin gels appear to maintain their structural integrity for 28 days

under solution, it is necessary to study the mechanical stability of the gel, especially as previously stated (Figure 5.6) the gel varies considerably in structural morphology once thrombin concentration is altered.

Figure 5.9 shows the gelation kinetics of acellular fibrin at a thrombin concentration of 5 U/mL, 20 U/mL and 40 U/mL. Figure 5.9A depicts the storage modulus whereas Figure 5.9B shows the corresponding loss modulus. It is evident from Figure 5.9 that the modulus at 3453s (58 min) is similar with all three concentrations used (1263 Pa as shown in Figure 5.9A and 757 Pa as shown in Figure 5.9B). This would suggest that the thrombin concentration makes little difference to the gelation time of fibrin. However, this does not correspond with morphological changes observed using SEM (Figure 5.6) where the fibres are seen to become thinner and longer with fewer junction points as the concentration of thrombin is increased. For such a morphological change some mechanical differences were expected, whereby the availability of higher concentrations of thrombin would allow clots to form faster as the fibrinopeptides are cleaved sooner and fibril formation occurs sooner. It is perhaps that the modulus of fibrin gels at increased concentrations also increases or that the images presented in Figure 5.6, as discussed earlier, are not a true representation of the gelled structure due to loss of liquid. Further characterisation and determination of liquid loss is needed, perhaps by a thermoanalytical technique such as differential scanning calorimetry.

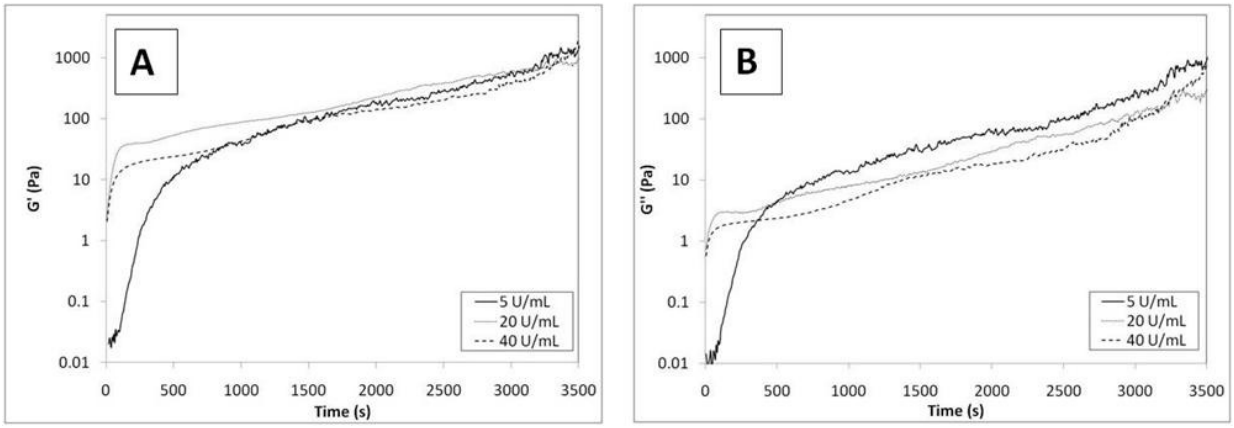

Figure 5.9 Storage modulus (A) and loss modulus (B) for fibrin over 1h at thrombin concentrations of 5 U/mL, 20 U/mL and 40 U/mL.

In order to investigate the modulus, one concentration (20 U/mL) was used. Figure 5.10 shows the storage and loss modulus for the acellular fibrin gel with an increasing angular frequency. It can be seen that in its acellular form, the scaffold exhibits a low storage modulus of 7 Pa at an angular frequency of 7 rad/s and 54 Pa at an angular frequency of 315 rad/s in comparison to other hydrogel scaffolds used for tissue engineering (Zustiak and Leach 2010). Zustiak and Leach reported a storage modulus of 5 kPa for a poly(ethylene glycol)-based gel at an angular frequency of 7 rad/s. It is the proliferation and subsequent attachment of cells within the matrix which would increase the modulus as the network is held tightly together. Rheological studies of cellular gels were not possible as the gel geometry was inconsistent between samples due to irregular contraction. Controlling the contraction rate would introduce further variables, such as inhibitors, making the study complex. Uninhibited contraction of cellular fibrin could not be measured using conventional rheometer plates available. In order to study the rheological

properties of cellular contracting gels, equipment with microNewton force sensitivity and micrometer displacement sensitivity would be needed (Cheneler 2010).

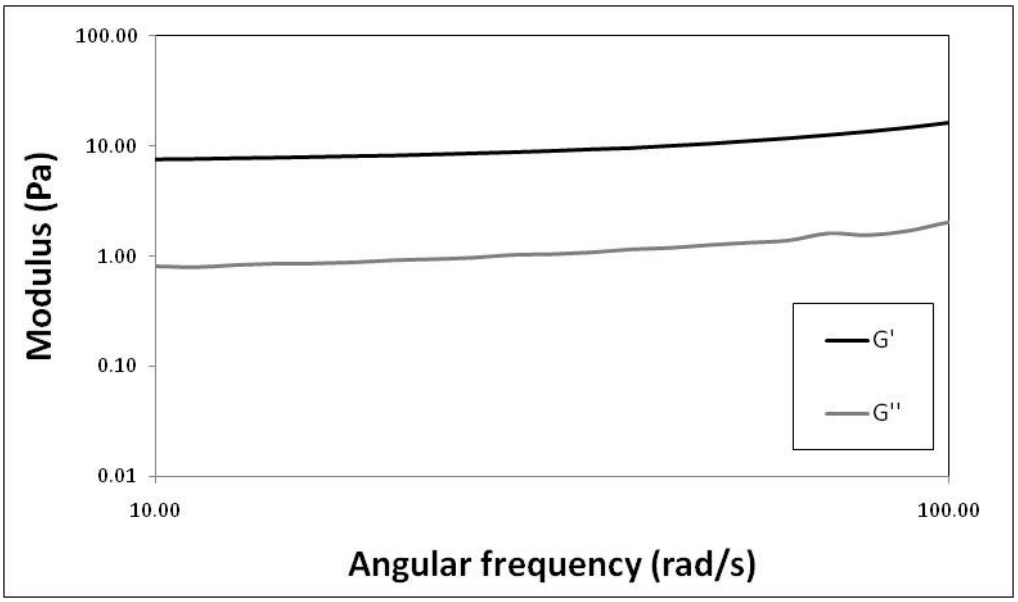

Figure 5.10 Storage and loss moduli for fibrin gel with increasing angular frequency.

The attachment and proliferation of cells on the scaffold is an important issue to consider in tissue engineering. As a preliminary investigation, the pull-off force, an indicator of adhesion force (described in Figure 4.7 using a 6 µm colloid probe) for acellular fibrin was measured. The pull-off force for fibrin gel was found to be 6.37 ± 0.10 µN. This pull-off force is similar to 2% w/v *κ*-carrageenan (6.32 ± 0.09 µN) whereby it was believed that the values may be explained by force interaction between the SiO_2 probe and the gel surface. However, it should be noted that

whilst these values may be similar for κ-carrageenan and fibrin, cells seeded on fibrin can cause extensive contraction of the scaffold thereby causing further structural changes within the network.

After assessing the mechanical integrity of fibrin, it's clotting behaviour and preliminary forces governing adhesion of cells to the gel, it is necessary to encapsulate cells within the gel matrix to ascertain compatibility and cellular morphology *in vitro*. As previously discussed in Chapter 4, all cells have a typical growth curve. For tendon and ligament engineering the cells of choice are tenocytes. Figure 5.11 shows a typical growth curve for tenocytes with the stationary phase beginning at day 7 and ending by day 21. These phases have previously been described in Figure 4.8. It is noted that experiments involving tenocytes will have to be conducted for a minimum of 21 days to ensure that the peak metabolic activity is recorded, after which natural cell death is to be expected. Should cell death occur before 21 days it is reasonable to assume that factors other than normal cell growth are affecting their behaviour.

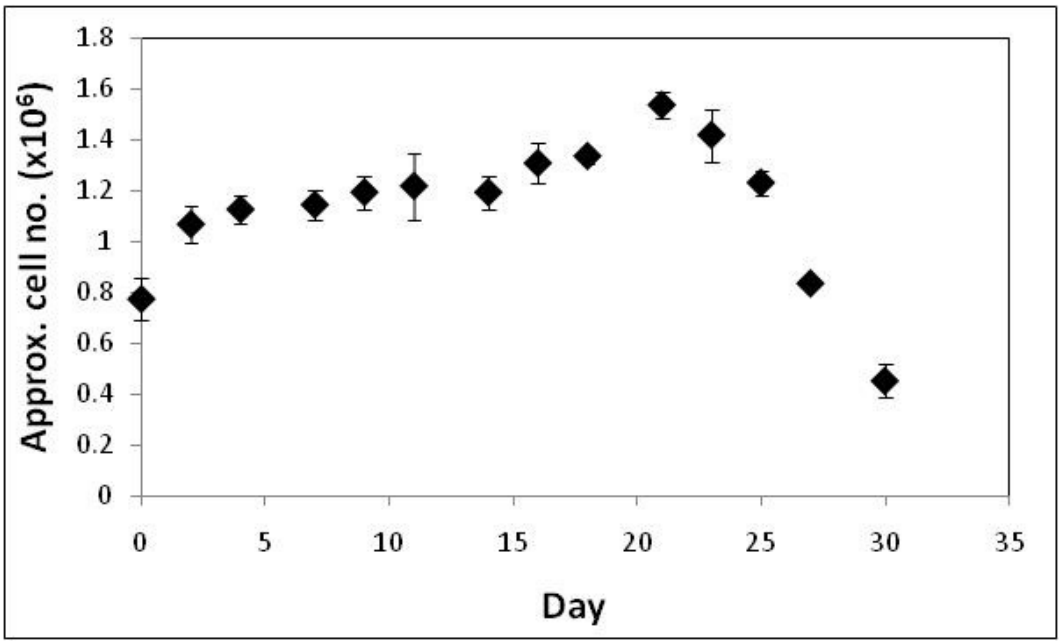

Figure 5.11 An MTT growth curve for isolated murine tenocytes showing a typical life cycle of the cells at passage 3 from isolation. The error bars shown represent the standard error of the mean.

After investigating the basic principles of tenocyte growth behaviour, rat tail tenocytes were encapsulated within fibrin and morphological changes were studied over a 28 day time frame. For comparative purposes NIH 3T3 murine fibroblasts were also encapsulated within the gel matrix (Figure 5.12). It was found through SEM imaging that initial attachment of 3T3 cells (Figure 5.12A) is more pronounced than for tenocytes for the same incubation period (Figure 5.12K). Attachment of the cells to the gel matrix is seen by the presence of elongated cells (>20µm in length). Live/ dead images for the same cells and incubation periods (Figure 5.12F and P) show that there is a higher number and a more even distribution of living cells, represented by the

green colour, visible for tenocytes in fibrin (Figure 5.12P). Furthermore, as cellular attachment and proliferation increases in both sets of images (Figure 5.12B-E and L-O) over the 28 days, an increase in cell number through fluorescence microscopy, Figure 5.12F-J and P-T, is also seen. The value of live/ dead fluorescent imaging is evident in Figure 5.12 where although cellular attachment is presented in Figure 5.12A-E and K-O, it is easy to assume that all cells viewed are indeed alive. However, it may be noted in Figure 5.12F-J and P-T that whilst NIH 3T3 cells proliferate, producing healthy cells (represented by the green colour) in fibrin, the same images for tenocytes encapsulated in fibrin show a higher proportion of red cells, i.e. dead cells. However, actual metabolic rate, and therefore cellular function, cannot be estimated from microscopy images alone. Furthermore, it is difficult to evaluate the attachment of cells to hydrogels due to their highly hydrated nature. Problems with visualising cellular morphology using SEM (Figure 5.12A-E and K-O), for example, include the collapse of the sample structure, caused by the fixation and dehydration process, thus producing an image which is not a true representation of the highly hydrated structure expected.

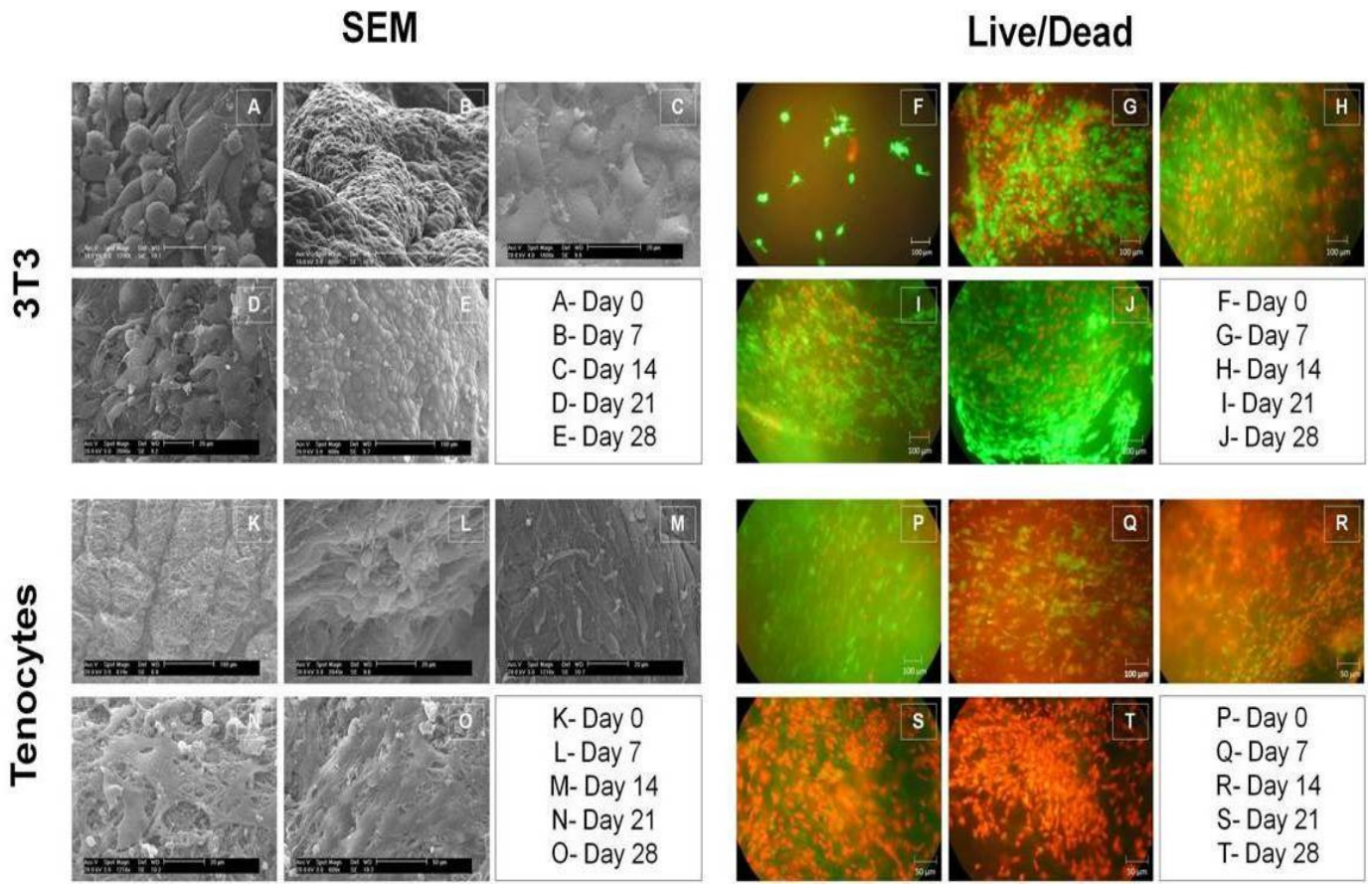

Figure 5.12 SEM and live/ dead images for NIH 3T3 murine fibroblasts (A-J) and rat tail tenocytes (K-T) encapsulated in fibrin gel over 28 days.

In order to obtain quantitative data for cell viability, a 3-(4,5-Dimethylthiazol-2-yl)-2,5-diphenyltetrazolium bromide assay (MTT) was used. The results of this assay are presented in Figure 5.13. Again for comparative purposes, the metabolic activity of both NIH 3T3 and tenocytes encapsulation has been presented on the days shown in Figure 5.12. Calculations of the approximate number of living cells in the gel sample from an absorbance standard show that whilst the NIH 3T3 cells follow their expected growth curve, demonstrated in Figure 4.8, and reach the stationary phase by day 14 (Figure 5.13A), the maximum viable cell number is estimated to be 9×10^5 in comparison to an almost 6-fold increase (5×10^6) in the number of viable tenocytes seen on day 7 after encapsulation (Figure 5.13B). Day 7 is within the stationary phase of tenocyte growth as seen in Figure 5.11. Whilst this initial spurt of cellular growth for tenocytes is observed, it is seen that by day 21 the number of viable cells has dramatically decreased to 5×10^5 (Figure 5.13B) whereas on day 21 for the NIH 3T3 cells the number has decreased only slightly and is estimated to be 7×10^5 cells (Figure 5.13A). The data presented in Figures 5.12 and 5.13 suggest that whilst cellular attachment and proliferation is seen for NIH 3T3 and tenocytes encapsulated in fibrin gel, the NIH 3T3 cells only achieve an estimated 1 million cell population in comparison to tenocytes where cell proliferation reaches approximately 5 million. However, the high growth is short-lived and the number of viable tenocytes in the gel drops within 3 weeks. It is perhaps the initial increase in cells which has lead to this sudden drop as the fibrin gel degrades with increased matrix enzymes and there is little room for cellular proliferative activity on diminishing scaffold material. As mentioned in the previous chapter, surface area for cell migration is necessary for growth. Furthermore, the high number of cells would also deplete the nutrient supply sooner in comparison to the NIH 3T3 cells. Therefore, as

the availability of nutrients diminishes and toxic by-products build up, the cell death phase is reached sooner (Figure 5.11) in comparison to cells where there is less competition for nutrients, as is the case for the NIH 3T3 cells.

For the MTT data collected, only an approximate metabolic rate may be presented. The absorbance readings from which the cell number has been calculated assumes that all cells within the sample measured had an equal mitochondrial dehydrogenase activity and therefore there was no variation in the physiological state of the cells present.

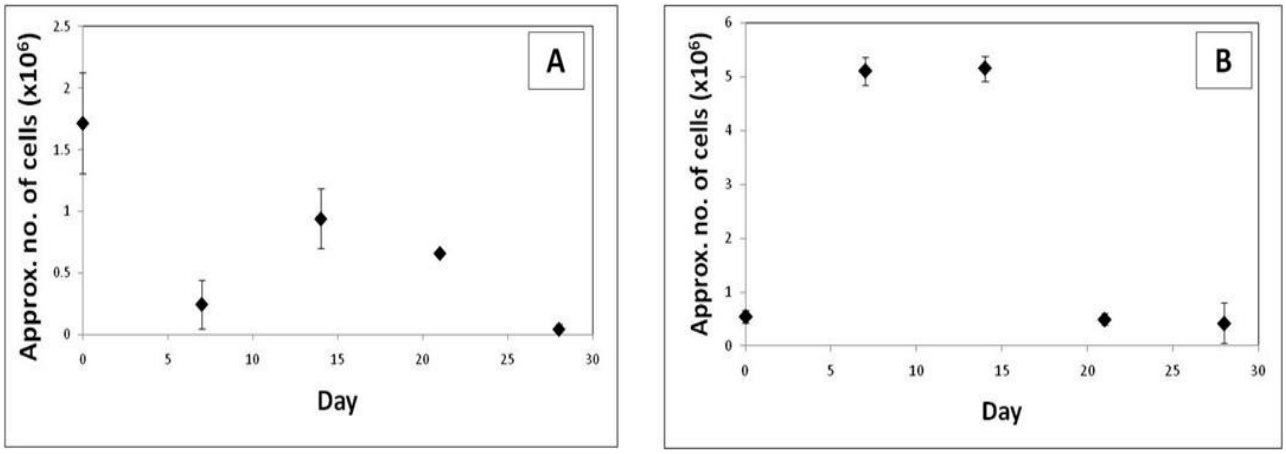

Figure 5.13 Approximate number of viable NIH 3T3 murine fibroblasts (A) and rat tail tenocytes (B) encapsulated in fibrin gel over 28 days. The error bars shown represent the standard error of the mean.

Whilst it has previously been mentioned that cellular fibrin gels are subject to contraction, it should be noted that measurement of the contraction rate is extremely difficult. Previous researchers have used digital observational methods (Rowe *et al*. 2007) or measurement through calipers or digital indicators (Tuan *et al*. 1996) to estimate the contraction. Whilst attempts were made to estimate the contraction rate using digital calipers, it was noted that the modulus of the gels was of such a low value that even when care was taken, the perimeter of the gel was inevitably squeezed by the caliper ends and therefore a true measurement was not possible (Figure 5.14B). Furthermore, it was noted that with no external restraints, the gel contracted in all directions and rarely by the same amount for different samples under the same conditions (Figure 5.14C). This is because cell proliferation is not uniform in all instances. As the cells grow and proliferate, adhesion to the fibrin fibres pulls the network, reducing the space taken up by liquid, and if there is insufficient physical restraint, the gel contracts in all directions, as is the case here.

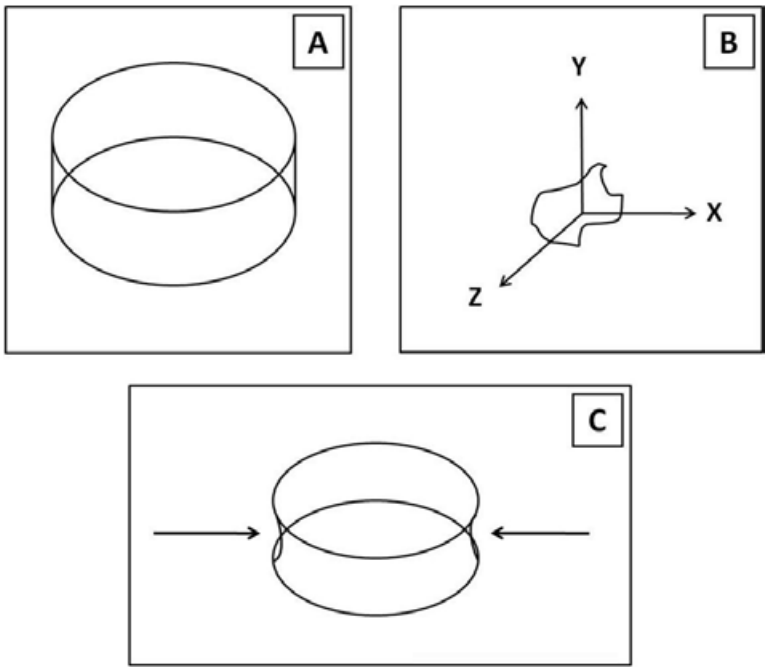

Figure 5.14 Diagrammatic representation of a crosslinked fibrin gel disc (A), irregular contraction (B) and deformation caused by calipers (C).

Digital observational methods, macro and micro level photography, was attempted with little success (Figure 5.15). It was found that the gel was difficult to photograph under solution whilst maintaining sterility (Figure 5.15A) and attempts at photographing the edge of the gel often lead to manufacturing imperfections in the plastic cell culture plate being wrongly imaged (arrow showing manufacturing error in Figure 5.15B). An ideal situation, out of the realms of the equipment available for this study, would be to have photography equipment in a sterile environment, such as the CO_2 incubator where cellular incubation and proliferation would facilitate gel contraction.

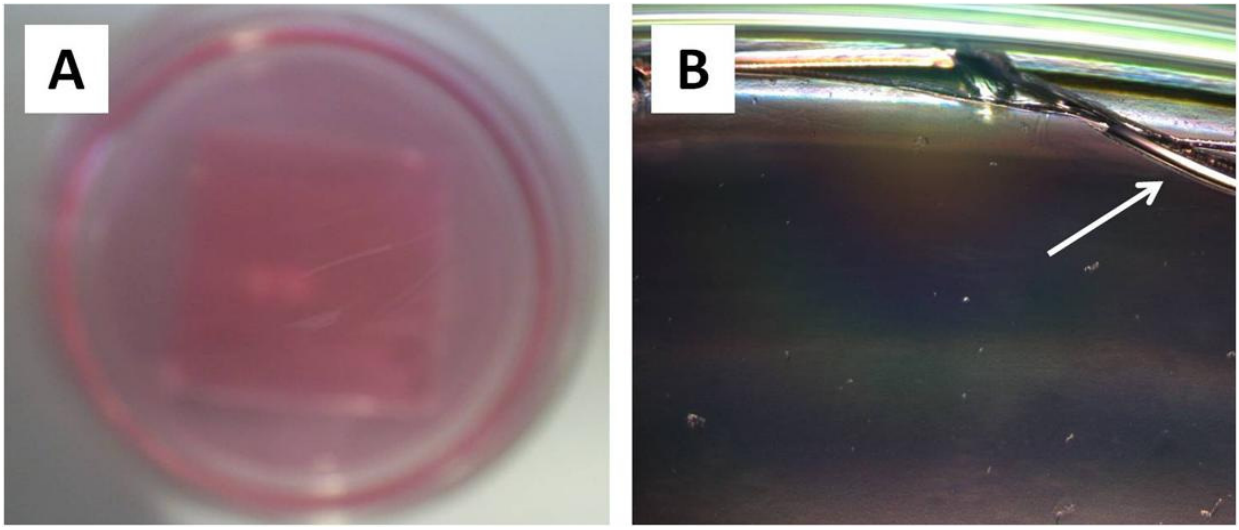

Figure 5.15 Attempts at photographing the contraction of cellular fibrin gel using a hand-held digital camera (A) and digital camera attached to a microscope (B). The arrow indicates an imperfection in the manufacture of the well plate.

Finally, a comparison was made to investigate the effect of cell encapsulation on fibrin degradation. This was compared to acellular fibrin gels (Figure 5.16). Whilst there is no statistical difference in the mass of the acellular fibrin gels over 28 days, gels containing tenocytes was shown to degrade by a minimum of 0.2 g over the same number of days. This is primarily due to the sudden increase in the proliferation of tenocytes by day 7 (Figure 5.13) which causes proteolytic degradation through an increase in the amount of ECM present, and therefore proteinases. It has been suggested that fibrin degradation *in vitro* may be controlled by incorporating enzyme inhibitors, such as ε-aminocaproic acid (Ahmann *et al*. 2010) or aprotinin (Smith *et al*. 2007), within the matrix. In order to investigate this further, characterisation of the

ECM products is needed. It should be noted that a repeat of this study is necessary and for a longer period as it appears as though fibrin containing tenocytes increases mass by the end of the study. A true trend may only be apparent over a longer period of time.

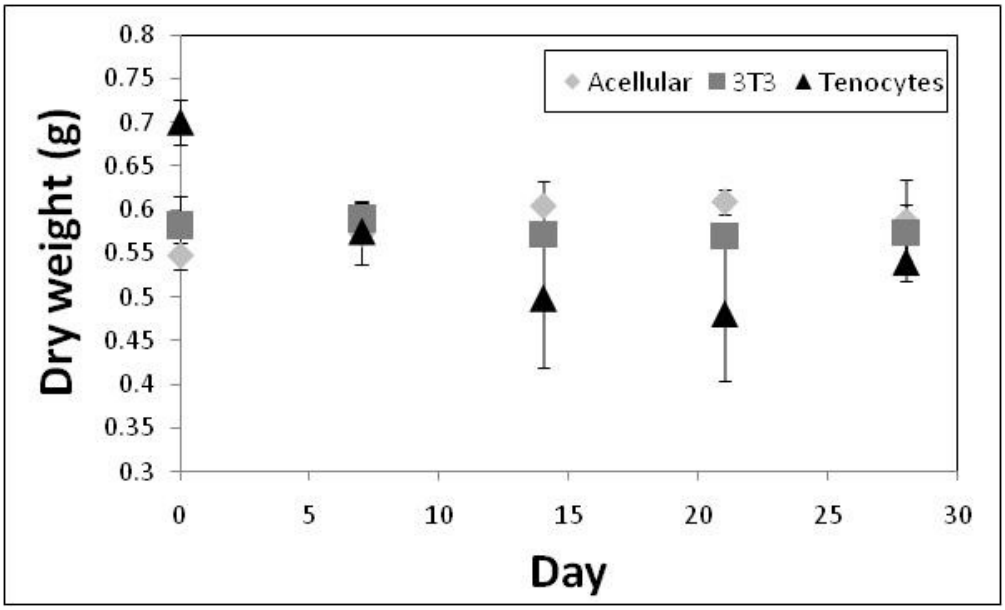

Figure 5.16 Degradation of acellular fibrin and with NIH 3T3 murine fibroblasts and rat tail tenocytes encapsulated within the matrix over 28 days. The error bars shown represent the standard error of the mean.

Whilst modifications to the gel network are entirely possible in order to enhance specific criteria, such as mechanical integrity, functionality of the cells is severely compromised by changing any of the previously mentioned factors (Linnes *et al*. 2007). In the study by Linnes *et al*. (2007), the

addition of the natural crosslinker extracted from the gardenia fruit, genipin, was used to increase the mechanical strength of fibrin gels. Furthermore, decreasing the thrombin concentration increases the size of the fibre bundles (Figure 5.6), introducing high porosity to the scaffold which allows free exchange of nutrients within the gel, a clotting time ideal for cell entrapment (Zhao *et al*. 2008) and an increased mechanical strength (Rowe *et al*. 2007). It is now believed that fibrin gels are initially weak (Linnes *et al*. 2007) and are often cultured with growth factors, or mixed with polymers and knitted fabrics to increase their strength (Weisel *et al*. 2004). This weakness in structure may be due to the fact that in a fibrinogen clot *in vivo*, only 0.25% of the total volume is fibrin with the rest being liquid occupying the large spaces between the fibre-forming protofibrils and the fibrin fibres themselves (Weisel *et al*. 2004).

5.3 Conclusion

This chapter sought to investigate the use of fibrin as potential tendon and ligament scaffold. To this end it was found that the crosslinking agent, thrombin, decreased the clotting time of fibrin as its concentration was increased. The change in clotting behaviour of fibrin, through changes in the thrombin concentration, was found to also affect the morphology of the network as well as the thickness of the overall fibres formed.

As the thickness of the fibres was shown, through SEM, to cause variation in pore morphology, it was noted that nutrient diffusion and cellular mobility would also be affected. The swelling behaviour of fibrin was assessed by investigating the water-uptake ratio of the gel. It was proposed that the initial decrease in the water-uptake ratio was caused by relaxation of the

network, allowing larger non-crosslinked molecules initially trapped in the network to leach out. This was followed by a constant water-uptake ratio, after 9 h whereby equilibrium is reached. This swelling behaviour did not affect the integrity of the gel over 28 days.

Cellular behaviour in fibrin gel was assessed by murine 3T3 encapsulation and isolated tenocyte encapsulation. It was found that initial growth is higher for tenocytes encapsulated in the gel. The growth of murine fibroblasts within the gel did not affect the degradation rate of the gel over 28 days. However, tenocyte encapsulation caused a 0.2 g decrease in the overall gel mass over 28 days.

It has been shown that fibrin is a highly versatile gel which has many current applications and promising future possibilities through modifications of the two part network, fibrinogen and thrombin. The ease of manipulation and exploitation of versatility and adaptability suggest that fibrin may be ideal as a potential scaffold material for the development of tenocyte-rich tendons and ligaments.

CHAPTER 6: UTILISING 3D POWDER PRINTING TECHNOLOGY TO PRODUCE CALCIUM PHOSPHATE BASED SCAFFOLDS

Characterisation techniques have previously been employed to investigate factors affecting gelation properties and structural changes within a fibrin scaffold used to tissue engineer tendons and ligaments. Furthermore, mechanical testing on the gels was performed in addition to cell compatibility studies to assess structural integrity and compare the viability of NIH 3T3 murine fibroblasts and isolated rat tail tenocytes. Fibrin was found to be suitable for soft tissue engineering owing to its versatility and the relative ease by which it can be structurally manipulated. In order to explore its potential as a fully functional ligamentous scaffold, it is necessary to study the interaction the soft tissue would have with hard tissue, i.e. at the enthesis. Here we investigate the use of 3D powder printing technology to produce CaP based bone scaffolds and subsequent characterisation of the printed structures.

6.1 Introduction

Bone may be healed natively after injury through remodelling, a process of breakdown and resorption via osteoclasts, reversal with mononuclear cells appearing on the surface and formation of ECM through osteoblasts (Jacobs 2000 and Hadjidakis and Androulakis 2006). The

replacement of bone is required when the extent of injuries is so great that treatments such as plate fixation (Porter *et al*. 2009) are insufficient in repairing the defect. Such deformities may be caused by an abnormal development of bone, such as Apert syndrome in which the fingers and toes are fused (Yang *et al*. 2008), by diseases such as osteoporosis and osteoarthritis (Porter *et al*. 2009 and Seong *et al*. 2010) or by trauma (Jabbarzadeh *et al*. 2008). Current methods of gross bone loss repair include allografts, autografts and xenografts. Whilst autografts are the most popularly used method of bone tissue repair, problems include donor site morbidity, long operating times, risk of infections at the harvest site and loss of function resulting in a permanently altered gait (Silber *et al*. 2003). Problems with allogenic bone, sourced from cadaveric or living donors (Cahn 2000) and xenografts, bone grafts taken from a different species, lie primarily with disease transmission (Laurencin and El-Amin 2008).

With all current methods of repair having a number of limitations, it is necessary to search for an alternative method of bone replacement. Consequently, a lot of research has focussed on the development of synthetic materials to replace bone. Biomaterials required for bone substitution need to match certain criteria exhibited by native bone, such as osteoinductivity and osteoconductivity, low inflammatory response and the ability to promote new bone formation (Takahashi *et al*. 2005).

Utilising synthetic scaffolds to eliminate risks of disease transmission, immunogenicity, long operating procedures and the number of procedures is one route of bone repair and regeneration. Materials such as polymers and ceramics have been used extensively for regenerating bone (Yoshikawa and Myoui 2005). Ceramics based on CaP are physicochemically similar to the mineral component of native bone (Porter *et al*. 2009) and have previously been used to repair

bony defects (Albee 1920), replace dentine (Aoki *et al*. 1977), and as graft material (Bohner *et al*. 2005 and Gross and Berndt 2002). It is the favourable cellular response *in vitro* and *in vivo* which has prompted the use of a variety of CaPs such as hydroxyapatite ($Ca_5(PO_4)_3(OH)$), brushite ($CaHPO_4.2H_2O$) and tricalcium phosphate ($Ca(PO_4)_2$) as potential bone replacement materials. Brushite, also known as dicalcium phosphate dihydrate, forms at a pH below 4.2 and has a higher resorption rate than hydroxyapatite (Lim *et al*. 2009 and Pina and Ferreira 2010) as it is sparingly soluble in physiological conditions.

Brushite is formed from the reaction of β-TCP with an acidic source of phosphate ions, such as phosphoric acid, as depicted in Equation 6.1.

$$Ca_3(PO_4)_2 + H_3PO_4 + 6H_2O \longrightarrow 3CaHPO_4.2H_2O \qquad (6.1)$$

The formation of brushite is rapid. Above 50°C brushite loses water of crystallisation to form monetite (Klammert *et al*. 2009). At the point of setting, brushite cements are acidic since dicalcium phosphate dihydrate precipitation requires solutions below pH 6 (Pina and Ferreira 2010). Eventually, through a dissolution and reprecipitation process, brushite forms the less soluble hydroxyapatite (HA) which degrades slowly due to low fluid exchange within the ceramic pores (Calafiori *et al*. 2007). Proteins from foetal bovine serum have been shown to inhibit the formation of HA and so degradation of brushite continues.

The fabrication of CaPs needs to be accurate for reproducibility and rapid to minimise the time required for manufacture. Computer-aided manufacturing techniques for scaffolds such as rapid prototyping, also known as solid freeform fabrication, are becoming increasingly popular due to ease of manufacture and accuracy (Sachlos and Czernuszka 2003; Bartolo *et al*. 2009 and Kim *et al*. 2010). Such methodologies, 3D printing, fused deposition modelling, 3D plotting and indirect rapid prototyping approaches (Salgado *et al*. 2004) involve the use of computer-aided design (CAD) to develop complex three-dimensional structures layer by layer. Advantages of using 3D printing over fused traditional systems include customised designs, precision manufacture and the ability to include biological materials, such as growth factors (Hutmacher 2000), within specified regions of the fabricated structure. Primary failures of fused deposition modelling, resin-curing stereolithography and selective laser sintering approaches require heat and ultraviolet mediated-fusion which cause protein denaturation within the scaffold and are prone to layer separation through presence of a 'seam' where the fabricated layers meet.

The thermosensitivity of rapid prototyping techniques is an area of much focussed research used to make the tissue engineering process quicker and more precise whilst tailoring tissues to specific wounds. Klammert *et al*. (2010) reported the use of 3D powder printing for the formation of magnesium ammonium phosphate, struvite, for bone replacement specifically with the intention of keeping the pH of the fabricated structures neutral. Previously Vorndran *et al*. (2010) have shown that 3D printing technology can be adapted to produce macroporous ceramic structures with localised delivery of bioactive drugs and proteins.

In this chapter 3D powder printing has been employed to produce CaP based structures for the intention of attaching a fibrin-based ligament scaffold (previously discussed in Chapter 5). The

cements produced have been characterised chemically, morphologically and their mechanical strength assessed under a compressive load. Changes to these characteristics have been monitored under cell culture conditions and the cellular compatibility of the scaffolds has been analysed. Selected results presented in this chapter have previously been published (see Appendix).

6.2 Results and discussion

CaP structures for this study were produced to investigate the capabilities of a rapid prototyping technique for precision printing bone scaffolds. The formation of CaP structures is shown in the diagrammatic representation in Figure 6.1B. Here it is shown that the process consists of a powder bed layer, in this case TCP, upon which a binder solution of 20% phosphoric acid is sprayed from a liquid reservoir in the geometry initially specified through a CAD drawing. As each layer is printed, a roller vertically compacts the layer and creates another powder layer above the bound TCP eventually producing a 3D structure. Figure 6.1A shows a disc and cylinder printed using this method. All printed structures were hardened in 20% phosphoric acid post-printing. This curing step is necessary to harden any unreacted powder on the outside of the monolith as it is lifted out of the powder bed. Traditional cement casting methods use a three-stage process of wax mould production followed by silicone mould production and finally filling with a cement paste to create specific structures, the geometry of which is limited by the original design of the wax mould (Paxton *et al*. 2010). The printing method outlined in this chapter eliminates the time consuming hand casting method whilst allowing large numbers of structures to be formed more accurately.

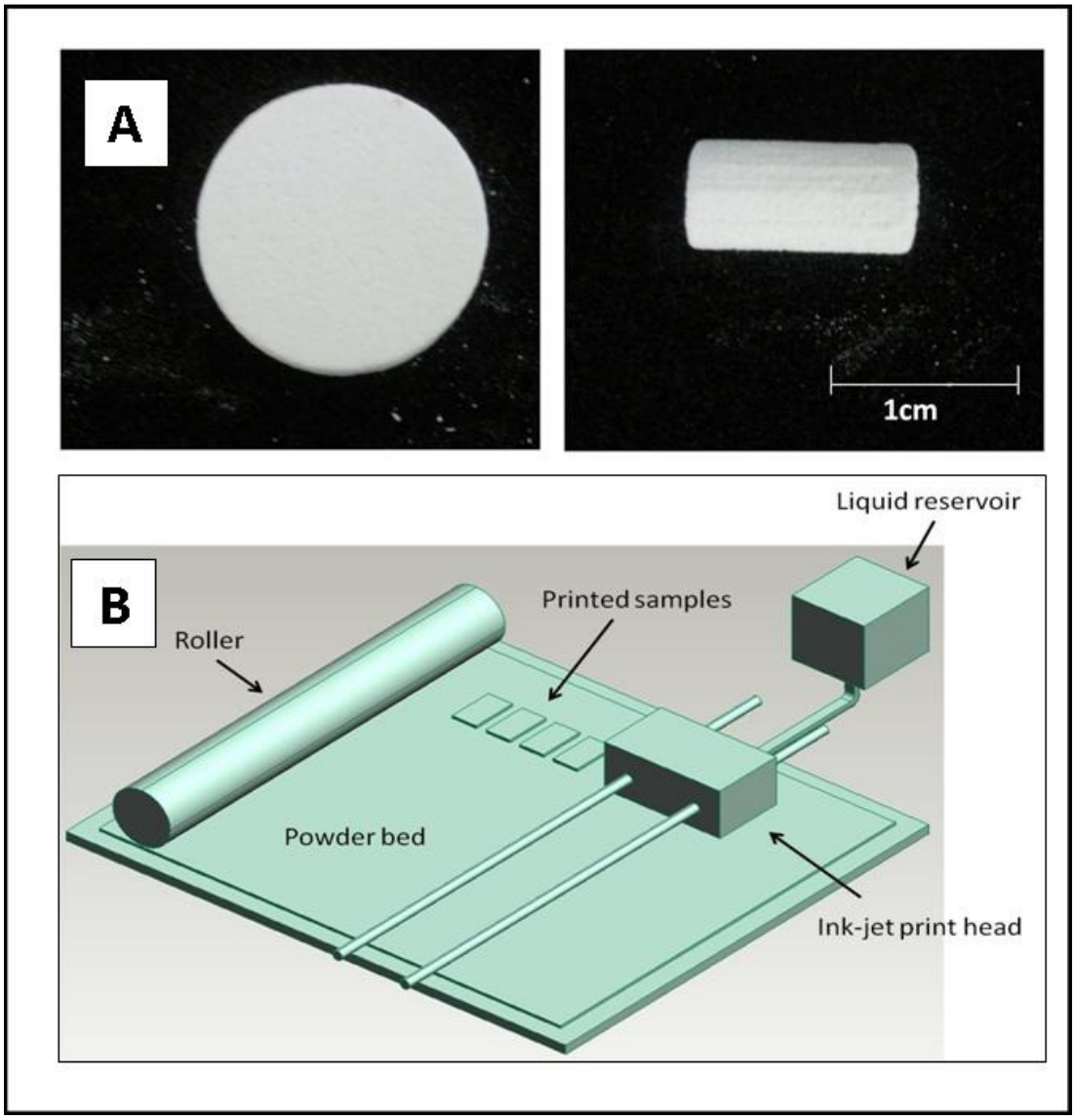

Figure 6.1 3D printed CaP disc and cylinder (A) and schematic of the printing process (B).

Upon investigation of the microstructure of the resultant monoliths it was found that whilst the raw powder used for the printing process, a mixture of α- and β-TCP, showed the presence of irregular particles alone (Figure 6.2A), both printed cylinders (Figure 6.2B) and printed discs

(Figure 6.2C) were structurally similar. Furthermore, both cylinders and discs showed the presence of long blade-like crystals, approximately 20µm in length and 2-5µm width, which is the morphology most frequently attributed to brushite (Bohner *et al*. 1996).

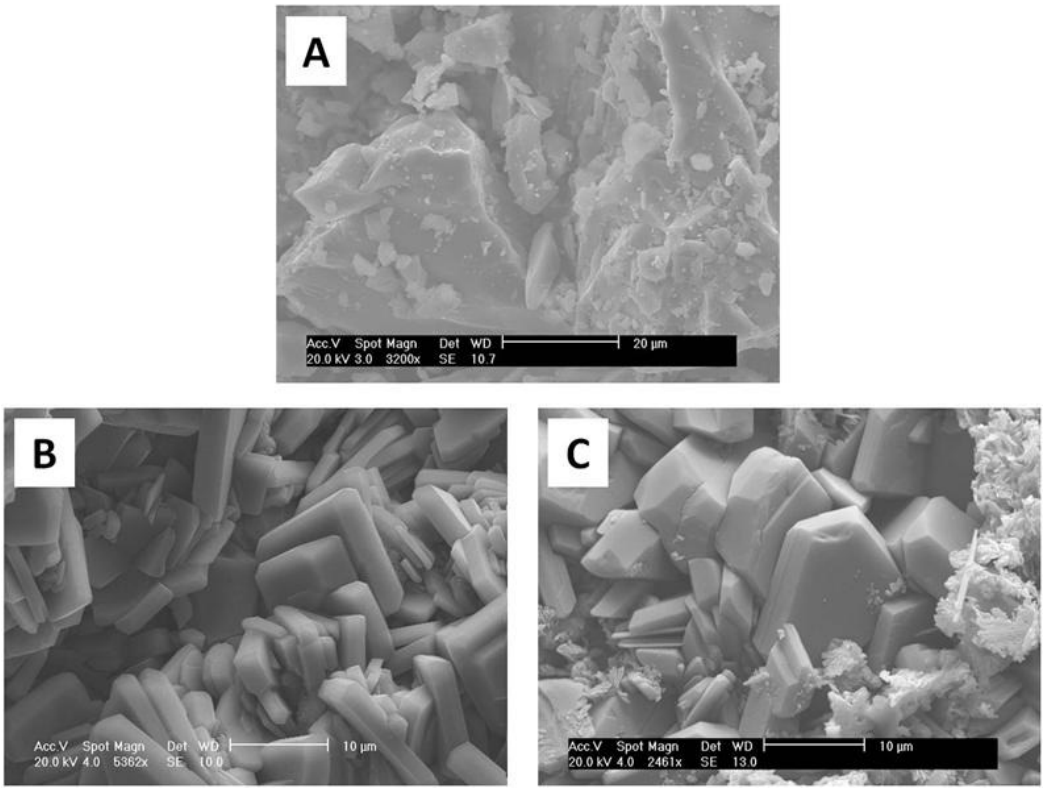

Figure 6.2 SEM images of TCP (A), a printed cylinder (B) and a printed disc (C).

The scanning electron micrographs of the materials were taken of fracture surfaces. Since the bulk and surface of cementitious materials has been shown to be significantly different, the

surface of the samples was characterised using white light interferometry. The surface properties of the material are especially important in this case, since cells seeded will be exposed to the surface rather than the bulk of the material. Figure 6.3 shows that an analysis of six separate areas on six printed discs yielded similar surface roughness values (an average of 17.4 ± 2.5 μm), similar to the size of the crystals as shown in Figure 6.2. This shows that the 3D printing process produces samples of consistent surface properties. This is to be expected as the printing process allows an even spray of acid to be deposited from the liquid reservoir each time it passes over the powder bed, assuming that there are no blockages in the print head.

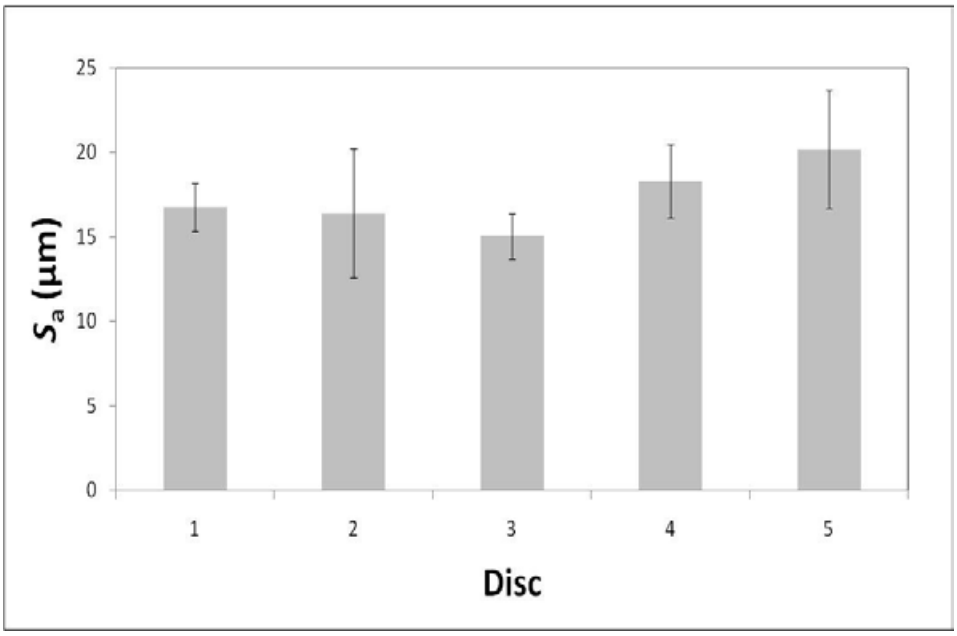

Figure 6.3 Surface roughness values obtained for 6 areas on 6 printed CaP discs. The error bars shown represent the standard error of the mean.

To determine whether the samples were homogeneous across the morphology of their surfaces, the chemistry of the samples were determined using confocal Raman microscopy. It was found that there was no variation in the spectra collected across all of the samples, indicating compositional homogeneity (Figure 6.4). From a comparison of the Raman spectra of the 3D printed and reference materials, it was apparent that the chemical composition of the ceramic structures was similar to the raw, unreacted powder used. A peak present at 372 cm^{-1} represented lattice vibrational modes and a strong peak at 944 cm^{-1} represents the v_1 vibrational mode of the HPO_4^{2-} ion. Further P-O stretching modes are seen at 1144-1454 cm^{-1} (v_2, and v_3 respectively) representative primarily of unreacted TCP. Overall the spectrum for the printed sample was more

similar in chemical bond composition to the unreacted powders than the brushite reference material and HA shown (Figure 6.4). It is thought that in the dry state; immediately after printing, the presence of unreacted surface powder is the cause of the spectra being more similar to the α- and β-TCP mix than the brushite or HA or that the extent of conversion was relatively low.

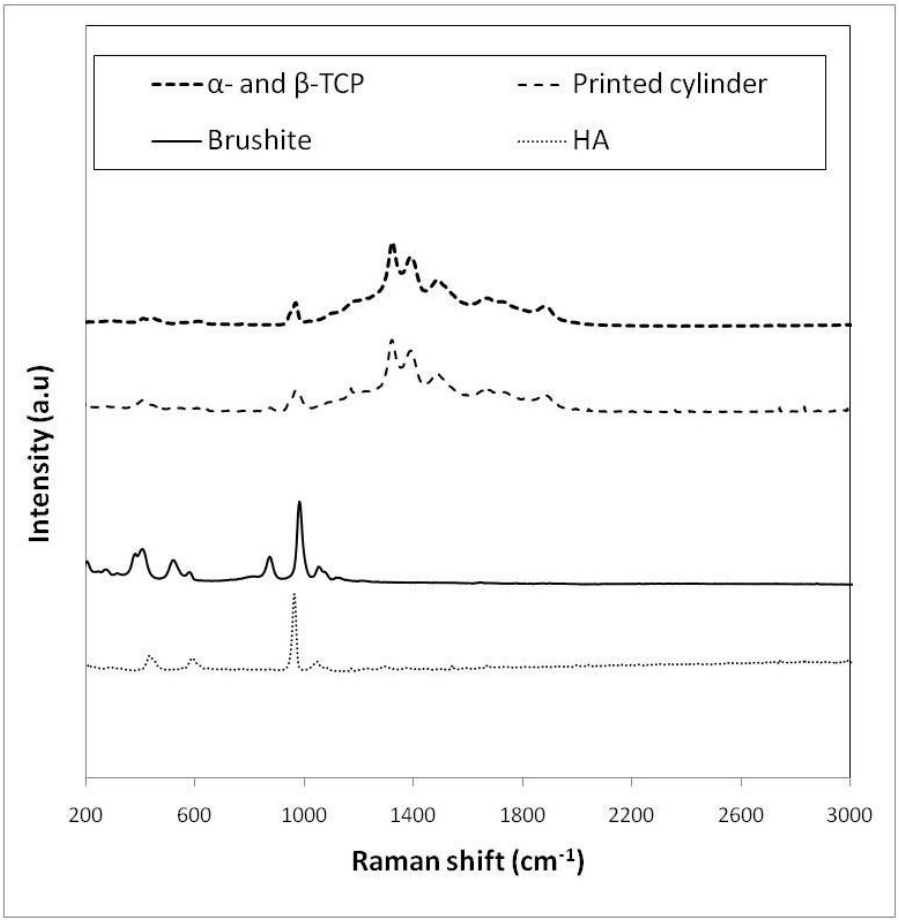

Figure 6.4 Raman spectra showing compositional vibrational frequencies for α- and β-TCP (bold dashed line), a printed cylinder (dashed line), brushite (bold solid line) and HA (dotted line).

In order to further investigate the chemical characteristics of the printed samples, the crystalline composition of the cements was evaluated using X-ray diffraction (XRD) (Figure 6.5). The diffraction pattern acquired indicated presence of β- and α-TCP which may be attributed to unreacted powder, marked by circles in Figure 6.5, but also showed the presence of brushite and some monetite (represented by squares and triangles, respectively). It has previously been suggested that a low localised pH due to the printing process and post-hardening steps may lead to the formation of monetite, which can form from the loss of water of crystallisation from brushite (Prado da Silva *et al*. 2001 and Mehrban *et al*. 2010). Furthermore, the introduction of excess phosphoric acid in the hardening of the printed samples increases monetite formation as demonstrated by Hofmann *et al*. (2006) who experienced similar results when using the setting retardant citric acid.

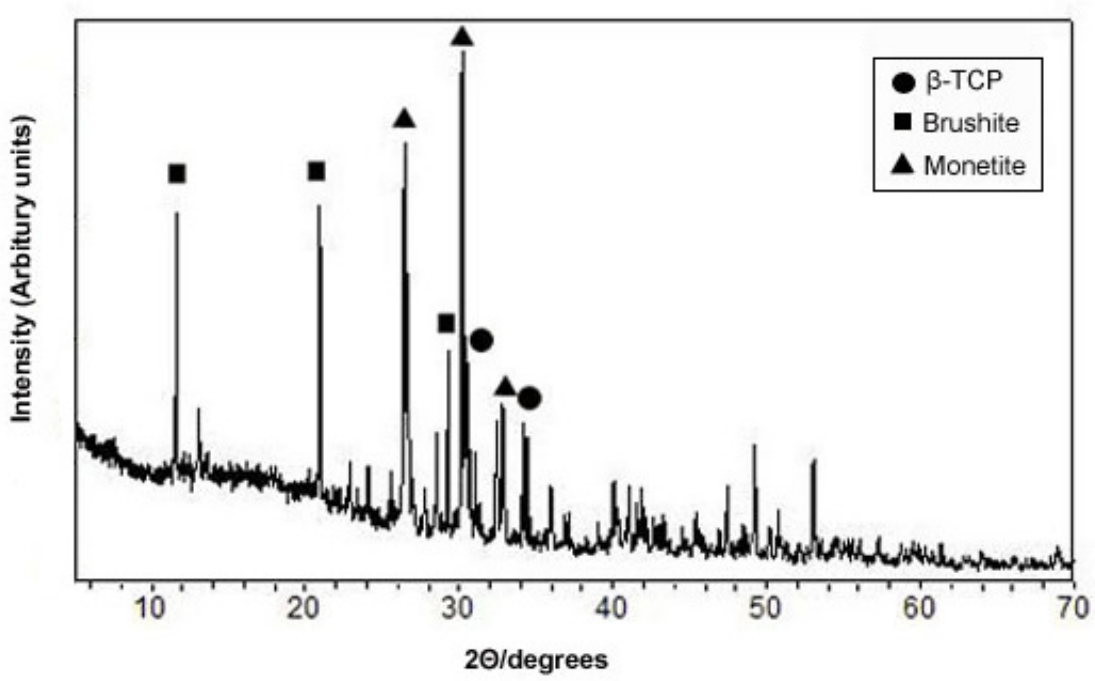

Figure 6.5 X-ray diffraction pattern showing phase composition of printed cement.

The composition of the cement matrix can influence the structure of the printed monoliths, which affect the ability of cells to attach to the scaffold. The presence of pores allows cells to migrate and proliferate as well as ensuring diffusion of nutrients and gases into and out of the scaffold. A porous surface also improves the interface between the scaffold and native bone by increasing the total surface area available for attachment (Karageorgiou and Kaplan 2005). Variation in pore sizes induces different responses to scaffolds. Whilst large pore sizes (100-200 μm) are ideal for bone growth *in vivo*, smaller pores (10-75 μm) may only be penetrated by soft tissue (Karageorgiou and Kaplan 2005). The pore size distribution for the 3D printed monoliths was found to be broad, ranging from 0.01 μm to 10 μm in their dry state (Figure 6.6). The presence of

a wide range of pore sizes is favourable for tissue engineering as the scaffold may facilitate cellular migration. The overall porosity of the printed cements was found to be higher, 35.9 ± 2.23%, than the hand-cast types owing to the presence of denser monetite, 2.89 g/cm^3, in comparison to brushite, 2.32 g/cm^3. Monetite formation caused by the dehydration of brushite could lead to cement matrix contraction and therefore a change in porosity within the structure.

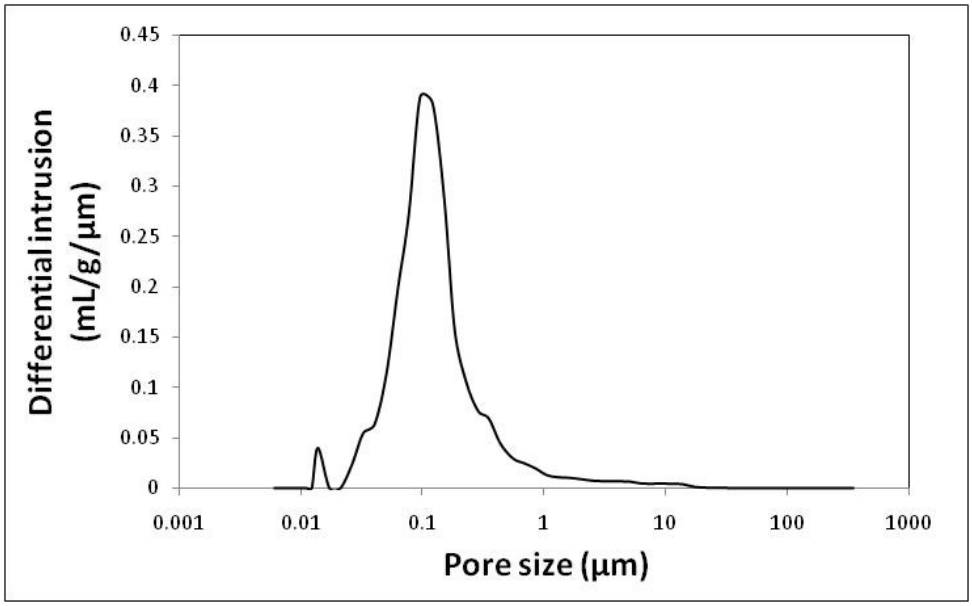

Figure 6.6 Pore size distribution of CaP samples as printed.

The degree of porosity further affects the mechanical strength of the overall scaffold; therefore the printed samples were also tested under a compressive load. Figure 6.7 shows the various modes of failure exhibited by the printed samples. Variation in the failure types exists because

stress concentrations within the sample vary depending upon the sample geometry used. In order to minimise stresses caused by corners of a sample, cylindrical samples are often the geometry of choice when testing the compressive strength of such cements. Figure 6.7 shows a comparison of the failure modes in cylindrical samples and disc samples. In Figure 6.7A, the compressive strain applied has led to a 'peeling effect' whereby the effect of the layer by layer printing process causes weaknesses between the printed sheets. This is further demonstrated in Figure 6.7B where it can be seen that the top layers of the printed disc have fallen away without damaging the entire disc. Conversely the opposite may also be true, as shown in Figure 6.7C and 6.7D, in which the disc has fractured directly across the middle of the entire sample, along the vertical diametral plane, as in Brazilian tests where a compressive load is used to measure the tensile strength of a material (Pittet and Lemaître 2000). The aforementioned researchers have explored the use of cardboard protection pads, insets, to minimise the radiance of fracture points on the sample where the compressive plate is in contact. However, this also serves to 'dampen' the effects of the force applied to the sample and the results obtained may not be a true reading of the resistance of the material being tested. Furthermore, since it was shown that the inset width strongly affected the number of fracture points on the sample, it is necessary to investigate inset geometry thereby complicating the test further. In cylindrical samples the formation of shear cones (Kendall 1980) due to stress points, created by the points of contact with the compressive plates lead to failure throughout the sample based on tensile stress distributed through the middle of the sample (Figure 6.7E and F). With many complex and different failure modes, cement samples under a compressive load may fail due to tensile or shear strain and distinction between the two is difficult to ascertain. It is noted that compressive testing is not the only method of mechanically

testing the cements produced. Tensile tests and bending tests allow accumulation of different data from variations in the type and distribution of strain applied. Therefore a comparison of such tests with those made previously by other researchers is difficult unless the conditions, sample geometry and test type are the same. Furthermore, for all printed samples used for compressive testing throughout this research cements of the same batch, with no visible defects were used.

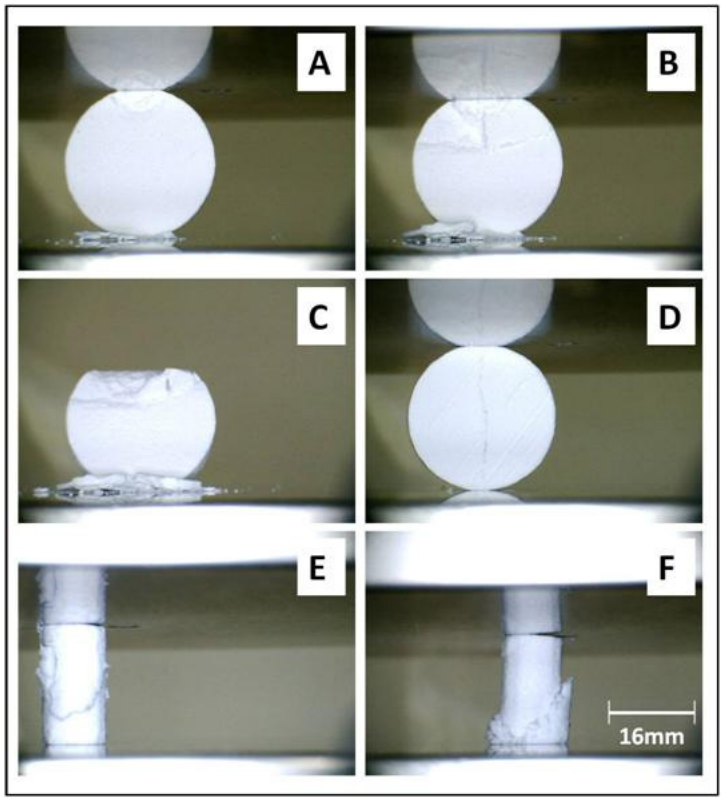

Figure 6.7 Images showing the different failure modes of printed CaP structures under a compressive load.

To test the compressive strength of the printed materials, experiments were limited to cylindrically shaped samples alone. To evaluate batch variation, two separate batches of printed cylinders were tested and it was found, as shown in Table 6.1, that there was a 3 MPa difference in the compressive strength of the cylinders. An average compressive strength of 18-21 MPa showed little statistical variation between batches indicating that the production of monoliths via 3D printing is reproducible. The overall compressive strength is considerably higher than that reported for hand-cast cements (12.04 ± 0.86 MPa) despite having an increased porosity, 2.67 ± 0.01 g/cm^3 (Mehrban *et al*. 2010).

Table 6.1 Differences in compressive strength of printed cylinders from different batches.

	Compressive strength (MPa)
Printed- Batch 1	21.0 ± 0.9
Printed- Batch 2	18.1 ± 1.7

After subjecting the samples to compressive loads the fracture surface was examined using SEM. Figure 6.8A demonstrates the microstructure of a crushed cylinder whilst Figure 6.8B shows the crystal structure inside a crushed disc. Both images show the presence of brushite-like crystals, as demonstrated in Figure 6.2, with the addition of unreacted powder. Since the print head used for the deposition of phosphoric acid onto the surface of the powder bed had a resolution of 118 ×

177 dots/ cm it is likely that the ceramic surface was evenly coated by the acid with the remaining unreacted powder hardened post-printing. Therefore, the unreacted particulates may have been caused by the compressive testing or have been present between printed layers at the start of the study.

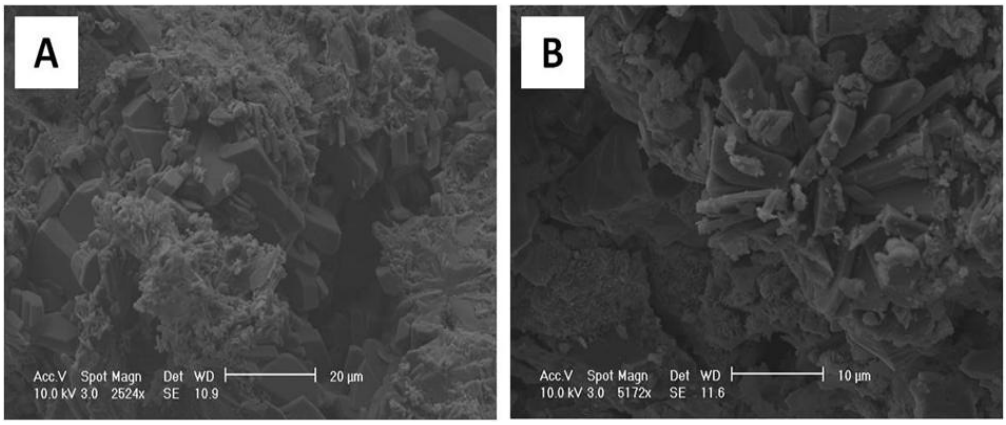

Figure 6.8 SEM images for the crystal morphology of a crushed cylinder (A) and crushed disc (B) showing loose powder surrounding brushite-like crystals.

In their printed, dry state the monoliths appear chemically and mechanically uniform. However, the structures will all be immersed in cell culture medium. Therefore characterisation of the printed samples was conducted in PBS, DMEM, S-DMEM, HAM and S-HAM, for suitability in the culture of murine NIH 3T3 fibroblasts and tenocytes isolated from rat tails. Figure 6.9 shows the crystal morphology on the surface of printed discs after immersion in the media for 28 days. It can be seen from all the images in Figure 6.9 that long, thin, plate-like crystals typical of

brushite are present throughout. All discs adopt rounded crystal morphology after 28 days of immersion in the various media indicating dissolution. Furthermore, discs immersed in HAM and S-HAM show presence of the 5µm thickness crystals. S-HAM was made with double the protein content of S-DMEM which may have caused a greater degree of dissolution on the surface of the samples.

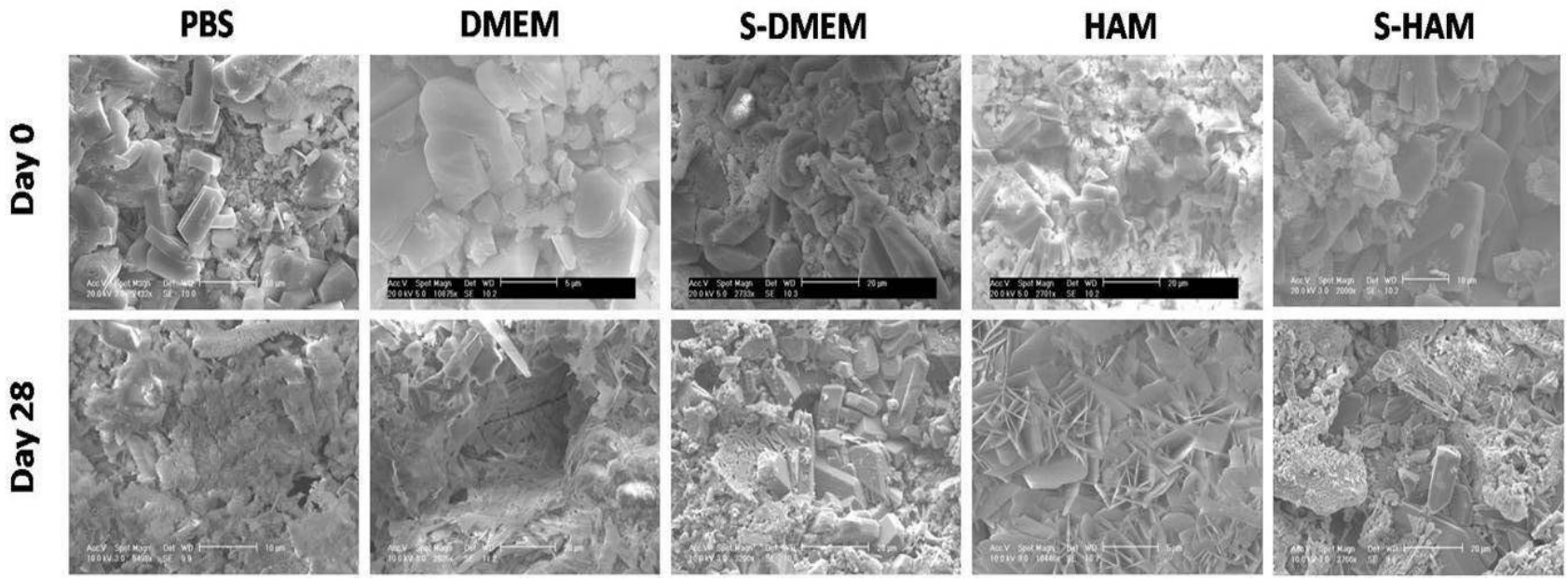

Figure 6.9 SEM images of printed discs after immersion in PBS, DMEM, S-DMEM, HAM and S-HAM on day 0 and 28.

It is well established that surface roughness of a material affects cellular attachment and growth independently of surface chemistry (Dos Santos *et al*. 2008). Analysis of the samples indicated that the roughness of the disc surfaces changed considerably over 28 days. Systematic surface dissolution of the CaPs caused by solution change every three days (Figure 6.10) is also followed by a statistically significant reduction of surface roughness (by approximately 6µm) to day 14 samples immersed in DMEM and S-DMEM (Figure 6.11 and 6.12). It has previously been reported that presence of ions, such as Ca^{2+}, Na^{+}, K^{+}, Mg^{2+}, Fe^{3+}, $H_2PO_4^{-}$, HCO_3^{-} and Cl^{-}, within DMEM cause a transformation of brushite to a precursor of apatite, octacalcium phosphate (OCP, $Ca_8(HPO_4)_2(PO_4)_4.5H_2O$) although evidence of octacalcium phosphate cannot be seen in the work reported here (Mandel and Tas 2010). Furthermore, the HAM and S-HAM media used for comparison also contained a high number of ions and no OCP formation was detected. Finally, the surface roughness of printed CaP samples immersed in HAM and S-HAM shows a statistically significant increase on day 14 of the study. This may be because there is a higher content of protein within these solutions and protein adsorption to the surface of the printed discs is causing an increase in apparent roughness (Figure 6.13 and 6.14) as a result of exchange at the solid-liquid interface in the multi-component system.

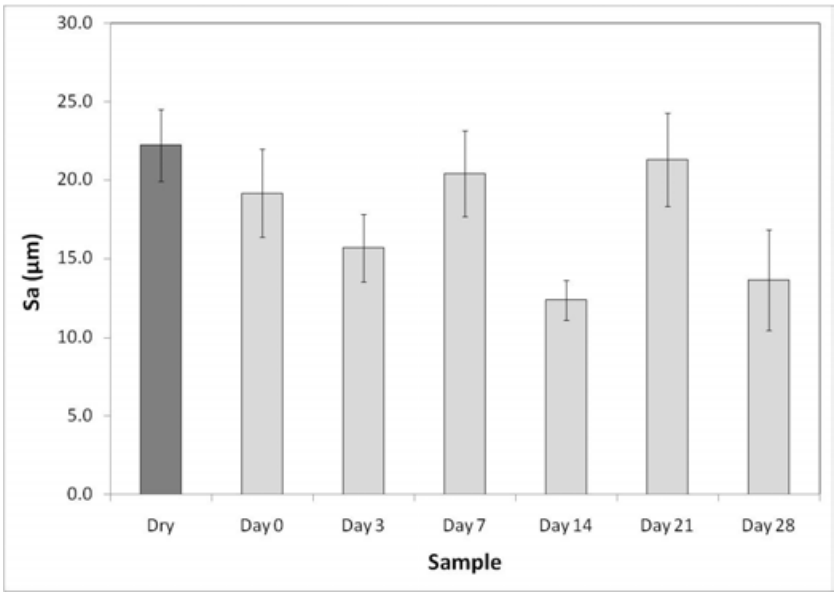

Figure 6.10 Surface roughness for CaP discs after immersion in PBS and dry discs for comparison. The error bars shown represent the standard error of the mean.

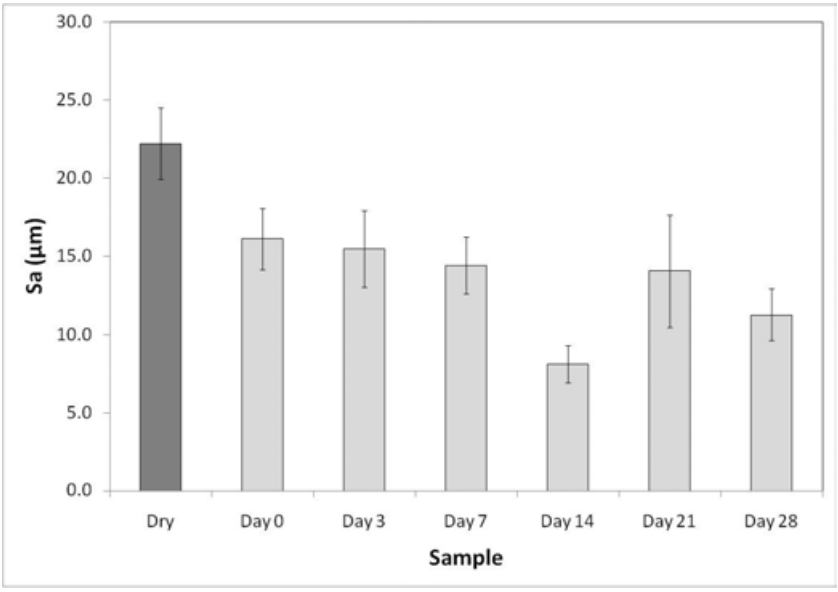

Figure 6.11 Surface roughness for CaP discs after immersion in DMEM and dry discs for comparison. The error bars shown represent the standard error of the mean.

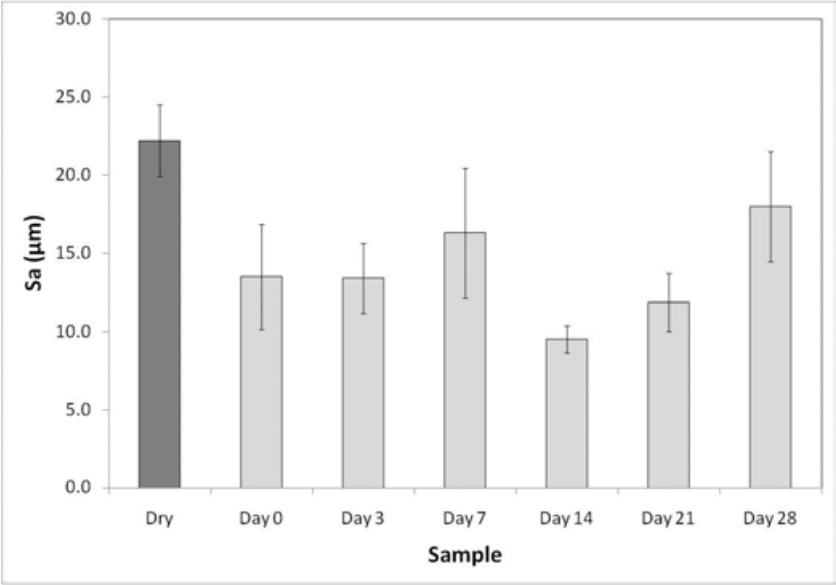

Figure 6.12 Surface roughness for CaP discs after immersion in S-DMEM and dry discs for comparison. The error bars shown represent the standard error of the mean.

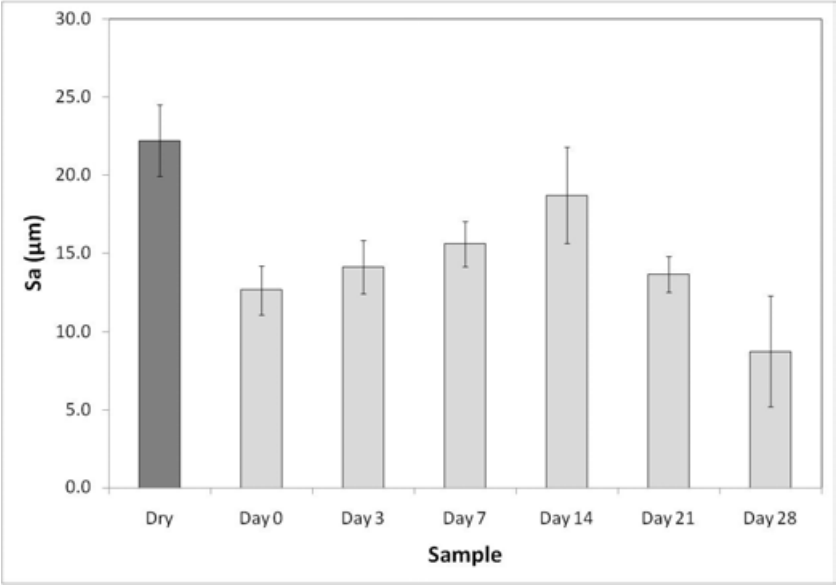

Figure 6.13 Surface roughness for CaP discs after immersion in HAM and dry discs for comparison. The error bars shown represent the standard error of the mean.

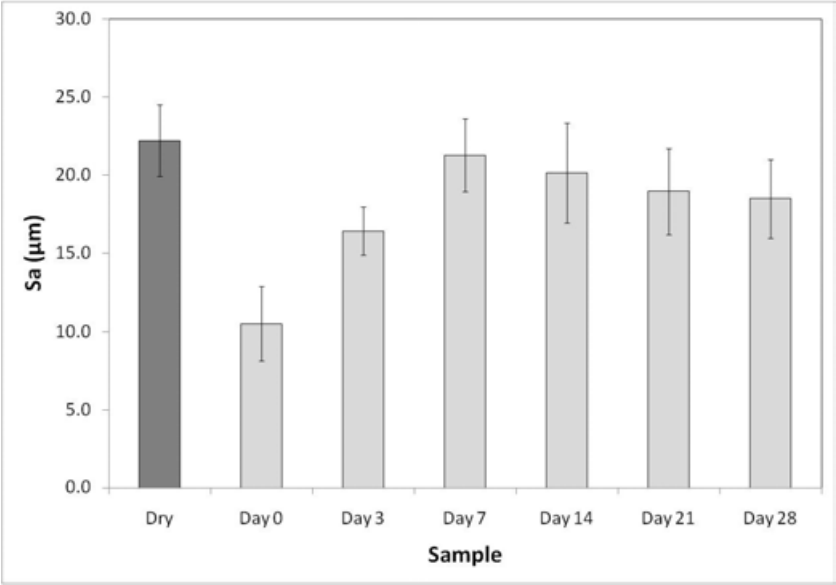

Figure 6.14 Surface roughness for CaP discs after immersion in S-HAM and dry discs for comparison. The error bars shown represent the standard error of the mean.

Upon observing a microstructural change in the surface morphology, the discs were analysed through confocal Raman microscopy to see whether a chemical change had been induced (results not presented). Raman spectroscopy showed that there was no difference in the chemical bonds of the samples after immersion in the various media over 28 days, further supporting the theory that no OCP was being produced.

The surface of the material changes over time as a consequence of protein adsorption and dissolution. As dissolution may also influence the internal structure of the brackets, porosity and pore size distribution has been investigated. Figure 6.15A shows the pore size distribution of discs immersed in PBS, DMEM, HAM, S-DMEM and S-HAM over 28 days. After the addition

of serum the pore size distribution shows a peak at over 1 µm, with samples without serum displaying a peak at 0.01-0.02 µm. The development of pores in all solutions over 28 days is caused by dissolution. Whilst it has been shown that sera proteins inhibit the formation of hydroxyapatite (Grover *et al*. 2003), the dissolution of the predominantly brushite scaffold continues. For the samples immersed in supplemented media either the smaller pores are merging together to create larger pores or the small pores are becoming coated with the protein from the serum, whilst dissolution of large pores continues.

Furthermore, the porosity of the brackets increases by approximately 16 ± 1.5 % in all solutions regardless of serum content (Figure 6.15B). *In vivo* osteogenesis induced by ceramics (Yuan *et al*. 1999) occurs in very porous ceramics within three months whereas ceramics with little to no pores showed no bone formation even after six months. Pores 0.1-0.5µm in size are known to have significant effects on bone resorption (Yokozeki *et al*. 1998) although, as previously suggested, some researchers argue that large pore sizes (typically 1.2-2.0 mm) with high surface area to volume ratios allow for better cellular migration, facilitating new tissue growth (Holly *et al*. 2000).

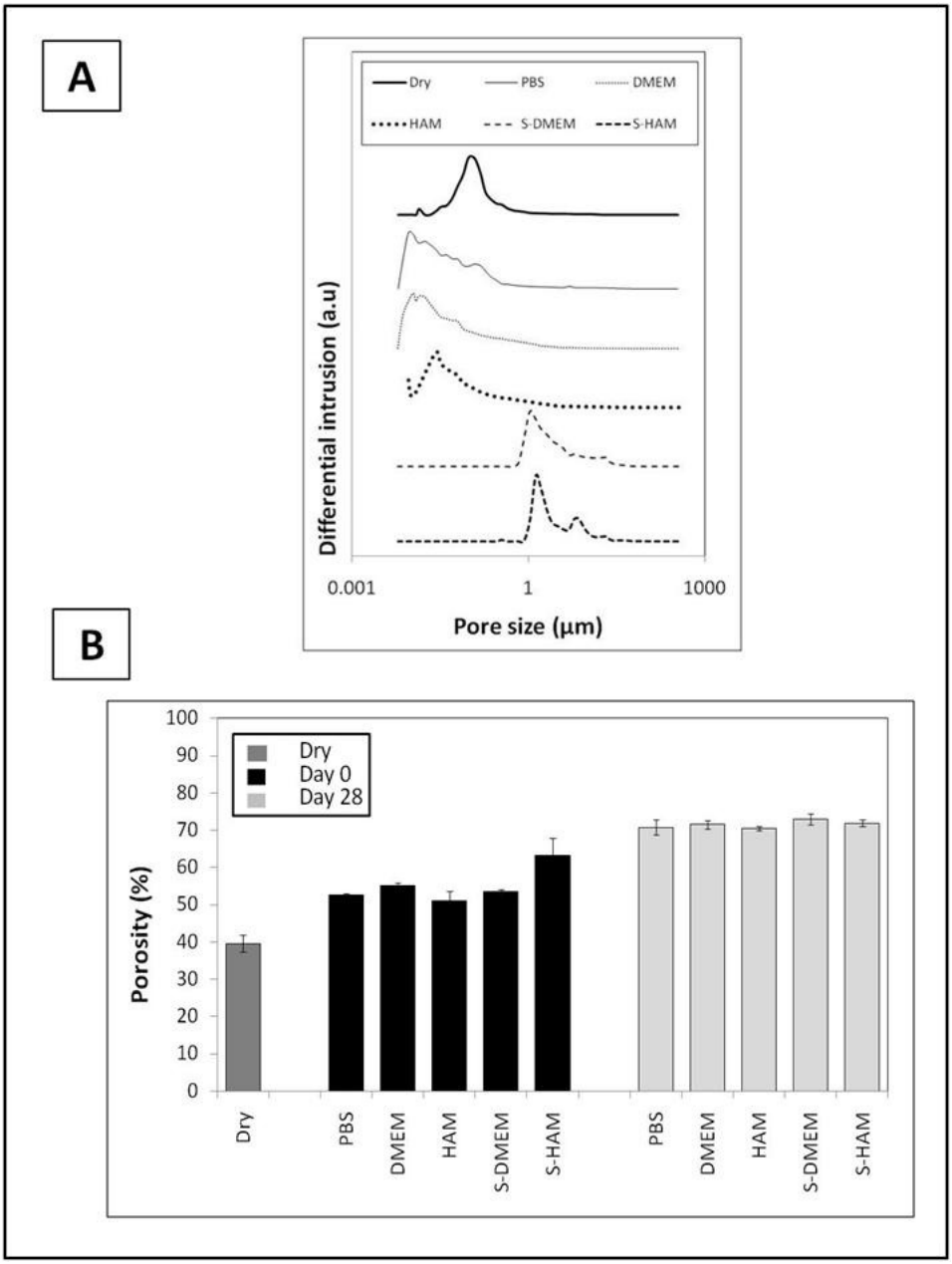

Figure 6.15 Pore size distribution of printed CaP samples immersed in PBS, DMEM, HAM, S-DMEM and S-HAM on day 28 (A) and porosity of printed CaP samples immersed in PBS, DMEM, HAM, S-DMEM and S-HAM on day 0 and day 28 (B). The error bars shown represent the standard error of the mean.

Surprisingly with the increase in porosity and pore size shown in Figure 6.15, Figure 6.16 shows that there was little change in the compressive strength of printed discs immersed in PBS, HAM and S-HAM over 28 days (from 11-15MPa). This preliminary study is indicative of a chemically stable scaffold which would be ideal for cellular support.

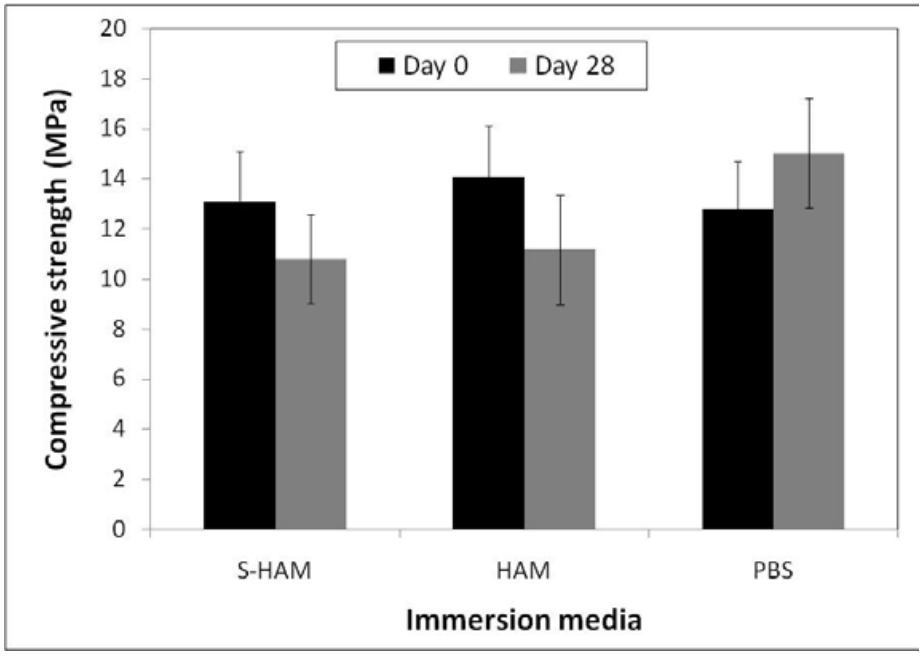

Figure 6.16 Compressive strength of printed CaP cylinders on days 0 and 28 after immersion in S-HAM, HAM and PBS. The error bars shown represent the standard error of the mean.

In order to further assess the mechanical stability of the printed scaffolds, a degradation study was undertaken which indicated in Figure 6.17, as in Figure 6.16, that the printed discs are able to

maintain mechanical integrity after immersion in PBS, HAM and S-HAM for 28 days. It has previously been reported that the degradation rate for brushite is 0.25 mm/ week (Ohura *et al*. 1996). In native bone formation this process involves two steps, dissolution and resorption with the latter being mainly osteoclast-mediated leading to osteoblastic matrix secretion (Schliephake *et al*. 2004).

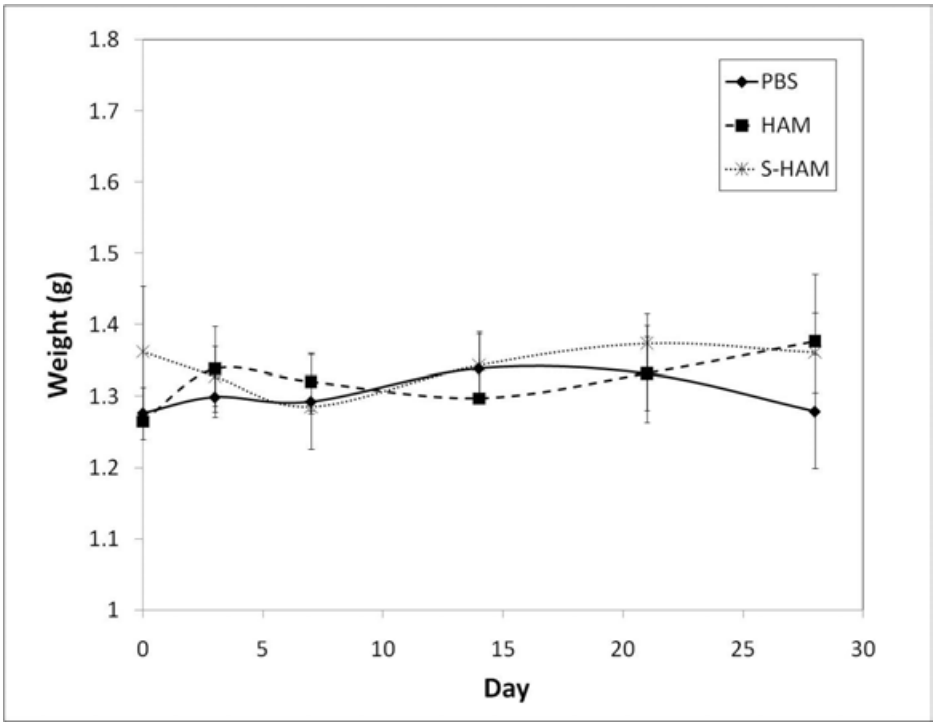

Figure 6.17 Weight of printed CaP discs in PBS, HAM and S-HAM over 28 days. The error bars shown represent the standard error of the mean.

After investigating some of the effects different solutions, particularly supplemented media, have on the printed CaP discs, it is necessary to establish why these effects may occur. Therefore, studying the effect the protein content, through foetal bovine serum (FBS) addition, has on the scaffolds is of vital importance in understanding cellular response to the printed monoliths. Foetal bovine serum (FBS), or foetal calf serum (FCS) as it is also known, is important for *in vitro* cell studies in providing an ideal environment for the development of focal adhesion plaques in cells, stimulating cell adhesion to a given surface (Gerharz *et al*. 1989 and Sallot *et al*. 1997). FBS is rich in proteins, albumin, polypeptides, hormones, amino acids and glucose among others (Liu *et al*. 2008). By providing a source of nutrients, FBS mimics *in vivo* conditions when added to cell culture medium for *in vitro* cell studies. It is therefore common practice to immerse samples in FBS prior to cellular experiments to promote cell attachment. Furthermore, the buffering effects of serum allow toxic by-products to be partially neutralised in medium.

Figure 6.18 shows the effect different concentrations of FBS have on the crystal morphology of printed CaP discs. It can be seen that crystal morphology changes dramatically for all concentrations of FBS used as individual crystals become difficult to distinguish, owing to a high degree of dissolution. It has previously been reported that the effect of ionic substitution, in this case from FBS, depends on the ionic radius of the substituting ion, for example substitution of Ca^{2+} ions with ions of different ionic radii can cause the β-TCP lattice to expand or shrink (Pina and Ferreira 2010). Since FBS is a complex mixture, it is difficult to ascertain which ions are affecting CaP morphology and chemistry.

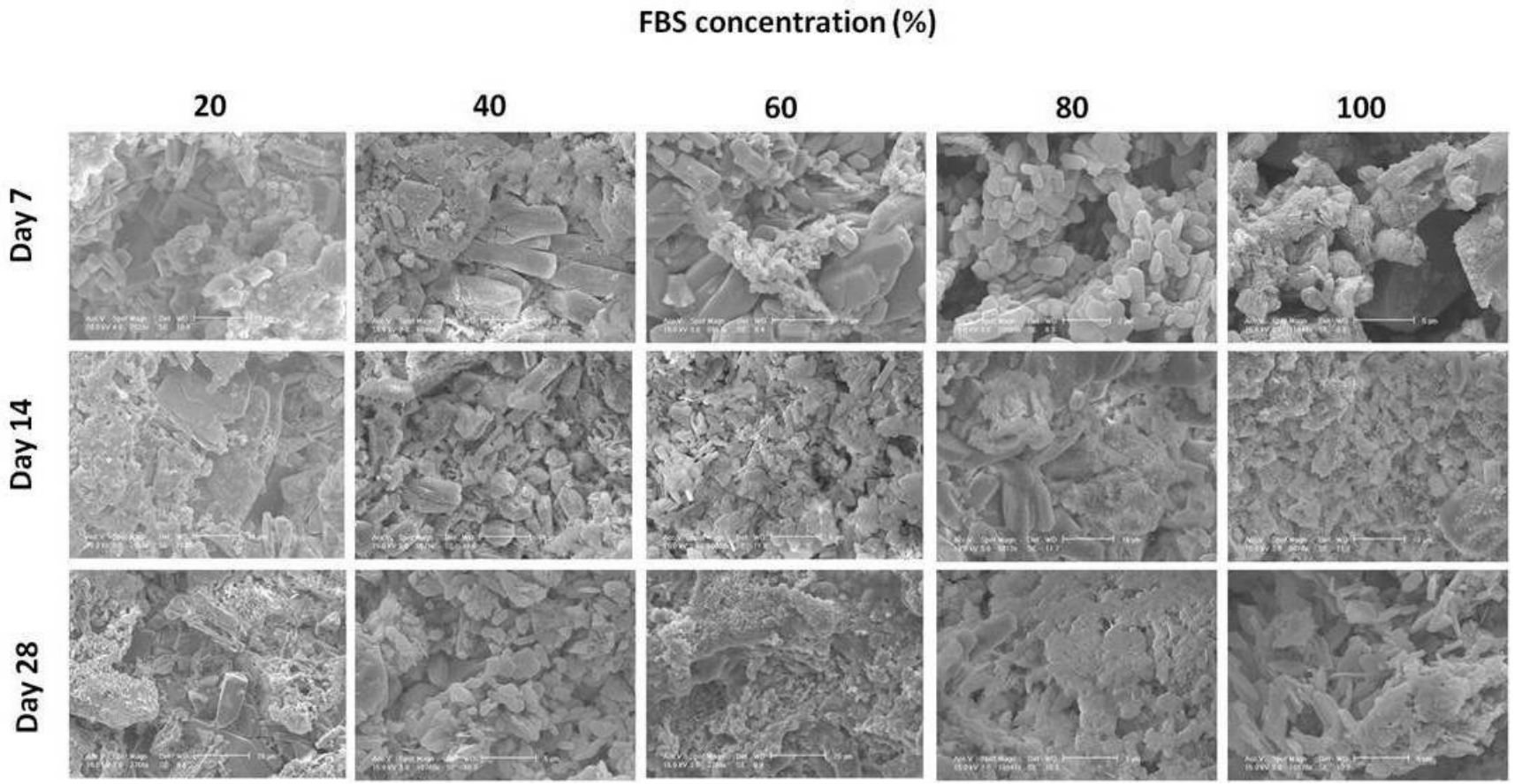

Figure 6.18 SEM images of printed CaP discs immersed in FBS at different concentrations for 7, 14 and 28 days.

In order to quantify the morphological changes seen in Figure 6.18, surface roughness measurements were taken. It can be seen in Figure 6.19 that the roughness values vary considerably between days 7 and 28 although at day 14 there is no statistically significant difference in the surface roughness of samples submerged in FBS and the dry printed samples. From this data, there appears to be no obvious relationship between FBS concentration and surface roughness. This may be because protein adsorption on the surface of the discs is obscuring the effects on the surface of the printed discs. Equally, an increase in protein should therefore lead to more adsorption on the CaP discs surface. Furthermore, although six measurements were taken on six separate samples, the roughness on day 7 after immersion in 40% v/v FBS (40 μm) seems unusually high and therefore the experiment may need to be repeated to include depth of protein adsorption over time.

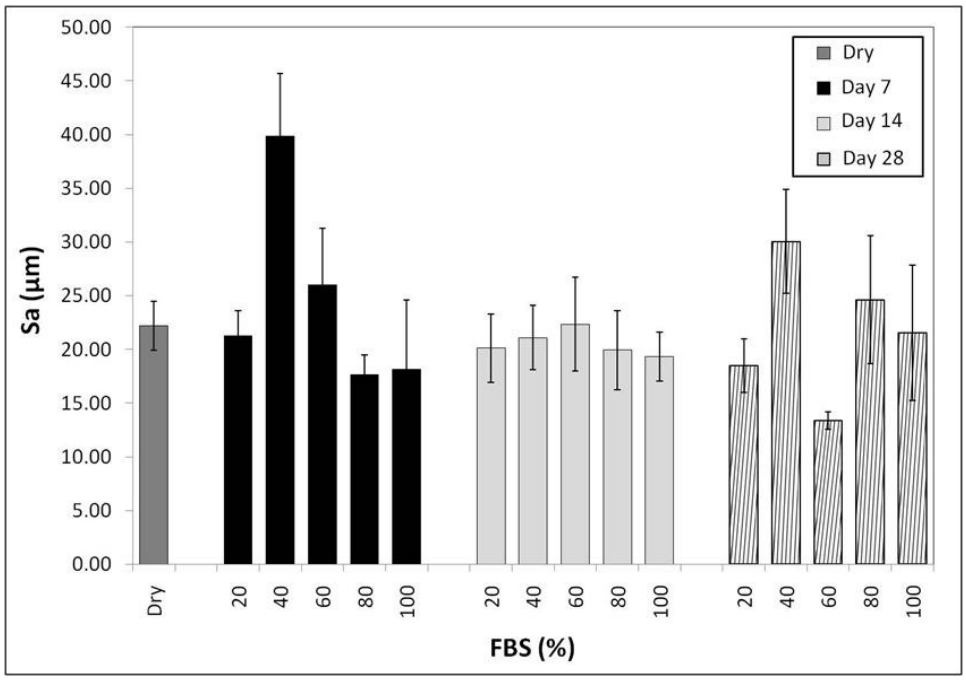

Figure 6.19 Surface roughness for printed CaP immersed in 20%, 40%, 60%, 80% and 100% v/v FBS on days 7, 14 and 28 post-immersion in comparison to a dry printed disc. The error bars shown represent the standard error of the mean.

It is evident that although there may be protein adsorbed to the surface of the printed discs, this does not affect the Raman data acquired, as seen in Figure 6.20. For biological material in particular it is common to find that the Raman signal is not flat and indicates a high level of adsorbed organic material. This was not seen for these samples. However, what can be seen in Figure 6.20 is that the intensity of peaks indicative of brushite and HA (at 350-600 and 1000 cm^{-1}) increases over the 28 day study. Both sets of peaks represent P-O bending and P-O stretching of the PO_4^{3-} ion respectively, neither of which are as strongly seen in the raw β-TCP

material. Other than dissolution and a strong indication of the presence of brushite, these spectra indicate that reprecipitation into the more stable HA is also occurring. Over such a short time frame, such changes to the network may affect the mechanical integrity of the scaffold which may be beneficial should the mechanical strength be required or a hindrance if dissolution is required.

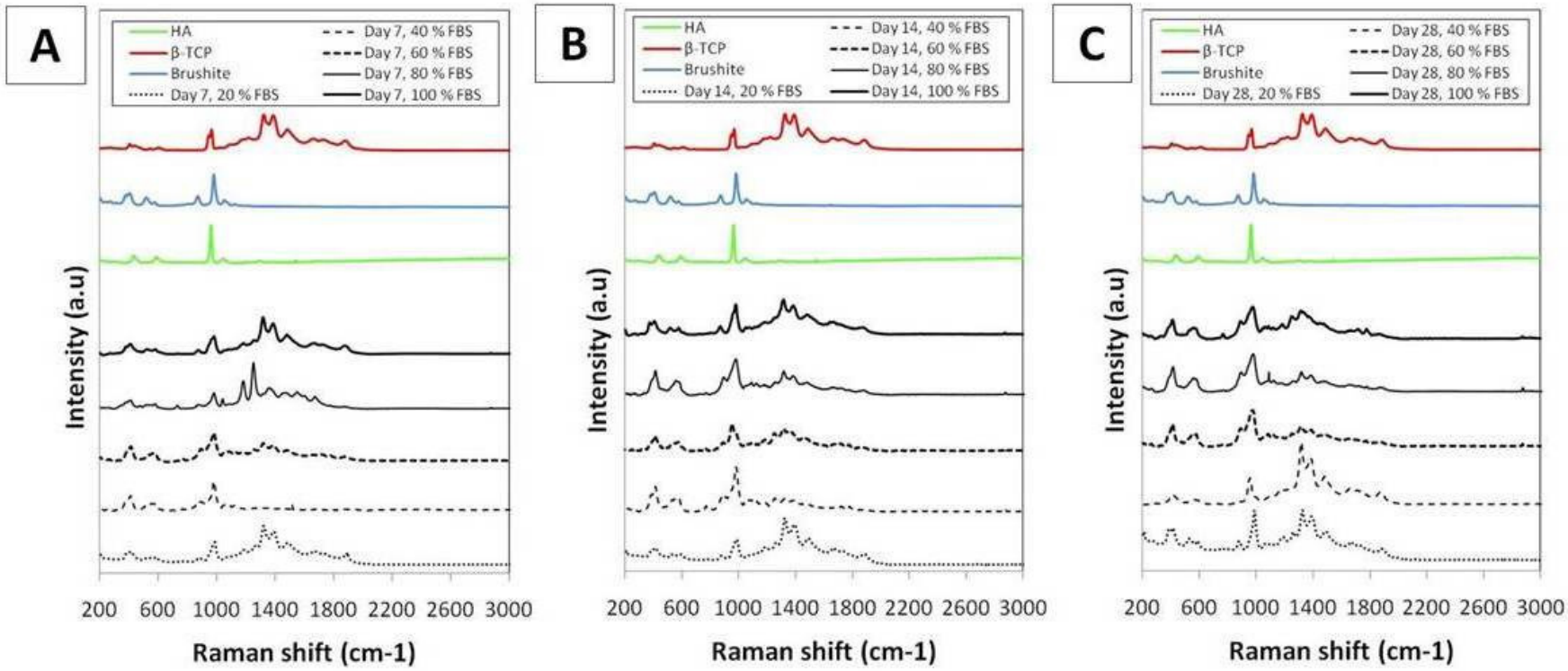

Figure 6.20 Raman spectra for printed CaP discs immersed in 20%, 40%, 60%, 80% and 100% v/v FBS for 7 days (A), 14 days (B) and 28 days (C). Spectra for HA (green), β-TCP (red) and brushite (blue) have been shown for comparison.

Formation of hydroxyapatite is further supported by the pore size distribution data collected (Figure 6.21A) where, although at 20% FBS the pore size increases considerably from its dry state, at higher concentrations of protein the pore sizes remain constant (0.1 μm). Whilst 20% v/v FBS may not be a sufficiently high concentration to prevent the formation of HA, higher FBS concentrations have led to the formation of a more stable phase of CaP which produces persistently uniform pore sizes. Unlike Figure 6.15, the pores are no longer aggregating through continued dissolution. Evidence of this is further seen in Figure 6.21B where the porosity of the monoliths is not significantly different between days 0 and 28, although porosity has significantly increased in all samples from their dry state. Porosity is highest on day 28 for 20% FBS (Figure 6.21B) which may be attributed to large pore dissolution at 20% in Figure 6.21A. Between days 0 and 28, large or small pores are no longer forming within the structure in their wet state.

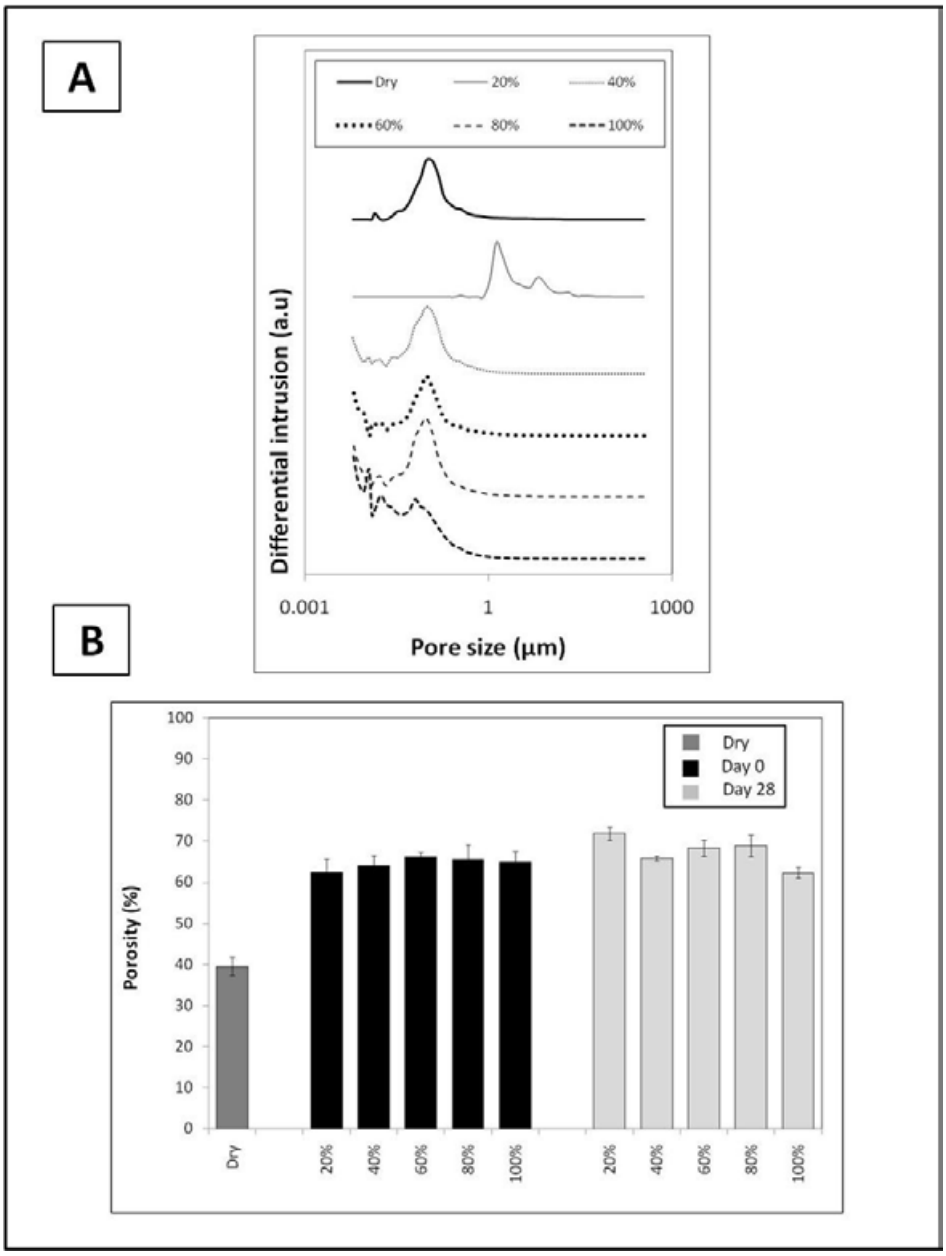

Figure 6.21 Pore size distribution of printed CaP samples immersed in 20%, 40%, 60%, 80% and 100% v/v FBS on day 28 (A) and porosity of printed CaP samples immersed in 20%, 40%, 60%, 80% and 100% v/v FBS on day 0 and day 28 (B). The error bars shown represent the standard error of the mean.

Furthermore, from Figure 6.22 it can be seen that there is between 19-27% difference in the dry weight of the CaP discs in comparison to their original weight at the beginning of the study. This difference can be seen in Figure 6.21B where the porosity of all wet samples has increased significantly from the printed dry state due to dissolution leading to overall mass loss. There is also no trend in the stability of the scaffold in comparison to the FBS concentration. This further supports the theory that a more stable CaP than brushite is being formed, i.e HA, when printed CaP samples are immersed in FBS regardless of the FBS concentration.

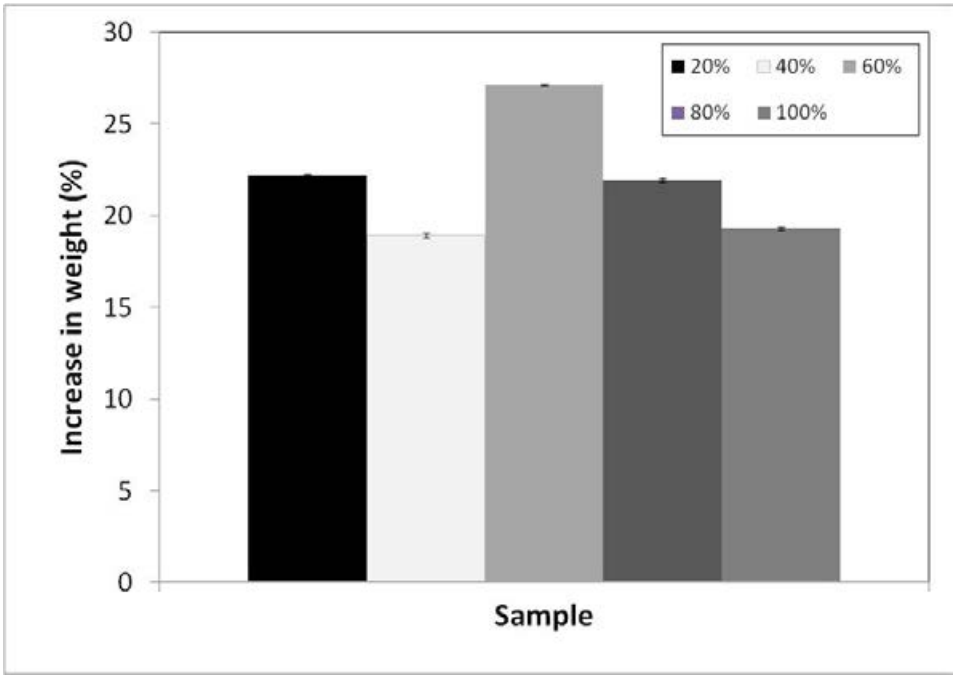

Figure 6.22 Percentage difference in the weight of printed CaP discs on days 0 and 28 after immersion in 20%, 40%, 60%, 80% and 100% v/v FBS. The error bars shown represent the standard error of the mean.

After investigating the effects of sera proteins on the CaP discs, cellular adhesion, via the proteins adsorbed to the CaP surface was studied. Cell adherence to a given surface occurs in stages where in the early stages, the protein from the extracellular matrix (ECM) adsorbs to the surface of the sample and the cell is attracted to the protein layer via ionic and van der Waals forces. Once on that surface, the integrin-ligand binding stage occurs, which adheres the cell to the sample surface. Intercellular integrin receptor clustering causes a state of permanent tension known as cytoskeletal prestress which, as the contact area between the cell and sample surface increases, increases the number of binding sites. Finally, the cell excretes its own ECM, containing more proteins which start the process again with surrounding cells (Anselme *et al*. 2010). Evidence of this may be seen in the SEM images shown in Figure 6.23. In Figure 6.23 it is shown that the tenocytes seeded onto the surface of the discs proliferate by day 3 (Figure 6.23B) until they are covering almost the entire surface by producing many cytoplasmic projections. These projections, indicating the binding sites of the cells to the CaP surface, begin to diminish by day 14 (Figure 6.23D) until there are little to no projections seen by day 28 (Figure 6.23F) whereby the crystal morphology of the cement can once again be seen as at the beginning of the study (Figure 6.23A). This may be because the protein layer adsorbed to the surface of the printed disc has been removed as the cell culture media is changed every three days. Loss of protein would also lead to a loss of cells adhering to the CaP surface.

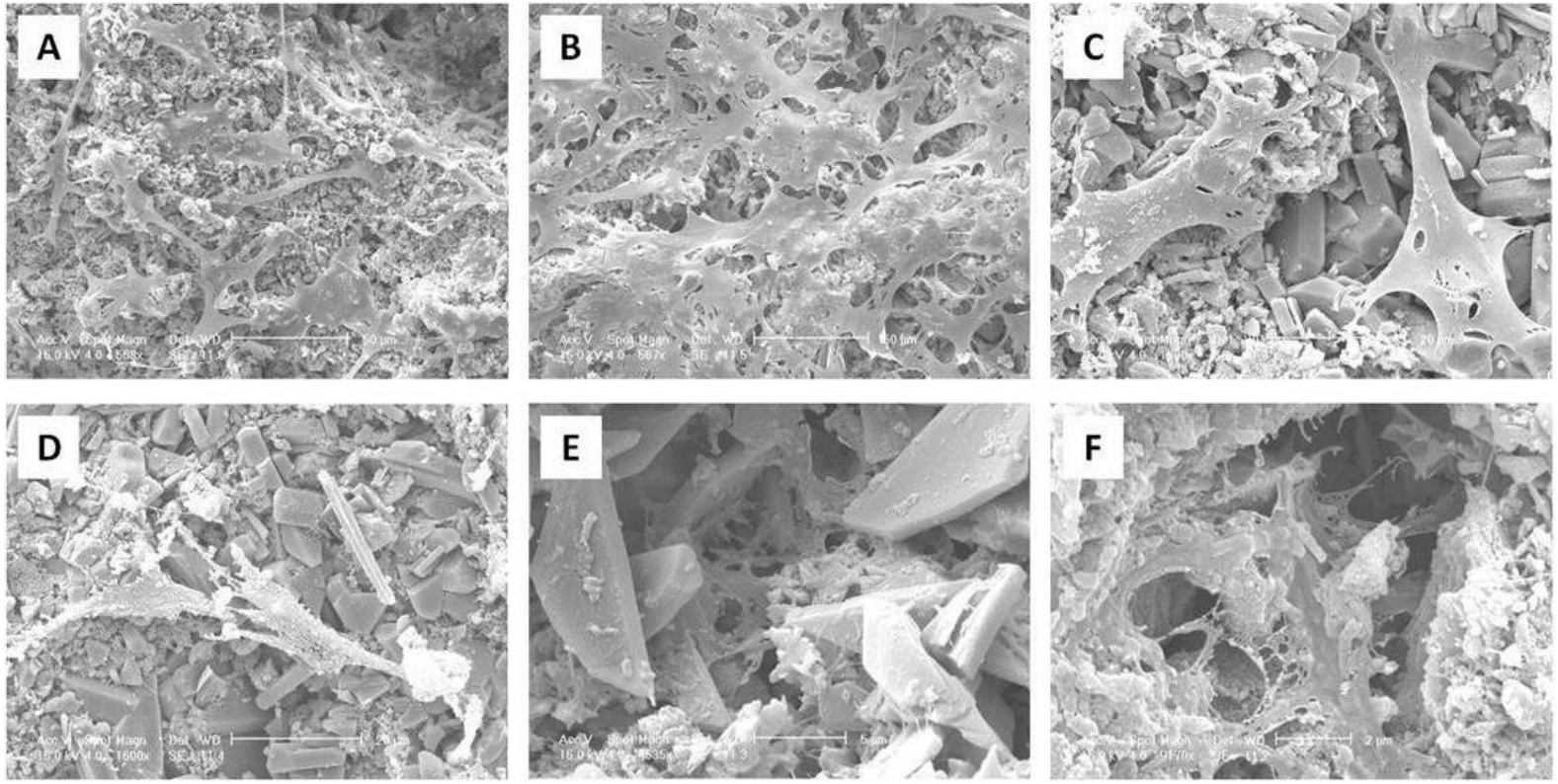

Figure 6.23 SEM images showing morphology of tenocytes on the surface of printed CaP discs on day 0 (A), day 3 (B), day 7 (C), day 14 (D), day 21 (E) and day 28 (F).

Quantification of the metabolic activity of tenocytes seeded onto the surface of the discs supports the trend shown in Figure 6.23 with the number of viable cells calculated from the metabolic activity absorbance (Figure 6.24) increasing from approximately 0.42 x 10^6 ± 0.04 x 10^6 cells to 1.44 x 10^6 ± 0.31 x 10^6 cells by day 3, after which the number of viable cells present decreases so that by day 28 the number of living cells remaining on the samples is approximately the same as on day 0 (0.54 x 10^6 ± 0.13 x 10^6 cells).

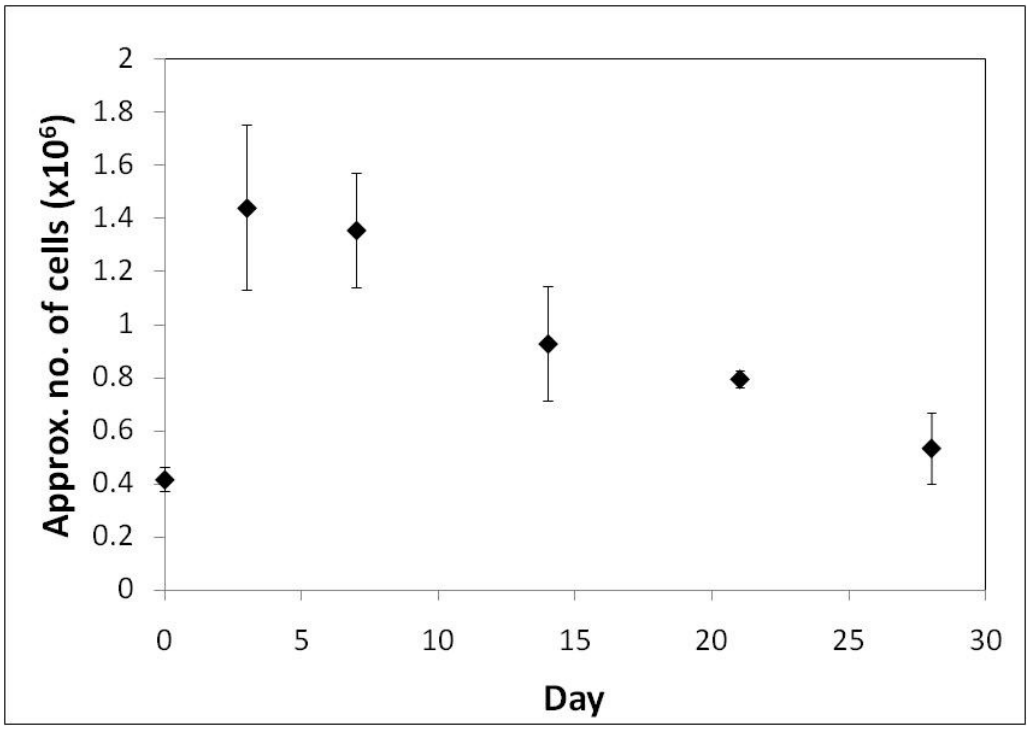

Figure 6.24 Approximate number of viable rat tail tenocytes on the surface of printed CaP discs over 28 days. The error bars shown represent the standard error of the mean.

It is important to investigate any changes the presence of cells may have on the roughness of the CaP discs as roughness affects cell attachment and alignment on the surface (above 50µm in width). However, cells are also able to bridge surface wells of up to 50µm in width (Rea *et al*. 2004). It has previously been shown that macro to nano scale changes affect osteoblastic growth independently of surface chemistry (Dos Santos *et al*. 2008). Consistency of surface arrangement allows for uniformity of cellular growth, with surfaces features below the size of the cell having a greater affect on cellular development than features of a larger size (Rea *et al*. 2004). For this study rapid production of ECM by day 3 does not affect the mechanical integrity of the CaP scaffolds, as indicated in Figure 6.25, whereby no change is seen in the surface roughness of five different samples over 28 days. Cellular proliferation, based on surface roughness alone, is unaffected by surface roughness changes on the scale investigated for this chapter.

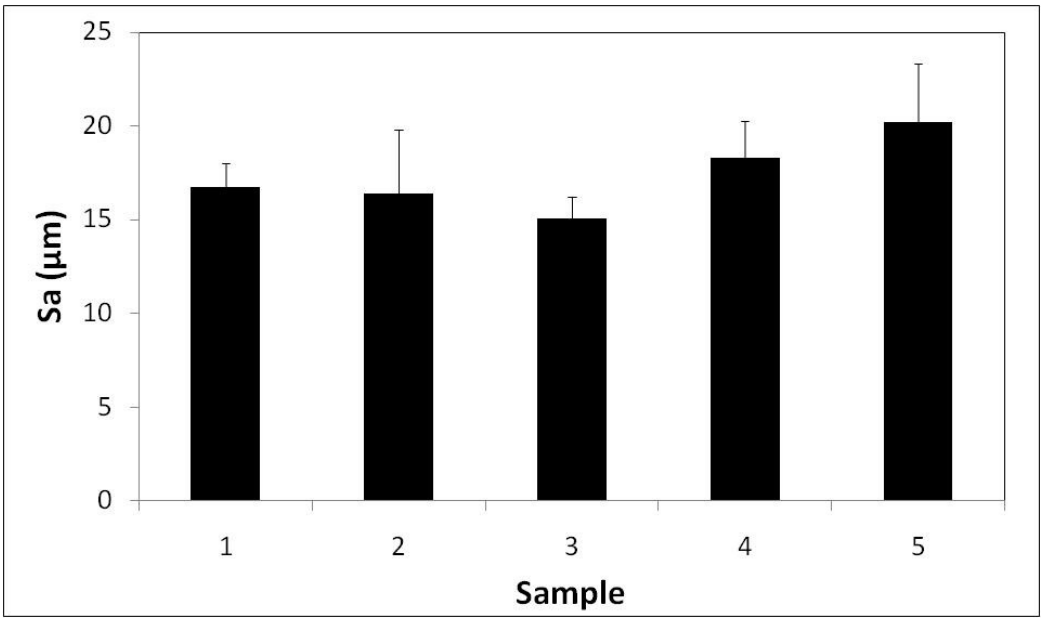

Figure 6.25 Surface roughness of 5 printed cellular CaP discs after 28 days in S-DMEM. The error bars shown represent the standard error of the mean.

Furthermore, as previously indicated in Figure 6.20, the chemical composition of the discs changes and the intensity of the HA peaks at 1000 cm^{-1} increases over the 28 days indicating a change of the structure to the more stable HA. A similarity between the day 21 spectrum and the raw β-TCP spectrum indicate that unreacted powder, possibly between the printed layers as dissolution of brushite occurs, is still present within the network (Figure 6.26). Further investigation of this is necessary to ascertain the extent of unreacted powder present within the samples and whether this is an indication of an incomplete reaction due to areas not covered/ penetrated to a sufficient depth by the phosphoric acid.

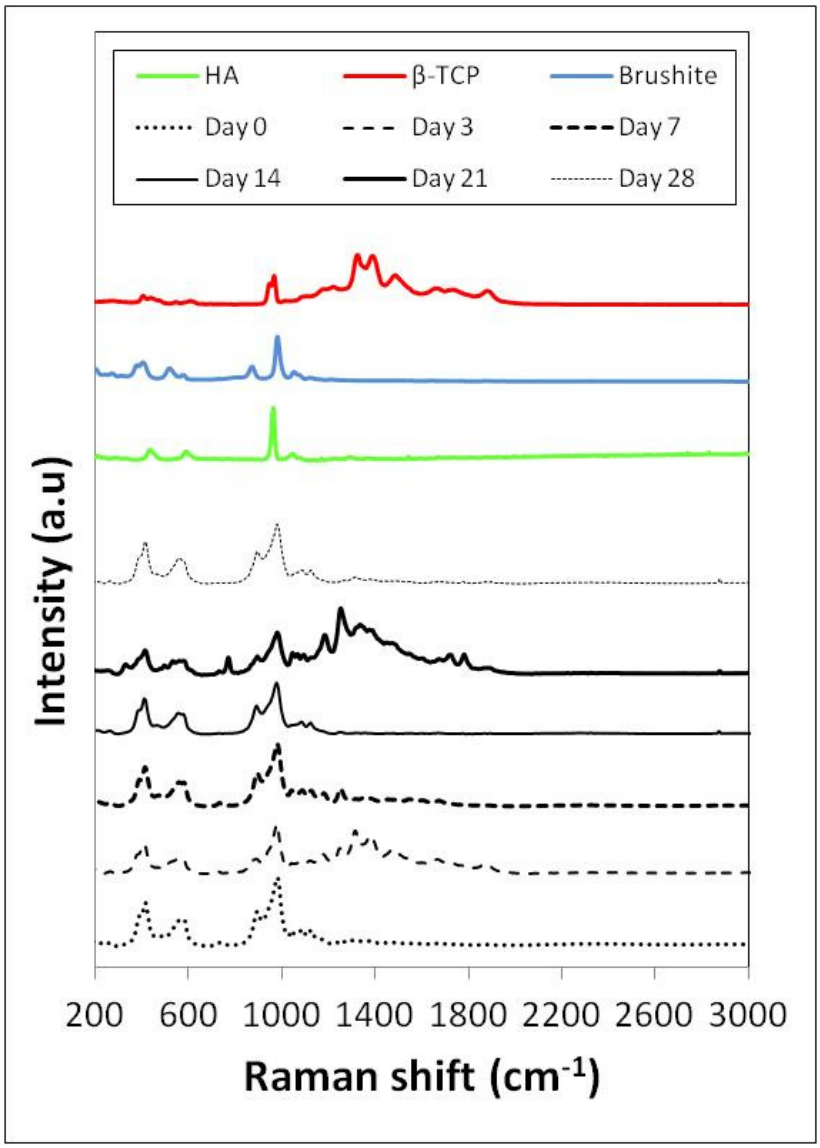

Figure 6.26 Raman spectra showing the chemical bonds present on the surface of cellular printed CaP discs.

Whilst evidence of HA formation has been presented, Figure 6.27A indicates that dissolution of the overall cement continues with large pores being created until day 14 of the study. Adsorption

of protein from immediate immersion in S-HAM can create a protective layer around the cement, preventing gross precipitation. However, as the ECM begins to degrade through enzymatic digestion, as indicated in Figure 6.23, the surface of the CaP is once more exposed, causing dissolution to take place (day 21 and day 28 of Figure 6.27A).

Furthermore, the porosity of the cements (Figure 6.27B) remains stable over 28 days with no statistically significant difference between days 0-21 and the dry samples. A decrease in porosity on day 28 may be attributed to matrix degradation products and cell debris, which may be blocking existing pores, as seen in Figure 6.23.

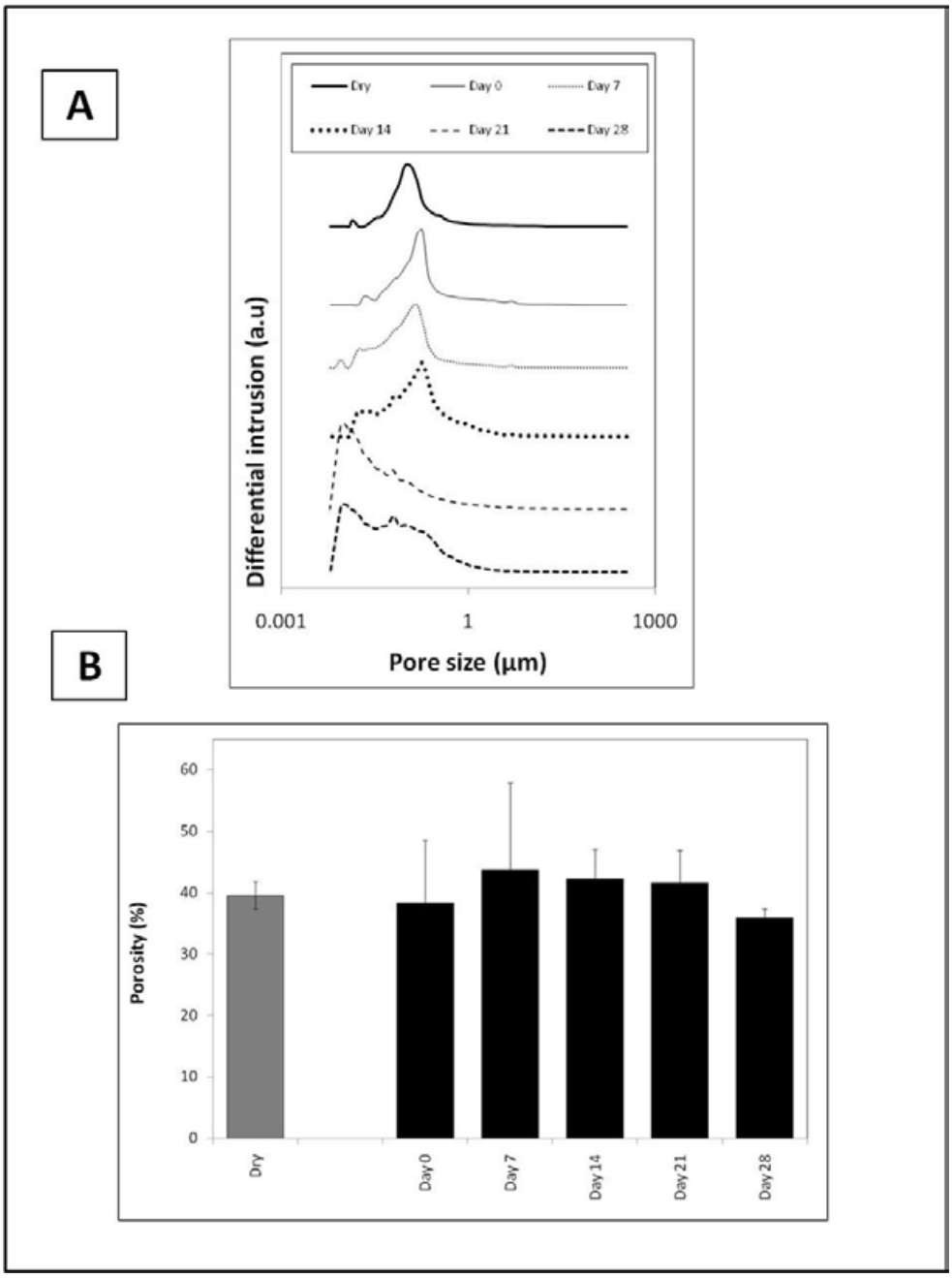

Figure 6.27 Pore size distribution of cellular CaP samples on day 28 (A) and porosity of cellular CaP samples on day 0, day 7, day 14, day 21 and day 28 (B). The error bars shown represent the standard error of the mean.

Finally, as in previous studies, the stability of the scaffold was investigated after the addition of cells. Although dissolution is apparent from the SEM images (Figure 6.23), there is no significant change in the dry weight of cellular CaP sample over 28 days, thereby supporting previous data on the scaffold generally being able to retain stability for 28 days.

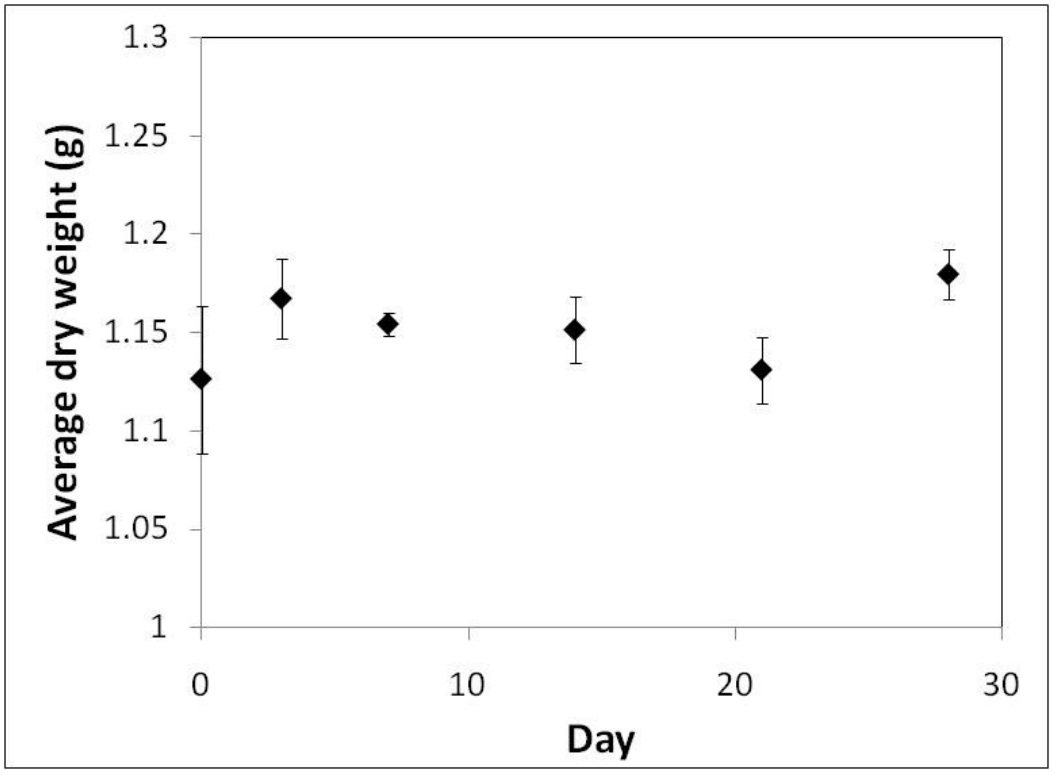

Figure 6.28 Average dry weights of cellular printed CaP discs after immersion in S-DMEM for 28 days. The error bars shown represent the standard error of the mean.

6.3 Conclusion

It has been shown that changes in the cell immersion media used with 3D powder printed CaP cements play a crucial role in cell adhesion, with the surface chemistry and reactivity of the printed structures affecting the stability of the cement and overall the ability for cells to adhere to that surface. Furthermore, the addition of sera proteins strongly influences the dissolution rate of the brackets and their pore sizes. Although the focus of this chapter has primarily been the rapid and accurate production of a bone scaffold for a ligamentous construct, the production of a bone scaffold has essentially been the primary objective. However, it should be noted that in order to utilise the printed structures as bone scaffolds there is a great need for further characterisation of the printed CaP, in particular cellular response to the structures. The cellular response reported here may be enhanced by the addition of growth factors, such as bone morphogenetic proteins (BMPs) and transforming growth factor-β (TGF-β), adding further chemical cues for increasing localised osteoinductivity or osteoconductivity through gene therapy or using bioreactors to recreate the *in vivo* conditions thereby promoting the production of ECM should the goal be to promote the growth of new bone.

For the purpose of this thesis it is concluded that as the surface of brushite dissolves and changes, the cellular response will inevitably change. However, surface modification may be employed to encourage cell adhesion through using techniques, such as the 3D powder printing method outlined in this study, to develop a scaffold of specific features favourable for cellular growth.

CHAPTER 7: PRODUCING A LIGAMENT CONSTRUCT USING CALCIUM PHOSPHATE AND FIBRIN GEL

In Chapters 5 and 6, fibrin gel and CaP have been separately evaluated as potential tissue engineering scaffolds. Chemical and morphological characterisation has been conducted and the cellular response to each scaffold determined. In this chapter fibrin and CaP have been combined and the powder printing technology investigated in Chapter 6 has been used to produce brackets designed with the goal of maximising adhesion between the two materials. Brackets of two sizes have been compared for their printing accuracy and reproducibility, and an evaluation has been made of the effects the CaP and fibrin combination has on cellular morphology and chemical response. In particular the tissue architecture has been compared to native connective tissue.

7.1 Introduction

Tendons and ligaments are prone to failure through rupture caused by excessive use (Hoffmann and Gross 2006) or degeneration (Rees *et al*. 2006) and current methods of repair, such as grafts (Robertson *et al*. 2007 and Bagnaninchi *et al*. 2007) have many limitations creating problems such as an altered gait, tendon shortening, lengthy operating times and the need for re-operation (Freedman *et al*. 2003 and Hankemeier *et al*. 2007). Therefore, there is a need to engineer a functional tendon or ligament which can be tailored to specific wound sites. Previous research in

this area includes using partly native tissue, such as porcine small intestinal submucosa, as a scaffold to minimise inflammatory responses (Badylak *et al*. 1999), the use of fibrin glue with bone marrow stromal cells (BMSCs) to improve patellar tendon healing (Hankemeier *et al*. 2007) and mesenchymal stem cells injected into collagen gels to repair defects in rabbit Achilles tendons (Young *et al*. 1998). As highlighted by Hankemeier *et al*. (2007), although the use of BMSCs is becoming highly popular in repairing tendon and ligament related wounds, problems with their use lie primarily in premature differentiation of the cells. Dressler *et al*. (2005) reported formation of calcified tissue when BMSCs were used. Whilst this may be useful in the enthesis region, calcified tissue is undesirable throughout the length of a tendon or ligament. Use of mature tendon-like cells, such as tenocytes, is likely to eliminate the worry of cell differentiation. Furthermore, it is important that the cells used continue proliferating for as long as they are required, producing the ECM needed to form new tissue. Quantification of glycosaminoglycans (GAGs), which is an important component of ECM can give an indication of how much ECM is present in comparative samples.

GAGs, are present as side chains on proteoglycans within the ECM (Shi *et al*. 2009 and Royce and Steinmann 2002). The GAG chain is a repeating unit consisting of one of two modified sugars (glucosamine or galactosamine) and uronic acid (Divya and Krishnan 2009). Almost all GAGs, other than hyaluronic acid, are covalently linked to protein cores in the Golgi apparatus forming proteoglycans (Preston *et al*. 1985). The GAG colourimetric assay is based on staining the sulphate components present on most GAGs. The standard used for this assay is based on the GAG chondroitin sulphate which is the most abundant GAG in connective tissue ECM (Riley *et al*. 1994).

As well as a high production of ECM, the development of new connective tissue may also be assessed by the amount of collagen produced since the dry weight of native tissue consist of over 70% collagen type I, and is responsible for the stiffness and strength of tendons (Freedman *et al*. 2003). It has previously been shown that the addition of L-proline (Reddy and Enwemeka 1996), and ascorbic acid enhance the production of collagen within a gel matrix as hydroxyproline is the most abundant protein within collagen (Carpenter and Hankenson 2004). Proline, and its hydroxylated form hydroxyproline, is present on every third repeating amino acid unit of the collagen polypeptide chain (Canty and Kadler 2002; Lanza *et al*. 1997 and Langrock *et al*. 2007) and whilst most researchers quantify the collagen content in engineered tissue by assessing the amount of hydroxyproline produced (Murphy *et al*. 2008; de Almeida *et al*. 2009 and Kirubanandan and Sehgal 2010) others have incorporated the proline directly into tissue and assessed the effects of mechanical stimulation on collagen concentration (Maeda *et al*. 2007). Both types of research intend to mimic the highly collagenous nature of tendons and ligaments. Furthermore, ascorbic acid, a natural antioxidant present in the body, has also been shown to stimulate the production of type I collagen and therefore promote tendon healing *in vivo* (Sarrafzadeh-Rezai *et al*. 2010 and Ramirez *et al*. 1997). Research also shows that deficiency in ascorbic acid directly leads to problems with collagen synthesis (Elliot 2002 and Murad *et al*. 1981).

The production of a more stable organised network, whereby pores are inevitably made smaller, should not inhibit the adhesion of the soft tissue to surrounding tissue. Problems with developing a tendon or ligament construct which meet these requirements lie in recreating the enthesis where a mismatch in the stress concentrations leads to repeated failure of the repaired tissue (Spalazzi *et*

al. 2006; Mikos *et al*. 2006 and Woo *et al*. 2006). The enthesis serves as a junction between hard and soft tissue and allows dissipation of stress through zones of transition. It is the gradual calcification within these zones which stops stresses applied to the area being centred at a specific spot. The recreation of the enthesis is particularly difficult when attempting to develop an entire construct mimicking the morphological and cellular characteristics of each zone (Spalazzi *et al*. 2006). Researchers have previously attempted to induce complex chemical pathways producing the transitional zones with graded mineral deposition, via gene therapy (Phillips *et al*. 2008), through the addition of bone-derived growth factors (Martinek *et al*. 2002), bone morphogenetic proteins (Wang *et al*. 2005) and cell therapy by introducing cells which promote the tissue healing process (Watanabe *et al*. 2002).

Although formation of zone specific tissue has previously been reported, gripping the soft tissue to accurately assess its mechanical strength is difficult. Attempts to test the tensile strength of such tissue has often led to new stress concentrations at the clamps, prematurely rupturing the soft tissue before completion of the test (Carpenter and Hankenson 2004). To overcome this issue researchers have used serrated clamps and frozen the ends leading to partial desiccation and cut the ends to fit into metallic grips (Carpenter and Hankenson 2004). In small animal models, and for constructs produced *in vitro*, this becomes a problem as the aforementioned methods all rely on the soft tissue being of a sufficient size to test after manipulating the ends. Production of an ideal ligamentous scaffold with the ability to grip the tissue without damaging the ends is one of the most important aspects of *in vitro* tissue testing which needs to be addressed.

In the previous chapter a powder printing method was used to develop bone scaffolds of specific geometries. Previous works have reported the success of this technique as a bone scaffold

(Leukers *et al*. 2005; Gbureck *et al*. 2007; Vorndran *et al*. 2008 and Bergmann *et al*. 2010). Similar methodology has been applied here to create a CaP based scaffolds to minimise slip.

7.2 Results and discussion

In order to create a ligament construct which may be gripped without damage to the ends, a series of CaP based brackets were designed using CAD software (Figure 7.1A-D). Rapid prototyping technology has previously been investigated for wax mould production in anchoring fibrin to cement (Paxton *et al*. 2010) and scaffolds with a hollow vascular system (Liu 2010). However, the use of 3D powder printing to directly produce cements specifically for gripping soft polymers has not been researched previously. The representative designs shown in Figure 7.1 (A-D) were created to reduce slippage by incorporating intricate channels on the surface of the scaffold, which cannot be made with hand moulding. The bespoke brackets printed consisted of a two-part structure with the base containing the grooved patterns to minimise slippage and a flat top half designed to hold the soft tissue scaffold in place (Figure 7.1E and F). The dimensional accuracy of the printed brackets was 95 ± 5 % (assessed by measuring the smallest printed feature of the brackets and comparing this to the original CAD diagram). This process had two advantages over a previously reported three-stage moulding process which required hand-casting cement into a silicone mould (Paxton *et al*. 2010) which did not enable the production of re-entrant angles and was of limited accuracy. Furthermore, 3D printing using the cement had advantages over laser sintering techniques, such as that used by Duan *et al*. (2010) to manufacture 3D nanocomposite scaffolds for bone tissue engineering, whereby the temperatures reached by the laser, in excess of

800˚C, such as the sintering temperatures used for the production of HA. The high temperature results in the production of a material with low specific surface area and precludes the incorporation of temperature sensitive therapeutic molecules.

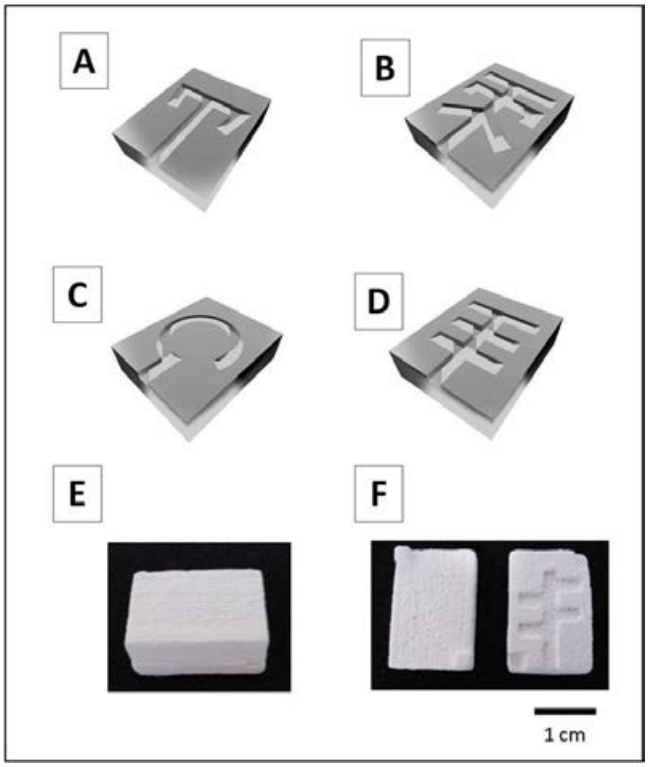

Figure 7.1 CAD images of bracket halves developed for the gripping of fibrin gel (A-D) using Thinkdesign software with the final representative printed structure (E) and the separated brackets (F) shown.

After sterilisation and formation of the construct, the cell-seeded gels began to contract. Figure 7.2 shows contraction of the gel around the brackets over 28 days. Image (Figure 7.2A) was taken 3h after the gel was added to the brackets. Evidence of contraction can be seen at the bottom of the image, where the gel is retreating from the plate sides. Tuan and Grinnell (1989) previously reported fibrin contraction of more than 50% after the addition of human dermal fibroblasts and whilst this is not the case in Figure 7.2A, anchorage of human fibroblasts is likely to be quicker than that of the tenocytes used in this study as attached human dermal fibroblast length (recorded as over 150µm by Oie *et al*. 2010) is vastly greater than that of tenocytes (~60µm). By day 7 (Figure 7.2B) the gel has contracted considerably, although the top of the image remains unchanged, suggesting some gel may be adhering to the side of the dish. A sterile scalpel was used to release the attached gel from the petri dish wall which allowed the fibrin to freely contract on all sides. Figure 7.2C shows the contracted gel on day 28 and formation of the ligament construct. Assessment of the construct beyond this period revealed no change to gel dimensions after alignment with the width of the brackets. This is because the CaP brackets have created a physical barrier stopping the gel from contracting any further. Results presented in Chapter 5 on fibrin alone shows that the gel will continue contracting in all directions, if there are no physical inhibitions (as supported by Atala and Lanza 2002 and Even-Ram 2009), by cellular attachment to the gel pulling the network closer on all sides.

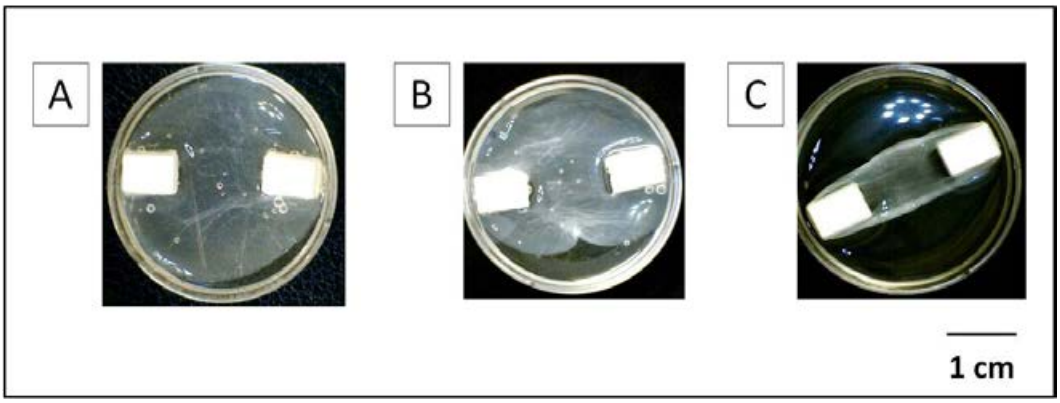

Figure 7.2 Contraction of cell-seeded fibrin gel around the printed CaP brackets on day 0 (A), day 7 (B) and day 28 (C).

Gel contraction was inhibited by the presence of the brackets. Figure 7.3 shows that after full gel contraction by day 14, the construct is self-supporting with no tears developing in the gel as it is lifted out of the petri dish, further supporting the theory that there is some adhesion between the gel and the CaP. Attempts to determine the extent of fibrin adhesion to the printed structures have previously been discussed in Chapter 6. Furthermore, the constructs are easily gripped with metallic implements without causing damage to the gel (Figure 7.3B). The ability to grip the soft tissue without causing damage is necessary for full mechanical testing of the gel. However, gripping the tissue induces stress concentrations causing either slippage or premature tearing (Maganaris *et al*. 2004) as previously discussed.

Initial assessment of the self-supporting nature of the construct revealed no slippage of soft tissue for any of the bracket designs used, indicating good attachment of gel to cement. Tensile testing of the constructs may reveal differences in gel slippage for the various designs used in this study.

Furthermore, it is also noted that whilst attachment may be sufficient between the two materials to create a self-supporting construct, studies would need to be conducted on the dissolution rate of CaP within the gel. The dissolution and precipitation of the cement, as previously discussed in Chapter 6, would ultimately provide a more realistic representation of the graded enthesis seen in native connective tissue. Over the 28 days of this study, no obvious changes were seen in the structural integrity of the cement, with all anchors retaining their original printed features suggesting that even with mechanical agitation by regular replenishment of supplemented media, the printed scaffolds do not degrade quickly. Lack of cement dissolution may also be indicative of formation of the more stable HA. Whilst the stability of hydroxyapatite allows for sufficient support in early tissue formation, this may be undesirable long-term *in vivo* where the new tissue would ultimately replace the temporary scaffolds introduced to the body. Chemical changes to printed CaP in supplemented media have previously revealed that there is no significant change to the structure. However, a combination of CaP, fibrin and cells in media is a new system and therefore this area would need further investigation.

One of the advantages of the 3D printing technique used in this study is that it may be utilised to incorporate growth factors, and other chemical stimuli, into the CaP promoting the development of a transitional area between the soft and hard tissue. The potential of this technique is such that denaturing by increased temperature, as is the case with some of the techniques previously discussed, can be avoided entirely.

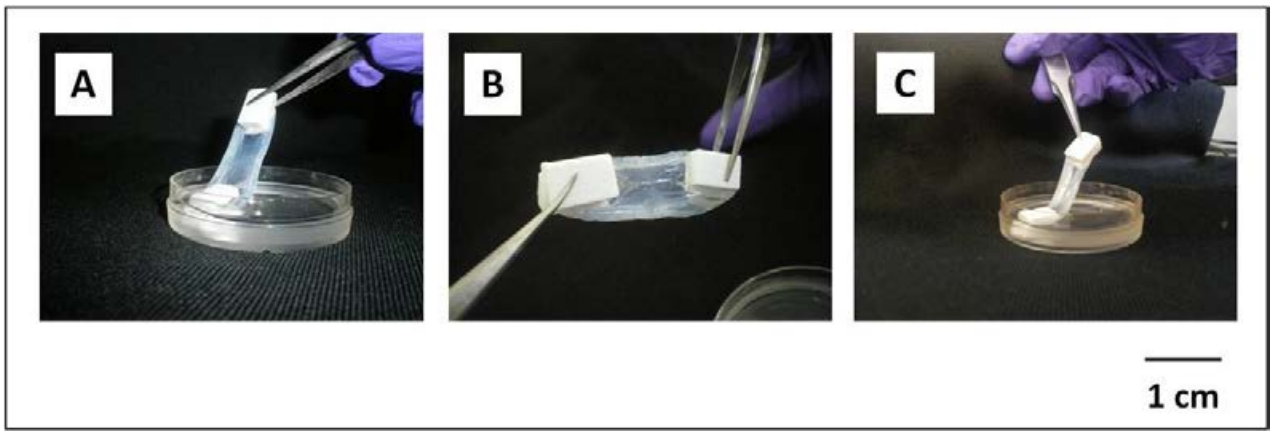

Figure 7.3 Photographs showing that the gel is self-supporting on day 14 (A), day 21 (B) and day 28 (C) after seeding.

Formation of a self-supporting construct has been supported by contraction of the gel around the printed cements. However, as the gel contracts, compressive forces at the edge of the gel as well as tensile forces in the centre of the gel are exhibited on the cells seeded within. The cellular response to gel contraction over 28 days was initially assessed via SEM (Figure 7.4). As the gel begins to contract, tension is created between the two ends where the gel is adhered to the CaP bracket which is known to cause cell proliferation and alignment (Sawaguchi *et al*. 2010). Initially, as depicted in Figure 7.4A, a rounded cellular morphology with no cytoplasmic projections and contact between cells. By day 3 (Figure 7.4B) an increase in cell number is apparent with attachment between groups of elongated cells, indicative of cell agglomerate formation. Agglomeration of cells in a fibrin network indicates gross cellular proliferation. After the tenocytes begin covering most of the surface area available for attachment (Figure 7.4C),

cellular alignment becomes evident (Figure 7.4D) with the cells arranged parallel to one another. Although cellular alignment may have occurred earlier than day 14 (depicted in Figure 7.4D), Figure 7.3A shows that it is by day 14 that the gel has contracted to the same width as the brackets. It is therefore likely that the tension caused between the brackets of the now fully contracted gel has caused this alignment of cells to occur. The alignment is favourable as tendon and ligament fibrils both contain cells arranged in a similar orientation (Vunjak-Novakovic *et al*. 2004) to increase tissue strength at sites where heavy loads are experienced, such as the knees, the heels of the foot and the wrists.

By day 21 (Figure 7.4E) cellular alignment persists, with cells fully populating the fibrin scaffold. However, as tendons are composed mostly of water (over 60%) and there are less than 5% cells present within the structure itself (Hoffmann and Gross 2006), cell proliferation on the gel matrix is of less importance in comparison to the alignment, the necessary precursor to fibril development (Ralphs *et al*. 1999). It has also been noted that cells isolated from tendons/ ligaments are not always aligned as cells extracted from the sheath are randomly orientated and those extracted from the connective tissue stroma are aligned (Chowdhury *et al*. 1991). Variation in cellular orientation after attachment was minimised in this study by using primary cells taken from isolated tendon fibres. After 28 days however (Figure 7.4F), the ECM between cells appears fragmented with debris visible around the construct. This would suggest that the death phase of the tenocyte life cycle has commenced. The addition of chemicals other than proline and ascorbic acid, stimulating production of ECM may be investigated since the ECM is composed of proteoglycans, structural glycoproteins, water, elastin and collagen (Dahlgren 2007), any of which may be quantified in the development of the new tissue.

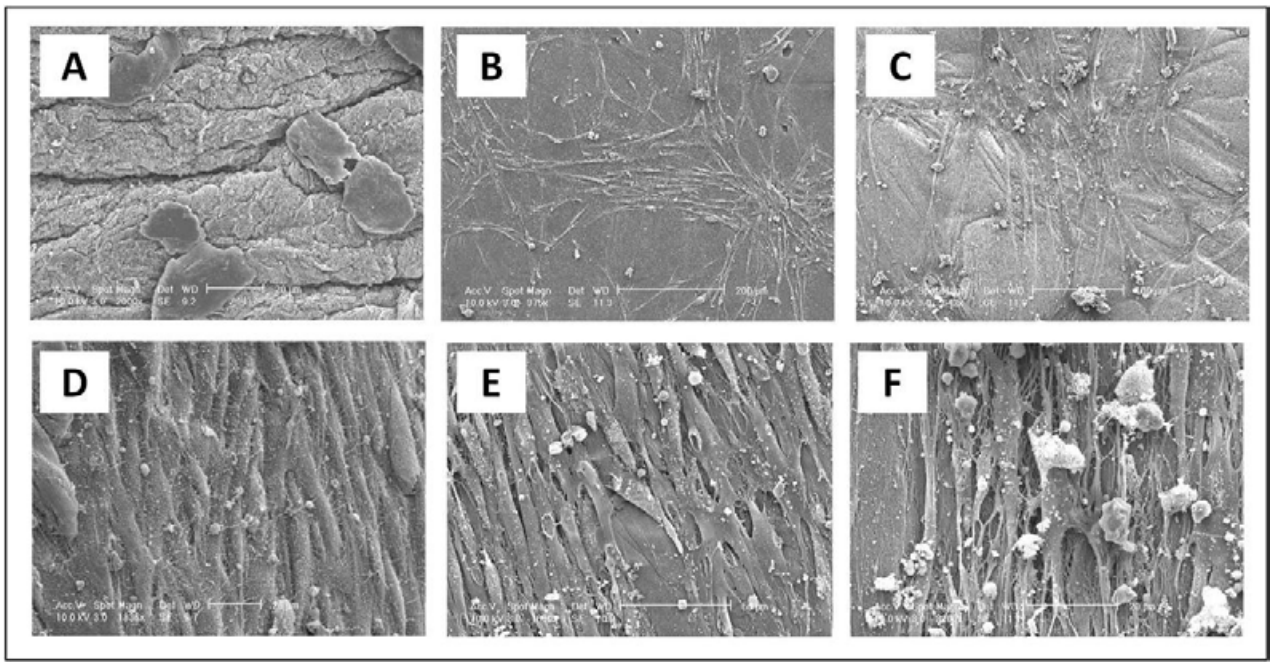

Figure 7.4 SEM images of tenocytes seeded onto fibrin gel on day 0 (A), day 3 (B), day 7 (C), day 14 (D), day 21 (E) and day 28 (F) showing gradual proliferation and alignment of cells. Scale bars equal to 20 µm (A and F), 200 µm (B and C) and 200 µm (D and E).

From the contraction of the gel shown in Figure 7.2, the tension at the centre of the construct is likely to differ from the ends where support is provided by the brackets. Previous research shows that cell morphology and function varies considerably upon varying mechanical stimuli (Janmey and McCulloch 2007 and Kim *et al*. 2009).

Investigation of cellular changes caused by a variation of forces between the two areas was attempted through fluorescence microscopy (Figure 7.5). Similar to Figure 7.4, cell alignment can be seen on day 14 (Figure 7.5D and J) with the number of viable cells greatly reduced by day

28 (Figure 7.5F and L). As previously stated, this is due to the life cycle of tenocytes, with cell death also leading to a build-up of toxic products within the matrix which affect the viability of the remaining cells (Hampson *et al*. 2008). Furthermore, there is no obvious difference in the morphology of the viable cells between the end attached to the CaP bracket and the central portion of the gel suggesting that either the stresses exhibited at the two locations are the same or that a difference in the stresses is not sufficient enough to cause morphological changes to the cells. From the size of the entire construct it is likely that the latter is true. In order to fully determine this further investigation would be needed of constructs with varying lengths whereby any changes in the stress at the end attached to the CaP in comparison to the middle of the gel would be apparent.

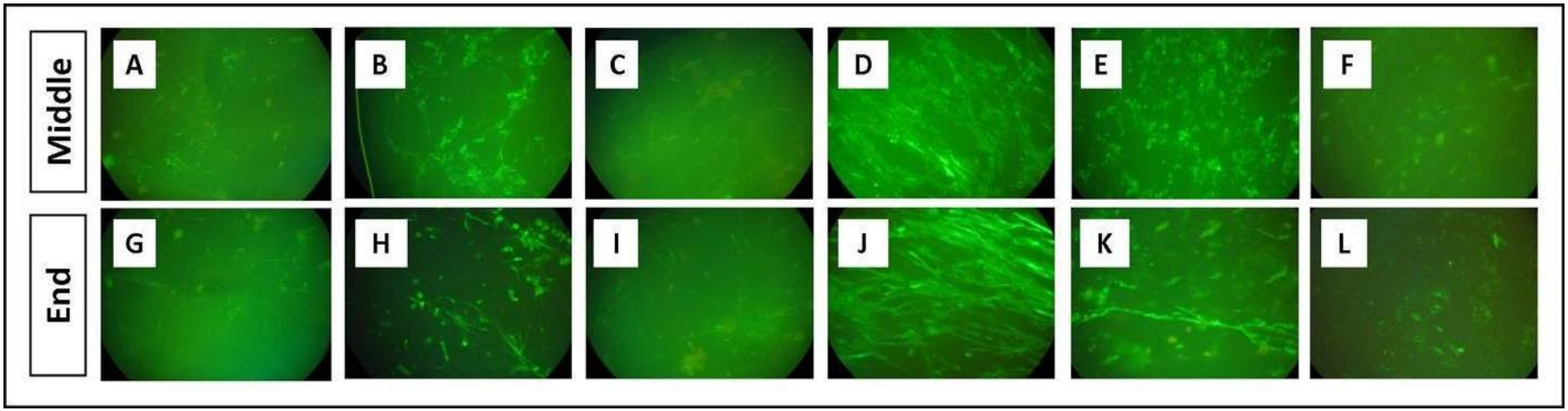

Figure 7.5 Fluorescent images showing the morphology of living cells seeded onto the ligament construct at the middle of the construct as well as the end on day 0 (A and G), day 3 (B and H), day 7 (C and I), day 14 (D and J), day 21 (E and K) and day 28 (F and L).

Figures 7.4 and 7.5 show tenocyte morphology in the construct over 28 days, with Figure 7.5 indicating the morphology of living cells alone. Figure 7.6 reports the approximate number of living cells in the ligament constructs based on the MTT assay (Sieuwerts *et al*. 1995). It can be seen from the results that there is a significant increase ($P<0.05$) in the number of viable cells present in the constructs on day 14 with cell death causing a decrease in the cell viability calculated by day 28. This supports the morphological changes observed in Figures 7.4 and 7.5. In native tissue as a tendon or ligament matures the number of cells within the tissue also decreases owing to maturation and remodeling (Carpenter and Hankenson 2004), therefore, even without mechanical stimulation the decrease in cell viability after 28 days in culture could be indicative of new tissue formation, as a collagen matrix is already being formed (evidence to support this is shown in Figure 7.7A-F).

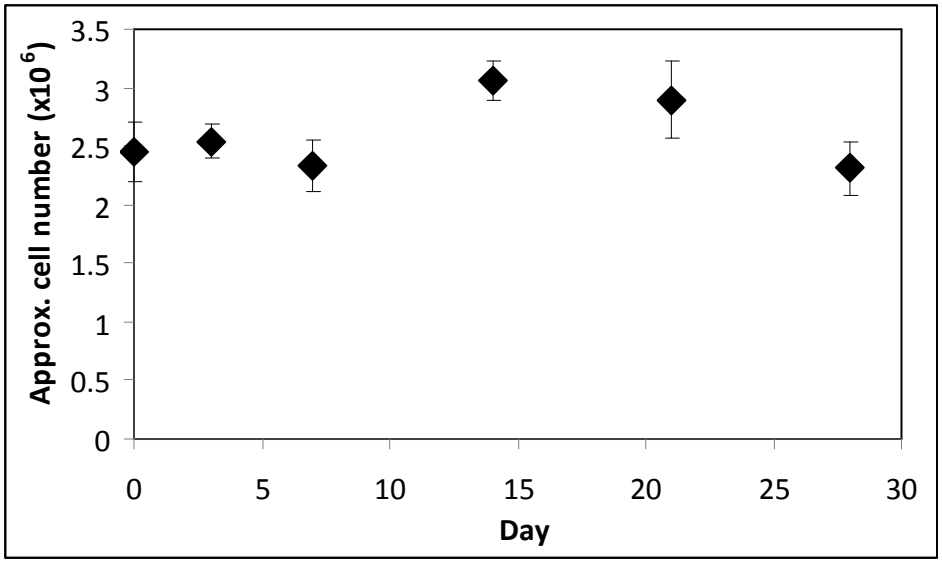

Figure 7.6 Approximate number of living cells in the construct over 28 days, determined by measuring the mitochondrial activity. The error bars shown represent the standard error of the mean.

Evidence of collagen production by the cells is shown by increasing amounts of cytoplasm being formed over 28 days (Figure 7.7G-L). Whilst cellular viability reaches a plateau by day 14 (Figure 7.5D and J), with aligned cells present throughout the soft tissue scaffold, it is also necessary to investigate the intracellular response. Firstly, the aligned orientation of the cells may be investigated further by focusing on the position of cell nuclei. Figure 7.7 (M-Q) shows the Weigert's iron hematoxylin stained cellular nuclei in 6 μm fibrin sections over 28 days in comparison to native tendon dyed using the same method. Whilst Figure 7.7M shows clear alignment of tenocyte nuclei, sections taken of the construct over time show nuclei leaching from the scaffold which may be caused by the sectioning technique. Sections for this research were

made using a stainless steel blade fixed into a manual cryotome. Although care was taken to position the fixed tissue as centrally on the blade, with fixative debris being removed between each section of sample cut, the size of the contracted gel meant that it was difficult to manipulate gel orientation within the cryogenic chamber. However, it can still be seen, most clearly in Figure 7.7O, that although the cells appear outside the gel matrix, their orientation may still be aligned. Further sectioning is necessary before this can be confirmed although the assumption strongly supports results reported in Figures 7.4 and 7.5. Fibroblastic orientation such as this has previously been shown to be a precursor to collagen fibrillogenesis (Benjamin and Ralphs 2000) supported by an assessment of the ECM deposited by the cells, using Beibrich scarlet-acid fuschin, where a gradual increase in matrix production over 28 days (Figure 7.7H-L) is evident. Although cellular activity has previously been shown to greatly diminish by day 28 (Figure 7.6), high levels of matrix can still be seen. Degradation of matrix proteins is caused by enzymatic digestion *in vivo* (Roycik *et al*. 2009) and although cells are dying over time, the number of dead cells does not affect the matrix which has already been deposited and that which is still being deposited by the remaining viable cells. Furthermore, the addition of aminohexanoic acid, a known enzyme inhibitor, could contribute to ECM integrity as previous studies by Wong *et al*. (1992) have shown that there is a strong correlation between ECM degradation and the amount of the enzyme plasmin present within culture medium. The increase in ECM seen suggests that the fibrin scaffold is being replaced by a more permanent support, which further indicates early tissue development (Ross and Tranquillo 2003).

Finally, an assessment of the collagen content of the scaffold was made. Tendons and ligaments are highly collagenous (Shinji *et al*. 2010) and for a true representation of connective tissue it is

necessary to replicate the formation of aligned collagen fibrils (Silver *et al*. 2006). Figure 7.7A shows clearly aligned collagen fibrils, stained with Analine blue, in native rat tail tendon. Figure 7.7B-F show presence of collagen within the developed constructs, evidence of collagen fibrillogenesis and therefore the initial stages of fibril development, precursor to end-to-end fibril assembly and fibril bundle formation (Zhang *et al*. 2005). Although the alignment is difficult to observe (Figure 7.7B-F), a steady increase in collagen production is evident in the fibrin scaffold, supporting previously published data by Hankemeier *et al*. (2007). Hankemeier further reports that cellular morphology on the surface of matrix deposition is most important, i.e. the depth of cellular penetration varies. The samples used in this study have been sectioned to a depth of 6 μm to ensure dye penetration and ease of visibility under a light microscope. Keeping the sectioning depth uniform for all samples being stained ensures that dye penetration is homogenous and therefore all stained sections are comparable. Furthermore, Woo *et al*. (1990) report a 6% penetration depth of cells on a rabbit anterior cruciate ligament. Since fibrin contracts readily in all directions, as previously discussed in Chapter 5, and it is difficult to control the contraction let alone ensure that the rate of contraction is the same for all ligament samples created; it is highly difficult to focus particularly on areas of this penetration depth. It is more feasible to replicate the studies of Hankemeier *et al*. (2007) remembering that morphological changes may be apparent for cells at varying depths throughout developed tissue. In order to address this issue, histological images were taken of at least 6 separate sections for each dye type.

From the SEM and fluorescence images (Figures 7.4 and 7.5) whereby cellular alignment and fibrillogenesis is evident, a longer study may be necessary to monitor morphological changes, particularly mature development of collagen fibril structures in bundles. Further assessment of

collagen fibril formation may be made by investigating the presence of fibripositors, areas of the matrix rich in the globular protein actin, where it is believed aligned collagen fibrils are formed (Bayer *et al*. 2010).

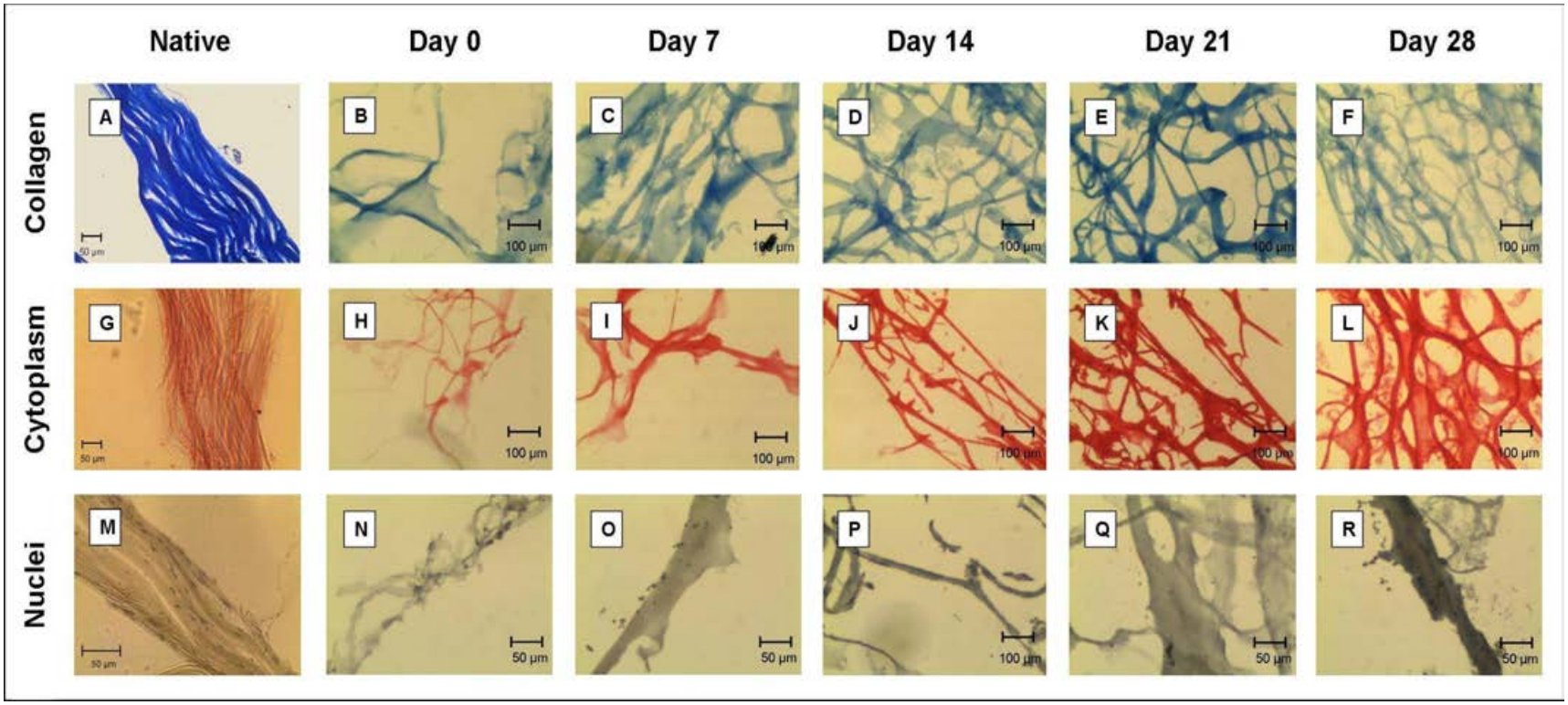

Figure 7.7 Histological staining of native tendon sections and fibrin-based construct sections using Analine blue for collagen (A-F), Beibrich scarlet-acid fuschin for cytoplasm (G-L) and Weigert's iron hematoxylin for nuclei (M-R).

Since there is no ECM compositional difference between tendons and ligaments (Tozer and Duprez 2005), distinction between tendons and ligaments cannot be made by studying the ECM alone. Quantitative analysis of ECM deposition within the fibrin gel over 28 days (Figure 7.8) showed that whilst the GAG content of native tendons was found to be 8.65 ± 0.01 µg/mg of tissue, the maximum GAG content for the large construct was 2.30 ± 1.01 µg/mg of construct with no significant difference between the middle and end regions. However, for the smaller construct it has been shown that there is a significantly higher amount of matrix produced after day 14 in the middle region of the construct (4.68 ± 0.63 µg/mg of construct). Whilst previous research by the group has shown that size of the ligamentous construct does not affect the amount of GAG produced, the results from Figure 7.8 indicate that the addition of chemical factors, inducing collagen synthesis and reducing scaffold degradation, contribute to a higher level of GAG produced with significant differences between the end and middle regions of the constructs, as noted by Flint (1972) who studied the GAG content along the entire length of a tendon. Whilst GAG content varies along the length of connective tissue (Rigozzi *et al*. 2009), changes in GAG production between the different regions in comparison to the large construct may be caused by the difference in the width of the brackets. As previously noted, contraction of cell-seeded fibrin is limited to the width of the bracket used and with smaller brackets having a smaller width (4 mm in comparison to 16 mm for the larger brackets) the fibrin is able to contract more, inducing higher compressive and tensile forces on the cells. The change in the forces leads to increased cellular stimulation and therefore a higher level of ECM deposited (Chiquet *et al*. 2003). This data supports the metabolic activity (Figure 7.6) shown for the cells whereby cellular activity reached its peak by day 14.

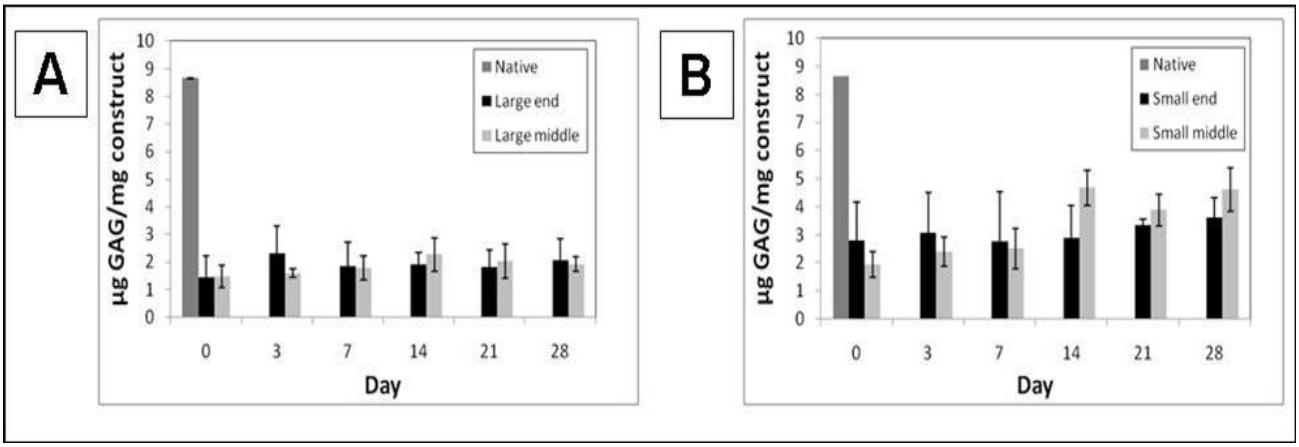

Figure 7.8 µg GAG per mg of construct made using large brackets (A) and small brackets (B). The error bars shown represent the standard error of the mean.

To support the histological images of collagen production, a hydroxyproline based assay was used to quantify the amount of collagen synthesised by the cells within the construct. Figure 7.9A shows diminished collagen production in the middle region of the construct on day 14 of the study, with higher levels of collagen produced on days 21 and 28 in comparison to the end region. From the cellular activity previously shown in Figure 7.4, Figure 7.5 and Figure 7.6, day 14 is when the highest levels of collagen production are expected. In the analysis of the smaller constructs, it is shown that on day 14 there is 10.78 ± 0.63 % w/v collagen present in the middle region of the construct in comparison to less than 8% on all other days. This would suggest that the experiment may need to be repeated for the larger constructs.

Results from the smaller constructs (Figure 7.9B) show a statistically significant difference between the amount of collagen deposited in the middle and end regions on days 7 and 14. The

highest level of collagen produced is seen on day 14 (10.78 ± 0.63 % w/w) when the maximum cellular viability was previously recorded (Figure 7.6). Native tendon collagen content has been reported to be over 70% of the dry weight of tendons (Meyer *et al*. 2009) and from the analysis of native rat tail tendon this was shown to be the same (77.17 ± 0.20 % w/w). Although, the levels of collagen obtained from the constructs is 14% that of native tissue, recreating the collagen levels of native tissue is vital for the strength of the overall construct (Wang *et al*. 1994). The amount of collagen produced by a cell is dependent upon the age of that cell and further chemical and mechanical stimulation of the cells may produce more ECM and therefore collagen deposition within the matrix.

Mechanical and chemical stimulation protocols have been developed and optimised within the research group (results not reported). In relation to the constructs reported here, the addition of ascorbic acid and proline has made a significant difference to the amount of collagen produced over 28 days. As previously discussed, in native tissue ascorbic acid is essential for collagen synthesis as without ascorbic acid a collagen-deficient system is likely to develop, affecting the tensile strength of the tissue (Kaplan *et al*. 2004). Successful promotion of collagen synthesis, through the addition of ascorbic acid and the essential collagenous protein, proline (Kaplan *et al*. 2004), is shown in Figure 7.9B, mimicking native tissue. The concentration of the added collagen promoters was established from previous work conducted within the laboratory and whilst the individual effects of the additional chemicals may be interesting, due to the limited amount of printed brackets available the optimal ascorbic acid and proline concentrations as previously established were used for the formation of the small brackets.

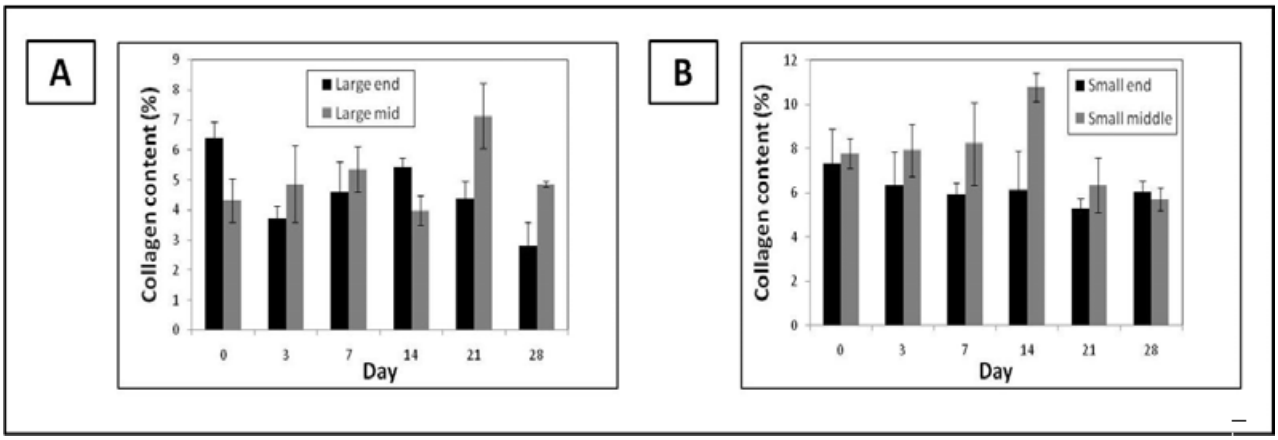

Figure 7.9 Collagen content of constructs made using large brackets (A) and small brackets (B). The error bars shown represent the standard error of the mean.

Whilst a colorimetric assay has been used for the analysis of hydroxyproline within the constructs, the method does not differentiate between the four hydroxyproline isomers for which more specific methods, such as reversed-phase high performance liquid chromatography have previously been reported (Langrock *et al*. 2007). Whilst histological and biochemical techniques were used to ascertain the amount of collagen within samples, this is not the only detectable protein available. Elastin and glycoproteins, such as decorin and fibronectin, may also be identified (Neurath and Stofft 1992), the importance of which were recognised by Kyriakides *et al*. (1998) and Svensson *et al*. (1999) where exclusion of certain proteoglycans, such as thrombospondin 2 and fibromodulin, resulted in abnormalities in the fibrillogenesis process of connective tissue in mice.

7.3 Conclusion

In this chapter powder printing technology has been used to develop 3D brackets for use in engineering tendons and ligaments. The self-supporting constructs developed have been characterised after the encapsulation of tendon-specific tenocytes and, where possible, compared to native tendons isolated from rat tails. Initially large constructs, with the larger brackets set and maintained 3 cm apart, were produced to prove the concept was feasible after which a smaller size, 2 cm, was also investigated since tendon length is known to vary considerably. A comparison of the cellular compatibility of the two sizes showed no significant differences. Further analysis of the middle and end regions of the constructs revealed little difference in cellular morphology although this may be because a longer construct would allow greater dissipation of stresses and therefore differences between regions would be clearer.

It was noticeable that the cells within the developed construct became aligned, similar to cellular orientation in native tendons, whilst production of ECM was recorded by measuring the GAG content. Furthermore, collagen content was also quantified and similar to the GAG content it was shown that the smaller constructs, containing additional proline and ascorbic acid, produced more ECM and more collagen. Histological analysis of the constructs supported the data obtained for GAG and collagen synthesis from the chemical assays. Whilst histological analysis showed deposition of matrix containing collagen, it was not possible to investigate the enthesis region specifically as the construct was too small.

Finally, whilst mechanical testing is the obvious next step for testing these novel constructs, as brackets were developed specifically to enhance gripping of the soft gel, the potential of the

construct, particularly the rapid production of brackets, has been realised. From this it is shown that analysis of the adhesion mechanism between the fibrin and CaP is necessary.

CHAPTER 8: GENERAL CONCLUSIONS

The research presented in this thesis aimed to investigate a suitable scaffold for the development of tendons and ligaments. For this purpose a number of polymeric scaffolds have been investigated with particular focus on fibrin as the soft tissue support. Powder printing technology has been used to rapidly develop bone tissue scaffolds of specific geometry to represent the bony ends of a ligamentous construct. The main conclusions of the topics investigated for this thesis have been presented in this chapter.

Three naturally derived polymers, agarose, gelatin and carrageenan were initially investigated as potential tissue engineering scaffolds. Both agarose and gelatin were found to be unsuitable for tissue engineering. This was due to their gelation times. *κ*-carrageenan was initially the preferred scaffold. The gel was able to withstand higher loads under compression and had a clotting time suitable for cell-seeding.

Cell viability and proliferation were shown to be enhanced on the surface of *κ*-carrageenan in comparison to within the gel, owing to restricted cell migration within the highly ordered network after cell encapsulation. Since carrageenan has three forms, the other two, *ι*- and *λ*-carrageenan were also considered. *λ*-carrageenan was found to be non-clotting and therefore is unsuitable for tissue engineering. However, the *ι*- form has fewer ester sulphate groups along the polymer chain, thus revealing a higher cell viability and proliferation rate after encapsulation within the gel in comparison to *κ*-carrageenan, with metabolic activity increasing over 28 days. Cellular

proliferation was shown to cause mass loss over time in both *κ*- and *ι*-carrageenan. However, the introduction of network manipulation agents, such as sucrose discussed in Chapter 4, have the ability to affect gelation kinetics which are in turn likely to affect the mechanical stability of the gelled networks.

The investigations into the suitability of carrageenan as a tissue engineering scaffold showed cell compatibility was achieved over the course of the study. However, reports have emerged of the carcinogenic effects of carrageenan with malignancies found in animal models. Whilst no ban on the use of carrageenan in the food industry currently exists, the rising concern with ulcers and tumours caused by carrageenan has lead to the search of an alternative scaffold for engineering tendons and ligaments for this thesis.

Fibrin was selected for use as the scaffold for the final constructs as it already exists within the human body, known to cause no toxic by-products or inflammation and is already used for clinical application, such as fibrin glue. In investigating the effect of fibrinogen to thrombin ratio upon clotting, it was found that the clotting time of fibrin decreases with higher concentrations of thrombin. Furthermore as the concentration of fibrinogen was reduced, the number of central zones/ nodules at which the thrombin cleaved on a fibrinogen monomer also decreased leading to fewer bridging points and an overall looser fibrin network.

Fibrin supports cellular growth and matrix deposition. In comparison to the previously investigated carrageenan, the fibrin network produced was shown to be stable in cell culture media with and without cells for 28 days suggesting the ECM produced by cells within the gel is of insufficient quantity to cause fibrin digestion. Even so the scaffold was able to support cellular

growth and proliferation, shown by a comparison of 3T3 fibroblasts and rat tail tenocytes. Whilst both cell types cause contraction of the gel matrix in all directions the scaffold was easy to handle and manipulate, and therefore with further manipulation may be tailored for specific tissue needs.

3D printed CaP is ideal for the attachment of soft tissue in a ligament construct. Stability of the printed structures was maintained and the chemical change, in the formation of hydroxyapatite, did not affect the stability of the overall structures although SEM micrographs showed evidence of dissolution after immersion in cell culture media which in turn affected surface roughness and the interaction of cells to the surface of the cement. Cellular adhesion to the CaP was further affected by changes to the porosity of the scaffold over time. However, cells were shown to be viable on the cements over 28 days after treatment with FBS. Mechanical agitation via removal of old media and replenishment of new media caused the physical removal of attached cells on the surface of the cements. Since the purpose of this research is not to investigate potential bone scaffolds, experiments related to scaffold manipulation for optimum cell adhesion was not investigated. From the cellular compatibility over the duration of the study, it was shown that the printed cements promoted cell attachment and proliferation and may be used in conjunction with fibrin as a ligament scaffold.

Bespoke brackets were printed to minimise slippage of soft tissue. After 28 days the construct was still seen to be self-supporting. The constructs were shown to produce ECM and collagen although after the addition of ascorbic acid and L-proline, production of GAGs and collagen was considerably higher. The high levels of collagen are necessary for a predominantly collagen based tissue.

Ligamentous constructs were successfully formed from the combination of fibrin and CaP. The construct showed cellular compatibility and no difference was found in the cellular morphology of large and small constructs. The alignment of cells, determined by SEM, fluorescent staining and histology, in the fibrin matrix was comparable to native tissue with no change being seen in cell orientation at the end and middle regions of the engineered ligament. An assessment of the metabolic activity within the constructs showed a slight peak at day 14 with little difference in overall cellular activity at the start and end of the study. The overall research showed that the construct had potential as an engineered ligament.

CHAPTER 9: FUTURE WORK

The research presented in this thesis has led to the successful development of a self-supporting ligamentous scaffold utilising powder printing technology to produce bespoke brackets, minimising slippage of polymer based soft scaffolds. In order to fully investigate the potential of the construct, further work is required. This chapter aims to highlight some of the areas which require further investigation and outline how the work will be beneficial to the research.

As a general statement it should be noted that natural variation exists in biological samples and the assumption throughout the work presented here is that cell function is always the same and therefore quantitative data is averaged. However, this is only an approximation as cellular function is variable. For more accurate representation of a cell population larger sample sizes would be ideal.

For the materials specifically used in this research, although a few gels have been investigated, the list of soft tissue scaffolds available, both natural and synthetic, is exhaustive. Some of these have briefly been mentioned in Chapter 4. Investigation of other gels is particularly necessary to ascertain the effects they will have on the function of the ligament construct produced in Chapter 7.

In the characterisation of fibrin, it was realised that variation of thrombin concentrations strongly affect fibril length, thickness and overall network morphology. After considering the effects on cellular compatibility and structural integrity when *ι*-carrageenan was submerged in cell culture

media and the SEM images of fibrin clotting behaviour with various concentrations of thrombin, it has been ascertained that less bridging points lead to a less ordered network. If the effects of fewer clotting points are similar to *ι*-carrageenan then the less bound fibrinogen chains in low concentrations of fibrinogen would create a mechanically weaker structure. Degradation of the structure may mean that there are optimal concentrations of fibrinogen and thrombin which may be used to maintain a stable structure whilst allowing nutrient diffusion and cell migration and proliferation. Therefore a thorough investigation of the effect changes in thrombin and fibrinogen concentration induce on cells may allow additional information to be collected on the suitability of the construct in tissue engineering. Initial investigations in this particular area could begin from an extension of the water uptake study investigated, as shown in Figure 5.7. Whilst it has been hypothesised that scaffold weight decrease may be caused by solutes leaching out of the network, confirmation must be attained. This may be done by collecting the submersion liquid over time and conducting protein assays or inductively coupled plasma- mass spectrometry (ICP-MS) to investigate whether there is an increase in solute content or by measuring the density of the gel over time via pycnometry.

The hard tissue scaffold used for the construct, the CaP, may also benefit from further exploration, particularly in consideration of the technique employed. The unreacted powder present within the cements, caused by the layer-by-layer printing technique may cause premature dissolution or a peeling effect whereby layers are separated from each other due to poor adhesion. Whilst there is some indication of unreacted powder present within the structures, no weight loss has been observed. However, the duration of all studies conducted for this thesis is 28 days, in accordance to the life cycle of the fibroblasts and tenocytes being used. For a more

comprehensive study, further investigation of dissolution beyond the surface of the cements is required particularly as the cements may help to grip the soft tissue and premature dissolution would cause weaknesses in this area leading to stress points and eventual loss of grip of the gel.

The construct discussed in Chapter 7 should be investigated further as the behaviour of fibrin and CaP individually behave very differently to the combination of the materials, as previously discussed. The contraction of fibrin is no longer uninhibited in all directions, as discussed in Chapter 5, but halted by the presence of the printed brackets. Whilst the contraction has been discussed in depth in Chapter 5, the effects of increasing the seeding density on a ligament construct are as yet unexplored. It is likely that increasing the seeding density will affect the contraction rate, with a higher number of viable cells causing the network to be pulled tighter and sooner than a low density of cells. The effect changes in cell number are likely to have on the ligament construct developed here must be explored, as cell changes will also affect the amount of ECM and collagen produced, in turn affecting the physical characteristics of the final ligament.

Furthermore, the production of GAG and collagen within the construct has been quantified. Whilst these are the only two markers investigated, a great many more markers for specific proteins such as the proteoglycan decorin which makes up approximately 90% of the proteoglycan content in fresh ligaments (Kuroda *et al*. 2010), exist which may also be used to reinforce the data presented in Chapter 7 and provide a fuller picture of cell function after encapsulation in a ligamentous scaffold.

As well as chemicals produced by the cells, chemicals introduced to the extracellular environment induce specific effects in the intracellular environment through integrin receptors on

the cell membrane (Nishimura *et al*. 2009). Whilst it has been established that addition of chemicals, such as L-proline and ascorbic acid, affects cell matrix production with particular reference to collagen production, these are not the only chemicals responsible for changes. It has been shown that adding poly(L)lactic acid increases the mechanical integrity of a ligament construct as well as promoting cell migration (Ide *et al*. 2001). Understanding changes induced by changing the chemical makeup of the cell culture media may help to optimise the efficiency of the construct as a realistic functional ligament model for clinical applications.

Furthermore, the effects of mechanical stimulation alone must also be investigated. Compressive and tensile loads applied to developing connective tissue have been shown to affect proteoglycan production directly (Benjamin and Ralphs 1998) and therefore the amount collagen synthesised (Screen *et al*. 2005). It has also been shown that cyclic tension on *in vitro* cultured chick tendons increases cell proliferation which increased the amount of collagen produced (Tanaka *et al*. 1995). Even when serum is removed from media Yang *et al*. (2004) showed that cyclic stretching alone can significantly increase the amount of cells proliferating within a scaffold. Whilst the brackets developed for the research presented here have been shown to successfully support a fibrin scaffold, the effects of compressive and tensile loads have not been explored. Slippage investigation in particular will benefit from tensile strain tests. The effects of mechanical stimulation in combination with an optimal chemical environment may produce higher levels of collagen than those reported here. However, it is necessary also to investigate the optimal level of stress application to the developing tendon or ligament and existing failure of connective tissue indicates that failure may be caused excessive stress application.

Application of mechanical stress upon the construct will also provide more information on the development of the enthesis and the adhesion of the soft tissue to the printed hard tissue as this information has been difficult to ascertain from the ligament constructs. As cell morphology changes, causing changes to the ECM, the effects on the fibrin scaffold as well as the CaP scaffold may be altered. This thesis provides a control for investigations needed to explore the effects of mechanical stimulation.

The duration of this study and continuation of the research presented here is also in need of further investigation. The assessment of fibrin adhesion to CaP has proved unsuccessful in this research. However, it is necessary to develop a method by which the enthesis may be looked at in its entirety. This will indicate whether regions of calcification exist between the two tissue types or whether the attachment is created by gel intrusion into the pores of the printed brackets. Although visual techniques exist for this purpose, such as the SEM used throughout this research, method of sample preparation require optimisation. Particular problems lie in sectioning the construct along the horizontal axis through two very different materials. Implements ideal for soft tissue sectioning do not section the hard tissue scaffold whereas those ideal for hard tissue are to crude for the weaker gel.

Finally the use of different cell types, such as BMSCs mentioned in Chapter 7, must be investigated as the age and type of cells used strongly affect the amount and type of ECM produced which may in turn affect the structure and function of the ligament.

Whilst the future work outlined here relates to areas of expansion or further investigation in the research presented in this thesis, the list is not exhaustive. As experimental procedures are

developed, further issues are likely to arise which require addressing such as instrumental limitations and material performance characteristics. All issues outlined in this chapter have been noted with the eventual goal of creating a tendon or ligament suitable for clinical applications.

REFERENCES

Abell AB, Willis KL and Lange DA (1999) Mercury Intrusion Porosimetry and Image Analysis of Cement-Based Materials. J.Colloid Interf. Sci., 211, pp. 39-44.

Adolfs MJP, Bonta IL and Bragt PC (1979) Increased lipid peroxidation and decreased hepatic aminopyrine metabolism during carrageenin-induced granulomatous inflammation in the rat. Proceedings of the BPS, 12-14 Sept, pp. 123P-124P.

Ahmann KA, Weinbaum JS, Johnson SL and Tranquillo RT (2010) Fibrin Degradation Enhances Vascular Smooth Muscle Cell Proliferation and Matrix Deposition in Fibrin-Based Tissue Constructs Fabricated. *In Vitro*, Tissue eng: Part A, 16, pp. 3261-3270.

Ahmed Z, Underwood S and Brown RA (2000) Low concentrations of fibrinogen increase cell migration speed on fibronectin/ fibrinogen composite cables. Cell Motil. Cytoskelet., 46, pp. 6–16.

Albee FH (1920) Studies in bone growth: Triple CaP as a stimulus to osteogenesis, Ann. Surg., 71, pp. 32-36.

Allison DD and Grande-Allen KJ (2006) Review: Hyaluronan: A powerful tissue engineering tool. Tissue Eng, 12, pp. 2131-2140.

Alter MJ. Science of flexibility, 3rd edition. Leeds: Human Kinetics 2004.

Ameye LG and Chee WSS (2006) Osteoarthritis and nutrition. From Nutraceuticals to functional foods: a systematic review of the scientific evidence. Arth. Res. Therap., 8, pp. R127.

Amiel D, Frank C, Harwood F, Fronek J and Akeson W (1984) Tendons and ligaments: A morphological and biochemical comparison. J.Orthop. Res., 1, pp. 257-265.

Andree C, Munder BI, Behrendt P, Hellmann S, Audretsch W, Voigt M, Reis C, Beckmann MW, Horch RE and Bach AD (2008) Improved safety of autologous breast reconstruction surgery by stabilisation of microsurgical vessel anastomoses using fibrin sealant in 349 free DIEP or fascia-muscle-sparing (fms)-TRAM flaps: a two centre study. Breast, 17, pp. 492-498.

Anselme K, Ploux L, Ponche A (2010) Cell/ Material Interfaces: Influence of Surface Chemistry and Surface Topography on Cell Adhesion. J. Adhes. Sci. Technol. 24, pp. 831–852.

Aoki H, Kato K, Ogiso M and Tabata T (1977) Studies on the application of apatite to dental materials. J. Dent. Eng., 18, pp. 86-89.

Arruda EM, Calve S, Dennis RG, Mundy K and Baar K (2006) Regional variation of tibialis anterior tendon mechanics is lost following denervation. J. Appl. Physiol., 101, pp. 113-1117.

Atala A and Lanza RP. Methods of tissue engineering. London: Academic Press, 2002.

Aylward GH. SI chemical data, 6th edition. New York: John Wiley & sons 2007.

Badylak S, Amoczky S, Plouhar P, Haut R, Mendenhall V, Clarke R and Horvath C (1999) Naturally occurring extracellular matrix as a scaffold for musculoskeletal repair. Clin. Orthop. Relat. Res., 367, pp. S333-S343.

Badylak SF, Tullius R, Kokini K, Shelbourne KD, Klootwyk T, Voytik SL, Kraine MR and Simmons C (1995) The use of xenogeneic small intestinal submucosa as a biomaterial for Achilles tendon repair in a dog model. J. Biomed. Mater. Res., 29, pp. 977-985.

Bagnaninchi P-O, Yang Y, El Haj AJ and Maffulli N (2007) Tissue engineering for tendon repair, J. Sports Med., 41, pp.1-5.

Baran ET, Tuzlagoklu K, Salgado AJ and Reis RL (2004) Multichannel mould processing of 3D structures from microporous coralline hydroxyapatite granules and chitosan support materials for guided tissue regeneration/ engineering. J. Mater. Sci.: Mat. Med., 15, pp. 161-165.

Barnes CP, Pemble CW, Brand DD, Simpson DG and Bowlin GL (2007) Crosslinking electrospun type II collagen tissue engineering scaffolds with carbodiimide in ethanol. Tissue Eng., 13, pp. 1593-1605.

Bartolo PJS, Almeida H and Laoui T (2009) Rapid prototyping and manufacturing for tissue engineering scaffolds. Int. J. Comp. App. Tech., 36, pp. 1-9.

Baxter LC, Frauchiger V, Texter M, Gwynn I and Richards RG (2002) Fibroblast and osteoblast adhesion and morphology on calcium phosphate surfaces. Europ. Cells Mat., 4, pp. 1-17.

Bayer ML, Yeung CY, Kadler KE, Qvortrup K, Baar K, Svensson RB, Magnusson SP, Krogsgaard M, Koch M and Kjaer M (2010) The initiation of embryonic-like collagen fibrillogenesis by adult human tendon fibroblasts when cultured under tension. Biomat., 13, pp. 4889-4897.

Becker P, Neumann H-G, Nebe B, Lüthen F and Rychly J (2004) Cellular investigation on electrochemically deposited calcium phosphate composites. J. Mat. Sci.: Mat. Med., 15, pp. 437-440.

Becktor JP, Hallström H, Isaksson S, Sennerby L (2008) The use of particulate bone grafts from the mandible for maxillary sinus floor augmentation before placement of surface-modified implants: Results from bone grafting to delivery of the final fixed prosthesis. J. Oral Maxillofac. Surg., 66, pp. 780-786.

Bell E, Ivarsson B, Merrill C (1979). Production of a tissue-like structure by contraction of collagen lattices by human fibroblasts of different proliferative potential *in vitro*. Proc. Natl. Acad. Sci., 76, pp. 1274-1278.

Benjamin M and Ralphs JR (1998) Fibrocartilage in tendons and ligaments - an adaptation to compressive load. J. Anat., 193, pp. 481-494.

Benjamin M and Ralphs JR (2000) The cell and developmental biology of tendons and ligaments. Int. Rev. Cytol., 196, pp. 85-130.

Benjamin M, Kumai T, Milz S, Boszczyk BM, Boszczyk AA and Ralphs JR (2002) The skeletal attachment of tendons-tendon 'entheses'. Compara. Biochem. Physio. Part A: Molec. Integ. Physio., 133, pp. 931-945.

Benjamin M, Toumi H, Ralphs JR, Bydder G, Best TM and Milz S (2006) Where tendons and ligaments meet bone: attachment sites ('entheses') in relation toexercise and/ or mechanical load. J. Anat., 208, pp. 471-490.

Bentley JP and Hanson AN (1969) The hydroxyproline of elastin. Biochem. et Biophy. Acta: Protein Struct., 175, pp. 339-344.

Bergmann C, Lindner M, Zhang W, Koczur K, Kirsten A, Telle R and Fischer H (2010) 3D printing of bone substitute implants using calcium phosphate and bioactive glasses. J. European Ceram. Soc., 30, pp. 2563-2567.

Bhat S, Tripathi A and Kumar A (2010) Supermacroporous chitosan-agarose-gelatin cryogels: *in vitro* characterisation and *in vivo* assessment for cartilage tissue engineering. J. R. Soc. Interface, 8, pp. 540-554.

Bilezikian JP, Raisz LG and Rodan GA. Principles of bone biology, 2nd edition, vol. 1. London: Academic Press, 2002.

Birk DE, Zycband EI, Woodruff S, Winkelmann DA and Trelstad RL (1997) Collagen fibrillogenesis in situ: Fibril segments become long fibrils as the developing tendon matures. Develop. Dynam., 208, pp. 291-298.

Bohner M, Gbureck U and Barralet JE (2005) Technological issues for the development of more efficient calcium phosphate bone cements: A critical assessment, Biomat., 26, pp. 6423-6429.

Bohner M, Lemaitre J and Ring TA (1996) Effects of sulfate, pyrophosphate, and citrate ions on the physicochemical properties of cements made of β-tricalcium phosphate-phosphoric acid-water mixtures. J. Am. Ceram. Soc., 79, pp. 1427-1434.

Bohnsack M, Rühmann O, Kirsch L and Wirth CJ (2000) Surgical shortening of the Achilles tendon for correction of elongation following healed conservatively treated Achilles tendon rupture. Z Orthop. Ihre Grenzgeb, 138, pp. 501-505.

Bonney RJ, Gery I, Lin T-Y, Meyenhofer MF, Acevedo W and Davies P (1978) Mononuclear phagocytes from carrageenan-induced granulomas. J. Exp. Med., 148, pp. 261-275.

Bowen J, Cheneler D, Walliman D, Arkless SG, Zhang Z, Ward MCL and Adams MJ (2010) On the calibration of rectangular atomic force microscope cantilevers modified by particle attachment and lamination. Meas. Sci. Technol., 21, 115106.

Braut-Boucher F, Pichon J, Rat P, Adolphe M, Aubery M and Font J (1995) A non-isotopic, highly sensitive, fluorimetric, cell-cell adhesion microplate assay using calcein AM-labelled lymphocytes. J. Immunolog. Meth. 178, pp. 41-51.

Brown GD and Ahmad CS (2007) The docking technique for medial patellofemoral ligament reconstruction. Operat. Techn. Orthop., 17, pp. 216-222.

Butler DL, Dressler M, Awad H. Functional tissue engineering: assessment of function in tendon and ligament repair. In: Guilak F, Butler D, Goldstein S, Mooney D, editors. Functional tissue engineering. New York: Springer; 2003.

Cahn F (2000) Review: Technologies and characteristics of tissue-engineered skin substitutes. J. Regen. Med., 1, pp. 145-155.

Calafiori AR, Di Marco G and Martino G (2007) Preparation and characterization of calcium phosphate biomaterials. J. Mater. Sci: Mater. Med., 18, pp. 2331-2338.

Calderon L, Collin E, Velasco-Bayon D, Murphy M, O'Halloran D and Pandit A (2010) Type II collagen-hyaluronan hydrogel- A step towards a scaffold for intervertebral disc tissue engineering. Euro. Cells Mat., 20, pp. 134-148.

Calve S, Dennis RG, Kosnik PE, Baar K, Grosh K and Arruda EM (2004) Engineering of a functional tendon. Tissue Eng., 10, pp. 755-761.

Campbell PG, Miller ED, Fisher GW, Walker LM and Weiss LE (2005) Engineered spatial patterns of FGF-2 immobilized on fibrin direct cell organization. Biomat., 26, pp. 6762-6770.

Canty EG and Kadler KE (2002) Collagen fibril biosynthesis in tendon: a review and recent insights. Comparative Biochem. Physio.: Part A., 133, pp. 979-985.

Caprise PA, Lester GE, Weinhold P, Hill J and Dahners LE (2001) The effect of NKISK on tendon in an *in vivo* model. J. Orthop. Res., 19, pp. 858-861.

Carpenter JE and Hankenson KD (2004) Animal models of tendon and ligament injuries for tissue engineering applications. Biomat., 25, pp. 1715-1722.

Cen L, Liu W, Cui L, Zhang W and Cao Y (2008) Collagen tissue engineering: development of novel biomaterials and applications. Pediatr. Res., 63, pp. 492-496.

Chen J, Xu J, Wang A and Zheng M (2009) Scaffolds for tendon and ligament repair: Review of the efficacy of commercial products. Expert Rev. Med. Devices, 6, pp. 61-73.

Chen X, Qi Y-Y, Wang L-L, Yin Z, Yin G-L, Zou X-H and Ouyang H-W (2008) Ligament regeneration using a knitted silk scaffold combined with collagen matrix, Biomat., 29, pp. 3683-3692.

Cheneler D (2010) The design and analysis of a microsqueeze flow rheometer. Ph.D. thesis, University of Birmingham.

Chernousov, M.A. and Carey, D.J. (2003) αVβ8 integrin is a Schwann cell receptor for fibrin. Exp. Cell. Res. 291, pp. 514-524.

Chiquet M, Renedo AS, Huber F and Flück M (2003) How do fibroblasts translate mechanical signals into changes in extracellular matrix production? Matrix Biol., 22, pp. 73-80.

Choi YS, Hong SR, Lee YM, Song KW, Park MH and Nam YS (1999) Study on gelatin-containing artificial skin: I. Preparation and characteristics of novel gelatin-alginate sponge. Biomat., 20, pp. 409-417.

Chokalingam K, Juncosa-Melvin N, Hunter SA, Gooch C, Frede C, Florert J, Bradica G, Wenstrup R and Butler DL (2009) Tensile Stimulation of Murine Stem Cell–Collagen Sponge Constructs Increases Collagen Type I Gene Expression and Linear Stiffness. Tissue Eng: Part A, 15, pp. 2561–2570.

Choueka J, Charvet JL, Koval KJ, Alexander H, James KS, Hooper KA and Khon J (1996) Canine bone response to tyrosine-derived polycarbonates and poly(L-lactic acid). J. Biomed. Mater. Res., 31, pp. 35-41.

Chowdhury P, Matyas JR and Frank CB (1991) The 'epiligament' of the rabbit medial collateral ligament: a quantitative morphological study. Connect. Tissue Res., 27, pp. 33-50.

Claudpierre P and Voisin M-C (2005) The enthuses: histology, pathology, and pathophysiology. Joint Bone Spine, 72, pp. 32-37.

Cooper JA, Bailey LO, Carter JN, Castiglioni CE, Kofron MD, Ko FK and Laurencin CT (2006) Evaluation of the anterior cruciate ligament, medial collateral ligament, achilles tendon and patellar tendon as cell sources for tissue-engineered ligament. Biomat., 27, pp. 2747–2754.

Cooper RR and Misol S (1970) Tendon and ligament insertion. A light and electron microscopic study. J. Bone Joint Surg. Am., 52, pp.1-20.

Cribb AM and Scott JE (1995) Tendon response to tensile stress: an ultrastructural investigation of collagen: proteoglycan interactions in stressed tendon. J. Anat., 187, pp. 423-428.

Dagher E, Hays PL, Kawamura S, Godin J, Deng X-H and Rodeo SA (2009) Immobilization Modulates Macrophage Accumulation in Tendon-Bone Healing. Clin. Orthop. Relat. Res., 467, pp. 281-287.

Dahlgren LA (2007) Pathobiology of tendon and ligament injuries. Clin. Tech. Equine Pract., 6, pp. 168-173.

Daniel-da-Silva AL, Lopes AB, Gil AM and Correia RN (2007) Synthesis and characterisation of porous κ-carrageenan/ calcium phosphate nanocomposite scaffolds. J. Mat. Sci., 42, pp. 8581-8591.

De Almeida FM, Tomiosso TC, Nakagaki WR, Gomes L, Matiello-Rosa SMG and Pimentel ER (2009) Effects of passive stretching on the biochemical and biomechanical properties of calcaneal tendon of rats. Connective Tissue Res., 50, pp. 279-284.

Dee KC, Puleo DA and Bizios R (2002) An introduction to tissue-biomaterial interactions. New Jersey: John Wiley & Sons, Inc.

Dejardin LM, Arnoczky SP, Ewers BJ, Haut RC and Clarke RB (2001) Tissue-engineered rotator cuff tendon using porcine small intestine submucosa: Histologic and mechanical evaluation in dogs. J. Sports. Med., 29, pp. 175-184.

Denissen HW, Kalk W, Veldhuis AA and van der Hooff A (1989) Eleven year study of hydroxyapatite implants, J. Prosthet. Dent., 61, pp. 706-712.

Di Stasio E, Nagaswami C, Weisel JW and Di Cera E (1998) Cl- regulates the structure of the fibrin clot. Biophys. J., 75, pp. 1973-1979.

DiGiovanna JJ, Helfgott RK, Gerber LH and Peck GL (1986) Extraspinal tendon and ligament calcification associated with long-term therapy with etretinate, N. Engl. J. Med., 315, pp. 1177-1182.

Divyap P and Krishnan LK (2009) Glycosaminoglycans restrained in a fibrin matrix improve ECM remodelling by endothelial cells grown for vascular tissue engineering. J. Tissue eng. Regen. Med., 3, pp. 377-388.

Doroski DM, Brink KS and Temenoff JS (2007) Techniques for biological characterisation of tissue-engineered tendon and ligaments. Biomat., 28, pp. 187-202.

dos Santos EA, Farina M, Soares GA and Anselme K (2008) Chemical and topographical influence of hydroxyapatite and β-tricalcium phosphate surfaces on human osteoblastic cell behaviour, J. Biomed. Mater. Res. A, pp. 510-520.

Doschak MR and Zernicke RF (2005) Structure, function and adaptation of bone-tendon and bone-ligament complexes. J. Musculoskelet. Neuronal Interact., 5, pp. 35-40.

Dressler MR, Butler DL and Boivin GP (2005) Effects of age on the repair ability of mesenchymal stem cells in rabbit tendon. J. Orthop. Res, 23, pp. 287-293.

Drury JL and Mooney DJ (2003) Hydrogels for tissue engineering: scaffold design variables and applications. Biomat., 24, pp. 4337-4351.

Duan B, Wang M, Zhou WY, Li ZY and Lu WW (2010) Three-dimensional nanocomposite scaffolds fabricated via selective laser sintering for bone tissue engineering. Acta Biomat., 6, pp. 4495-4505.

Elliot WL (2002) Role of vitamin C in collagen biosynthesis and connective tissue health. J. Bodywork Movement Ther., 6, pp. 221-224.

Even-Ram S (2009) Fibrin gel model for assessment of cellular gel contractility. Methods Mol. Bio., 522, pp. 251-259.

Everman DB and Robin NH (1998) Hypermobility syndrome. Paediatrics rev., 19, pp. 111-117.

Eyrich D, Brandl F, Appel B, Weise H, Maier G, Wenzel M, Staudenmaier R, Goepferich A and Blunk T (2007) Long-term stable fibrin gels for cartilage engineering. Biomat., 28, pp. 55-65.

Ferry JD. Viscoelastic Properties of Polymers, 3rd edition. New York: John Wiley & Sons, 1980.

Fini M, Torricelli P, Giavaresi G, Rotini R, Castagna A and Giardino R (2007) *In vitro* study comparing two collagenous membranes in view of their clinical application for rotator cuff tendon. J. Orthop. Res., 25, pp. 98-107.

Flint M (1972) Interrelationships of mucopolysaccharide and collagen in connective tissue remodelling. J. Embryol. Exp. Morph., 27, pp. 481-495.

Freedman KB, D'Amato MJ, Nedeff DD, Kaz A and Bach BR Jr. (2003) Arthroscopic Anterior Cruciate Ligament Reconstruction: A Metaanalysis Comparing Patellar Tendon and Hamstring Tendon Autografts, Am. J. Sports Med., 31, pp. 2–11.

Fröhlich M, Grayson WL, Wan LQ, Marolt D, Drobnic M and Vunjak-Novakovic G (2008) Tissue engineered bone grafts: biological requirements, tissue culture and clinical relevance. Curr. Stem. Cell. Res. Ther., 3, pp. 254-264.

Fu S-C, Cheuk Y-C, Chan K-M, Hung L-K and Wong MW-N (2007) Is cultured tendon fibroblast a good model to study tendon healing? J. Orthop. Res., 26, pp. 374-383.

Gabl M, Reinhart C, Lutz M, Bodner G, Rudisch A, Hussl H and Pechlaner S (1999) Vascularised bone graft from the iliac crest for the treatment of nonunion of the proximal part of the scaphoid with an avascular fragment. J. Bone Joint Surg., 81, pp. 1414-1428.

Galarneau A, Lefèvre B, Cambon H, Coasne B, Valange S, Gabelica Z, Bellat J-P and Di Renzo F (2008) Pore shape affects the determination of the pore size of ordered mesoporous silicas by mercury intrusion. Stud. Surface Science Catalysis, 174, pp. 957-960.

Gans H and Lowman JT (1967) The uptake of fibrin and fibrin-degradation products by the isolated perfused rat liver. Blood, 29, pp. 526-539.

Gbureck U, Hölzel T, Klammert U, Würzler K, Müller FA and Barralet JE (2007) Resorbable dicalcium phosphate bone substitutes prepared by 3D powder printing. Advan. Func. Mat., 17, pp. 3940-3945.

Gbureck U, Barralet JE, Spatz K, Grover LM and Thull R (2004) Ionic dification of calcium phosphate cement viscosity. Part I: Hypodermic injection and strength improvement of apatite cement. Biomat., 25, pp. 2187-2195.

Gbureck U, Dembski S, Thull R and Barralet JE (2005) Factors influencing calcium phosphate shelf-life. Biomat., 26, pp. 3691-3697.

Gerharz CD, Gabbert HE, Biesalski HK, Engers R, Luley C (1989) Fetal calf serum and retinoic acid affect proliferation and terminal differentiation of a rat rhabdomyosarcoma cell line (BA-HAN-1C). British J. Cancer, 59, pp. 61-7.

Gillery P, Bellon G, Coustry F and Borel JP (1989) Cultures of fibroblasts in fibrin lattices: models for the study of metabolic activities of the cells in physiological conditions. J. Cell Physiol., 140, pp. 483-490.

Gillmor JR, Connelly RW, Colby RH and Tan JS (1999) Effect of Sodium Poly(styrene sulfonate) on Thermoreversible Gelation of Gelatin. J. Polymer Sci: Part B: Polymer Phys., 37, pp. 2287-2295.

Ginebra MP, Traykova T and Planell JA (2006) Calcium phosphate cements as bone drug delivery systems: A review. J. Cont. Rel., 113, pp. 102-110.

Goldner J (1938) A modification of the Masson Trichrome technique for routine laboratory purposes. Am. J. Path., 14, pp. 237-243.

Gottsauner-Wolf F, Egger EL, Schultz FM, Sim FH and Chao EYS (1994) Tendons attached to prostheses by tendon-bone block fixation: An experimental study in dogs. J. Orthop. Res., 12, pp. 814-821.

Goyenvalle E, Guyen NJM, Aguado E, Passuti N and Daculsi G (2003) Bilayered calcium phosphate coating to promote osseointegration of a femoral stem prosthesis. J. Mat. Sci.: Mat. Med., 14, pp. 219-227.

Graham HK, Holmes DF, Watson RB and Kadler KE (2000) Identification of collagen fibril fusion during vertebrate tendon morphogenesis. The process relies on unipolar fibrils and is regulated by collagen-proteoglycan interaction. J. Molec. Biol., 295, pp. 891-902.

Granero AJ, Razal JM, Wallace GG and Panhuis M in het (2010) Conducting gel-fibres based on carrageenan, chitosan and carbon nanotubes. J. Mater. Chem., 20, pp. 7953-7956.

Grenha A, Gomes ME, Rodrigues M, Santo VE, Mano JF, Neves NM and Reis RL (2009) Development of new chitosan/ carrageenan nanoparticles for drug delivery applications. J. Biomed. Mat. Res., 92A, pp. 1265-1272.

Griffin Global Systems (2006) Everything about Achilles tendons [on-line]. New York: Griffin Global Systems. Available from:- http://www.achillestendon.com/ [Accessed 26 October 2007].

Gross KA and Berndt CC (2002) Phosphates: Geochemical, geobiological and materials importance. Mineralog. Soc. Am.: Washington DC, USA, pp. 631-672.

Grover LM, Knowles JC, Fleming GJP and Barralet JE (2003) *In vitro* ageing of brushite calcium phosphate cement. Biomat., 24, pp. 4133-4141.

Hadjidakis DJ and Androulakis II (2006) Bone remodelling, Ann. N. Y. Acad. Sci., 1092, pp. 385-396.

Hampson K, Forsyth NR, El Haj A and Maffulli N (2008) Tendon tissue engineering in Topics in tissue engineering, Vol. 4, pp. 1-21.

Hankemeier S, van Griensven M, Ezechieli M, Barkhausen T, Austin M, Jagodzinski M, Meller R, Bosch U, Krettek C and Zeichen J (2007) Tissue engineering of tendons and ligaments by human bone marrow stromal cells in a liquid fibrin matrix in immunodeficient rats: Results of a histologic study. Arch. Orthop. Trauma Surg., 127, pp. 815-821.

Hariharan P. Basics of Interferometry, 2nd edition. New York: Academic Press: Elsevier, 2007.

Harpel PC, Gordon BR and Parker TS (1989) Plasmin catalyzes binding of lipoprotein (a) to immobilized fibrinogen and fibrin. PNAS, 86, pp. 3847-3851.

Hashimoto Y, Yoshida G, Toyoda H and Takaoka K (2007) Generation of tendon-to-bone interface "entheses" with use of recombinant BMP-2 in a rabbit model. J. Orthop. Res., 25, pp. 1415-1424.

Hausmann E and Neuman WF (1961) Conversion of proline to hydroxyproline and its incorporation into collagen. J. Bio. Chem., 236, pp. 149-152.

Hayakawa T, Yoshinari M, Nemoto K, Wolke JG and Jansen JA (2000) Effect of surface roughness and calcium phosphate coating on the implant/ bone response. Clin. Oral. Implants. Res., 11, pp. 296-304.

Heath JP and Dunn GA (1978) Cell to substratum contacts of chick fibroblasts and their relation to the microfilament system. A correlated interface-reflexion and high-voltage electron microscope study. J. Cell Sci., 29, pp. 197-212.

Hechler B, Magnenat S, Zighetti ML, Kassack MU, Ullmann U, Cazenava J-P, Evans R, Cattaneo M and Gachet C (2005) Inhibition of platelet functions and thrombosis through selective or nonselective inhibition of the platelet P2 receptors with increasing doses of NF449 [4,4',4'',4'''-(Carbonylbis(imino-5,1,3-benzenetriylbis-(carbonylimino)))tetrakis-benzene-1,3-disulfonic Acid Octasodium Salt]. J. Pharmac. Exp. Therap., 314, pp. 232-243.

Heimann RB (1999) Design of novel plasma sprayed hydroxyapatite-bond coat bioceramic systems. J. Therm. Spray Technol., 8, pp. 597-604.

Heinemann C, Heinemann S, Lode A, Bernhardt A, Worch H and Hanke T (2009) *In vitro* evaluation of textile chitosan scaffolds for tissue engineering using human bone marrow stromal cells. Biomacromol., 10, pp. 1305-1310.

Hildebrand KA, Frank CB and Hart DA (2004) Gene intervention in ligament and tendon: current status, challenges, future directions. Gene Therap., 11, pp. 368-378.

Hiltner A, Cassidy JJ and Baer E (1985) Mechanical properties of biological polymers. Ann. Rev. Mater. Sci., 15, pp. 455-482.

Hoffmann A and Gross G (2006) Tendon and ligament engineering: from cell biology to *in vivo* application. Regen. Med., 1, pp. 563-574.

Hofmann MP, Young AJ, Gbureck U, Nazhat SN and Barralet JE (2006) FTIR-monitoring of a fast setting brushite bone cement: effect of intermediate phases. J. Mat. Chem., 16, pp. 3199 - 3206.

Holly CE, Schoichet MS and Davies JE (2000) Engineering three-dimensional bone tissue *in vitro* using biodegradable scaffolds; Investigating initial seeding density and culture period. J. Biomed. Mater. Res., 51, pp. 376-382.

Holmbeck K, Bianco P, Caterina J, Yamada S, Kromer M, Kuznetsov SA, Mankani M, Robey PG, Poole AR, Pidoux I, Ward JM and Birkedal-Hansen H (1999) MT1-MMP-deficient mice develop dwarfism, osteopenia, arthritis and connective tissue disease due to inadequate collagen turnover. Cell, 99, pp. 81-92.

Holmes DF, Graham HK and Kadler KE (1998) Collagen fibrils forming in developing tendon show an early and abrupt limitation in diameter at the growing tips. J. Molec. Biol., 283, pp. 1049-1058.

Houglum PA. Therapeutic exercise for musculoskeletal injuries, 3rd edition. Leeds: Human Kinetics 2010.

Hsu S-L, Liang R and Woo SLW (2010) Functional tissue engineering of ligament healing. Sports Med., Anthros., Rehab., Therap. Tech., 2, pp. 1-10.

Hunt L, Hacker DL, Grosjean F, Jesus MD, Uebersax L, Jordan M and Wurm FM (2005) Low-temperature pausing of cultivated mammalian cells. Biotech. Bioeng., 89, pp. 157-163.

Hutmacher DW (2000) Scaffolds in tissue engineering bone and cartilage. Biomat., 21, pp. 2529-2543.

Ide A, Sakane M, Chen GP, Shimojo H, Ushida T, Tateishi T, Wadano Y and Miyanaga Y (2001) Collagen hybridization with poly(L-lactic acid) baid promotes ligament cell migration. Mater. Sci. Eng. C Biomimetic Supramol. Syst., 17, pp. 95-99.

Ikema Y, Tohyama H, Yamamoto E, Kanaya F and Yasuda K (2007) *Ex vivo* infiltration of fibroblasts into the tendon deteriorates the mechanical properties of tendon fascicles but not those of tendon bundles. Cli. Biomech., 22, pp. 120-126.

Iler RK. The Chemistry of Silica: Solubility, Polymerisation, Colloid and Surface Properties, and Biochemistry. New York: John Wiley & sons 1979.

Isaji M, Miyata H, Ajisawa Y, Takehana Y and Yoshimura N (1997) Tranilasts inhibits the proliferation, chemotaxis and tube formation of human microvascular endothelial cells *in vitro* and angiogenesis *in vivo*. British J. Pharm., 122, pp. 1061-1066.

Israelachvili JN. Intermolecular and surface forces: With applications to colloidal and biological systems (colloid science), 2nd edition. New York: Academic Press 1991.

Jabbarzadeh E, Starnes T, Khan YM, Jiang T, Wirtel AJ, Deng M, Lv Q, Nair LS, Doty SB and Laurencin CT (2008) Induction of angiogenesis in tissue-engineered scaffolds designed for bone repair: A combined gene therapy– cell transplantation approach. PNAS, 105, pp. 11099-11104.

Jacobs CR (2000) The mechanobiology of cancellous bone structural adaption, J. Rehabil. Res. Dev., 37, pp. 209-216.

Jain A, Kima Y-T, McKeonb RJ and Bellamkonda RV (2006) In situ gelling hydrogels for conformal repair of spinal cord defects, and local delivery of BDNF after spinal cord injury. Biomaterials, 27, pp. 497-504.

Janmey PA and McCulloch CA (2007) Cell mechanics: Integrating cell responses to mechanical stimuli. Ann. Rev. Biomed. Eng., 9, pp. 1-34.

Janmey PA, McCormick ME, Rammensee S, Leight JL, Georges PC and MacKintosh FC (2007) Negative normal stress in semiflexible biopolymer gels. Nat. Mater., 6, pp. 48-51.

Janmey PA, Winer JP and Weisel JW (2009) Fibrin gels and their clinical and bioengineering applications. J. R. Soc. Interface, 6, pp. 1-10.

Jeon O, Song SJ, Lee K-J, Park MH, Lee S-H, Hahn SK, Kim S and Kim B-S (2007) Mechanical properties and degradation behaviours of hyaluronic acid hydrogels crosslinked at various crosslinking densities. Carbohyd. Polym., 70, pp. 251-257.

Jockenhoevel S, Zund G, Hoerstrup SP, Chalabi K, Sachweh JS, Demircan L, Messmer BJ and Turina M (2001) Fibrin gel- advantages of a new scaffold in cardiovascular engineering. Eur. J. Cardiothor. Surg., 19, pp. 424-230.

Johnson PJ, Parker SR and Sakiyama-Elbert SE (2010) Fibrin-based tissue scaffolds enhance neural fibre sprouting and delay the accumulation of reactive astrocytes at the lesion in a subacute model of spinal cord injury. J. Biomed. Mater. Res. A, 92, pp. 152-163.

Jukes JM, van der Aa LJ, Hiemstra C, van Veen T, Dijkstra PJ, Zhong Z, Feijen J, van Bitterswijk CA and de Boer J (2010) A newly developed chemically crosslinked dextran-poly(ethylene glycol) hydrogel for cartilage tissue engineering. Tissue Eng. Part A, 16, pp. 565-573.

Juncosa-Melvin N, Matlin KS, Holdcraft SW, Nirmalanandhan VS and Butler DL (2007) Mechanical stimulation increases collagen type I and collagen type III gene expression of stem cell-collagen sponge constructs for patellar tendon repair. Tissue Eng., 13, pp. 1219-1226.

Kaelin Jr WG (2005) Proline hydroxylation and gene expression. Annu. Rev. Biochem., 74, pp. 115-128.

Kaneshiro ES, Wyder MA, Wu Y-P and Cushion MT (1993) Reliability of calcein acetoxy methyl ester and ethidium homodimer or propidium iodide for viability assessment of microbes. J. Microbiol. Methods, 17, pp. 1-16.

Kannus P (2000) Structure of the tendon connective tissue. Scandinav. J. Med. Sci. Sports, 10, pp. 312-320.

Kaplan B, Gönül B, Dinçer S, Kaya ND and Babül A (2004) Relationships between tensile strength, ascorbic acid, hydroxyproline and zinc levels of rabbit full-thickness incision wound healing. Surg. Today, 34, pp. 747-751.

Karousou E, Ronga M, Vigetti D, Passi A and Maffulli N (2008) collagens, proteoglycans, MMP-2, MMP-9 and TIMPs in human Achilles tendon rupture. Clin. Orthop. Relat. Res., 466, pp. 1577-1582.

Kastelic J, Galeski A and Baer E (1978) The multi-composite structure of tendon. Connect. Tissue Res., 6, pp. 11-33.

Kendall K (1980) Complexities of compression failure. Proceeding of the Royal Society, London, pp. 245-361.

Keppeler S, Ellis A and Jacquier JC (2009) Crosslinked carrageenan beads for controlled release delivery systems. Carbohyd. Polym., 78, pp. 973-977.

Ker RF (2007) Mechanics of tendon, from an engineering perspective. Int. J. Fatigue, 29, pp. 1001-1009.

Kim GH, Ahn S, Kim YY, Cho Y and Chun W (2011) Coaxial structured collagen-alginate scaffolds: fabrication, physical properties, and biomedical application for skin tissue regeneration. J. Mat. Chem., 21, pp. 6165-6172.

Kim JY, Lee T-J, Cho D-W and Kim B-S (2010) Solid free-form fabrication-based PCL/ HA scaffolds fabricated with a multi-head deposition system for bone tissue engineering. J. Biomat. Sci., 21, pp. 951-962.

Kim S, Yun J and Shin JH (2009) Effects of mechanical stimulus on cells via multi-cellular indentation device. 13th Internat. Conf. Biomed. Eng., 23, pp. 1949-1951.

Kirubanandan S and Sehgal PK (2010) Regeneration of soft tissue using porous bovine collagen scaffold. J. Optoelectronics Biomed. Mat., 2, pp. 141-149.

Klammert U, Reuther T, Jahn C, Kraski B, Kübler AC and Gbureck U (2009) Cytocompatibility of brushite and monetite cell culture scaffolds made by three-dimensional powder printing. Acta Biomater., 5, pp. 727-734.

Klammert U, Vorndran E, Reuther T, Müller FA, Zorn K and Gbureck U (2010) Low temperature fabrication of magnesium phosphate cement scaffolds by 3D powder printing, J. Mater. Sci: Mater. Med., 21, pp. 2947-2953.

Konno T and Ishihara K (2007) Temporal and spatially controllable cell encapsulation using a water-soluble phospholipids polymer with phenylboronic acid moiety. Biomat., 28, pp.1770-1771.

Könönen M, Hormia M, Kivilahti J, Hautaniemi J and Thesleff I (1992) Effect of surface processing on the attachment, orientation and proliferation of human gingival fibroblasts on titanium. J. Biomed. Mater. Res., 26, pp. 1325-1341.

Krishnamurti C, Vukelja SJ and Alving BM (1994) Inhibitory effects of lysine analogues on t-PA induced whole blood clot lysis. Thromb. Res., 73, pp. 419-430.

Kuroda S, Goto N, Suzuki M, Kaneda K, Ohya K, Shimokawa H and Kasugai S (2010) Regeneration of bone-and tendon/ ligament-like tissues induced by gene transfer of bone morphogenetic protein-12 in a rat bone defect. J. Tissue Eng., pp. 1-8, doi:10.4061/2010/891049.

Kyriakides TR, Zhu YH, Smith LT, Bain SD, Yang Z, Lin MT, Danielson KG, Iozzo RG, La Marca M, McKinney CE, Ginns EI and Bornstein P (1998) Mice that lack thrombospondin 2 display connective tissue abnormalities that are associated with disordered collagen

fibrillogenesis, an increased vascular density and a bleeding diathesis. J. Cell. Bio, 140, pp. 419-430.

Lai VMF, Wong PA-L and Li C-Y (2000) Effects of cation properties on sol-gel transition and gel properties of κ-carrageenan. J. Food Sci: Food Eng. Physical Prop., 65, pp. 1332-1337.

Langrock T, García-Villar N and Hoffmann R (2007) Analysis of hydroxyproline isomers and hydroxylysine by reversed-phase HPLC and mass spectrometry. J. Chromat. B, 847, pp. 282-288.

Lanza R, Langer R and Vacanti J. Principles of tissue engineering, 3rd edition. London: Academic Press: Elesvier, 1997.

Laurencin CT and El-Amin SF (2008) Xenotransplantation in orthopaedic surgery, J. Am. Acad. Orthop. Surg., 16, pp. 4-8.

Leukers B, Gülkan H, Irsen SH, Milz S, Tille C, Schieker M and Seitz H (2005) Hydroxyapatite scaffolds for bone tissue engineering made by 3D printing. J. Mater. Sci. Mater. Med., 16, pp. 1121-1124.

Lévesque SG, Lim RM and Schoichet MS (2005) Macroporous interconnected dextrans scaffolds of controlled porosity for tissue-engineering scaffolds. Biomat., 26, pp. 7436-7446.

Levitt GE, Crayton PH and Monroe EA (1969) Forming methods for apatite prosthesis, J. Biomed. Mater. Res, 3, pp. 683-685.

Lewis SD, Janus TJ, Lorand L and Shafer JA (1985) Regulation of Formation of Factor XIIIa by Its Fibrin Substrates. Biochem., 24, pp. 6772-6777.

Li Z, Ramay HR, Hauch KD, Xiao D and Zhang M (2005) Chitosan-alginate hybrid scaffolds for bone tissue engineering. Biomat., 26, pp. 3919-3928.

Liao S, Watari F, Zhu Y, Uo M, Akasaka T, Wang W, Xu G and Cui F (2007) The degradation of the three layered nano-carbonated hydroxyapatite/ collagen/ PLGA composite membrane *in vitro*. Dental Mat., 23, pp. 1120-1128.

Lim HN, Huang NM, Yarmo MA, Khiew PS and Chiu WS (2009) Preparation and characterization of brushite crystals using high internal phase emulsion. Colloid J., 71, pp. 793-802.

Limpanuphap S and Derby B (2002) Manufacture of biomaterials by a novel printing process. J. Mat. Sci: Mat. Med., 13, pp. 1163-1166.

Lin TW, Cardenas L and Soslowsky LJ (2004) Biomechanics of tendon injury and repair. J. Biomech., 37, pp. 865-877.

Linnes MP, Ratner BD and Giachelli CM (2007) A fibrinogen-based precision microporous scaffold for tissue engineering. Biomat., 28, pp. 5298–5306.

Liu J-C (2010) A novel strategy for engineering vascularised grafts *in vitro*. World J. Stem Cells, 2, pp. 93-96.

Liu W, Chen B, Deng D, Xu F, Cui L and Cao Y (2006) Repair of tendon defect with dermal fibroblast engineered tendon in a porcine model. Tissue Eng., 12, pp. 775-778.

Louie L, Yannas I and Spector. Editors: M Patrick Jr. C, Mikos A and McIntire L.Tissue engineered tendon. New York: Elsevier Science Ltd., 1998.

Lu HH, Cooper JA, Manuel S, Freeman JW, Attawia MA, Ko FK and Laurencin CT (2005) Anterior cruciate ligament regeneration using braided biodegradable scaffolds: *in vitro* optimization studies. Biomat., 26, pp. 4805–4816.

MacArtain P, Jacquier JC and Dawson KA (2003) Physical characteristics of calcium induced *κ*-carrageenan networks. Carbohyd. Polym., 53, pp. 395–400.

Maeda E, Shelton JC, Bader DL and Lee DA (2007) Time dependence of cyclic tensile strain on collagen production in tendon fascicles. Biochem. Biophys. Res. Comm., 362, pp. 399-404.

Maganaris CN, Narici MV and Reeves ND (2004) *In vivo* human tendon mechanical properties: Effect of resistance training in old age. J. Musculoskelet. Neuron. Interact., 4, pp. 204-208.

Majima T, Irie T, Sawaguchi N, Funakoshi T, Iwasaki N, Harada K, Minami A and Nishimura S-I (2007) Chitosan-based hyaluronan hybrid polymer fibre scaffold for ligament and tendon tissue engineering. J Eng. In Med., 221, pp. 537-546.

Mandel S and Tas AC (2010) Brushite ($CaHPO_4.2H_2O$) to octacalcium phosphate ($Ca_8(HPO_4)_2(PO_4)4.5H_2O$) transformation in DMEM solutions at 36.5°C. Mater. Sci. Eng. C, 30, pp. 245-254.

Mangione MR, Giacomazza D, Bulone D, Martorana V, Cavallaro G and San Biagio PL (2005) K^+ and Na^+ effects on the gelation properties of *κ*-carrageenan, Biophys. Chem., 113, pp.129-135.

Mannucci PM (1997) Desmopressin (DDAVP) in the treatment of bleeding disorders: The first 20 years. Blood, 90, pp. 2515-2521.

Marenzana M, Wilson-Jones N, Mudera V and Brown RA (2006) The origins and regulation of tissue tension: Identification of collagen tension-fixation process *in vitro*. Exp. Cell res., 312, pp. 423-433.

Martinek V, Latterman C, Usas A, Abramowitch S, Woo SL, Fu FH and Huard J (2002) Enhancement of tendon-bone integration of anterior cruciate ligament grafts with bone morphogenetic protein-2 gene transfer: A histological and biomechanical study. J. Bone Joint Surg. Am., 84, pp. 1123-1131.

Martins RS, Siqueira MG, Da Silva CF and Plese JPP (2005) Overall assessment of regeneration in peripheral nerve lesion repair using fibrin glue, suture or a combination of the 2 techniques in a rat model. Which is the ideal choice? Surg. Neurol., 64, pp. 10-16.

Marx J, Hudry-Clergeon G, Capet-Antonini F and Bernard L (1979) Laser Raman spectroscopy study of bovine fibrinogen and fibrin. Biochem. et Biophys. Acta, 578, pp. 107-115.

Mastrojalos DS, Springer J, Siebold R and Paessler HH (2005) Donor site morbidity and return to the preinjury activity level after anterior cruciate ligament reconstruction using ipsilateral and contralateral patellar tendon autograft: a retrospective, nonrandomized study. Am. J. Sports Med., 33, pp. 85-93.

Matsumoto T, Sasaki J-A, Alsberg E, Egusa H, Yatani H and Sohmura T (2007) Three-dimensional cell and tissue patterning in a strained fibrin gel system. PLoS ONE, 2, e1211.

Matsuno A, Tanaka H, Iwamuro H, Takanashi S, Miyawaki S, Nakashima M, Nakaguchi H and Nagashima T (2006) Analyses of the factors influencing bone graft infection after delayed cranioplasty. Acta Neurochir. (Wien), 148, pp. 535-540.

Mauck RL, Soltz MA, Wang CC, Wong DD, Chao PH, Valhmu WB, Hung CT and Ateshian GA (2000) Functional tissue engineering of articular cartilage through dynamic loading of chondrocyte-seeded agarose gels. J. Biomech. Eng., 122, pp. 252-260.

Mauney JR, Volloch V and Kaplan DL (2005) Role of adult mesenchymal stem cells in bone tissue engineering applications: current status and future prospects. Tissue Eng., 11, pp. 787-802.

Mazzieri R, Masiero L, Zanetta L, Monea S, Onisto M, Garbisa S and Mignatti P (1997) Control of type IV collagenase activity by components of the urokinase-plasmin system: a regulatory mechanism with cell-bound reactants. The EMBO J., 16, pp. 2319-2332.

McGuigan AP and Sefton MV (2007) Modular tissue engineering: fabrication of a gelatin-based construct. J. Tissue Eng. Regen. Med., 1, pp. 136-145.

McGuigan AP and Sefton MV (2007) Modular tissue engineering: fabrication of a gelatin-based construct. J. Tissue Eng. Regen. Med., 1, pp. 136-145.

McManus MC, Boland ED, Koo HP, Barnes CP, Pawlowski KJ, Wnek JE, Simpson DG and Bowlin GL (2006) Mechanical properties of electrospun fibrinogen structures. Acta Biomater., 2, pp. 19-28.

Mehrban N, Hunt N, Smith AM and Grover LM (2009) A comparative study of iota-carrageenan, kappa-carrageenan and alginate hydrogels as tissue engineering scaffolds, in

Williams PA, Phillips GO, Gums and Stabilisers for the Food Industry 15, Royal Society of Chemistry, Cambridge University Press, 2009 [ISBN (print): 978-1-84755-199-3].

Mehrban N, Paxton JZ, Bowen J, Vorndran E, Gbureck U and Grover LM (2011) Comparing the physicochemical properties of printed and hand-cast biocements designed for ligament replacement, Advances in Applied Ceramics: Structural, Functional and Bioceramics, 110, pp. 162-167.

Mendias CL, Bakhurin KI and Faulkner JA (2008) Tendons of myostatin-deficient mice are small, brittle, and hypocellular. Natio. Acad. Sci. USA, 105, pp. 388-393.

Meyer U, Meyer T, Handschel J, Wiesmann HP. Fundamentals of tissue engineering and regenerative medicine. Berlin: Springer-Verlag, 2009.

Mikos AG, Herring SW, Ochareon P, Elisseeff J, Lu HH, Kandel R, Schoen FJ, Toner M, Mooney D, Atala A, Van Dyke ME, Kaplan D and Vunjak-Novakovic D (2006) Engineering complex tissues. Tissue Eng., 12, pp. 3307-3339.

Mitkevich OV, Shainoff JR, DiBello PM, Yee VC, Teller DC, Smejkal GB, Bishop PD, Kolotushkina IS, Fickenscher K and Samokhin GP (1998) Coagulation Factor XIIIa undergoes a conformational change evoked by glutamine substrate. J. Biol. Chem., 273, pp. 14387-14391.

Moermans JP (1997) Place of segmental aponeurectomy in the treatment of dupuytren's disease [on-line]. Brussels: Clinique du Parc Léopold. Available from:-

http://www.jpmoermans.be/Scientific%20Activities_files/thesis-4.pdf [Accessed 26 October 2007].

Molinari BL, Tasat DR, Palmieri MA and Cabrini RL (2005) Kinetics of MTT-formazan exocytosis in phagocytic and non-phagocytic cells. Micron., 36, pp. 177-183.

Monis B and Valentich MA (1986) Ultrastructure of macrophages of carrageenan granuloma in the rat with data on gamma-glutamyltranspeptidase activity. J. Leukocyte Biol., 39, pp. 133-140.

Morris VJ (1998) Gelation of polysccharides. In Functional properties of food macromolecules, Ed. Hill SE, Ledward DA and Mitchell JR, Gaithersburg, MD, USA: Aspen Publication. pp. 143–226

Mosmann, T. (1983) Rapid colorimetric assay for cellular growth and survival: application to proliferation and cytotoxicity assays. J. Immunol. Methods, 65, pp. 55-63.

Murad S, Grove D, Lindberg KA, Reynolds G, Sivarajah A and Pinnell SR (1981) Regulation of collagen synthesis by ascorbic acid. Proc. Natl. Acad. Sci., 78, pp. 2879-2882.

Murphy KD, Mushkudiani IA, Kao D, Levesque AY, Hawkins HK and Gould LJ (2008) Successful incorporation of tissue-engineered porcine small-intestinal submucosa as substitute flexor tendon graft is mediated by elevated TGF-beta1 expression in the rabbit. J. Hand Surg. Am, 33, pp. 1168-1178.

Mutané J, Fernandez Y, Mitjavila S and Mitjavila MT (1993) Hepatic changes during a carrageenan induced granuloma in rats. Mediators Inflamm., 2, pp. 79-83.

Nakagawa S, Pawelek P and Grinnell F (1989) Extracellular matrix organization modulates fibroblast growth and growth factor responsiveness. Exp. Cell Res., 182, pp. 2572-2582.

Narayanan J, Xiong J-Y and Liu X-Y (2006) Determination of agarose gel pore size: Absorbance measurements vis a vis other techniques. J. Physics: Conference Series, 28, pp. 83-86.

Nesti LJ, Li WJ, Shanti RM, Jiang YJ, Jackson W, Freedman BA, Kuklo TR, Giuliani JR and Tuan RS (2008) Intervertebral disc tissue engineering using a novel hyaluronic acid-nanofibrous scaffold (HANFS) amalgam. Tissue Eng. Part A, 14, pp. 1527-1537.

Neurath MF and Stofft E (1992) Structure and function of matrix components in the cruciate ligaments. Acta. Anat., 145, pp. 387-394.

Nickerson MT, Darvesh R and Paulson AT (2010) Formation of calcium-mediated junction zones at the onset of the sol-gel transition of commercial *κ*-carrageenan solutions. J. Food Sci. E: Food Eng. Physical Prop., 75, pp. E153-E156.

Nickerson MT, Paulson AT and Hallett FR (2004) Dilute solution properties of *κ*-carrageenan polysaccharides: effect of potassium and calcium ions on chain conformation, Carbohyd. Polym., 58, pp.25-33.

Nishimura K, Blume P, Ohgi S and Sumpio BE (2009) The effect of different frequencies of stretch on human dermal keratinocyte proliferation and survival. J Surg. Res., 155, pp. 125-131.

Nishinari K, Watase M, Williams PA and Phillips GO (1990) *κ*-carrageenan gels: Effect of sucrose, glucose, urea and guanidine hydrochloride on the rheological and thermal properties. J. Agric. Food Chem., 38, pp. 1188-1193.

Nishida E, Sasaki T, Ishikawa SK, Kosaka K, Aino M, Noguchi T, Teranaka T, Shimizu N and Saito M (2007) Transcriptome database KK-Periome for periodontal ligament development: Expression of the extracellular matrix genes. Gene, 404, pp. 70-79.

Nutton RW, Mclean I and Melville E (1999) Tendon allografts in knee ligament surgery. J. R. Coll. Surg. Edinb., 44, pp. 236-240.

Ohura K, Bohner M, Hardouin P, Lemaitre J, Pasquier G and Flautre B (1996) Resorption of, and bone formation from, new β-tricalcium phosphate cements: An *in vivo* study. J. Biomed. Mater. Res. B, 30, pp. 193-200.

Oie Y, Hayashi R, Takagi R, Yamato M, Takayanagi H, Tano Y and Nishida K (2010) A novel method of culturing human oral mucosal epithelial cell sheet using post-mitotic human dermal fibroblast feeder cells and modified keratinocyte culture medium for ocular surface reconstruction. Br. J. Opthalmol., 94, pp. 1244-1250.

Okuda Y, Gorski JP, An K-N and Amadio PC (1987) Biochemical, histological and biomechanical analysis of canine tendon. J. Orthop. Res., 5, pp. 61-68.

Olesen JL, Heinemeier KM, Gemmer C, Kjær M, Flyvbjerg A and Langberg H (2007) Exercise-dependent IGF-1, IGFBPs, and type I collagen changes in human peritendinous connective tissue determined by microdialysis. J. Appl. Physiol., 102, pp. 214-220.

Omae H, (2006) Effects of interconnecting porous structure of hydroxyapatite ceramics on interface between grafted tendon and ceramics. J. Biomed. Mater. Res., Part A, pp.329-337.

Özbek H and Pekcan Ö (2004) Critical exponents of thermal phase transitions in κ-carrageenan-water system. J.Molec. Struct: Theochem., 676, pp. 19-27.

Pal K, Banthia AK and Majumdar DK (2006) Polyvinyl Alcohol–Gelatin patches of Salicylic Acid: preparation, characterization and drug release studies. J. Biomat. App., 21, pp. 75-91.

Pan Y, Dong S, Hao Y, Chu T, Li C, Zhang Z and Zhou Y (2010) Demineralised bone matrix gelatin as scaffold for tissue engineering. Afr. J. Microbiol. Res., 4, pp. 865-870.

Paoloni J, De Vos RJ, Hamilton B, Murrell GAC and Orchard J (2011) Platelet-rich plasma treatment for ligament and tendon injuries. Clin. J. Sport Med., 21, pp. 37-45.

Parfitt AM, Mathews CH, Villanueva AR, Kleerekoper M, Frame B and Rao DS (1983) Relationships between surface, volume and thickness of iliac trabecular bone in ageing and in osteoporosis. Implications for the microanatomic and cellular mechanisms of bone loss. J. Clin. Invest., 72, pp. 1396-1409.

Patel S, Rodriguez-Merchan EC and Haddad FS (2010) The use of fibrin glue in surgery of the knee. J. Bone Joint Surg., 92-B, pp. 1325-1331.

Paul W and Sharma CP (2007) Effect of calcium, zinc and magnesium on the attachment and spreading of osteoblast like cells onto ceramic matrices. J. Mater. Sci: Mater. Med., 18, pp. 699-703.

Paulson F, Kimpel M, Lockemann U and Tillmann B (2000) Effects of ageing on the insertion zones of the human vocal fold. J. Anat., 196, pp. 41-54.

Paxton JZ and Baar K (2007) Tendon mechanics: the argument heats up. J. Applied Physiol., 103, pp. 423-424.

Paxton JZ, Donnelly K, Keatch RP, Baar K and Grover LM (2010) Factors affecting the longevity and strength in an *in vitro* model of the bone-ligament interface. Annals. Biomed. Eng., 38, pp. 2155-2166.

Pecheva E, Pramatarova L and Altankov G (2007) Hydroxyapatite grown on a native extracellular matrix: Initial interactions with human fibroblasts. Langmuir, 23, pp. 9386-9392.

Pedersen, J.A. and Swartz, M.A. (2005) Mechanobiology in the third dimension. Annals Biomed. Eng., 33, pp. 1469–1490.

Pendegrass CJ, Oddy MJ, Cannon SR, Briggs T, Goodship AE and Blunn GW (2004) A histomorphological study of tendon reconstruction to a hydroxyapatite-coated implant: regeneration of a neo-entheses *in vivo*. J. Orthop. Res., 22, pp. 1316-1324.

Penel G, Leroy N, Van Landuyt P, Flautre B, Hardouin P, Lemaître J and Leroy G (1999) Raman microspectrometry studies of brushite cement: *In vivo* evolution in a sheep model. Bone, 25, pp. 81S-84S.

Petersen W and Tillmann B (1999) Structure and vascularisation of the cruciate ligaments of the human knee joint. Anat. Embryol., 200, pp. 325-334.

Phillips JE, Burns KL, Le Doux JM, Guldberg RE and Garcia AJ (2008) Engineering graded tissue interfaces. PNAS, 105, pp. 12170-12175.

Pick TP and Howden R. Gray's anatomy: Anatomy, descriptive and surgical, 1901 edition. Pennsylvania: Running Press 1974.

Picker KM (1999) Matrix tablets of carrageenans. I. A comparative study. Drug Dev. Ind. Pharm., 25, pp. 329-337.

Pina S and Ferreira J-MF (2010) Brushite-forming Mg-, Zn- and Sr-substituted bone cements for clinical applications, Materials, 3, pp. 519-535.

Pittet C and Lemaître J (2000) Mechanical characterization of brushite cements: A Mohr Circles' approach.J. Biomed. Mater. Res. Part A, 53, pp. 769-780.

Porter JR, Ruckh TT and Popat KC (2009) Bone tissue engineering: A review in bone biomimetics and drug delivery strategies. Biotech. Prog., 25, pp. 1539-1560.

Prado Da Silva MH, Lima JHC, Soares JA, Elias CN, de Andrade MC, Best SM and Gibson IR (2001) Transformation of monetite to hydroxyapatite in bioactive coatings on titanium. Surf. Coat. Tech., 137, pp. 270-276.

Preston SF, Regula CS, Sager PR, Pearson CB, Daniels LS, Brown PA and Berlin RD (1985) Glycosaminoglycan synthesis is suppressed during mitosis and elevated during early G1. J. Cell Bio., 101, pp. 1086-1093.

Provenzano PP and Vanderby R (2006) Collagen fibril morphology and organization: Implications for force transmission in ligament and tendon. Matrix Biol., 25, pp. 71-84.

Qin TW, Yang ZM, Wu ZZ, Xie HQ, Qin J and Cai SX (2005) Adhesion strength of human tenocytes to extracellular matrix component modified poly(DL-lactide-co-glycolide) substrates. Biomat., 26, pp. 6635–6642.

Ragetly GR, Slavik GJ, Cunningham BT, Schaeffer DJ and Griffon DJ (2010) Cartilage tissue engineering on fibrous chitosan scaffolds produced by a replica molding technique. J. Biomed. Mater. Res. A, 93, pp. 46-55.

Ralphs JR and Benjamin M (1999) Cell and matrix organization in tendons and ligaments. In: The biology of synovial joint. Gordon and Breach: Amsterdam: The Netherlands, pp. 267-273.

Ramirez A, Schwane JA, McFarland C and Starcher B (1997) The effect of ultrasound on collagen synthesis and fibroblast proliferation *in vitro*. Med. Sci. Sport Exc., 29, pp. 326-332.

Rea SM, Brooks RA, Schneider A, Best SM and Bonfield W (2004) Osteoblast-like cell response to bioactive composites- surface topography and composition effects, J. Biomed. Mat. Res. B Appl. Biomat., 70, pp. 250-261.

Reddy GK and Enwemeka CS (1996) A simplified method for the analysis of hydroxyproline in biological tissue. Clin. Biochem., 29, pp. 225-229.

Rees DA (1981) Polysaccharide shapes and their interactions- some recent advances. Pure Applied Chem., 53, pp. 1-14.

Rees JD, Wilson AM and Wolman RL (2006) Current concepts in the management of tendon disorders. Rheumatology (Oxford), 45, pp. 508-521.

Reeves KD and Hassanein KM (2003) Long term effects of dextrose prolotherapy for anterior cruciate ligament laxity. Alternative Therap., 9, pp. 58-62.

Rigozzi S, Muller R and Snedeker JG (2009) Local strain measurement reveals a varied regional dependence of tensile tendon mechanics on Glycosaminoglycan content. J. Biomech., 42, pp. 1547-1552.

Riley GP, Harrall RL, Constant CR, Chard MD, Cawston CE and Hazleman BL (1994) Glycosaminoglycans of human rotator cuff tendons: changes with age and in chronic rotator cuff tendinitis. Ann. Rheum. Dis., 53, pp. 367-376.

Robertson WJ, Hatch JD and Rodeo SA (2007) Evaluation of tendon graft fixation using α-BSM calcium phosphate cement. Anthroscopy: J. Anthros. Relat. Surg., 23, pp. 1087-1092.

Robinson G, Manning CE and Morris ER (1991) In Food Polymers Gels und Colloids, Ed. Dickinson E, Royal Society of Chemistry, Cambridge, pp. 22-33.

Robinson PS, Lin TW, Reynolds PR and Derwin KA (2004) Strain-rate sensitive mechanical properties of tendon fascicles from mice with genetically engineered alterations in collagen and decorin. J. Biomech. Eng., 126, pp. 252-257.

Ross JJ and Tranquillo RT (2003) ECM gene expression correlates with *in vitro* tissue growth and development in fibrin gel remodelled by neonatal smooth muscle cells. Matrix Biol., 22, pp. 477-490.

Rowe SL, Lee SY and Stegemann JP (2007) Influence of thrombin concentration on the mechanical and morphological properties of cell-seeded fibrin hydrogels. Acta Biomater., 3, pp. 59–67.

Royce PM and Steinmann B. Connective tissue and its heritable disorders: Molecular, genetic and medical aspects, 2nd edition. New York: John Weily & sons: Weily-Liss, 2002.

Roycik MD, Fang X and Sang QX (2009) A fresh prospect of matrix hydrolytic enzymes and their substrates. Curr. Pharm. Des., 15, pp. 1295-1308.

Rufai A, Ralphs JR and Benjamin M (1995) Structure and histopathology of the insertional region of the human Achilles tendon. J. Orthop. Res., 13, pp. 585-593.

Sachlos E and Czernuszka JT (2003) Making tissue engineering scaffolds work. Review on the application of solid freeform fabrication technology to the production of tissue engineering scaffolds. Eur. Cells and Mater., 5, pp. 29-40.

Sachlos E, Reis N, Ainsley C, Derby B and Czernuszka JT (2003) Novel collagen scaffolds with predefined internal morphology made by solid freeform fabrication. Biomat., 24, pp. 1487-1497.

Sahoo S, Cho-Hung JG and Siew-Lok T (2007) Development of hybrid polymer scaffolds for potential applications in ligament and tendon tissue engineering. Biomed. Mater., 2, pp. 169-173.

Sahoo S, Ouyang H, Goh C-HJ, Tay TE and Toh SL (2006) Characterisation of a novel polymeric scaffold for potential application in tendon/ ligament tissue engineering. Tissue Eng., 12, pp. 1-9.

Sakai S, Hashimoto I and Kawakami K (2007) Synthesis of an Agarose-Gelatin Conjugate for Use as a Tissue Engineering Scaffold. J. Biosci. Bioeng., 103, pp. 22-26.

Salgado AJ, Coutinho OP and Reis RL (2004) Bone tissue engineering: State of the art and future trends. Macromol. Biosci., 4, pp. 743-765.

Sallot M, Lascombe I, Bermont L, Jouvenot M (1997) Comparison of the effects of epidermal growth factor and fetal calf serum in human endometrial carcinoma RL95-2 cells. Anticancer Res., 17, pp. 3499-504.

Sano H, Yamashita T, Wakabayashi I and Itoi E (2007) Stress distribution in the supraspinatus tendon after tendon repair: Suture anchors versus transosseous suture fixation. Am. J. Sports Med., 35, pp. 542-546.

Sant S, Hancock MJ, Donnelly JP, Iyer D and Khademhosseini A (2010) Biomimetic gradient hydrogels for tissue engineering. Canad. J. Chem. Eng., 88, pp. 899-911.

Santo VE, Frias AM, Carida M, Cancedda R, Gomes ME, Mano JF and Reis RL (2009) Carrageenan-based hydrogels for the controlled delivery of PDGF-BB in bone tissue engineering applications. Biomacromol., 10, pp. 1392-1401.

Sarrafzadeh-Rezaei F, Farshid A-A, Dalir-Naghadeh B, Saifzadeh S, Abbasnia P and Jarolmasjed S-H (2010) Effects of ascorbic acid and α-tocopherol on collagen fibril stereological parameters in rabbits. Bull. Vet Inst. Pulawy, 54, pp. 377-382.

Sawaguchi N, Majima T, Funakoshi T, Shimode K, Harada K, Minami A and Nishimura S-I (2010) Effect of cyclic three-dimensional strain on cell proliferation and collagen synthesis of fibroblast-seeded chitosan-hyaluronan hybrid polymer fibre. J. Orthop. Sci., 15, pp. 569-577.

Schense, J.C. and Hubbell, J.A. (1999) Crosslinking Exogenous Bifunctional Peptides into Fibrin Gels with Factor XIIIa. Bioconj. Chem., 10, pp. 75-81.

Schliephake H, Gruber R, Dard M, Wenz R and Scholz S (2004) Repair of calverial defects in rats by prefabricated hydroxyapatite cement implants. J. Biomed. Mat. Res. A, 69, pp. 382-390.

Schuenke M, Schulte E, Schumacher U. THIEME Atlas of anatomy. In: Ross L, Lamperti E, Eds. General anatomy of the musculoskeletal system. New York: Thieme New York 2006.

Screen HR, Shelton JC, Bader DL and Lee DA (2005) Cyclic tensile strain upregulates collagen synthesis in isolated tendon fascicles. Biochem. Biophys. Res. Commun., 336, pp. 424-429.

Screen HRC, Bader DL, Lee DA and Shelton JC (2004) Local strain measurement within tendon. Strain, 40, pp. 157-163.

Screen HRC, Shelton JC, Chhaya VH, Kayser MV, Bader DL and Lee DA (2005) The influence of noncollagenous matrix components on the micromechanical environment of tendon fascicles. Annals. Biomed. Eng., 33, pp. 1090-1099.

Seitz H, Rieder W, Irsen S, Leukers B and Tille C (2005) Three-dimensional printing of porous ceramic scaffolds for bone tissue engineering. Wiley Periodicals, pp. 782-788.

Seong JM, Kim B-C, Park J-H, Kwon IK, Mantalaris A and Hwang Y-S (2010) Topical review: Stem cells in bone tissue engineering. Biomed. Mater., 5, pp. 1-15.

Sharma P and Maffulli N (2005) Tendon injury and tendinopathy: Healing and repair. J. Bone Joint Surg., 87-A, pp. 187-202.

Shi H, Wang J, Dong F, Wang X, Li H and Hou Y (2009) The effect of proteoglycans inhibited by RNA interference on metastatic characters of human salivary adenoid cystic carcinoma. BMC Cancer, 9, pp. 456.

Shinji K, Nobuhiro G, Michiko S, Kazutaka K, Keiichi O, Hitoyata S and Shohei K (2010) Regeneration of bone- and tendon/ ligament-like tissues induced by gene transfer of bone morphogenetic protein-12 in a rat bone defect. J. Tissue Eng., Article ID 891049, 8 pages doi:10.4061/2010/891049.

Sieuwerts AM, Klijn JG, Peters HA, Foekens JA (1995) The MTT tetrazolium assay scrutinised: How to use this assay reliably to measure metabolic activity of cell cultures *in vitro* for the assessment of growth characteristics, IC50-values and cell survival. Eur. J. Clin. Chem. Clin. Biochem., 33, pp. 813-823.

Silber JS, Anderson DG, Daffner SD, Brislin BT, Leland JM, Hilibrand AS, Vaccaro AR and Albert TJ (2003) Donor site morbidity after anterior iliac crest bone harvest for single-level anterior cervical discectomy and fusion, Spine, 28, pp. 134-139.

Silver FH, Freeman JW and Bradica G (2006) Structure and function of ligament, tendon and joint capsule. Orthop. Biol. Med., 2006, Part II, 15-47, DOI: 10.1385/1-59259-942-7:015.

Smith JD, Chen A, Ernst LA, Waggoner AS and Campbell PG (2007) Immobilization of aprotinin to fibrinogen as a novel method for controlling degradation of fibrin gels, Bioconjug. Chem., 18, pp. 695-701.

So K, Fujibayashi S, Neo M, Anan Y, Ogawa T, Kokubo T and Nakamura T (2006) Accelerated degradation and improved bone-bonding ability of hydroxyapatite ceramics by the addition of glass. Biomat., 27, pp. 4738-4744.

Sogal A and Tofe AJ (1999) Risk of bovine spongiform encephalopathy transmission through bone graft material derived from bovine bone used for dental applications. J. Periodontal., 70, pp. 1053-1063.

Solchaga LA, Dennis JE, Goldberg VM and Caplan AI (1999) Hyaluronic acid-based polymers as cell carriers for tissue-engineered repair of bone and cartilage. J. Orthop. Res., 17, pp. 205-213.

Sommerfeldt DW and Rubin CT (2001) Biology of bone and how it orchestrates the form and function of the skeleton. Eur. Spine. J., 10, pp. S86-S95.

Spalazzi JP, Doty SB, Moffat KL, Levine WN and Lu HH (2006) Development of controlled matrix heterogeneity on a triphasic scaffold for orthopaedic interface tissue engineering. Tissue Eng., 12, pp. 3497-3508.

Spiekermann H, Donath K, Hassell T, Jovanovic S and Richter J. Color atlas of dental medicine: Implantology. New York: Thieme, 1995.

Srinivasan S, Dollin M, McAllum P, Berger Y, Rootman DS and Slomovic AR (2009) Fibrin Glue Versus Sutures for Attaching the Conjunctival Autograft in Pterygium Surgery: A Prospective Observer Masked Clinical Trial. British J. Ophthalmol., 93, pp. 215-218.

Stephens MM (1994) Haglund's deformity and retrocalcaneal bursitis. Orthop. Clin. North Am., 25, pp. 41-46.

Stevens A and Lowe J. Human histology, 2nd edition. Edinburgh: Harcourt Publishers Limited: Mosby, 1997.

Stevens MM, Mayer M, Anderson DG, Weibel DB, Whitesides GM and Langer R (2005) Direct patterning of mammalian cells onto porous tissue engineering substrates using agarose stamps. Biomat., 26, pp. 7636-7641.

Stine IA and Vangsness Jr. CT (2009) Analysis of the capsule and ligament insertions about the acromioclavicular joint: A cadaveric study. Anthros.: J. Anthros. Relat. Surg., 25, pp. 968-974.

Stokols S, Sakamoto J, Breckon C, Holt T, Weiss J and Tuszynski MH (2006) Templated agarose scaffolds support linear axonal regeneration. Tissue Eng., 12, pp. 2777-2787.

Svensson L, Aszodi A, Reinholt FP, Fassler R, Heinegard D and Oldberg A (1999) Fibromodulin-null mice have abnormal collagen fibrils, tissue organization and altered lumican deposition in tendon. J. Bio. Chem., 274, pp. 9636-9647.

Takada A, Ohashi H, Matsuda H and Takada Y (1979) Effects of tranexamic acid, CIS-AMCHA, and 6-aminohexanoic acid on the activation rate of plasminogen by urokinase in the presence of clot. Thrombosis Res., 14, pp. 915-923.

Takahashi Y, Yamamoto M and Tabata Y (2005) Enhanced osteoinduction by controlled release of bone morphogenetic protein-2 from biodegradable sponge composed of gelatin and β-tricalcium phosphate. Biomat., 26, pp. 4856-4865.

Tamimi F, Torres J, Lopez-Cabarcos E, Bassett DC, Habibovic P, Luceron E, Barralet JE (2009) Minimally invasive maxillofacial vertical bone augmentation using brushite based cements. Biomat., 30, pp. 208-216.

Tanaka H, Manske PR, Pruitt DL and Larson BJ (1995) Effect of cyclic tension on lacerated flexor tendons *in vitro*. Am. J. Hand Surg., 20, pp. 467-473.

Tateishi T, Chen G and Ushida T (2006) Polyfunctional scaffolds for tissue engineering. J. Biomech. Sci. Eng., 1, pp. 8-15.

te Nijenhuis K (1997) On the nature of crosslinks in thermoreversible gels. Polymer Bulletin, 58, pp. 27-42.

Tobacman JK (2001) Review of harmful gastrointestinal effects of carrageenan in animal experiments. Environ. Health Perspec., 109, pp. 983-994.

Tozer S and Duprez D (2005) Tendon and ligament: Development, repair and disease. Birth Defects Res. (Part C), 75, pp. 226-236.

Triplett DA (2000) Coagulation and bleeding disorders: Review and update. Clinical Chem., 46, pp. 1260-1269.

Trotter JA and Wofsy C (1989) The length of collagen fibrils in tendon. Transactions of the Orthopaedic research society, 14, pp. 180.

Tuan TL and Grinnell F (1989) Fibronectin and fibrinolysis are not required for fibrin gel contraction by human skin fibroblasts. J. Cell Physiol., 140, pp. 577-583.

Tuan T-L, Song A, Chang S, Younai S and Nimni ME (1996) *In Vitro* fibroplasia: matrix contraction, cell growth, and collagen production of fibroblasts cultured in fibrin gels. Exp. Cell Res., 223, pp. 127–134.

Vacanti CA and Upton J (1994) Tissue-engineered morphogenesis of cartilage and bone by means of cell transplantation using synthetic biodegradable polymer matrices. Clin. Plast. Surg., 21, pp. 445–462.

Van Vlierberghe S, Dubruel P and Schacht E (2011) Biopolymer-based hydrogels as scaffolds for tissue engineering applications: A review. Biomacr., 21388145.

Venu P, (2004) Effect of coating techniques on the creation of a calcified zone for implant-tendon entheses. Bioeng. Conf. Proceedings IEEE 30th Ann. Northeast, USA pp. 138-139.

Vinatier C, Gauthier O, Masson M, Malard O, Moreau A, Moreau F, Bilban M, Spaethe R, Goppelt A, Daculsi G, Weiss P and Guicheux J (2006) Nasal chondrocytes and fibrin sealant for cartilage tissue engineering. Euro. Cells Mat., 12, pp. 43.

Vogel KG (2004) What happens when tendons bend and twist? Proteoglycans. J. Musculoskelet. Neuron Interact., 4, pp. 202-203.

von Doernberg M-C, von Rechenberg B, Bohner M, Grünenfelder S, van Lenthe GH, Müller R, Gasser B, Mathys R, Baroud G and Auer J (2006) *In vivo* behaviour of calcium phosphate scaffolds with four different pore sizes. Biomat., 27, pp. 5186-5198.

Vorndran E, Klammert U, Ewald A, Barralet JE and Gbureck U (2010) Simultaneous immobilisation of bioactives during 3D powder printing of bioceramic drug-release matrices. Advan. Func. Mater., 20, pp. 1585-1591.

Vorndran E, Klarner M, Klammert U, Grover LM, Patel S, Barralet JE and Gbureck U (2008) 3D powder printing of β-tricalcium phosphate ceramics using different strategies. Advan. Eng. Mater., 10, pp. B67-B71.

Vunjak-Nuvakovic G, Altman G, Horan R and Kaplan DL (2004) Tissue engineering of ligaments. Ann. Rev. Biomed. Eng., 6, pp. 131-156.

Wang JHC (2006) Mechanobiology of tendon. J. Biomech., 39, pp. 1563-1582.

Wang L, Shelton RM, Cooper PR, Lawson M, Triffitt JT and Barralet JE (2003) Evaluation of sodium alginate for bone marrow cell tissue engineering. Biomat., 24, pp. 3475-3481.

Wang M-C, Pins GD and Silver FH (1994) Collagen fibres with improved strength for the repair of soft tissue injuries. Biomat., 15, pp. 507-512.

Wang Q-W, Chen Z-L and Piao Y-J (2005) Mesenchymal stem cells differentiate into tenocytes by bone morphogenetic protein (BMP) 12 gene transfer. J. Biosci. Bioeng., 100, pp. 418-422.

Wardle EN and Taylor G (1968) Fibrin breakdown products and fibrinolysis in renal disease, J. Clin. Path., 21, pp. 140-146.

Washburn NR, Simon CG, Tona A, Elgendy HM, Karim A and Amis EJ (2002) Co-extrusion of biocompatible polymers for scaffolds with co-continuous morphology. J. Biomed. Mater. Res., 60, pp. 20-29.

Watanabe N, Woo SL-Y, Papageorgiou C, Celechovsky C and Takai S (2002) Fate of donor bone marrow cells in medial collateral ligament after stimulated autologous transplantation, Micros. Res. Tech., 58, pp. 39-44.

Watase M and Nishinari K (1986) Rheological and thermal properties of agarose and kappa-carrageenan gels containing urea, guanidine hydrochloride or formamide. Food Hydrocolloids, 1, pp. 25-36.

Wear KA (1999) Frequency dependence of ultrasonic backscatter from human trabecular bone: Theory and experiment. J. Acoust. Soc. Am., 106, pp. 3659-3664.

Wehrli FW (2007) Structural and functional assessment of trabecular and cortical bone by micromagnetic resonance imaging. J. Mag. Res. Imag., 25, pp. 390-409.

Weinstein SL and Buckwalter JA. Turek's orthopaedics: Principles and their application, 6th edition. Pennsylvania: Lippincott Williams & Wilkins, 2005.

Weisel JW and Litvinov RI (2008) The biochemical and physical process of fibrinolysis and effects of clot structure and stability on the lysis rate. Cardiovasc. hematol. Agents Med. Chem., 6, pp. 161-180.

Weisel, J.W. (2004) The mechanical properties of fibrin for basic scientists and clinicians. Biophys. Chem., 112, pp. 267-276.

Weisel, J.W. (2005) Fibrinogen and fibrin. Advanc. Protein Chem., 70, pp. 247-299.

Weisel, J.W. (2007) Which knobs fit into which holes in fibrin polymerization. J. Thromb. Haemost., 5, pp. 2340-2343.

Weisel JW, Nagaswami C and Makowski L (1987) Twisting of fibrin fibres limits their radial growth. Proc. Natl. Acad. Sci. 84, pp. 8991-8995.

Whitlock PW, Smith TL, Poehling GG, Shilt JS and Van Dyke M (2007) A naturally derived, cytocompatible, and architecturally optimized scaffold for tendon and ligament regeneration. Biomat., 28, pp. 4321-4329.

Williams RC (1981) Morphology of bovine fibrinogen monomers and fibrin oligomers. J. Molec. Biol., 150, pp. 399-408.

WoldeMeskel D, Abate G, Lakew M, Goshu S, Selassie A, Miomer H and Aseffa A (2005) Evaluation of a direct colorimetric assay for rapid detection of rifampicin resistant Mycobacterium tuberculosis. Ethiop. J. Health Dev., 19, pp. 51-54.

Wolfman NM, Hattersley G, Cox K, Celeste AJ, Nelson R, Yamaji N, Dube JL, DiBlasio-Smith E, Nove J, Song JJ, Wozney JM and Rosen V (1997) Ectopic induction of tendon and ligament in rats by growth and differentiation factors 5, 6, and 7, members of the TGFb gene family. J. Clin. Invest., 100, pp. 321–330.

Wong AP, Cortez SL and Baricos WH (1992) Role of plasmin and gelatinase in extracellular matrix degradation by cultured rat mesangial cells. Am. J. Physiol., 263, pp. F1112-F1118.

Woo SL, Abramowitch SD, Kilger R and Liang R (2006) Biomechanics of knee ligaments: injury, healing and repair. J. Biomech., 39, pp. 1-20.

Yang F, Wang Y, Zhang Z, Hsu B, Jabs EW and Elisseeff JH (2008) The study of abnormal bone development in the Apert syndrome $Fgfr2^{+}$/S252W mouse using a 3D hydrogel culture model. Bone, 43, pp. 55-63.

Yang G, Crawford RC and Wang JH (2004) Proliferation and collagen production of human patellar tendon fibroblasts in response to cyclic uniaxial stretching in serum-free conditions. J. Biomech., 37, pp. 1543-1550.

Yang YI, Seol DL, Kim HI, Cho MH and Lee SJ (2007) Composite fibrin and collagen scaffold to enhance tissue regeneration and angiogenesis. Current App. Phys., 7SI, pp. e103-e107.

Yee VC, Pratt KP, Côté HCF, Trong IL, Chung DW, Davie EW, Stenkamp RE and Teller DC (1997) Crystal structure of a 30kDa C-terminal fragment from the γ chain of human fibrinogen. Structure, 5, pp. 125-138.

Yoon JH and Halper J (2005) Tendon proteoglycans: biochemistry and function. J. Musculoskelet. Neuronal Interact., 5, pp. 22-34.

Yoshikawa H and Myoui A (2005) Bone tissue engineering with porous hydroxyapatite ceramics. J. Artific. Organs, 8, pp. 131-136.

Young RG, Butler DL, Weber W, Caplan AI, Gordon SL and Fink DJ (1998) Use of mesenchymal stem cells in a collagen matrix for Achilles tendon repair. J. Orthop. Res., 16, pp. 406-413.

Yung CW, Wu LQ, Tullman JA, Payne GF, Bentley WE and Barbari TA (2007) Transglutaminase crosslinked gelatin as a tissue engineering scaffold. J. Biomed. Mat. Res. A, 83, pp. 1039-1046.

Zhai Y and Cui FZ (2006) Recombinant human-like collagen directed growth of hydroxyapatite nanocrystals. J. Crystal Growth, 291, pp. 202-206.

Zhang G, Young BB, Ezura Y, Favata M, Soslowsky LJ, Chakravarti S and Birk DE (2005) Development of tendon structure and function: Regulation of collagen fibrillogenesis. J. Musculoskelet. Neuronal Interact., 5, pp. 5-21.

Zhang Y, Ni M, Zhang M and Ratner B (2003) Calcium phosphate-chitosan composite scaffolds for bone tissue engineering. Tissue Eng., 9, pp. 337-345.

Zhao H, Ma L, Zhou J, Mao Z, Gao C and Shen J (2008) Fabrication and physical and biological properties of fibrin gel derived from human plasma. Biomed. Mat., 3, 015001.

Zheng Shu X, Liu Y, Palumbo FS, Luo Y and Prestwich GD (2004) In situ crosslinkable hyaluronan hydrogels for tissue engineering. Biomat., 25, pp. 1339-1348.

Zustiak S and Leach JB (2010) Hydrolytically Degradable poly(ethylene glycol) hydrogel scaffolds with tunable degradation and mechanical properties, Biomac., 11, pp. 1348-1357.

APPENDIX

Mehrban N, Hunt N, Smith AM and Grover LM (2009) A comparative study of iota-carrageenan, kappa-carrageenan and alginate hydrogels as tissue engineering scaffolds, in Williams PA, Phillips GO, Gums and Stabilisers for the Food Industry 15, Royal Society of Chemistry, Cambridge University Press, 2009 [ISBN (print): 978-1-84755-199-3].

Mehrban N, Smith AM, Grover LM. Evaluation of Iota carageenan as a potential tissue engineering scaffold. Submitted for Oral Presentation at the 8th World Congress of Chemical Engineering, Montreal, Canada, August 23rd – 27th, 2009 (conference proceeedings).

Mehrban N, Gbureck U, Grover LM. 3D printing of calcium phosphate cements for regenerating the hard/ soft tissue interface. Cement and Concrete Science, Leeds, September 2009 (conference proceedings).

3D printing of calcium phosphate cements for regenerating the hard/ soft tissue interface.

Nazia Mehrban, School of Chemical Engineering, College of Physical Science and Engineering, Edgbaston, Birmingham, B15 2TT, UK, NXM741@bham.ac.uk.

Uwe Gbureck, Department of Functional Materials in Medicine and Dentistry, University of Wuerzburg, Wuerzburg, D-97070, Germany, uwe.gbureck@fmz.uni-wuerzburg.de

Liam M Grover*, School of Chemical Engineering, College of Physical Science and Engineering, Edgbaston, Birmingham, B15 2TT, UK, L.M.Grover@bham.ac.uk.

* corresponding author

Abstract: Cement based materials have an important role to play in a diverse range of fields including tissue engineering. Whilst many ceramics require thermal processing, leading to difficulties in the incorporation of active biological moieties, cements often set with little exotherm. This allows active biological molecules to be immobilised in the material with minimal loss in activity. Recent advances in 3D powder printing have enabled the production of calcium phosphate cement based materials which can be readily formed in a range of precise and complex morphologies (Vorndran et. al. 2008). For this study, a tricalcium phosphate powder layer was sprayed with a binder solution of 20% phosphoric acid and developed into a layer by layer 3D construct. Triplicate immersion in 20% phosphoric acid completed the hardening process. Structural geometries of the brackets were designed using thinkdesign 2007 software for eventual use as anchors in the tensile tissue engineered ligament constructs. Initially, carrageenan gel was used to represent the soft tissue component in the tissue engineered ligament construct. The bracket design was chosen to minimise fracture between the hard/ soft tissue interface where unbalanced stress caused by clamping results in serious distortions of the soft tissue structure ultimately leading to premature failure.

1.Introduction

Composed mainly of tenocytes embedded within a matrix of collagen, tendons are responsible for the attachment of muscle to bone and ligaments are responsible for the attachment of bone to bone. They are often damaged through overuse or lack of use (e.g. being bedridden), with most ligament and tendon related injuries (such as ectopic calcification and tearing) occurring amongst athletes, causing extreme pain and a decrease in the functionality of the joint. Current methods of repair encounter problems when restoring original joint biomechanics and maintaining good healing at the site of injury (Doroski, et. al., 2007) due to the poor regenerative capabilities of the tissue. Recent advances in the repair of damaged connective tissue have involved engineering the tissue using biological scaffolds seeded with cells. Some workers have successfully grown

harvested tenocyte cells between two anchor points forming a self-aligned structure of collagen fibres (naturally present in both ligaments and tendons). One limiting factor with this approach is the weak attachment of the tissue engineered construct to bone. In order to create a strong bond, it is necessary to recreate the calcified transition zone between the soft and hard tissue (Venu et. al. 2004).
It is well established that calcium phosphates can form an intimate bond with both soft and hard tissues and consequently they have successfully been used to coat prostheses such as hip implants, thus increasing attachment. Calcium phosphate based ceramics have also been used as a bone regeneration scaffold onto which precursor cells have been seeded (Vacanti and Upton, 1994). The development of a range of calcium phosphate cement materials that could be processed to a desired shape with little or no exotherm during setting, has enabled the incorporation of biologically active molecules into the solid material. Recently, we have reported the production of 3D powder printed calcium phosphate based bracket that can have tightly defined geometries. Importantly, with this process we were able to precisely deposit growth factors to further enhance tissue attachment and reduce the chances of interface failure. In this pilot study we have used a 3D powder printing process where a phosphoric acid binder was sprayed onto a bed of β-tricalcium phosphate (β-TCP) in order to produce a range of 3D printed brackets between which tissue engineered ligaments will be grown. It is hoped that these scaffolds will ultimately allow for the formation of a strong bond between the bone and the cell-seeded soft tissue scaffold following implantation.

2. Materials and methods

2.1 3D printing

Tricalcium phosphate (TCP) was synthesised by heating an equimolar mixture of dicalcium phosphate anhydrous (DCPA, $CaHPO_4$ monetite) (Merck, Darmstadt, Germany) and calcium carbonate (CC, CaCO3, calcite) (Merck, Darmstadt, Germany) to 1400°C for 14h followed by quenching to room temperature. The sintered cake was crushed with a pestle and mortar and passed through a 160µm sieve. Milling was performed in a planetary ball mill (PM400, Retsch, Germany) at 200rpm with 500ml agate jars, 4 agate balls with a diameter of 30mm and a load of 125g TCP per jar for 30 mins. Printing of cement samples was performed with a multi-colour 3D-powder printing system (Spectrum ZS10, Z-Corporation, USA) using the TCP powder and a binder solution of 20% phosphoric acid (Merck, Darmstadt, Germany) with a layer thickness of 125µm, a binder/ volume ratio of 0,371 and an isotropic scaling x=y=z= 1.0. Structure geometries were designed using thinkdesign 2007 software (Fa. Think3). After the printing process the samples were cleaned with compressed air and hardened afterwards by triplicate immersion in 20% phosphoric acid for 30 seconds. Printed calcium phosphate brackets were formed based on the CAD's. All brackets were hand cleaned and hardened before use and their matching brackets were checked for precise fitting.

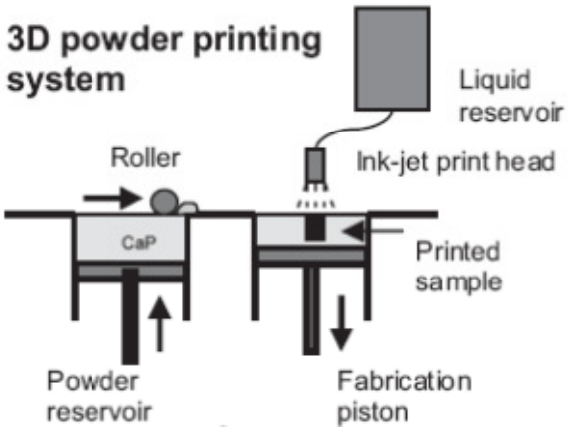

Figure 1: Schematic of the powder printing methodology reported in this paper (Adapted form Vorndran et al. 2008).

2.2 Gel formation

2% kappa-carrageenan (w/v) was prepared on a hotplate stirrer at 60°C. The liquid gel was then poured over the channel in a mold designed to hold the split-brackets and provide a groove to allow the formation of a gel fibre (Figure 2).

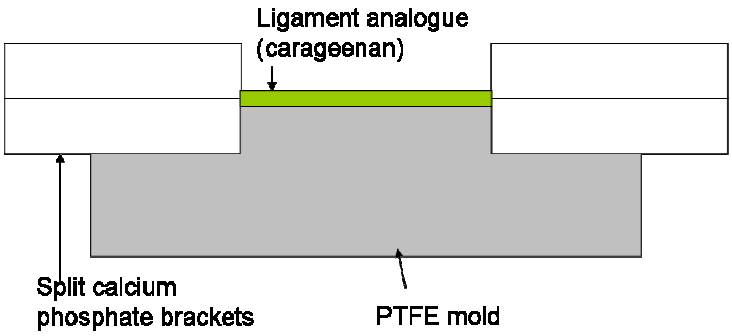

Figure 2. A schematic diagram showing the mold onto which the split calcium phosphate brackets were placed and between which the ligament analogue (carrageenan) was cast.

3. Results and Discussion

A range of brackets were designed for the purpose of minimising slippage of the ligament analogue when placed under tensile strain (Figure 3). Curvature at the opening of the channel was believed to enhance the grip and avoid tear directly at the interface between the gel and the

calcium phosphate bracket. In this study, we have designed various brackets to maximise grip and used 3D powder printing facilities to rapidly and accurately reproduce the calcium phosphate structures. All bracket designs were fabricated to within 1% accuracy of their CAD model, and the resulting structures exhibited sufficient mechanical integrity to retain their original morphology following immersion in culture medium (Figure 4).

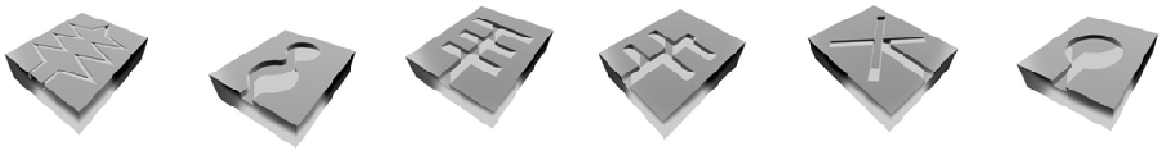

Figure 3: 3D powder printed brackets designed on thinkdesign 2007 software.

By employing a PTFE mold (Figure 2) it was possible to cast a fibre of carrageenan between the two calcium phosphate brackets onto which tenocytes could be seeded. The resulting structure was a self-supporting gel between two sets of calcium phosphate brackets (Figures 4 and 5). 3D printing has allowed us to successfully produce precisely defined structures enabling the fabrication of tissue engineered ligament which has two attachment points which could be integrated into bone following implantation. The technique has previously been used to print 3D structures of a defined geometry and a range of different chemistries (Vorndran et. al., 2008 and Khalyfa et. al., 2007).

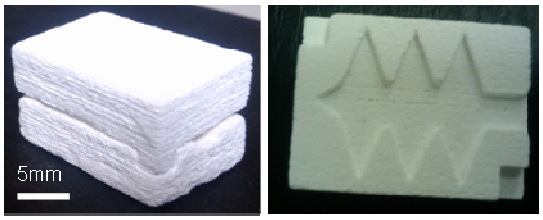

Figure 4: 3D calcium phosphate brackets printed on the 3D powder printing system (Spectrum ZS10, Z-Corporation, USA). Images show two brackets as well as the internal design of a printed bracket.

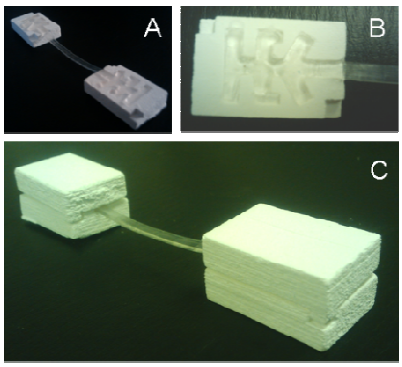

Figure 5: The fabrication of a a tissue engineered ligament scaffold using A) two calcium phosphate brackets, B) Onto which a carrageenan gel was cast. C). The resulting structure was self supporting and could act as a functional scaffold for tissue engineering ligaments.

4. Conclusions

Here we report a preliminary study that demonstrates the efficacy of a 3D powder printing approach for the fabrication of brackets used for the tissue engineering of ligaments. We hope to be able to use the printed brackets in the near future to develop cell-seeded structures between calcium phosphate grips. These will be used for the investigation of tensile strain on the cells within the gel and the mechanical strength of the gel used in order to gain a better understanding of the causes of failure in current methods of tendon/ ligament repair.

Acknowledgments

We would like to thank Dr. James Bowen, Neeraj Jumbu and Sarika Patel for their contribution, and the BBSRC for the provision of a studentship (N. Mehrban).

References

Bauer, T.W. et. al. (1999) Hydroxyapatite-coated femoral stems. Histological analysis of components retrieved at autopsy. Journal of Bone and Joint Surgery. Vol 73 (10): 1439-1452.

Doroski, D. M. et. al. 92007) Techniques for biological characterisation of tissue-engineered tendon and ligaments. Biomaterials. Vol. 28 (2): 187-202.

Khalyfa, A. et. al. (2007) Development of a new calcium phosphate powder-binder system for the 3D printing of patient specific implants. J. Material Science: Mate. Medicine, 18: 909-916.

Vacanti, C.A., Upton, J., 1994. Tissue-engineered morphogenesis of cartilage and bone by means of cell transplantation using synthetic biodegradable polymer matrices. Clin. Plast. Surg. 21 (3), 445–462

Venu, P. et. al. (2004) Effect of coating techniques on the creation of a calcified zone for implant-tendon entheses. Bioengineering Conference, 2004. Proceedings of the IEEE 30th Annual Northeast. 138-139.

Vorndran et al. Adv Eng Mater 2008;10:12:B67-B71.

A COMPARATIVE STUDY OF IOTA CARRAGEENAN, KAPPA CARRAGEENAN AND ALGINATE HYDROGELS AS TISSUE ENGINEERING SCAFFOLDS

N Mehrban, N Hunt, AM Smith and LM Grover

School of Chemical Engineering, University of Birmingham, Edgbaston, Birmingham, UK

1 INTRODUCTION

The increasingly aging population and lack of donor tissue has pushed tissue regeneration to the forefront of modern biomedical research and biopolymers traditionally found in the food and pharmaceutical industry are increasingly being used in tissue engineering. The development of tissue engineering provides the opportunity to take a sample of cells from a patient which are then cultured *in vitro* to organise into functional tissue that can then be implanted back into the patient, ultimately, overcoming problems of tissue rejection and the need for donor tissue. To grow replacement tissue requires a suitable substrate or scaffold for cells to attach, proliferate and organise into viable tissue that can be safely implanted into the body. Biopolymers and hydrogel forming biopolymers in particular, have been shown to be a promising scaffold material due having properties that resemble the environment of the mammalian extracellular matrix (ECM). In addition properties such as mild gelation conditions, potential for good mass transport of nutrients and waste molecules, nontoxic nature and biological compatibility provide an advantage over synthetic polymers and ceramic and metallic materials which have also been used as tissue engineering scaffolds.

As well as supporting cell growth and proliferation, the scaffold must have the mechanical characteristics needed to retain its structure for as long as it is needed [1]. Ideally gels used as scaffolds for tissue engineering would have a mild sol-gel reaction that can be controlled at 37°C and at physiological pH, have rapid gelation kinetics and be robust enough for 3D culture and implantation. This explains why much of the research on biopolymers for tissue engineering has been performed on materials such as alginate[2] and chitosan[3] collagen[4] agarose[5] and fibrin[6]. The relative success of the cell culture of the mentioned biopolymers has generated interest in other gel forming biopolymers such as gellan gum[7] and chemically modified gels such as RGD alginate[8]. Performance of the cells when encapsulated in these biopolymers varies due to the cellular interaction with the polymer chemistry and gel network structure.

In this study we have investigated the use of carrageenan as a 3D tissue engineering scaffold for mammalian cells and looked at the impact of structural differences between kappa and iota

carrageenan has on the attachment, survival and proliferation of fibroblasts and in comparison with alginate which, is widely used in tissue regeneration. Carrageenan has been used in bacterial culture[9] and has been evaluated as a delivery vehicle for growth factors for mammalian tissue engineering applications[10] however there have been no reports of carrageenan being used exclusively for the 3D culture of mammalian cells.

2 METHODS AND RESULTS

Unless otherwise specified all reagents were obtained form Sigma Aldrich (Poole, UK).

2.1. Formation of hydrogel scaffolds for encapsulation of fibroblasts

NIH 3T3 murine fibroblasts were added to 2% (w/v) Na-alginate at a density of 0.75 x 10^6 cells/ml. The cell-gel suspension was then added drop wise into a bath of 100mM $CaCl_2$ and left to incubate at 37ºC for 2h to form crosslinked spheres of 3.0 ± 0.2 mm diameter.

1% *kappa* and 2% *Iota* carrageenan discs were formed using 3ml autoclaved gel which was cooled to 40°C before a 0.75 x 10^6 NIH 3T3 murine fibroblast cell suspension was added and pipetted repeatedly to ensure homogenisation. No extra cations were added to the gel solution as there were sufficient salts present within the supplemented media added to cell suspensions to cause the gel to crosslink.

All samples were cultured in high glucose Dulbecco's Modified Eagle's Media (DMEM) supplemented with 10% v/v foetal bovine serum (FBS) (PAA, Somerset, UK), 1% v/v penicillin-streptomycin (P/S), 2.25% v/v HEPES and 2% v/v L-glutamine and maintained at 37ºC with 5% CO_2 and 100% relative humidity and media was changed three times weekly. Control samples without cell seeding were also prepared for degradation studies.

2.2 Formation of hydrogel scaffolds for surface seeding

Alginate discs were prepared using sterile 2% low viscosity Na-alginate. The discs were formed by covering 3ml Na-alginate with 100 mM $CaCl_2$ for 2h in 6-well tissue culture plates. Following crosslinking, NIH 3T3 murine fibroblasts were seeded on the surface of the alginate at a density of 0.44×10^6 cells/ml

Iota and *Kappa* carrageenan gel cylinders were formed using sterile 2% (w/v) *iota*-carrageenan and 1% (w/v) *kappa* carrageenan in 12-well culture plates containing 3ml of the gel solution per well before addition of 1 ml 200 mM KCl. The crosslinked *kappa* and *iota*-carrageenan discs were then seeded at a cell density of 0.75×10^6. The gel discs were topped with supplemented DMEM and maintained at 37ºC with 5% CO_2 and 100% relative humidity.

2.3 Analysis of cell morphology and survival

Following 10 days in culture, samples of the gels were removed and the cells were analysed using a Live/ Dead® Viability/Cytotoxicity Kit. This procedure, based on the uptake of calcein AM and conversion to fluorescent calcein (green) by intracellular esterases in live cells and the uptake of propidium iodide (red) by cells with damaged plasma membranes, was used in conjunction with fluorescence microscopy to assess cellular responses to the alginate and carrageenan scaffolds. The results for the encapsulated samples showed that >95% of cells remained viable in alginate. The rounded morphology, however, also indicate that they were not well attached to the gel (Fig. 1A). Similarly cells encapsulated in *kappa*-carrageenan are rounded in appearance on day 10 (Fig 1B) with > 95% of the cells remaining live. Samples of *iota*-carrageenan (Fig. 1C) also had a >95% survival, however, the appearance of thin projections and overall elongation of the cells suggests attachment of the cells to the hydrogel. It is hypothesised that the lack of ionically bound junction zones within the structure of iota-carrageenan gels provides spaces between the polymer chains that are sufficient in allowing the cells to grow and proliferate similar to the findings of Jeon et. al. (2007)[11]. For surface seeded samples only a few cells were seen to be attached to alginate and *iota*-carrageenan after 10 days (Fig. 2A and 2B). These cells were shown to be alive, but with a rounded morphology without cytoplasmic projections indicating that the cells were poorly attached to the surface of the gel. Although the cells in alginate exhibit similar behaviour to kappa carrageenan when they are encapsulated, there is a marked reduction in cell number (<50%) and overall lack of attachment to the surface of the alginate samples. This poor attachment was similar to reported found by Harris *et al* (2007) who used gellan gum for surface seeding. The authors hypothesised that poor attachment was due to poor cell traction which prevented the cells from adhering to the surface of the material and exerting forces sufficient to allow migration, which may be the case for alginate and kappa carrageenan. Indeed, it has been shown that modifying alginate with the tri-peptide RGD dramatically improves cell attachment[8]. For *iota*-carrageenan, however, the cells appear to be attached to the surface of the gel although this cannot be truly confirmed without performing assaying for the presence of focal contacts or adhesion proteins.

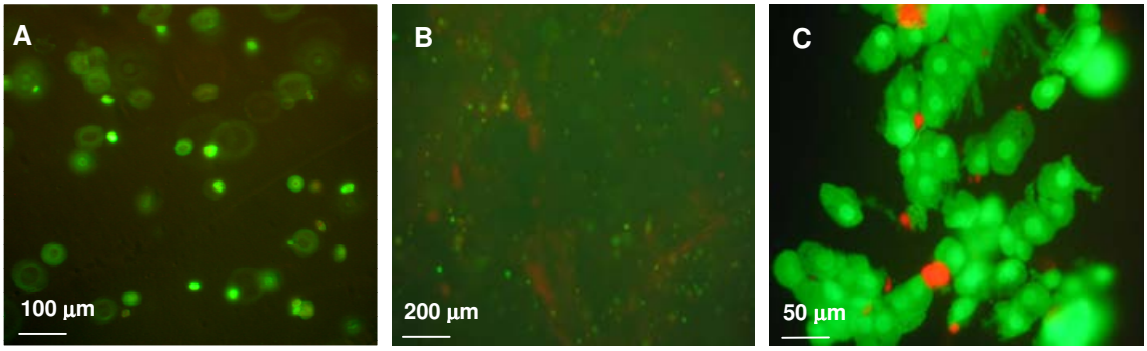

Fig. 1. 3T3 Fibroblasts stained with calcein-AM and PI 10 days post encapsulation in alginate (A), *kappa*-carrageenan (B) and *iota*-carrageenan (C).

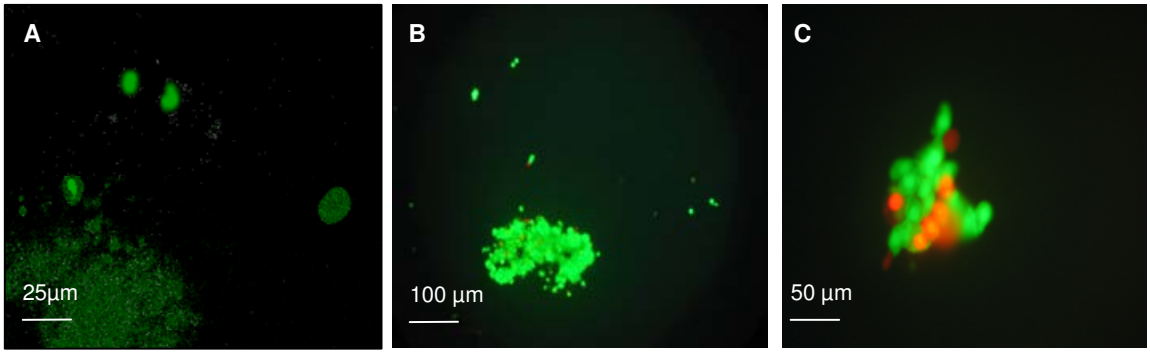

Fig. 2. 3T3 Fibroblasts stained with calcein-AM and PI 10 days after application to the surface of alginate (A), *kappa* -carrageenan (B) and *iota*-carrageenan (C).

2.2 MTT (3-(4,5-Dimethylthiazol-2-yl)-2,5-diphenyltetrazolium bromide) assay

To identify and quantify any cell proliferation within the gels an MTT assay was performed, whereby the tetrazolium ring of the MTT is cleaved by the mitochondrial dehydrogenases in living cells, producing purple formazan crystals. Dissolving these crystals and measuring the absorbance is an indication of the cell population's metabolic activity. This assay was applied to the cultures by adding 200 µl MTT to a 2 ml gelled sample. The absorbance readings (at 620 nm) obtained from the MTT assay over 12 days were used to determine the number of viable cells present in each daily sample. Figure 3 shows a comparison of the calculated cell number for all three gels. It can be seen that whilst there was a significant difference between the cell counts of all three gels ($P < 0.05$) there appeared to be no proliferation in the number of cells encapsulated in alginate. Cells encapsulated in *iota*-carrageenan show a gradual increase in the cell number over 5 days. This may be explained by the fact that iota-carrageenen gels have the ability to spontaneously reform below their melting point following mechanical disruption[12] allowing cells to migrate throughout the gel without disrupting the network, unlike in kappa-carrageenan and alginate where the cells are confined within a more tightly bound gel network. After 5 days in culture, this number reduced (from 4.9×10^6 to 1.1×10^6 by day 12). Proliferation was also seen in *kappa*-carrageenan, however, not at the same rate as in *iota*-carrageenan and it was not until day 10 that the cells in kappa carrageenan were of comparable number to those in the iota-carrageenan.

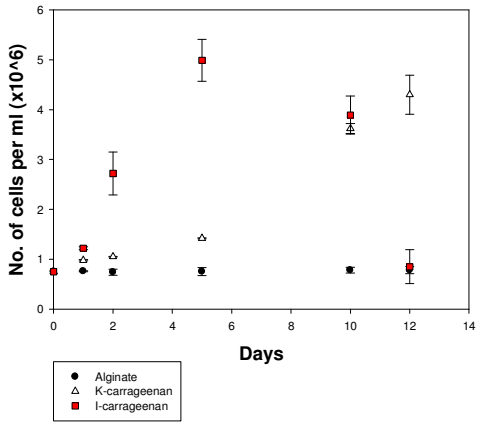

Fig. 3: Number of viable cells calculated from the absorbance of formazan of the encapsulated cells. Vertical error bars represent the standard deviation of the reported mean values (n=3).

2.3 Degradation

The changes in mass of gels with and without cells was determined by measuring the dry mass of the samples (by slow vacuum drying) on a daily basis in a vacuum freeze-drier (Edwards, EF03, Sussex, UK) for 16h. This was to quantify any fluctuations in mass within the samples which may occur as a consequence of polymer degradation, protein absorption from the culture media or formation of extracellular matrix.

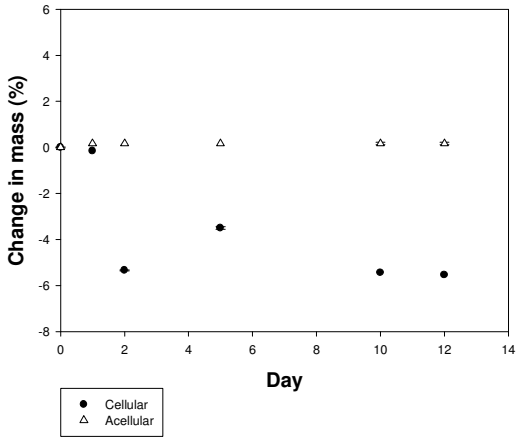

Fig. 4: Changes in the mass for *Kappa*-carrageenan with and without cells. Vertical error bars represent the standard deviation of the reported mean values (n=3).

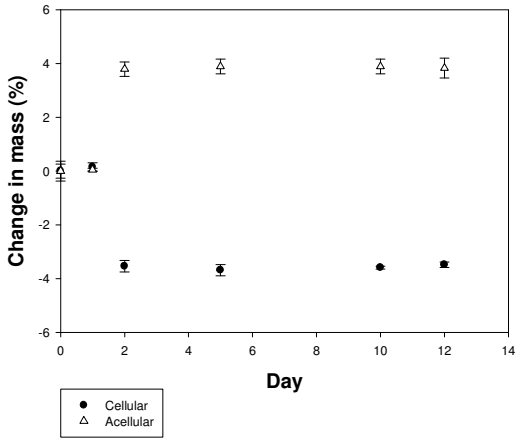

Fig. 5: Changes in the mass for *Iota*-carrageenan with and without cells. Vertical error bars represent the standard deviation of the reported mean values (n=3).

The degradation rates of the three gels were found to vary considerably, with no statistical difference seen between the cellular and acellular samples of alginate ($P > 0.05$) (results not shown). The acellular samples of *kappa*-carrageenan remained unchanged for the duration of the study, however, the addition of cells within the gel caused a gradual loss in total mass suggesting degradation of the polymer. The gel mass of acellular samples of *iota*-carrageenan increased by a total of 3.9% 2 days post encapsulation indicating the possibility of protein absorption from the culture media to the carrageenan, enabling cell attachment. This supports the findings from the proliferation assay and the observations of cell attachment. The *iota*-carrageenan containing cells showed a 3.5% reduction in mass which, is thought to be due to degradation of the gel which was visually apparent when samples were being transferred to the freeze dryer for measurements. The kappa carrageenan samples where observed to be more robust than the iota-carrageenan however the gel integrity of both types did reduce through the duration of the study. Kappa-carrageenan was initially observed to be a stronger gel in comparison with iota-carrageenan and interestingly, these physical properties may be the cause of initial cell proliferation observed in iota-carrageenan which were not seen in the kappa form. Eventual dissolution of iota-carrageenan lead to difficulty in quantifying the proliferation of encapsulated cells within the polymer at day 12 which accounts for the reduction in cellular proliferation measured using the MTT assay. The gel network of the kappa-carrageenan samples also began to lose its integrity, however, this was not apparent until day 10 of the study which correlates with a dramatic increase in the proliferation of encapsulated cells. This is in contrast to the alginate samples which appeared unchanged throughout. This demonstrates the necessity of investigating the mechanical properties of hydrogel scaffolds in relation to cellular behaviour.

3.0 CONCLUSION

In conclusion we have shown that cells can be encapsulated and remain viable in both kappa and iota carrageenan for up to 12 days which is comparable with alginate which is a widely used tissue engineering substrate. There was no evidence of attachment of cells to the alginate or the kappa carrageenan however some attachment was evident when using iota carrageenan as the scaffold for both encapsulated cells and surface seeded cells. It was also shown that proliferation of the cells within the scaffolds occurs at different rates possibly due to the mechanical properties and network architecture of the gels. Fluctuations in mass were also measured in the scaffolds which correlated with changes in cellular proliferation.

Subsequently, this study has highlighted the need for investigations into the mechanical properties of hydrogels when applied as cell scaffolds. The potential for utilising biopolymers and mixtures of biopolymers traditionally used in the food and pharmaceutical industry for this

purpose is apparent as the subtle differences in gel architecture can have a dramatic effect on cell culture. This preliminary study suggests that both kappa and iota-carrageenan may be suitable hydrogels for use as a scaffold for tissue engineering purposes and as a tool for examining cells as proliferation occurs. Iota-carrageenan in particular, may have applications as a cell delivery vehicle due to the initial proliferation and subsequent dissolution. Furthermore, chemical modifications, and the development of polymer blends to change the structure and gelation behaviour may be of use to tailor the scaffolds further.

Acknowledgements

We would like to acknowledge the EU for the provision of a studentship under FP6 (N Hunt, NanoBioTact) and the BBSRC for the provision of a studentship (N Mehrban).

REFERENCES

1 J.J. Harris, A.M. Smith, S. Campbell-Lynch & R.M. Shelton (2008) *In Gums and stabilisers for the food industry 14*. 79-86

2 JL. Drury & DJ. Mooney (2003) *Biomaterials.* 24, 4337-4351

3 B Baroli (2007) *J. Pharm. Sci.* 96, 2197-2223

4 Z. Feng, M. Yamato, T. Akutsu, T. Nakamura, T. Okano, and M. Umezu (2003) *Artificial Organs* 27, 84 – 91

5 M.A. DiMicco, J.D. Kisiday, H. Gong and A.J. Grodzinsky (2007) *Osteoarthr. Cartilage* 15 1207–1216

6 K. Baar. (2007). Uniaxial stretch increases collagen synthesis in fibrin-based engineered tendons. *Tissue Engineering* 13, 1773.

7 A.M Smith, R.M Shelton, Y. Perrie, & JJ.Harris (2007) *J. Biomater. Appl.* 3, 241-54.

8 J T. Connelly, A J. García & M E. Levenston (2007) *Biomaterials.* 28, 1071-1083
9 J. Woodward (1998). *Journal of microbiological Methods,* **8**, 91-102.
10 V. Espírito Santo, A.M. Frias, M. Carida, R. Cancedda, M.E. Gomes, J.F Mano & R.L. Reis (2009) Biomacromolecules

11 O. Jeona, S.J Songa, K. Leea, M.H. Parkb, S. Leed, S.K. Hahne, S. Kimf & B.S. Kimc (2007) *Carbohydr. Polym*. 70, 251-257

12 H.J. Bixler, K. Johndro & R. Falshaw (2001) *Food Hydrocolloids* 15, 619-63

EVALUATION OF *IOTA*-CARRAGEENAN AS A POTENTIAL TISSUE ENGINEERING SCAFFOLD

Nazia Mehrban, Alan M. Smith, Liam M. Grover

School of Chemical engineering, University of Birmingham, UK.

Abstract: The present study evaluates the use of *iota*-carrageenan as a potential tissue engineering scaffold. Cell viability and cell attachment studies were performed on 3T3 fibroblasts cultured for a period of 12 days on the surface and when encapsulated within a 2% *iota*-carrageenan hydrogel. It was found that 3T3 fibroblasts seeded onto the surface of the gel did not show signs of attachment and the proportion of live cells decreased by 33% over a period of 12 days. The proportion of live cells encapsulated within the gel remained constant and there was evidence of cell proliferation throughout the 12 day study (4-fold increase in cell number). The extent of degradation of the gel for both encapsulated and non cell-seeded forms was also evaluated and showing no significant degradation for both types. These results indicate that *iota*-carrageenan may be a suitable scaffold material for use in tissue engineering and a potential tool for studying cell proliferation in three dimensions.

Keywords: *iota*-carrageenan, encapsulation, 3T3 fibroblasts, tissue engineering.

1. INTRODUCTION

Tissue engineering (TE) offers the potential for alleviation of problems associated with an ageing population, a shortage of donor organs and immune rejection of such tissue post-transplantation. Current methods used to enhance repair and regeneration of tissues include cell therapy, growth factors, gene delivery systems and biological scaffolds (Calve et. al., 2004). Seeding a patients' own cells onto a biodegradable scaffold which is inserted into the body, following culture *in vitro,* is of particular interest in regenerative medicine.

Recent research has focussed on the use of water soluble polymers for the encapsulation of cells (Konno and Ishihara, 2007), producing a temporary non-cytotoxic scaffold closely resembling the extracellular matrix of native soft tissue. Certain hydrogels, such as PHEMA (poly(hydroxyethylmethacrylate)) are able to retain water at a concentration similar to living tissue but do not degrade easily. Having a predictable degradation rate is an important factor to account for in tissue engineering as the gel acts as a temporary support to the cells, allowing the cells to grow and proliferate, providing mechanical support whilst the scaffold dissolves and is cleared from the body. The swelling of the gels allows nutrients to diffuse into the network whilst allowing cellular waste to diffuse out of the network (Jeon et. al., 2007). The mechanical properties exhibited by gels are also affected by the surfaces to which they adhere to (Jeon et. al., 2007). Poly(glycolic acid) (PGA) based scaffolds were the earliest successful degradable polymers to be implanted into humans and since then copolymers of PGA and poly(lactic acid) (PLA) have also been developed for the same purpose.

In addition to the use of synthetic hydrogel scaffolds for tissue engineering there is a growing trend towards the use of natural hydrogel scaffolds (such as fibrin, alginate and chitosan). The benefit of using natural hydrogels is the mild and simple approach to 3D cell immobilization. However, some of the gels mentioned (such as alginate) have been known to contract after cells have been incorporated (Awad et. al., 1999). The investigation of proliferation and cell expansion abilities within the scaffolds is necessary as this is a prerequisite for tissue formation.

Carrageenan is a linear sulphated polysaccharide extracted from several species of red seaweeds (*Rhodophyceae*). There are three types of carrageenan commercially available *kappa*, *iota* and *lambda* of which *kappa* and *iota* can form self supporting hydrogels (*lambda* is non-gelling). The primary structure of all types of carrageenan is based on an alternating sequence of □□1-3) linked and □(1-4) linked D-galactose residues. The 4-linked residues in *kappa* and *iota* occur

mainly as the 3,6 anhydride which are required for gel formation. The idealised structure of *iota*-carrageenan has one sulphate on every residue whereas idealised *kappa*-carrageenan has one sulphate group per disaccharide repeat unit. The central process of gelation in *iota* and *kappa*-carrageenan is the formation of intermolecular double helices on cooling (Rees *et al* 1982) and only chain sequences with the 4-linked residues in the anhydride form are compatible for helix formation. Sol-gel transition of both *iota* and *kappa*-carrageenan can be displaced to higher temperatures by addition of salts, for *iota* this is a result of increasing ionic strength (Picullel *et al* 1993), however for *kappa* there is evidence of binding with specific cations in particular K^+ which results in suppression of the electrostatic repulsion between the negatively charged carrageenan helices which enables aggregation and ultimately increased gel strength. *Iota*-carrageenan is not believed to undergo cation mediated aggregation and requires substantially higher polymer concentrations for gel formation. An interesting feature of *iota*-carrageenen hydrogels is their ability to spontaneously reform below their melting point following mechanical disruption (Bixler *et al* 2001) unlike *kappa*-carrageenan and alginate, which may impact on degradation rates when used as cell scaffolds.

Whilst literature is widely available on the entrapment of bacterial cells within carrageenan gels (Lopez, A. et. al., 1997 and Woodward, J., 1998) little is known on the interaction of mammalian cells with carrageenan. We investigated the response of fibroblasts to *iota*-carrageenan. Previous, unpublished experiments, show good cell survival and attachment to the *kappa*- form. Degradation, cell attachment to the surface of the gel, cell behaviour upon encapsulation and the proliferation of encapsulated cells were studied in depth.

2. MATERIALS AND METHODS

2.1Materials

All experiments requiring sterile conditions were conducted under laminar flow. Supplemented media consisted of 10% foetal calf serum, 2.4% L-glutamine, 2.4% HEPES buffer and 1% penicillin-streptomycin (P/S). Foetal calf serum was obtained from PAA (PAA Laboratories Ltd., Somerset, UK). All other chemicals were ordered from Sigma Aldrich (Sigma Aldrich, Poole, UK).

2.2 Methods

Surface seeding. 2% sterile *iota*-carrageenan (w/v) was prepared to form 3ml gelled discs in 12-well cell culture plates and incubated at 37°C for 20 minutes. The gelled discs were seeded with 0.50 x 10^6 NIH 3T3's and 3ml supplemented media. Discs were incubated at 37°C and 5% CO_2 and the media changed every 3 days.

Encapsulation. 0.75 x 10^6 NIH 3T3's were encapsulated in 2% sterile *iota*-carrageenan (w/v) to form 3ml gel discs (created in 12-well culture plates). To ensure cells were evenly distributed within the gel, the cell suspension was repeatedly pipetted in liquid gel. Gelled discs were incubated at 37°C for 20 minutes to ensure gelation. All discs were topped with 3ml supplemented media and incubated at 37°C and 5% CO_2. The media was changed every 3 days to ensure a fresh supply of nutrients reached the cells.

Fluorescence- live/ dead assay. 1ml of gelled samples (both encapsulated and surface-seeded samples) was stained with 2µl calcein-AM and 25µl propidium iodide (PI). The stained samples were each cut to an approximate 1mm thickness (with surface-seeded samples cut horizontally) and observed under ultraviolet light using a fluorescent microscope (Carl Zeiss Ltd, Hertfordshire, UK) at magnifications of x10 and x20. Live (green) and dead (red) cells were photographed using a Canon digital camera attached to the microscope (Powershot G5, Canon UK Ltd, Surrey, UK). Five representative samples were randomly chosen from both the surface seeded and encapsulated gels to determine the proportions of live and dead cells on a daily basis.

MTT (3-(4,5-Dimethylthiazol-2-yl)-2,5-diphenyltetrazolium bromide) assay. The proliferation of encapsulated cells was evaluated by adding 200µl MTT (10% tetrazolium MTT in phosphate buffer solution) to a 2ml gelled disc. Calibration curves were initially conducted to determine the amount of MTT needed per gelled disc and the incubation time needed to obtain the maximum dissolution of MTT using HCl-isopropanol (1ml HCl in 24ml isopropanol). After 18 hs incubation at 37°C, 1ml HCl-isopropanol was added to the well and incubated at 37°C and 5% CO_2 for a further 75 minutes. Absorbance was measured on a daily basis, in triplicate, at 620nm (Cecil C-7500, 7000 Series spectrophotometer, Cecil Instruments Limited, Cambridge, UK). Absorbance measurements obtained from the MTT assay were used to calculate the number of metabolising cells present in each daily sample.

Degradation. Degradation of gels with and without encapsulated cells was conducted by measuring daily wet and dry weights. Dry weights were obtained by slow vacuum drying in an Edwards model EF03 freeze dryer (High Vacuum Ltd., Crawley, UK). All measurements were taken in triplicate. Gels were suspended in 2ml of supplemented media and incubated at 37°C and 5% CO_2 with media being changed every 3 days.

Statistical Analysis. Comparisons among groups were made by the unpaired t-student's test or by analysis of variance (ANOVA) followed by post hoc Tukey test. Differences were determined statistically significant with $p < 0.05$. Data are expressed as mean ± SD.

3. RESULTS

3.1 Fluorescence- live/ dead assay.

Figure 1 clearly illustrates that encapsulated cells remain alive and appear to proliferate with small, thin projections showing possible attachment to the hydrogel. However, cells seeded on the surface of the gel gradually reduce in number and do not aggregate. At day 12, very few cells (alive and dead) remained on the gel surface. The majority of cells photographed when both encapsulated and surface-seeded remain green, indicating that the cells remain alive.

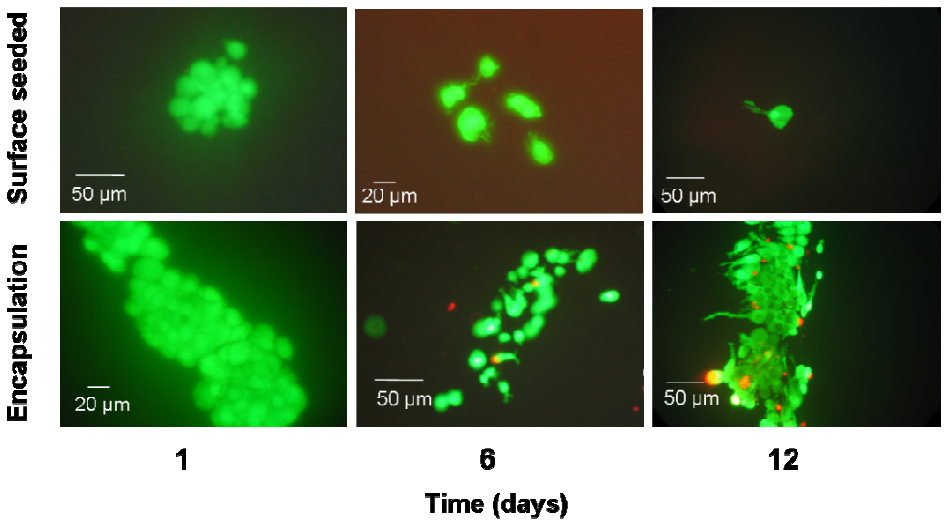

Figure. 1. Fluorescence microscopy images of encapsulated and surface-seeded cells stained with calcein-AM and PI on days 1, 6, and 12 days. Live cells are stained green and dead cells red.

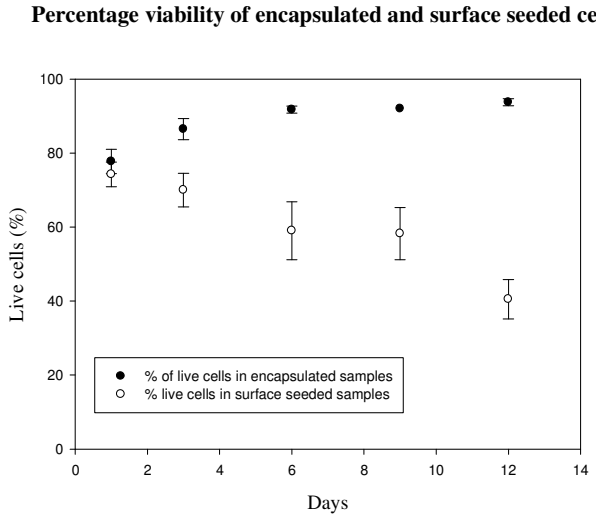

Figure. 2. Percentage of live encapsulated cells as visualised using the live/ dead assay. Cell counts were conducted on days 1, 3, 6, 9 and 12.

Live cell counts shown in Figure 2 reveal that cell viability remains high (80 to 90%) when encapsulated. Indeed, a steady increase in the proportion of live encapsulated cells was witnessed (a total increase of 16%). In contrast, the proportion of live surface seeded cells showed a gradual reduction with a total loss of 33% over the 12 day study. It was also noticed that there was a dramatic reduction of the number of cells on the surface of the gel (live and dead) by day 12.

3.2 MTT cell proliferation assay.

Proliferation of cells was determined from daily absorbance readings of formazan. Figure 3 shows a four-fold increase in the daily number of encapsulated cells. The steady increase in cell number supports previous data obtained from the live/ dead assay and subsequent cell counts (Figures 1 and 2).

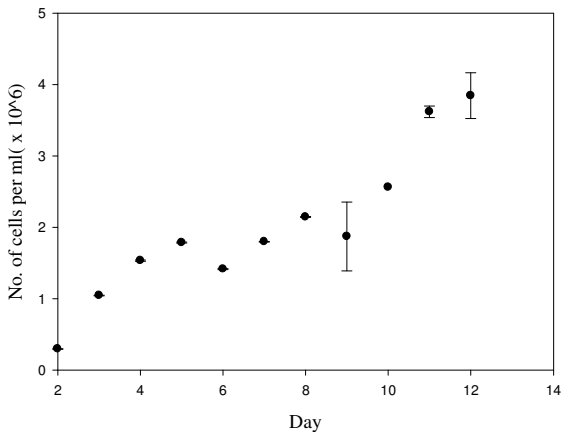

Figure. 3. Number of metabolising cells encapsulated within the carageenan matrix following various periods of culture. As determined using the MTT assay.

3.3 Degradation

From the degradation comparison given in Figure 4 no significant difference is seen between the cell-seeded and non-seeded gels over the 12 day study and both sets of samples lost insignificant proportions of their original mass in this time.

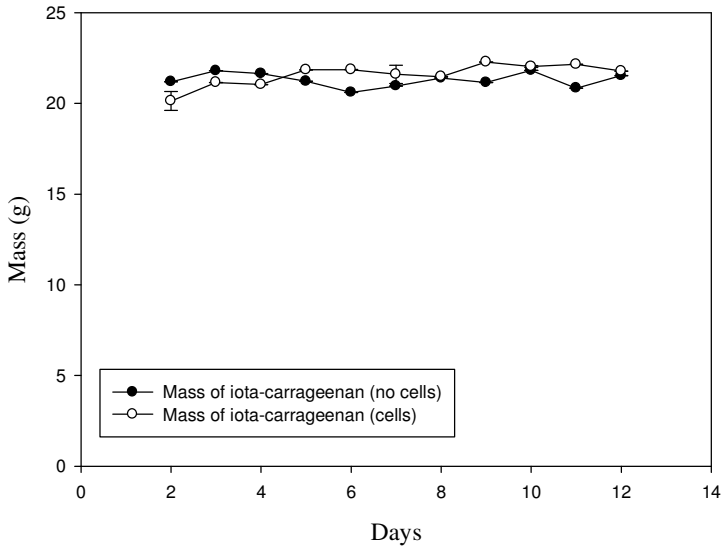

Figure 4. Mass lost from samples of *iota*-carrageenan in supplemented media over the duration of the study. Comparison of gels containing no cells to those containing cells.

4. DISCUSSION

Iota-carrageenan was chosen for investigation due to its well-known thermoreversible and thixotropic nature. We have investigated the attachment, viability and proliferation of the 3T3 fibroblasts in relation to *iota*-carrageenan gel. We have also looked at the degradation rate of *iota*-carrageenan, with and without cells.

Generally, to achieve gelation of carrageenan (*kappa* and *iota* forms), a source of cations (such as potassium) are required (as suggested by Picullel et. al., 1993), however in our system the salts present in the supplemented culture media were sufficient to crosslink the gel. Therefore, no additional cations were needed for gelation to occur offering extremely mild route to immobilising cells in 3D.

After encapsulation and surface seeding, live/ dead assays (using calcein-AM and PI) were conducted on the gelled discs to investigate the viability and attachment of the cells to the gel. From the representative fluorescent images seen in Figure 1, it is immediately apparent that whilst both gels contain live cells on day 1, for the surface seeded samples these quickly diminish. At day 12, there are very few cells to be found on the surface of the gel. It is thought that weak attachment to the surface of the *iota*-carrageenan led to the cells being washed away when the media was changed. However, for the encapsulated cells, the cells appear to be proliferated. Cell counts based on the visual inspection of five fluorescent images (Figure 2), show an increase in cell number when encapsulated and a reduction in cell counts when seeded on the surface of the gel. Although there is no significant difference between the two seeded gel types on day 1, by day 3 statistically significant ($P < 0.05$) differences are apparent.

These results suggest that after 12 days, *iota*-carrageenan allowed sufficient nutrients to diffuse to the centre of the gelled discs keeping cells alive throughout the construct whilst allowing waste products to diffuse out into the surrounding media. This may be explained by the fact that the structure of *iota*-carrageenan is not so orderly and spaces between the polymer chains caused by the swelling of the gel are sufficient in allowing the cells to grow and proliferate similar to the findings of Jeon et. al. (2007).

The increase in cell number seen in the encapsulated cells was further determined by MTT assay. Cell proliferation in encapsulated fibroblasts was evaluated through the reduction of yellow tetrazolium to purple formazan crystals. Changes in the metabolic activity of cells leads to changes in the amount of purple formazan produced (caused by mitochondrial dehydrogenases of viable cells cleaving the tetrazolium ring). The increasing optical density measured spectrophotometrically at 620nm was used in conjunction with the linear calibration curve obtained for MTT to calculate the number of viable cells in daily samples. The results, shown in Figure 3, exhibit the same general trend in cell viability and proliferation, indicated by the fluorescence images and cell counts. Cell number in encapsulated gel samples increases from 0.298×10^6 per ml to 4.297×10^6 per ml 12 days after encapsulation.

As well as a possible tissue engineering scaffold, this rapid proliferation of cells in *iota*-carrageenan makes the gel suitable for the expansion and proliferation of cells in three-dimensional (3D) conditions. This study shows that minimal work is required to obtain cells capable of producing their own extracellular matrix. Traditional two-dimensional (2D) cell culture techniques are time-consuming, requiring constant monitoring and the conditions required for their expansion are not mirrored by the conditions experienced upon implantation. In comparison to encapsulation in unmodified alginate, which is also an ionic binding gel (Constantinidis, I., 2007), cells have been shown to remain viable with little proliferation. The lack of proliferation is thought to be caused by minimal protein adsorption promoted by alginate hydrogels (Rowely, J. A., 1999).

Scaffold degradation studies shown in Figure 4 revealed no significant differences in degradation of samples containing cells in comparison to those containing no cells. This would suggest that although cells remain viable and proliferate in *iota*-carrageenan, they do not affect the degradation rate of the hydrogel and therefore it's overall structure. The reordering properties of *iota*-carrageenan gels are thought to be sufficient in allowing the cells to proliferate throughout the gel, over a 12 day of culture period. It is possible however that as the cells proliferate to a higher rate, the structure of *iota*-carrageenan will be affected. This initial degradation study further adds to the suitability of *iota*-carrageenan as a cell support, initially providing stability. Furthermore, chemical modifications may be made to *iota*-carrageenan to change its gelation behaviour and structure (Picullel et. al., 1993), which may be of use to engineer the scaffold further.

In conclusion, we have shown that although cells do not attach to *iota*-carrageenan, they remain viable and proliferate for up to 12 days when encapsulated, with no significant degradation. However, attachment of cells may be improved with the addition of cell adhesion factors. This

preliminary study suggests that *iota*-carrageenan may be a suitable hydrogel for use as a scaffold for tissue engineering purposes and as a tool for examining cells as proliferation occurs.

REFERENCES

Awad, H.A. *et. al*. (1999) Autologous mesenchymal stem cell-mediated repair of tendon. *Tissue engineering* **5 (3)**, 267- 276.

Bixler, H.J. *et al* (2001) Kappa-2 carrageenan: Structure and performance of commercial extracts. II. Performance in two simulated dairy applications. *Food Hydrocolloids* **15,** 619-630

Calve. S. *et. al*. (2004) Engineering of a functional tendon. *Tissue engineering,* **10 (5/6)**, 755-761.

Constantinidis, I. *et.al*. (2007) Non-invasive evaluation of alginate/poly-l-lysine/alginate microcapsules by magnetic resonance microscopy. *Biomaterials,* **28 (15)**, 2438-2445.

Jeon, O. *et. al*. (2007) Mechanical properties and degradation behaviours of hyaluronic acid hydrogels crosslinked at various crosslinking densities. *Carbohydrate polymers,* **70**, 251-257.

Konno, T. and Ishihara, K. (2007) Temporal and spatially controllable cell encapsulation using a water-soluble phopholipid polymer with phenylboronic acid moiety. *Biomaterials,* **28 (10)**, 1770-1777.

Lopez, A. *et. al.* (1997) The interphase technique: a simple method of cell immobilization in gel-beads. *Journal of microbiological methods,* **30**, 231-234.

Piculell, L. *et al* (1993) Gelation of (some) seaweed polysaccharides. In: *Food hydrocolloids-structures properties and functions*. 35-44. Plenum Press, New York.

Rees,D.A. *et al.* (1982) *Shapes and interactions of carbohydrate chains. In: The polysaccharides*, Vol. 1 (ed. G.O. Aspinall), 195-290. Academic press, New York.

Rowely, J.A. *et. al.* (1999) Alginate hydrogels as synthetic extracellular matrix materials. *Biomaterials,* **20 (1)**, 45-53.

Woodward, J. (1998) Methods of immobilization of microbial cells. *Journal of microbiological Methods,* **8**, 91-102.